National Library
of Canada

Acquisitions and
Bibliographic Services Branch

395 Wellington Street
Ottawa, Ontario
K1A 0N4

Bibliothèque nationale
du Canada

Direction des acquisitions et
des services bibliographiques

395, rue Wellington
Ottawa (Ontario)
K1A 0N4

Your file Votre référence

Our file Notre référence

NOTICE

The quality of this microform is heavily dependent upon the quality of the original thesis submitted for microfilming. Every effort has been made to ensure the highest quality of reproduction possible.

If pages are missing, contact the university which granted the degree.

Some pages may have indistinct print especially if the original pages were typed with a poor typewriter ribbon or if the university sent us an inferior photocopy.

Reproduction in full or in part of this microform is governed by the Canadian Copyright Act, R.S.C. 1970, c. C-30, and subsequent amendments.

AVIS

La qualité de cette microforme dépend grandement de la qualité de la thèse soumise au microfilmage. Nous avons tout fait pour assurer une qualité supérieure de reproduction.

S'il manque des pages, veuillez communiquer avec l'université qui a conféré le grade.

La qualité d'impression de certaines pages peut laisser à désirer, surtout si les pages originales ont été dactylographiées à l'aide d'un ruban usé ou si l'université nous a fait parvenir une photocopie de qualité inférieure.

La reproduction, même partielle, de cette microforme est soumise à la Loi canadienne sur le droit d'auteur, SRC 1970, c. C-30, et ses amendements subséquents.

Canada

UNIVERSITY OF ALBERTA

Investigation of the Electropolymerization Kinetics and Deposition Processes During the Formation of Electronically Conducting Polypyrrole.

©

BY

Daniel Edward Raymond

A Thesis Submitted
To The Faculty of Graduate Studies and Research
In Partial Fulfillment Of The Requirements For The Degree Of **Doctor of Philosophy**

Department of Chemistry

Edmonton, Alberta

Spring, 1993

National Library
of Canada

Acquisitions and
Bibliographic Services Branch

395 Wellington Street
Ottawa, Ontario
K1A 0N4

Bibliothèque nationale
du Canada

Direction des acquisitions et
des services bibliographiques

395, rue Wellington
Ottawa (Ontario)
K1A 0N4

Your file Votre référence

Our file Notre référence

The author has granted an irrevocable non-exclusive licence allowing the National Library of Canada to reproduce, loan, distribute or sell copies of his/her thesis by any means and in any form or format, making this thesis available to interested persons.

L'auteur a accordé une licence irrévocable et non exclusive permettant à la Bibliothèque nationale du Canada de reproduire, prêter, distribuer ou vendre des copies de sa thèse de quelque manière et sous quelque forme que ce soit pour mettre des exemplaires de cette thèse à la disposition des personnes intéressées.

The author retains ownership of the copyright in his/her thesis. Neither the thesis nor substantial extracts from it may be printed or otherwise reproduced without his/her permission.

L'auteur conserve la propriété du droit d'auteur qui protège sa thèse. Ni la thèse ni des extraits substantiels de celle-ci ne doivent être imprimés ou autrement reproduits sans son autorisation.

ISBN 0-315-81985-5

Canada

University of Alberta
Edmonton

Department of Chemistry
Faculty of Science

Canada T6G 2G2

E3-44 Chemistry Bldg., Tel. (403) 492-3254 Fax (403) 492-8231

Prof. D. Jed Harrison
February 3, 1993

To whom it may concern:

This letter is to inform you that I am a co-author with Daniel E. Raymond in a publication titled "Observation of Soluble Electroactive Intermediates during the Anodic Formation of Conducting Polypyrrole Films". This article was published in the Journal of Electroanalytical Chemistry in 1990 (Vol **296**, pp 269-273, 1990). I hereby agree that this material may be included in his thesis.

Best regards,

D. Jed Harrison
Associate Professor of Chemistry
Phone (403) 492-2790
Fax (403) 492-8231

UNIVERSITY OF ALBERTA

RELEASE FORM

NAME OF AUTHOR: **Daniel Edward Raymond**

TITLE OF THESIS: **Investigation of the Electropolymerization Kinetics and Deposition Processes During the Formation of Electronically Conducting Polypyrrole.**

DEGREE: **Doctor of Philosophy**

YEAR THIS DEGREE GRANTED: **1993**

Permission is hereby granted to the University of Alberta Library to reproduce single copies of this thesis and to lend or sell such copies for private, scholarly or scientific research purposes only.

The author reserves all other publication and other rights in association with the copyright in the thesis, and except as hereinbefore provided neither the thesis nor any substantial portion thereof may be printed or otherwise reproduced in any material form whatever without the author's prior written permission.

AUTHOR'S SIGNATURE: Dan Raymond

PERMANENT ADDRESS:
#8-10554 85th Avenue
Edmonton, Alberta
T6E 2K4

DATE: **February 3, 1993**

UNIVERSITY OF ALBERTA

FACULTY OF GRADUATE STUDIES AND RESEARCH

The undersigned certify that they have read, and recommend to the Faculty of Graduate Studies and Research for acceptance, a thesis entitled **Investigation of the Electropolymerization Kinetics and Deposition Processes During the Formation of Electronically Conducting Polypyrrole** submitted by **Daniel Edward Raymond** in partial fulfillment of the requirements for the degree of **Doctor of Philosophy**.

SUPERVISOR: ____________________
Dr. D. J. Harrison

____
Dr. N. Dovichi

James A. Plambeck
Dr. J. Plambeck

Dennis D. Tanner
Dr. D.D. Tanner

Reg Eadie
Dr. R.L Eadie

EXTERNAL EXAMINER: S. Holdcroft
Dr. S. Holdcroft
Simon Fraser University

DATE: **January 28, 1993**

To my Family.

Abstract

Rotating ring-disk electrode (RRDE) and spectroelectrochemical evidence are presented which show bipyrrole is formed in solution during the anodic polymerization of pyrrole in acetonitrile (ACN). Spectroelectrochemistry shows a measurable solution concentration is built up, but the RRDE collection efficiency, N_R, of 9×10^{-3} (0.22 theoretical) demonstrates the yield is low. Other intermediates were observed and the presence of H^+ and protonated pyrrole is discussed. An absorbance peak at 242 nm formed during electropolymerization is identified as protonated pyrrole. Authentic bipyrrole underwent two oxidations at an RRDE, with $E_{1/2}$ values of 0.55 and 1.15 V vs SSCE in 0.1*M* $NaClO_4$. The first $E_{1/2}$ was pH independent, while the second shifted to 0.55 V in 0.1*M* $NaClO_4$, 0.1 *M* pyridine to give a single wave. Polybipyrrole formed from oxidation of bipyrrole in ACN has an oxidation peak at -0.35 V vs SSCE in aqueous ClO_4^-, compared to greater than -0.05 V for polypyrrole. The polybipyrrole oxidation peak is narrower and shows a more well defined range of redox states that does polypyrrole, and coincides with a shoulder often observed for polypyrrole.

RRDE evidence is presented for the identification of the primary pyrrole radical cation species formed during the electropolymerization of pyrrole. An $E^{\circ\prime}$ for this species of + 1.1 V vs SSCE in 0.1 *M* $NaClO_4$ ACN solution is estimated, in agreement with cyclic voltammetric observations by others. At constant disk potential an induction period before the onset of significant pyrrole oxidation was observed, and the rapid rise in current coincides with a substantial, transient increase in the production of pyrrole radical species. During this rapid current increase polymer is deposited non-uniformly on the disk electrode in a pattern indicating the hydrodynamic flow profile at the rotating electrode controls polymer growth. The pattern indicates that soluble, reactive pyrrole oxidation products play a key role in the growth of the film. Finally, finite difference analysis of the polymerization process yielded an overall polymerization rate constant of 10^8 liters/mol-sec, indicating near diffusion control.

Acknowledgements

One would think that of all the sections of the thesis the acknowledgments would be the easiest to write, however, it is difficult to express my gratitude to everyone without feeling melancholy. In the time spent at the University of Alberta I have been very lucky to have met and become friends with some good people. Each in their own way has contributed to my education and have helped me through the thick and thin of graduate school life.

I am indebted to Professor D. Jed Harrison for allowing me the freedom to wander during my research project, but also for having the insight to bring me back when I went too far. Before I met you I had no understanding what a mentor was, now I can safely say I truly understand its meaning. Thank you for your patience, guidance and friendship.

To all the past and present members of " the Harrison Crew " : Andy Chan, Paul Glavina, Sabeth Verpoorte, Xizhong Li, Rob Turner, Kwok-Keung Shiu, Alebachew Demoz, Kurt Seiler, Karl Fluri, Francis Moussy, Aaron Neufeld, Zhonghui Fan, and Zhong Li, thanks for all the interesting times.

I would like to thank all those within the Chemistry Department that have helped me throughout my stay. In particular, Karen McLeod (Dr. Karen McDonald) for all the academic advice, but more importantly for the friendship and laughs. Dr. Jim Nolen has been an invaluable source of information on the digital simulation work and a safe haven during the throes of writing. I extend my appreciation to the electronics and glass shops within the Chemistry Department, the expertise is second to none. Specifically, I want to thank Henry Stolk for his patience during the repair processes. Also, thanks to George and Jackie Agnes for the backpacking escapes to the woods.

I wish to thank my parents, Fred and Linda Raymond, for their love, support and enthusiasm throughout the course of my education. Finally, I can not begin to express my gratitude for the patience, love and continual support from my best friend, Lis Winther. Thanks for everything Lis and sorry it took so long!

Table of Contents.

Chapter 1 Introduction..1

1.1 Pyrrole Chemistry..2
1.2 The Rotating Ring-Disk Electrode..4
1.3 Electropolymerization..9
  1.3.1 Historical Perspective..9
  1.3.2 Electropolymerization Mechanism..10
  1.3.3 Electrodeposition Process..17
1.4 References..22

Chapter 2 Observation of Soluble Electroactive Intermediates During the Anodic Formation of Conducting Polypyrrole Films........27

2.1 Introduction..27
2.2 Experimental..29
  2.2.1 Chemicals..29
  2.2.2 Instrumentation..30
2.3 Procedure..30
  2.3.1 RRDE Analysis of Pyrrole..30
  2.3.2 Bipyrrole Electrochemistry..31
2.4 Synthesis of Bipyrrole..31
  2.4.1 Protection of pyrrole amine group with 2,6-dichlorobenzoyl chloride..31
  2.4.2 Coupling of 1-(2,6-dichlorobenzoyl) pyrrole using $Pd(OAc)_2$ 37
  2.4.3 Hydrolysis of the protecting group..43
2.5 Results and Discussion..50
  2.5.1 Simultaneous sweeps of the Ring and Disk Potentials.........50
  2.5.2 Observation of Hydrogen Oxidation during Pyrrole Polymerization..53

  - 2.5.3 Bipyrrole Electrochemistry....53
  - 2.5.4 Effect of Added Pyridine....59
- 2.6 Conclusions....63
- 2.7 References....65

Chapter 3 Observation of Pyrrole Radical Cations as Transient Intermediates During the Anodic Formation of Conducting Polypyrrole Films....67

- 3.1 Introduction.... 67
- 3.2 Experimental....69
  - 3.2.1 Chemicals....69
  - 3.2.2 Instrumentation....70
- 3.3 Procedures.... 70
  - 3.3.1 Study of Ring Reduction Transient Time Dependence....70
  - 3.3.2 Acid Addition at RRDE using Luggin type capillary....70
  - 3.3.3 Evaluation of Diffusion Coefficients using the Taylor Dispersion Method.... 71
- 3.4 Results and Discussion.... 72
  - 3.4.1 Candidates for the Reducible Intermediate....72
  - 3.4.2 Ring Current Potential Dependence.... 75
  - 3.4.3 Time Dependence of Ring and Disk Currents.... 78
  - 3.4.4 Evidence for the role of Solution Species in Polymer Deposition.... 82
  - 3.4.5 Effect of Electrolyte.... 84
  - 3.4.6 Effect of Radical Dimerization on Kinetics....85
- 3.5 Conclusions....90
- 3.6 References....92

Chapter 4 Spectroelectrochemical Investigation of the Electropolymerization of Pyrrole....94

- 4.1 Introduction.... 94

4.2 Experimental.....95
    4.2.1 Chemicals.....95
    4.2.2 Spectroelectrochemical cell.....95
4.3 Procedures.....95
    4.3.1 Spectroelectrochemical Analysis.....95
    4.3.2 Acidic Polymerization of Pyrrole.....97
4.4 Results and Discussion.....99
    4.4.1 Potential and Time Dependent Spectra.....99
    4.4.2 Bipyrrole and Terpyrrole Spectra.....99
    4.4.3 Acid Polymerization Spectra.....106
4.5 Conclusions.....115
4.6 References.....117

Chapter 5 Analysis of Polymerization of Pyrrole using Standard Rotating Ring-Disk Electrode Kinetic Theory and Digital Simulation.....119

5.1 Introduction.....119
5.2 Rotating Ring-Disk Theory.....120
    5.2.1 The RRDE Collection Efficiency.....120
    5.2.2 First Order Homogeneous Kinetics.....121
    5.2.3 Second Order Homogeneous Kinetics.....123
    5.2.4 Digital Simulation via Finite Difference.....126
5.3 Experimental.....132
    5.3.1 Chemicals.....132
    5.3.2 Instrumentation.....132
5.4 Results and Discussion.....133
    5.4.1 Evaluation of "n" and the reaction order using the RDE.....133
    5.4.2 Kinetic Analysis of Pyrrole Polymerization at the RRDE.....141
        5.4.2-1 First Order Kinetic Analysis.....145
        5.4.2-2 Second Order Kinetic Analysis.....145
        5.4.2-3 Digital Simulation: Finite Difference Analysis.....158
        5.4.2-4 Discrimination between Reaction Schemes.....179

5.4.2-5 Analysis of Pyrrole Polymerization in Propylene Carbonate........ 180
5.4.2-6 Effect of Added Water on the Observation of Bipyrrole during the Polymerization of Pyrrole in Acetonitrile.. 180
5.5 Conclusions........ 185
5.6 References........ 187

Chapter 6 Conclusions 189

6.1 Summary of Contributions........ 189
6.2 Future Research........191
6.3 References........ 193

Appendix A1 Chapter 3: Calculation of Ring Current-Voltage Curves........194

Appendix A2 Chapter 5: Feldberg's Explicit Finite Difference Program........202

List of Tables

Table

2.1 Comparison of the experimental proton NMR ($CDCl_3$) results of 1-(2,6-dichlorobenzoyl)pyrrole to the literature values..............34

2.2 Mass spectral results for 1-(2,6-dichlorobenzoyl)pyrrole..............36

2.3 Comparison of the experimental proton NMR ($CDCl_3$) results of coupled 1-(2,6-dichlorobenzoyl)pyrrole to the literature values......40

2.4 Mass spectral results for coupled 1-(2,6-dichlorobenzoyl)pyrrole.. 42

2.5 Comparison of the experimental proton NMR ($CDCl_3$) results of bipyrrole to the literature values...46

2.6 Comparison of the experimental proton NMR (DMSO-δ6) results of bipyrrole to the literature values... 48

3.1 Diffusion Coefficients obtained via Taylor Dispersion method..... 88

4.1 Potential of the Ag (s) pseudo reference electrode versus the saturated calomel electrode in the various solvent systems studied 98

4.2 Summary of the spectral data obtained for electropolymerization of 50 m*M* pyrrole in acetonitrile with 0.1 *M* $NaClO_4$ as electrolyte...113

4.3 Summary of the spectral data obtained for the electropolymerization of 50 m*M* pyrrole in various electrolytes and solvents...116

5.4.1 Summary of the values of "n" obtained for polymerization of pyrrole in various solvent systems...137

5.4.2 Summary of literature values of "n" obtained for polymerization of pyrrole in various solvent systems................ 138

5.4.3 Summary of calculated diffusion coefficients for pyrrole in propylene carbonate..140

5.4.4 Second order rate constants obtained for various pyrrole concentrations in acetonitrile containing 0.1 *M* $NaClO_4$............ 153

5.4.5 Second order rate constants obtained for various pyrrole concentrations in acetonitrile containing 0.1 *M* $TBABF_4$............154

5.4.6 Second order rate constants obtained for various pyrrole concentrations in acetonitrile containing 0.1 *M* TBAP...............155

5.4.7 Overall polymerization rate constants obtained using Finite Difference Method for various pyrrole concentrations in acetonitrile containing 0.1 *M* $NaClO_4$. Different reactions schemes as shown..176

5.4.8 Overall polymerization rate constants obtained using Finite Difference Method for various pyrrole concentrations in acetonitrile containing 0.1 *M* TBAP. Different reactions schemes as shown..177

5.4.9 Overall polymerization rate constants obtained using Finite Difference Method for various pyrrole concentrations in acetonitrile containing 0.1 *M* $TBABF_4$. Different reactions schemes as shown..178

A1 Parameters used in Ring Current Calculations....................... 201

List of Figures.

Figure

1.2.1 Schematic of Rotating Ring-Disk Electrode.................................. 5

1.2.2 Schematic of the stream lines to a Rotating Ring-Disk Electrode....6

1.3.1 Schematic showing typical current-time response obtained from a potential step at the electrode...18

2.1 Proton NMR of 1-(2,6-dichlorobenzoyl)pyrrole in $CDCl_3$...............33

2.2 Electron impact mass spectrum of 1-(2,6-dichlorobenzoyl)pyrrole.. 35

2.3 Proton NMR of coupled 1-(2,6-dichlorobenzoyl)pyrrole in $CDCl_3$...39

2.4 Electron impact mass spectrum of coupled 1-(2,6-dichlorobenzoyl)pyrrole.. 41

2.5 Proton NMR of bipyrrole in $CDCl_3$...45

2.6 Proton NMR of bipyrrole in DMSO-d6.......................................47

2.7 Splitting pattern from the proton NMR of bipyrrole in a) $CDCl_3$ and b) DMSO-d6...49

2.8 The Pt ring electrode current is shown as a function of the ring potential (100 mV/s,3600 rpm) at several values of the disk potential, E_D (± 20 mV, since the disk was also swept at 5 mV/s). The inset shows the disk electrode current for pyrrole oxidation versus disk potential (5 mV/s,3600 rpm)..................................51

2.9 The Pt ring electrode current is shown as a function of the ring potential (500 mV/s,3600 rpm) at several values of the disk potential, E_D (± 20 mV, since the disk was also swept at 10 mV/s). The inset shows the disk electrode current for pyrrole oxidation versus disk potential (10 mV/s,3600 rpm).................................52

2.10 Cyclic voltammogram of 10 m*M* $HClO_4$ in CH_3CN containing 0.1 *M* $NaClO_4$. Obtained using a Pt disk electrode at a scan rate of 500 mV/s...54

2.11 The Pt ring electrode current is shown as a function of the ring potential (100 mV/s,3600 rpm) for the first oxidation wave of 0.03 m*M* bipyrrole and 0.1 *M* $NaClO_4$ in acetonitrile........56

2.12 a) The Pt ring electrode current-voltage curve (10 mV/s, 4500 rpm) for the oxidation of 0.03 m*M* bipyrrole in acetonitrile containing 0.1 *M* $NaClO_4$.

b) Cyclic voltammograms of deposited polybipyrrole obtained at various deposition potentials.
1. blank.
2. first oxidation plateau: 1 deposition cycle.
3. second oxidation plateau: 1 deposition cycles..57

2.13 Comparison of cyclic voltammograms of (a) polypyrrole and (b) polybipyrrole obtained in aqueous 0.1 *M* $NaClO_4$ after deposition from acetonitrile solution..58

2.14 The Pt ring electrode current is shown as a function of the ring potential (100 mV/s,3600 rpm) at several values of the disk potential, E_D (± 20 mV, since the disk was also swept at 5 mV/s). The inset shows the disk electrode current for pyrrole oxidation versus disk potential (5 mV/s,3600 rpm). Solution contained 100 m*M* pyridine..60

2.15 The Pt ring electrode current-voltage curve (10 mV/s, 4500 rpm) for the oxidation of 0.03 m*M* bipyrrole in acetonitrile containing 0.1 *M* $NaClO_4$ with added pyridine (arrows) and without added pyridine..................61

2.16 The Pt ring electrode current is shown as a function of the ring potential (500 mV/s,3600 rpm) at several values of the disk potential, E_D (± 20 mV, since the disk was also swept at 10 mV/s). The inset shows the disk electrode current for pyrrole oxidation versus disk potential (10 mV/s,3600 rpm). Solution contained 100 m*M* pyridine..........62

3.1 Typical RRDE current-voltage curve obtained from the polymerization of a 0.1 m*M* pyrrole solution with 0.1 *M* $NaClO_4$ as electrolyte. Rotation rate of 4500 rpm. Ring potential of 0.65 V vs SSCE. Disk potential scanned 0.0 V to 1.6 V..73

3.2 Ring current dependence on ring potential obtained from the polymerization of a 0.1 m*M* pyrrole solution with 0.1 *M* $NaClO_4$ as electrolyte. Disk potential scanned 0.0 V to 1.6 V. Rotation rate of 4500 rpm..76

3.3 Ring current dependence on ring potential obtained from the polymerization of a 0.1 m*M* pyrrole solution with 0.1 *M* $NaClO_4$ as electrolyte. Disk potential scanned 0.0 V to 1.6 V. Rotation rate of 4500 rpm..77

3.4 Ring reduction transient analysis during the polymerization of a 0.1 m*M* pyrrole solution with 0.1 *M* $NaClO_4$ as electrolyte. Ring potential held at 0.65 V vs SSCE. Rotation rate of 4500 rpm. Maximum disk potential applied was 1.15 V vs SSCE, as indicated by the dashed line..79

3.5 Ring reduction transient analysis during the polymerization of a 0.1 m*M* pyrrole solution with 0.1 *M* $NaClO_4$ as electrolyte. Ring potential held at 0.65 V vs SSCE. Rotation rate of 4500 rpm. Maximum disk potential applied was 1.125 V vs SSCE, as indicated by the dashed line..81

3.6 Photograph of Pt RDE surface taken after experiment was terminated during the rapid rise in disk current. Solution contained 0.1 m*M* pyrrole in acetonitrile with 0.1 *M* $NaClO_4$ as electrolyte. Maximum disk potential was 1.125 V vs SSCE. Rotation rate was 4500 rpm..83

3.7 Ratio of reduction current to bipyrrole oxidation current (absolute value) versus pyrrole concentrations. Ring potential held at 0.65 V vs SSCE. Disk potential scanned from 0.0 V to 1.6 V vs SSCE. Rotation rate of 4500 rpm................86

3.8 Results from calculations for 0.1 m*M* pyrrole solution. Rotation rate of 4500 rpm, 1.6 μm thick annulus and a rate constant of 1 x 10^8 liters/mole-sec...89

4.1 Schematic of the Spectroelectrochemical cell.............................96

4.2 Potential dependent spectra obtained in acetonitrile containing 50 m*M* pyrrole and 0.1 *M* $NaClO_4$ as electrolyte. Spectra taken 30 second after electrolysis at the indicated applied potentials. The working electrode was in the path of the spectrometer light beam while the spectra were taken......100

4.3 Time dependent spectra obtained in acetonitrile containing 50 m*M* pyrrole and 0.1 *M* $NaClO_4$ as electrolyte. The time after electrolysis the spectra were acquired is given. The working electrode was in the path of the spectrometer light while the spectra were taken...101

4.4 Spectrum obtained in acetonitrile containing 50 m*M* pyrrole and 0.1 *M* $NaClO_4$ as electrolyte. The spectrum was taken after electrolysis with the working electrode out of the path of the spectrometer light beam.......102

4.5 Spectrum of bipyrrole in acetonitrile containing 0.1 *M* $NaClO_4$ as electrolyte. Spectrum was taken in spectroelectrochemical cell without electrodes.......104

4.6 Plot of Absorbance versus λ_{max} for (a) pyrrole, (b) thiophene, (c) benzene and their respective oligomers in CH_3OH.......105

4.7 Spectrum obtained during acid polymerization. Acquired 30 minutes after addition of $HClO_4$ to 1 m*M* pyrrole in acetonitrile containing 0.1 *M* $NaClO_4$ as electrolyte. Spectrum was taken in spectroelectrochemical cell without electrodes.......111

4.8 Plot of Absorbance versus Time for protonated pyrrole (top) and protonated bipyrrole (bottom).......112

4.9 Spectrum obtained in propylene carbonate containing 50 m*M* pyrrole and 0.1 *M* TBAP as electrolyte. Spectrum was taken 30 seconds after electrolysis with the working electrode in the path of the spectrometer light beam.......114

5.2.1 Schematic of reaction zones and corresponding diffusion layer titration curve....... 125

5.2.2 Schematic of the methodology of finite difference analysis....... 128

5.2.3 RRDE discretization.......131

5.4.1 a) Cumulative Levich plot for various concentrations of pyrrole in acetonitrile containing 0.1 *M* $NaClO_4$.
b) Cumulative Koutecky-Levich plot for various concentrations of pyrrole in acetonitrile containing 0.1 *M* $NaClO_4$.......134

5.4.2 a) Cumulative Levich plot for various concentrations of pyrrole in acetonitrile containing 0.1 M $TBABF_4$.
b) Cumulative Koutecky-Levich plot for various concentrations of pyrrole in acetonitrile containing 0.1 M $TBABF_4$....... 136

5.4.3 Dependence of the collection efficiency on $\omega^{1/2}$ for various concentrations of pyrrole in acetonitrile containing either 0.1 *M* $NaClO_4$ or 0.1 *M* $TBABF_4$ 142

5.4.4 Dependence of ring current on $\omega^{1/2}$ for various concentrations of pyrrole in acetonitrile containing either 0.1 *M* $NaClO_4$ or 0.1 *M* $TBABF_4$ 143

5.4.5 RRDE First Order Working Curve 146

5.4.6 First order kinetic plot for 0.1 m*M* pyrrole with 0.1 *M* NaClO4 in acetonitrile (circles) and with 0.1 *M* $NaClO_4$ in propylene carbonate (squares). Triangles are for 0.1 m*M* pyrrole with 0.1 *M* $TBABF_4$ in acetonitrile 147

5.4.7 Second order plot: Kinetic collection efficiency versus ω/C^* or various concentrations of pyrrole in acetonitrile containing 0.1 *M* $NaClO_4$ 148

5.4.8 Second order plot: Ring (bipyrrole) current versus $\omega^{3/2}$ for various concentrations of pyrrole in acetonitrile containing 0.1 *M* $NaClO_4$ 149

5.4.9 Second order plot: Kinetic collection efficiency versus ω/C^* for various concentrations of pyrrole in acetonitrile containing 0.1 *M* $TBABF_4$ 150

5.4.10 Second order plot: Ring (bipyrrole) current versus $\omega^{3/2}$ for various concentrations of pyrrole in acetonitrile containing 0.1 *M* $TBABF_4$ 151

5.4.11 Second order rate constant as a function of pyrrole concentration in acetonitrile containing 0.1 *M* $NaClO_4$ and 0.1 *M* TBAP 156

5.4.12 Second order rate constant as a function of pyrrole concentration in acetonitrile containing 0.1 *M* $TBABF_4$ 157

5.4.13 Radical-radical coupling scheme used in digital simulation 160

5.4.14 Radical-monomer coupling scheme used in digital simulation 162

5.4.15 Comproportionation with radical-radical coupling scheme used in digital simulation 163

5.4.16 Plot of dimensionless rate parameter (obtained from experimental collection efficiencies) versus ω^{-1} for various concentrations of pyrrole in acetonitrile containing 0.1 *M* $NaClO_4$....164

5.4.17 Plot of dimensionless rate parameter (obtained from experimental collection efficiencies) versus ω^{-1} for various concentrations of pyrrole in acetonitrile containing 0.1 *M* $TBABF_4$.... 166

5.4.18 Set of curves demonstrating the effect the number of polymerization steps has on the working curves for the radical-radical coupling scheme....167

5.4.19 Normalized working curves used to evaluate pyrrole polymerization in acetonitrile containing 0.1 *M* $NaClO_4$, 0.1 *M* TBAP and 0.1 *M* $TBABF_4$....171

5.4.20 Dependence of the overall polymerization rate constant on the concentration of pyrrole in acetonitrile and 0.1 M $NaClO_4$....172

5.4.21 Dependence of the overall polymerization rate constant on the concentration of pyrrole in acetonitrile and 0.1 M TBAP....173

5.4.22 Dependence of the overall polymerization rate constant on the concentration of pyrrole in acetonitrile and 0.1 M $TBABF_4$.... 174

5.4.23 Plot of the experimental collection efficiency and the ring current versus $\omega^{1/2}$ obtained during pyrrole polymerization in propylene carbonate containing 0.1 *M* $NaClO_4$....181

5.4.24 Plot comparing the experimental collection efficiency versus ω^{-1} obtained during pyrrole polymerization in propylene carbonate containing 0.1 *M* $NaClO_4$ to the results obtained in acetonitrile containing 0.1 *M* $TBABF_4$ and 0.1 *M* TBAP....182

5.4.25 Plot of experimental collection efficiency versus $\omega^{1/2}$ demonstrating the effect of added water on the yield of bipyrrole during polymerization of pyrrole from 0.1 m*M* pyrrole and 50 m*M* pyrrole in acetonitrile containing

0.1 M $NaClO_4$ ... 184

A1 Schematic of Rotating Ring-Disk Electrode with radial distances applicable to treatment of the outer annulus of the disk as part of a Rotating Double Ring Electrode ... 195

List of Schemes

Scheme

1.1 Linear polymerization reaction schemes via radical-radical coupling or radical-monomer coupling...............12

1.2 Polymerization reaction scheme involving comproportionation and radical-radical coupling...................... 14

2.1 Electropolymerization mechanism..28

2.2 Bipyrrole Synthesis: Protection of pyrrole amine group...............32

2.3 Bipyrrole Synthesis: Coupling of 1-(2,6-dichlorobenzoyl)pyrrole....37

2.4 Bipyrrole Synthesis: Intramolecular Coupling of 1-benzoylpyrrole..38

2.5 Bipyrrole Synthesis: Hydrolysis of protecting group....................44

4.1 Acidic polymerization: formation of pyrrole trimer...................108

4.2 Formation of 2,2'-(1'-pyrrolinyl)pyrrole...................................109

Chapter 1

Introduction.

The study of conducting polymers, or organic metals, has been quite extensive during the past 15 years, and has developed into an interdisciplinary field focussing on both basic research and technical applications. The materials now classified as conducting polymer have long been known to exist. However, the study of organic metals gained impetus in 1977 after the discovery by Heeger and MacDiarmid that doping polyacetylene with iodine gave the polymer metallic properties and increased the conductivity by ten orders of magnitude. This discovery led to a concentrated effort to obtain a rechargeable polymer battery. In the course of this research new polymers, such as polypyrrole and polythiophene, which possessed similar properties to polyacetylene, were discovered.

Conducting polymers are fundamentally different from redox polymers, in that they possess conjugated backbones and the monomeric units interact via the π-electron system. Although redox polymers contain electro-active centers their backbones are not conjugated and the polymers are non-conducting electronically. The various technical applications of conducting polymers include polymer batteries, electrochromic displays, electrocatalysis, polymer based electronic devices (diodes and transistors), chemical sensors, devices for controlled drug release, and anti-corrosion layers in the microelectronic industry.

In general, with the exception of polyacetylene, all important conducting polymers can be formed electrochemically by anodic oxidation. Variations in the deposition conditions, such as solvent and electrolyte, were observed to result in polymer films of differing morphologies and physical properties. This drive to obtain a highly conductive polymer resulted in a vast empirical knowledge of polymer preparation. However, a more detailed understanding of the electropolymerization mechanism would allow direct control of the polymerization process and ultimately yield a polymer with desired properties. Therefore, the electrosynthetic method has also stimulated electrochemical studies of the mechanism of polymerization.

At the onset of this thesis work investigations into the electropolymerization of pyrrole were limited to chronoamperometric investigations of the deposition process [refs from chapter 2]. Speculation as to the involvement of soluble intermediate species in the electropolymerization of pyrrole initiated the mechanistic investigation that comprises this thesis [1]. The electrochemical method employed was the rotating ring-disk electrode, RRDE, which has proven to be an invaluable tool for electrochemically based mechanistic studies. The observation of bipyrrole as a soluble oligomeric intermediate is presented in Chapter 2, while the observation of the primary pyrrole radical cation is discussed in Chapter 3. In Chapter 4 spectroelectrochemical evidence for bipyrrole and other solution species is given. Chapter 5 describes the kinetic analysis of the bipyrrole current observed by conventional RRDE theory and by digital simulation. The mechanism of electropolymerization has been the source of controversy and speculation, with three mechanisms being proposed. The mechanisms are radical-radical coupling, radical-monomer coupling and a comproportionation process, each of which was examined using a finite difference technique.

Before presenting the thesis, a brief discussion of the properties and basic chemistry of pyrrole is given, followed by a description of the rotating ring-disk electrode. Finally, to gain a perspective on the current state of research into the electropolymerization of conducting polymers, the electropolymerization mechanisms and the studies used to investigate them are discussed.

1.1 Pyrrole Chemistry.

The term pyrrole was first used by Runge in 1834 [2] based on his observation that coal tar and bone oil contain a substance that imparts a red colour to pine splinters moistened with mineral acid. The compound was isolated from bone oil and purified by conversion into its potassium salt by Anderson in 1857 [3,4]. In 1870 [5] the structural formula was established. The Union of Pure and Applied Chemistry (IUPAC) numbering system is given in (1) along with the commonly used nomenclature in which the 2(5) positions are designated as α (α ') and the 3(4) positions as ß (ß'). The ring system, which is widely distributed in nature, is a subunit of haem, the chlorophylls, vitamin B and the bile pigments. The pyrrole ring also occurs in a number of naturally occurring antibiotics. Polymers based on the pyrrole ring system show promise as semiconducting and conducting materials. Doped polypyrrole films, generally prepared electrochemically, display metallic conductivity typically in the range 40-200 Ω^{-1} cm^{-1}, whereas films derived from N-methylpyrrole have much lower conductivities characteristic of semiconductors (ca. 10^{-3} Ω^{-1} cm^{-1}).

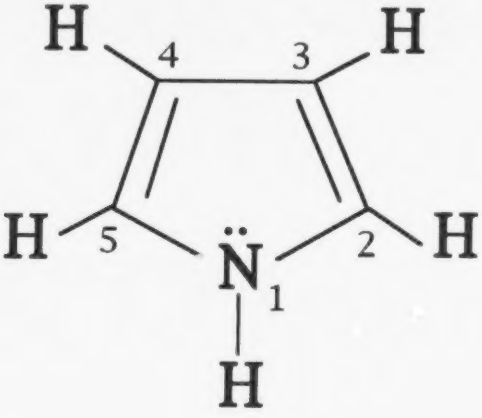

(1)

Pyrrole is a colourless liquid with a boiling point of 129.8 °C at 760 torr, a melting point of 23.4 °C, and a density of 0.970 g/ml at 20 °C. Pyrrole is gradually oxidized in air and its odor somewhat resembles that of chloroform. It has a low solubility in water (ca. 6%) but is miscible with most organic solvents. The physical and chemical properties of pyrrole are characteristic of those expected for an aromatic system in which the nitrogen lone pair is delocalized into the ring system.

The involvement of the nitrogen lone pair in the pyrrole π-system is reflected in its dipole moment. N-methylation of pyrrolidine leads to a reduction in the overall moment from 1.58 debye to 1.10 debye [6], whereas N-methylation of pyrrole leads to an increase in moment from 1.76 to 1.91 D [7]. This indicates that the moments of pyrrole and pyrrolidine are in opposite directions and that the σ-moment of pyrrole is opposed to the π-moment [8]. This is also supported by proton nuclear magnetic resonance, ^{1}H NMR, chemical shift data measured in CCl_4, C_6D_6, and D_6F_6 solutions [6]. As a consequence, pyrrole has negligible basicity compared with typical secondary amines. The pK_a in water for N-protonated pyrrole has been estimated [9] as -10, compared with 11.3 for pyrrolidine, therefore protonation occurs preferentially at carbon rather than nitrogen. The

pK_a for protonation in water at the 2-position is -3.80 [10], while that at the 3-position is -4.44 [10]. This is supported by the results of most molecular orbital (MO) calculations and ^1H NMR measurements [10-13]. The basicity of the pyrrole ring increases considerably with alkyl substitution. The N-H hydrogen atom undergoes rapid exchange with protic solvents at all pH values. Exchange of the C-H hydrogen atoms is catalyzed by acid and occurs more rapidly at the β position than at the α position, although the α–protonated salts are generally the thermodynamically stable species [14-16].

Estimates of the pK_a of pyrrole for N-H ionization to give the pyrrolyl anion vary somewhat depending on the solvent and analytical method. Recent values are 23.05 in dimethylsulfoxide (DMSO) [17] and 21.9 in 5% H_2O - 95% DMSO [18]. The former value should be compared with the value of 44 estimated for pyrrolidine, demonstrating the stabilizing effect of two α-carbon-carbon double bonds. The N-H acidity of substituted pyrroles increases as the substituents electron-withdrawing capabilities increases. Substitutions at the α–position have a greater effect than at the β-position.

1.2 The Rotating Ring-Disk Electrode (RRDE).

The rotating ring-disk electrode, RRDE, was first developed by Frumkin and Nekrasov [19] to detect unstable intermediates in electrode reactions. The RRDE consists of a central disk electrode surrounded by a concentric insulating annulus which separates the disk from a concentric ring electrode. The RRDE is shown in Figure 1.2-1. The RRDE is characterized by the disk electrode region, the gap region and the ring electrode region which are defined by the disk electrode radius, r_1, the inner ring electrode radius, r_2, and outer ring electrode radius, r_3. Individual control of the potentials and currents of each electrode allows the dual electrode system to be used to investigate processes at the disk electrode, or to use the disk electrode as a generator and the ring electrode as a detector of unstable intermediates. The RRDE has been successfully and extensively used to study organic electrode processes [20-24].

Figure 1.2-2 shows some schematic stream-lines for the rotating ring-disk system. The top of Figure 1.2-2 indicates that as the electrode is rotated centrifugal force produces shearing of the liquid at the surface of the electrode and drives it outward from the center. The liquid flung radially outward can only be replaced by liquid flowing toward the

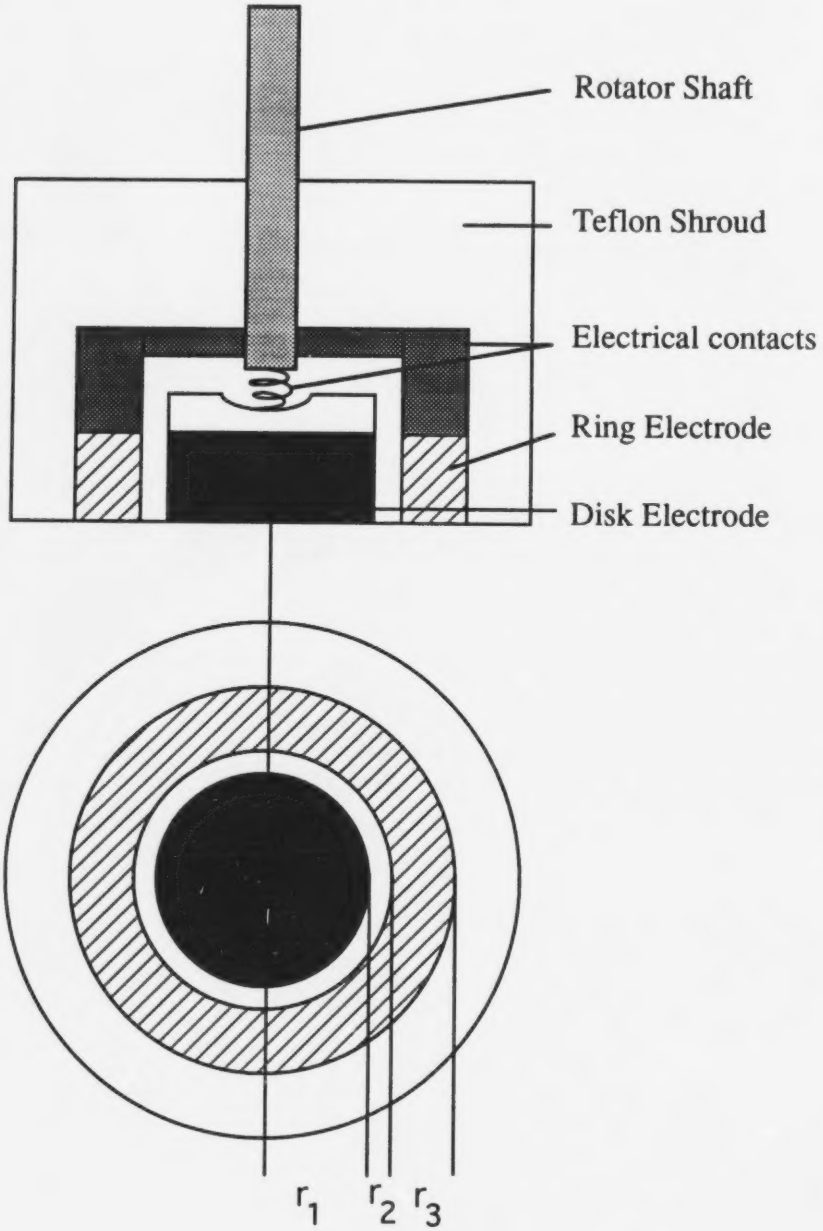
Rotator Shaft
Teflon Shroud
Electrical contacts
Ring Electrode
Disk Electrode
r_1
r_2
r_3

Figure 1.2-1. Schematic of the Rotating Ring-Disk Electrode.

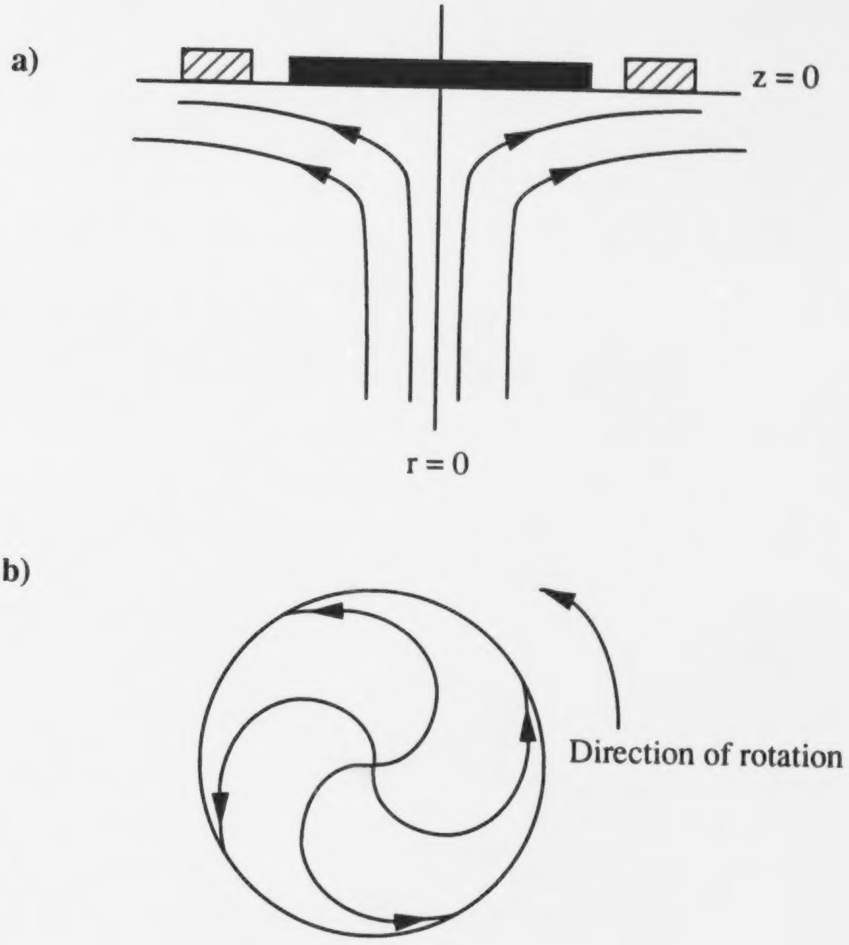
a)
z = 0
r = 0
b)
Direction of rotation

Figure 1.2-2. Schematic of the Stream lines to a Rotating Ring-Disk Electrode.

a) Below electrode surface.

b) Near electrode surface.

electrode from beneath. Thus, the electrode acts as a pump, drawing solution towards it from the bulk and flinging it out centrifugally close to the electrode surface. The bottom of the figure shows the characteristic stream-lines near the electrode surface, which are also called the hyrodynamic flow profiles at the electrode surface. The basic differential equation describing transport of a species of concentration c from the bulk of solution to the disk electrode surface under steady state conditions is given in Equation 1.2.1.

(1.2.1)
$$D\left(\frac{\delta^2 c}{\delta r^2} + \frac{\delta c}{r\delta r} + \frac{\delta^2 c}{\delta z^2}\right) = v_r \frac{\delta c}{\delta r} - v_z \frac{\delta c}{\delta z}$$

The subscripts r and z are the radial and normal components respectively. Equation 1.2-1 does not contain an angular component (ϕ) since, due to the cylindrical symmetry, there are no variations in the velocities and concentrations with respect to ϕ. Hence all derivatives with respect to ϕ are equal to zero. This equation was solved by V.G. Levich [25] and the equation which bears his name is given in Equation 1.2.2. The equation predicts that the limiting disk current is proportional to the concentration of bulk species and to the square root of rotation rate ($\omega^{1/2}$).

(1.2.2)
$$I_L = 0.62nFAD^{2/3}\nu^{-1/6}\omega^{1/2}C^*$$

where:
I_L is the limiting disk current.
n is the number of electrons involved in the electrochemical process.
F is the faraday.
A is the electrode area.
D is the diffusion coefficient of the bulk species.
ν is the kinematic viscosity defined as the ratio of solution viscosity to the density (ρ/d).
ω is the angular velocity.
C^* is the concentration of the bulk species.

To quantitatively describe the yield of species collected at the ring electrode from the amount initially generated at the disk electrode, the transport behaviour of the species from the disk electrode to the ring electrode must be described. An approximate solution to this problem was first obtained by Ivanov and Levich [26] and a more exact analytical expression was derived by Albery and Bruckenstein [27, 28]. In the simplest sense the disk electrode can be regarded as the source from which a constant flux of intermediates is generated. The resulting disk current is then a measure of the quantity of intermediates generated. If the ring electrode is set at a potential such that all the intermediates that reach it are consumed, then the ring current is a measure of the quantity of intermediates "collected" at the ring electrode. This is situation is given below.

$$\begin{array}{ll} \text{DISK} & A \pm n_D e^- \longrightarrow B \\ \text{RING} & B \mp n_R e^- \longrightarrow A \end{array}$$

Thus, the "collection efficiency" is defined as the ratio of the ring current, I_R to the disk current, I_D and is given in Equation 1.2.3.

$$N_0 = -\frac{I_R}{I_D} \qquad (1.2.3)$$

The collection efficiency is always less than unity due to the loss of intermediate species by diffusion into the bulk solution. The negative sign is due to the currents passing in opposite directions.

The theoretical value of the collection efficiency is a function of the electrode geometry and can be calculated using Equation 1.2.4.

$$N_0 = 1 - F\left(\frac{\alpha}{\beta}\right) + \beta^{\frac{2}{3}}[1-F(\alpha)] - (1+\alpha+\beta)^{\frac{2}{3}}\left[1-F\left(\frac{\alpha}{\beta}\right)(1+\alpha+\beta)\right] \qquad (1.2.4)$$

$$\text{with} \quad \alpha = \left(\frac{r_2}{r_1}\right)^3 - 1 \quad \text{and} \quad \beta = \left(\frac{r_3}{r_1}\right)^3 - \left(\frac{r_2}{r_1}\right)^3$$

and r_1 is the disk radius, r_2 is the inner ring radius and r_3 is the outer ring radius. The function, F, dependent on α and β is shown in Equation 1.2.5. This function is for x less than 1.

$$F(x) \equiv \frac{\sqrt{3}}{4\pi} \ln\left[\frac{\left(1 + x^{1/3}\right)^3}{1 + x}\right] + \frac{3}{2\pi} \arctan\left[\frac{2x^{1/3} - 1}{\sqrt{3}}\right] + \frac{1}{4} \qquad (1.2.5)$$

These equations describing the theoretical collection efficiency were obtained by solving the differential equation (Equation 1.2.6) which describes the transport of species B from the disk electrode to the ring electrode under steady state conditions.

$$\frac{\delta c}{\delta t} = D\left(\frac{\delta^2 b}{\delta r^2} + \frac{\delta b}{r \delta r} + \frac{\delta^2 b}{\delta z^2}\right) - v_r \frac{\delta b}{\delta r} - v_z \frac{\delta b}{\delta z} \qquad (1.2.6)$$

The theoretical collection efficiency is independent of rotation rate, and the experimental value obtained from detection of stable intermediates should be identical to the theoretical value. However, if the intermediate undergoes a chemical reaction before it reaches the ring, then the collection efficiency will exhibit a rotation rate dependence. The two factors which dictate whether species B can be detected at the ring electrode are the rotation rate, which defines the time interval between generation and detection, and the rate of the chemical step. Consequently, for a given chemical reaction the value of N will increase with increasing rotation rate and in the limit approach the value for a stable intermediate in an uncomplicated electron transfer.

1.3 Electropolymerization.

1.3.1 Historical Perspective.

It was well over a century ago that the first electrochemical syntheses of what are now classified as organic metals were performed. In 1862 Lethby [29] reported the anodic oxidation of aniline in a solution of dilute sulfuric acid. The blue-black, shiny powder deposited on the platinum electrode was reported to be insoluble in water, alcohol, and other organic solvents. Goppelsroeder [30] conducted further experiments in 1876 and postulated that "oligomers" were formed during the oxidation of aniline. However, it was electrosyntheses of other systems [31]. During the anodic oxidation of pyrrole in dilute sulfuric acid a brittle film of pyrrole black was observed to deposit on a platinum electrode. A conductivity of 8 S/cm was obtained from the isolated materials, indicating the potential of the films as organic conductors.

The first flexible, stable polypyrrole films with high conductivity (100 S/cm) were reported by Diaz *et al.* in 1979 [32-34]. However, rather than forming polypyrrole from an aqueous sulfuric acid solution, the polymer was deposited on a platinum electrode by anodic oxidation in acetonitrile. Electropolymerization in organic solvents to obtain smooth and manageable films of good conductivity became a popular method of preparation from other monomers, since the then known chemical methods of synthesis usually produced low conductivity powders [35-37]. In 1982 Tourillon and Garnier produced polythiophene, polyfuran, polyindole and polyazulene by anodic oxidation of the respective hetero- and homocyclic monomers [38]. This method of synthesis has been used to polymerize numerous substituted heterocyclic compounds of pyrrole and thiophene as well as other parent substances [39]. The number of conducting polymer systems from new monomers is still increasing and by structural modifications of existing parent monomers new properties, such as solubility, have been obtained [40].

1.3.2 Electropolymerization Mechanism.

In general conducting polymers are prepared by anodic oxidation. The two distinct advantages this method has over chemical syntheses is that the polymer is formed in its conducting state, i.e. doped, and that the films often possessed favourable mechanical properties. Anodic oxidation of pyrrole and thiophene has an electrochemical stoichiometry of 2.07 to 2.7 faraday/mol of reacting monomer. It has been demonstrated from elemental analysis and various studies of polypyrrole and polythiophene deposition [41-43] that the film forming process requires 2 faraday/mol and the additional charge is due to the partial, reversible oxidation (doping) of the polymer film. The processes of film formation and film oxidation occur simultaneously since the potential required for monomeric oxidation is always significantly higher than that for charging of the polymer [44]. The complete reaction equation for the polymerization of a species HMH is:

$$(n+2)\ HMH \text{ -------> } HM(M)_nMH^{(nx)+} + (2n+2)\ H^+ + (2n+2+nx)\ e^-$$

where (2n+2) electrons are used for the polymerization reaction, while the additional charging of the polymer requires nx electrons. In general x lies between 0.25 and 0.4 which implies that every third to fourth monomeric subunit in the film is charged.

The mechanism of electropolymerization has been the subject of debate and has not been completely explained. The only point of general acceptance is that in the very first step the neutral monomer is oxidized to a radical cation. However, beyond this two possible propagation modes are have been suggested, radical-radical coupling and radical-monomer coupling. A third mechanism has been proposed which involves comproportionation, however the propagation mode within the mechanism is still a radical-radical coupling process. Scheme 1.1 shows the two main propagation mechanisms proposed. Diaz *et al* have suggested [41,45] that the polymerization of pyrrole occurs via radical-radical coupling and is analogous to known coupling reactions of radical cations of aromatic compounds [46,47]. In this scheme protons are subsequently eliminated from the doubly charged dihydrodimer (**6**) forming the neutral species (**7**). The dimer is more easily oxidizable than the monomer [44] and is therefore immediately reoxidized to the cation. Chain growth occurs by addition of new cations of the monomeric pyrrole to the already charged oligomers (dimers). This is followed by further proton elimination and oxidation of propagating oligomers. This reaction scheme can be described as a cascade of ECCE steps.

In opposition to radical-radical coupling a radical-monomer coupling mechanism has been proposed [48-51] based on the argument that the strong coulombic repulsion between small cation radicals would make the direct dimerization of such particles improbable. Scheme 1.1 shows the radical-monomer mechanism in which an electrophilic attack by radical cation on neutral monomer produces the singly charged dihydroderivative (**5**). Proton elimination to form the neutral oligomer occurs only after further oxidation of species (**5**) to species (**6**). A recent study of the polymerization of 3-alkyl thiophenes with small amounts of 2,2'-bithiophene or 2,2':5'2"-terthiophene, plus similar studies of pyrrole polymerization with 2,2'-bipyrrole, indicated a radical-monomer propagation process [52,53]. However, other recent interpretations have pointed to a radical-radical coupling process [54]. Furthermore, it has been shown using the Debye-Smoluchovski theory [55,56] that small particles with the same charge are able to associate at diffusion-controlled rate. Further evidence to support radical-radical coupling is given below.

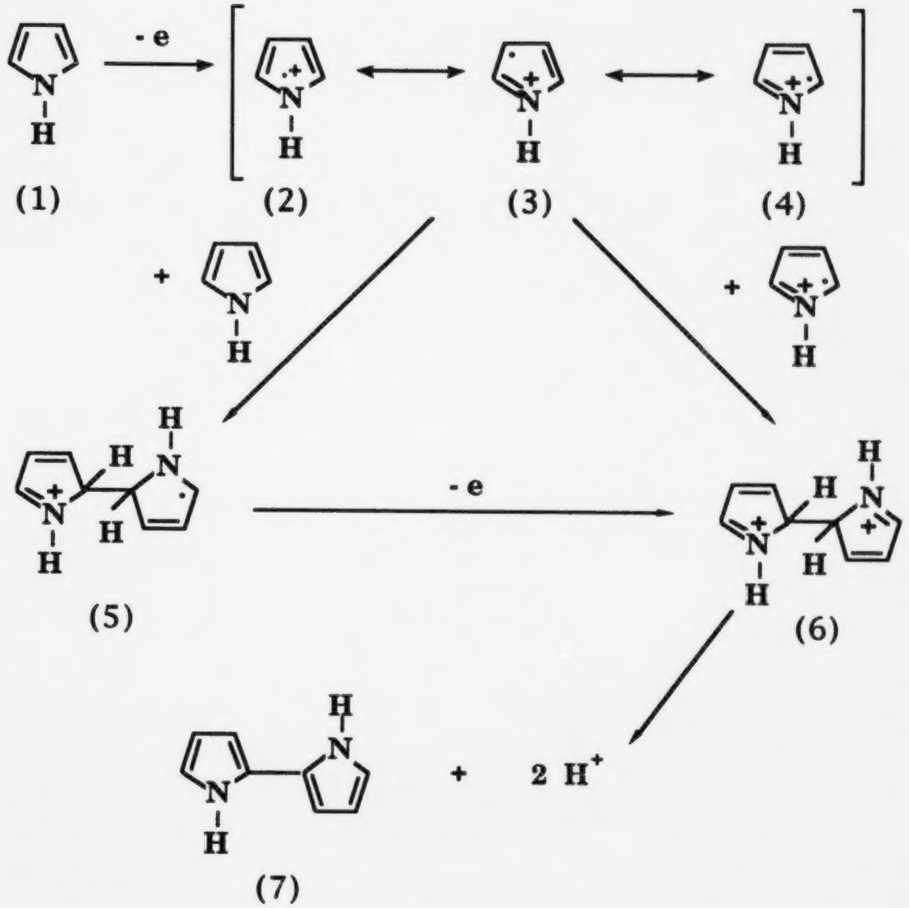
- e
(1)
(2)
(3)
(4)
+
+
(5)
- e
(6)
+ 2 H⁺
(7)

Scheme 1.1 Linear polymerization reaction schemes via radical-radical coupling or radical-monomer coupling.

Due to the available time scales of electrochemical techniques, the fast reaction rates encountered during the electropolymerization of pyrrole and thiophene have made the unequivocal characterization of the electropolymerization mechanism via kinetic analysis difficult . However, the anodic oxidation of N-phenylcarbazole has provided information on the initial stages of electropolymerization since its coupling reaction is "slower" than other polymerizable systems [57]. Using cyclic voltammetric studies the polymerization of N-phenylcarbazole was observed to begin at a formation potential well before the thermodynamic redox potential of the monomer species. Also, current-voltage trace-crossing effects, similar to those observed with pyrrole and thiophene, were obtained. From these observations the authors suggested that electropolymerization cannot be explained by a simple linear reaction scheme (scheme 1.1) because such a scheme indicates competing homogeneous and heterogeneous electron transfer processes. Detailed kinetic studies in conjunction with digital simulation confirmed that radical-radical coupling occurs as well as the oxidation of the resulting dimer to its dication. It was also shown that in addition to the heterogeneous process a homogeneous redox reaction occurs between the dimer dication and monomer, producing dimer radical cation and monomer radical cation. This sequence is shown in Scheme 1.2. The dimerization continually disturbs the comproportionation equilibrium by removing monomer radical cation, hence, monomer radical cation is formed homogeneously in the diffusion layer. The kinetic analyses gave a dimerization rate constant of 1.2 x 10^6 liters/mol-sec for the "slow" coupling of N-phenylcarbazole. Therefore, the corresponding dimerization rate constant for pyrrole and thiophene must be greater by some orders of magnitude.

Chronoabsorptiometric measurements [45] demonstrated that polypyrrole films grow in time linear to t and not to $t^{1/2}$. These measurements involved obtaining absorbance spectra as function of time at a constant potential analogous to measuring the current as a function of time for a potential step to a constant value. From this observation it was concluded that the rate-determining step during film growth is the radical-ion coupling step and not the diffusion of uncharged monomer to the electrode surface. Further proof of purely ionic radical-radical coupling is obtained from the observation that pyrrole polymerization apparently occurs considerably faster in the presence of polar H_2O (ε =79) than in dry aprotic solvents [31,41,58,59]. This has been attributed to the large dielectric constant of water which reduces the coulombic repulsion between the radicals. In contrast to this, thiophene polymerization in acetonitrile is dramatically reduced in the presence of small quantities of water. This inhibiting effect was assigned to the formation of a non-

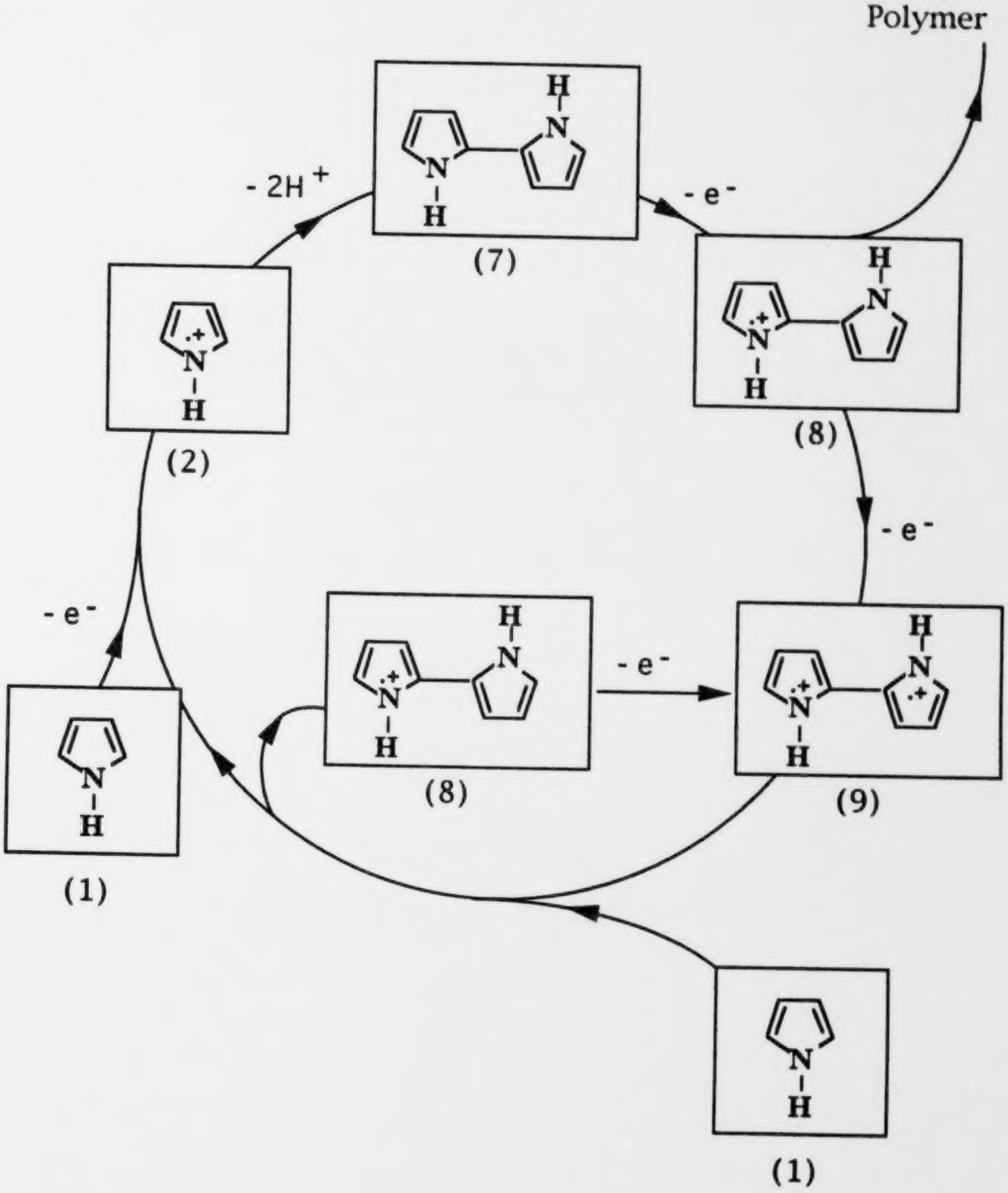
Polymer
- 2H +
- e-
(7)
- e-
(2)
(8)
- e-
- e-
(1)
(8)
(9)
(1)

Scheme 1.2 Polymerization reaction scheme involving comproportionation and radical-radical coupling.

conducting passivating layer on the platinum electrode or on the polythiophene surface [60]. Similar passivating effects were observed when benzene was oxidized in dry acetonitrile [61], but if dry SO_2 was used instead, adhesive polyparaphenylene films with suitable mechanical properties were formed [62].

The difference in polymerization behaviour between monomers is due to competition between reaction paths which are dependent upon both the reactivities of the anodically generated radical and the polymer film, as well as the reactivity of the solvent/electrolyte system used. The polymerization rate of a particular monomer can change dramatically as the nucleophilicity of the solvent increases. The solvents commonly used in electropolymerization are given below in increasing nucleophilic power: $HF < CF_3COOH < SO_2 < CH_3NO_2 < CH_2Cl_2 <$ propylene carbonate $< CH_3CN < H_2O$. Only pyrrole can be successfully polymerized in water [63-66]. The large dielectric constant of water accelerates the coupling reaction, while because of the low oxidation potential the nucleophilic reactivity between water and the polymer is diminished. Thiophene polymerizes easily in acetonitrile but due to its higher oxidation potential it is more reactive than pyrrole and, therefore, small amounts of water are sufficient for nucleophilic addition to block further growth of the oligomer chain.

An important factor which affects the rate of propagation is the extensive delocalization of the radical cation along the oligomeric chain [52]. The cationic character of the α-carbons at the chain ends decreases as the chain length increases because of this delocalization [44,67]. As the chain length increases the cationic character at the chain ends decreases resulting in decreased reactivity of the radical cation, and this leads to lower reaction rates for radical cations of longer oligomers [68,69]. A similar argument based on the respective oxidation potentials of the oligomeric chains can be used. The oxidation potentials of oligomeric species have been shown to decrease as the chain length increases [42] and, therefore, the radical cations of longer chain oligomers should be more stable than than those generated from shorter chains [52]. Consequently, the reactivity of the growing polymer chain decreases, particularly in the initial stages of growth. It is clear that the reactivity of the chain is dependent on its charge, which, in turn, is a function of the electrode potential and the respective degree of polymerization. The oxidation potential decreases rapidly as the chain length increases from the monomer to the tetramer but slows down as further increases occur, and eventually levels off as the polymer forms [44]. Thus, the coupling rate falls rapidly until it reaches a steady state characterized by a constant number of charges per segment despite an increasing degree of polymerization.

It is quite evident from the above discussion that the electropolymerization mechanism is complex. The relationship between the physical properties of the starting monomers and their tendency to polymerize has been extensively investigated by systematically varying polymerization parameters, such as solvent, electrolyte, or monomer substituents. Pyrrole and thiophene have been popular candidates for studying the effect of added substituents on the rate of polymerization and the properties of the resulting polymer film. N-substitution of pyrrole [70] has shown that sterically crowded substituents, such as *tert*-butyl- or the cyclohexyl-group, totally block polymerization, whereas long alkyl chains [71], or halogen substituents [72] produce films with poor conductivity and mechanical properties. Similarly, substitution at the 2 and 5 positions of pyrrole also block polymerization [73]. The electronic influences of the substituents is less clear than those of steric effects. In general, parent substances with high oxidation potentials will preferably form polymers with electron-donating substituents, and those with low oxidation potentials with electron-withdrawing substituents [74].

The intermediate radical cations formed at the electrode have in principle a choice of three reaction paths [67,75,76]. The first is the polymerization reaction (k_p), the second is the diffusion of stable radicals into solution (k_d), and third, for very reactive radicals, reaction with the solvent or the anions of the supporting electrolyte at the electrode interface ($k_n([solv] + [X^-])$). The fraction of the radical cations which electropolymerize is given by equation 1.3.1.

$$f_p = \frac{k_p}{k_p + k_d + k_n([solv] + [X^-])} \tag{1.3.1}$$

Thus, polymerization will always occur when $k_p \gg k_n([solv] + [X^-])$. For highly electron-donating substituents the radical cation may be stable enough such that $k_d \gg k_p + k_n([solv] + [X^-])$ and consequently, most of the radicals diffuse into solution. On the other hand, the combination of electron-withdrawing substituents and large oxidation potentials result in $k_n([solv] + [X^-]) \gg k_p + k_d$ and the nucleophilic addition will dominate while polymerization will be suppressed.

1.3.3 Electrodeposition Process.

Description of the processes involved in the deposition of polymer on the electrode surface has remained elusive despite the volume of knowledge acquired on the chemistry of electropolymerization. The induction stage of film formation of polypyrrole [51,59,77,78], polythiophene [60,79] and polyaniline [80] have been intensively studied using potential step and voltammetric experiments. In the first cycle in all voltammograms a trace-crossing is observed on the reverse sweep, provided that the scan reversal occurs near the peak potential. Similar trace-crossings are obtained during electrochemical deposition of metals on foreign substrates, e.g. lead on graphite, and are referred to as nucleation curves. The initial process of metal deposition requires an additional nucleation overpotential, while during the reverse scan metal is deposited on an identical metallic surface at the thermodynamically favourable potential. This potential is smaller relative to the nucleation overpotential resulting in metal deposition occurring at less positive potentials and the generation of a trace-crossing on the current-voltage curve.

The trace-crossings in electrochemical deposition of polymers only occur on freshly polished electrodes. Therefore, the similarities between the electrochemical deposition of metals and the electrochemical deposition of polymers has been taken as proof of the start of a nucleation process [51,77]. The increase in current with each cycle of a multisweep CV is a direct measure of the increase in the surface of the redox active polymer and, hence a suitable measure of relative growth rates [52,53]. The relative growth rate per cycle is calculated from the peak current of the respective polymer oxidation as the number of cycles increases.

The deposition processes of pyrrole, thiophene and aniline have been extensively investigated using potential step experiments. In this technique the potential is stepped from a value at which no faradaic process is occurring at the electrode, to a constant value at which the mass transport limited current is obtained. The resulting current is then monitored as a function of time. The top of Figure 1.3.1 shows a schematic of a typical current-time (i-t) curve obtained from a potential step experiment involving a reversible electrode process with a species that does not deposit on the electrode surface. The initial current spike is due to the non-faradaic charging of the double-layer, while the current decay is primarily due to depletion of the electroactive species near the electrode surface. The current decay at a planar electrode is described by the Cottrell equation (Equation 1.3.2) given below [81].

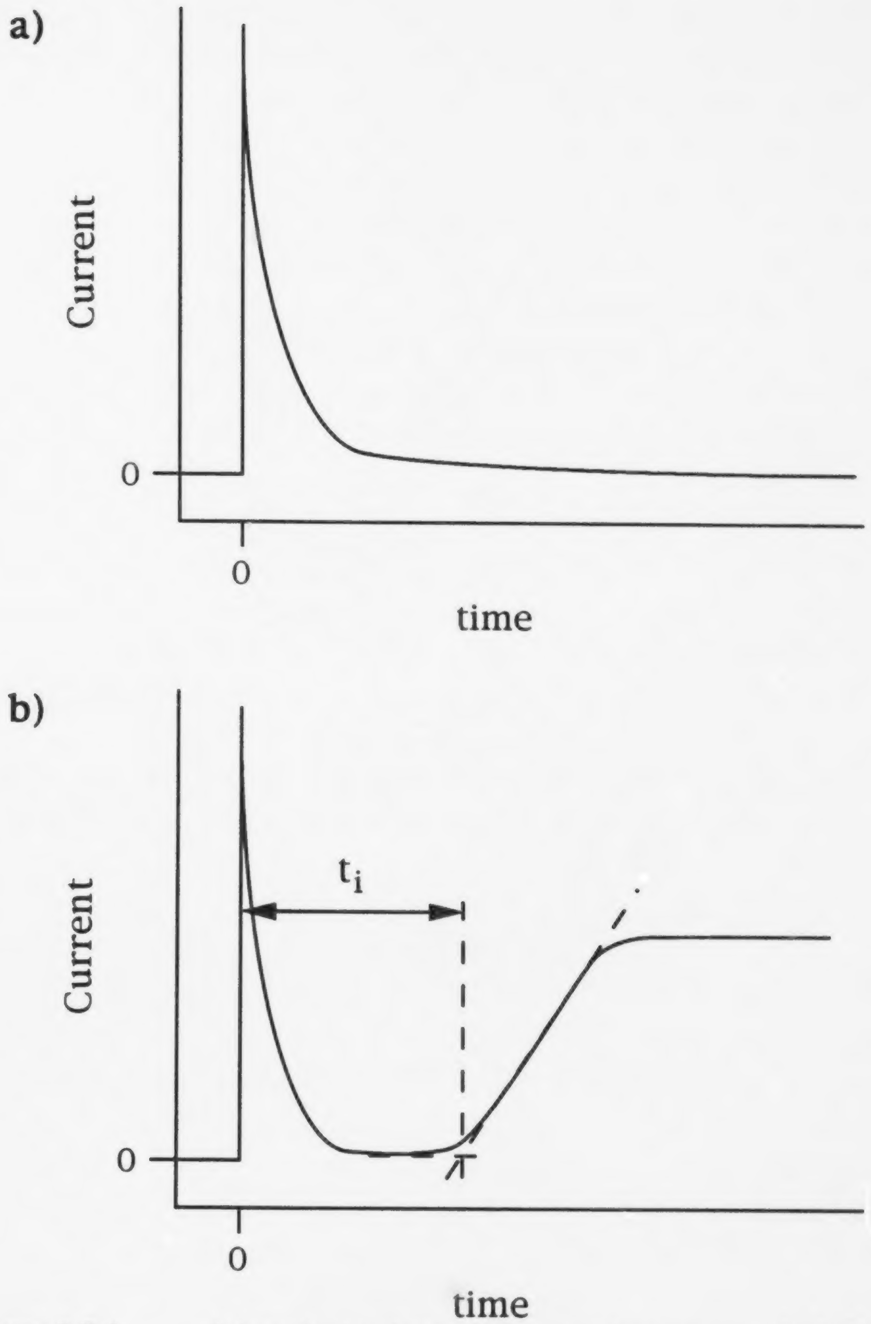

Figure 1.3.1. Schematic showing typical current-time response obtained from a potential step at the electrode.

a) Reversible electrode process without deposition.
b) Deposition onto electrode surface.

(1.3.2)

$$I(t) = \frac{nFAD_o^{1/2}C_o^*}{\pi^{1/2}\, t^{1/2}}$$

The current for the faradaic process decays as $t^{-1/2}$, while the non-faradaic current decays exponentially with a time constant R_uC_d, where R_u is the uncompensated resistance and C_d is the double-layer capacitance. Within the period of the time constant some contribution of the charging current to the total measured current occurs. However, after this time period the observed current is due solely to the faradaic process.

The bottom of Figure 1.3.1 shows the current-time curve obtained for the deposition of a metal under potential step conditions. After the initial decay the current grows rapidly to a constant value. This growth is attributed to the increase in the electrode surface area as the metal deposits. The time prior to the rapid growth is called the induction period, t_i, and it is during this period that the formation of nuclei occur. The equation describing instantaneous three-dimensional nucleation and growth is given in Equation 1.3.3, while progressive three-dimensional nucleation and growth is described by Equation 1.3.4 [82].

(1.3.3)

$$I(t) = \frac{2zF\pi M^2}{\rho^2} N_o k^3 t^2$$

(1.3.4)

$$I(t) = \frac{2zF\pi M^2}{3\rho^2} A k^3 t^3$$

The observed relationship between current and time is then used to assign the growth process.

In potential-step experiments with thiophene, pyrrole, and aniline monomers the observed relationship between current and time, after induction periods of varying lengths, is $i \approx t^2$. In most publications [59,77-80] this relationship is interpreted as being due to instantaneous nucleation and three-dimensional hemispherical growth. However, this interpretation is based on the models developed for nucleation and growth of metallic phases and anodically deposited oxide films [83,84]. The chemistry of the elementary steps of these processes differ fundamentally from the processes involved in the electropolymerization of organic metals. In three dimensional nucleation and growth random formation of nuclei occur, initiated by adsorption of metal cations onto the substrate which then react electrochemically generating a metal atom. Growth and overlap of these nuclei on the substrate surface then results in formation of the metallic phase. Conversely, in electropolymerization of conducting polymers formation of "nuclei" occurs in solution which subsequently precipitate onto the substrate surface. Growth results from continual electro-precipitation and by direct reaction at the surface. Thus, even though the i-t curves for both processes are superficially alike, the events which give rise to the curves are completely different. Also, a prerequisite for the postulated three-dimensional growth is chain-branching reactions, for which there is no support in the available data on structure of the polymers. Therefore, the electrochemical deposition of polymers can not be satisfactorily described as instantaneous nucleation and three dimensional growth.

Using optical measurements based on differential ellipsometry to study the deposition of 2-methylthiophene in acetonitrile Costa and Garnier [85] concluded that the intermediate radical cations form oligomers via coupling reactions in solution near the electrode interface with a degree of polymerization of 3-4. Above a critical chain length insoluble oligomers form, which deposit onto the electrode surface. The optical signal used to monitor polymer deposition during the potential step was observed to increase only when the current on the current-voltage curve began to rise again after the typical $t^{-1/2}$ decay. The observed oxidation currents and the optical signal were found to be dependent on the scan rate. The slower the scan rate, the more visible the electrode coating and the greater the rise in the oxidation currents, indicating the presence of soluble species.

Recently, a study of pyrrole deposition using *in-situ* differential ellipsometry [86] drew similar conclusions. Once above a critical length the oligomers precipitate onto active sites and grew homogeneously by addition to the free end of the polymer chain. The electric field at the end of the chain is the driving force for this growth process, assuming the polymer chains extend freely into solution. After these chains on the electrode surface reach a length such that the potential drop along their length precludes further growth, the polymer "fills in" via nucleation and growth on the remaining exposed electrode surface. Additional growth on the original chains may occur at the β-positions. Eventually the whole surface is covered and the film continues to grow outward. Studies utilizing the unique mass transport behavior characteristic of microelectrodes [87] concluded that polymer growth on the electrodes, after initial solution polymerization and precipitation, results from "continual electroprecipitation". These observations contradict the assumption of primary adsorption of monomers on the electrode surface, followed by oxidation and polymerization in the adsorbed state to form a single polymeric layer on the electrode [51,79,87-89].

The contribution from this thesis work on the electropolymerization of pyrrole to this array of information on the electropolymerization mechanism and the deposition process of conducting polymers is anticipated to be three-fold. Firstly, the direct observation and identification of the primary radical cation and the product of the first coupling reaction, bipyrrole, would allow insight into the the effects of solution conditions on the polymer formation mechanism. Secondly, the location of the polymerization process, whether it occurs in solution or on the electrode surface, has been a point of contention and it is hoped that the RRDE investigations can help clarify this situation. Finally, the RRDE is an invaluable tool for mechanistic studies and coupled with digital simulation has been used to obtain rate constants for complex reaction systems. It is anticipated that by using these techniques the overall rate constant for the polymerization of pyrrole, and a distinction between the proposed mechanisms can be found. Then, with this basis, the effect of solution conditions on the overall rate constant can be obtained

1.4 References

1. Miller, L.L.; Zinger, B.; Zhou, Q.X., *J. Am. Chem. Soc.*, **1987**, 109, 2267.
2. Runge, R., *Ann. Physik.*, **1834**, 31, 67.
3. Anderson, T., *Trans. Roy. Soc. Edinburgh.*, **1857**, 21, 571.
4. Anderson, T, *Liebigs Ann. Chem.*, **1858**, 105, 349.
5. Baeyer, A.; Emmerling H., *Chem. Ber.*, **1870**, 3, 517.
6. Barton, T.; Roth, R.W.; Verkade, J.G., *J. Am. Chem. Soc.*, **1972**, 94, 8854.
7. Mauret, P.; Fayet, J.-P.; Fabre, M., *Bull. Soc. Chim. Fr.*, **1975**, 1675.
8. Marino, G., *J. Heterocycl. Chem.*, **1972**, 9, 817.
9. Chen, H.J.; Hakka, L.E.; Hinman, R.L.; Kresge, A.J.; Whipple, E.B., *J. Am. Chem. Soc.*, **1971**, 93, 5102.
10. Chiang, Y.; Whipple, E.B., *J. Am. Chem. Soc.*, **1963**, 85, 2736.
11. Chiang, Y.; Hinman, R.L.; Theodoropulus, S.; Whipple, E.B., *Tetrahedron.*, **1967**, 23, 745.
12. Abraham, R.J.; Bullock, E.; Mitra, S.S., *Can. J. Chem.*, **1959**, 37, 1859.
13. Whipple, E.B.; Chiang, Y.; Hinman, R.L., *J. Am. Chem. Soc.*, **1963**, 85, 26.
14. Murano, Y.; Akimoto, J.; Yoshihara, K.; *Radiochim Acta.*, **1985**, 38, 11.
15. Catalan, J.; Yanez, M., *J. Am. Chem. Soc.*, **1984**, 106, 421.
16. Houriet, R.; Schwarz, H.; Zummack, W.; Andrade, J.G.; von R. Schleyer, P., *Nouv. J. Chim.*, **1981**, 5, 505.
17. Bordwell, F.G.; Drucker, G.E.; Fried, H.E., *J. Org. Chem.*, **1981**, 46, 632.
18. Halle, J.C.; Pouet, M.J.; Simonin, M.P.; Debleds, F.; Terrier, F.,*Can. J. Chem.*, **1982**, 60, 1988.
19. a) Frumkin, A.N.; Nekrasov, L.N.; Dokl Akad Nauk SSR, **1959**, 126, 115;
    b) Frumkin, A.N.; Nekrasov, L.N.; Levich, B.; Ivanov, Yu., *J. Electroanal. Chem*, **1959-1960**, 1, 84.
20. Albery, W.J.; Hitchman, M.C., *"Ring-Disk Electrodes"*, Oxford Press, London, **1971.**
21. a) Nekrasov, L.N.; Korsun, A.D., *Electrokhymiya.*, **1968**, 4, 489.

b) Nekrasov, L.N.; Korsun, A.D., *Electrokhymiya.*, **1968**, 4, 539.
c) Nekrasov, L.N.; Korsun, A.D., *Electrokhymiya.*, **1968**, 4, 996.
d) Korsun, A.D.; Nekrasov, L.N., *Electrokhymiya.*, **1969**, 5, 212.

22. a) Prater, K.B.; Bard, A.J., *J. Electrochem. Soc.*, **1970**, 117, 207, 335.
b) Prater, K.B.; Bard, A.J., *J. Electrochem. Soc.*, **1970**, 117, 207, 1517.

23. a) Puglisis, V.J.; Bard, A.J., *J. Electrochem Soc.*, **1972**, 119, 829.
b) Puglisis, V.J.; Bard, A.J., *J. Electrochem Soc.*, **1972**, 119, 833.
c) Puglisis,, V.J.; Bard, A.J., *J. Electrochem Soc.*, **1973**, 120, 748.

24. a) Neubert, B.; Prater, K.B., *J. Electrochem Soc.*, **1974**, 121, 745.
b) Korotov, A.P.; Nekrasov, L.N., *Soviet Electrochem.*, **1982**, 18, 35.
c) Yeh, Lun-Shu R.; Bard, A.J., *J. Electrochem. soc.*, **1977**, 124, 189.
d) Yeh, Lun-Shu R., *J. Electroanal Chem.*, **1977**, 84, 159.
e) Funt, B. Lionel; Severs, W.; Glasel, A., *J. Polym. Sci. Polym. Ed.*,**1976**, 14, 2763.
f) Funt, B. Lionel; Verigin, Victor, *Can. J. Chem.*, **1974**, 52, 1642.
g) Raymond, D.E.; Harrison, D. Jed, *J. Electroanal. Chem.*, **1990**, 296, 269.

25. Levich, V.G., *Acta. Phys. Chim. URSS.*, **1942**, 11, 257.

26. Ivanov, Y.B.; Levich, V.G., *Dokl. Akad. Nauk SSSR.*, **1959**, 126, 1029.

27. Albery, W.J., *Trans. Faraday Soc.*, **1966**, 62, 1915.

28. Albery, W.J.; Bruckenstein, S., *Trans. Faraday Soc.*, **1966**, 62, 1920.

29. Lethby, H., *J. Chem. Soc.*, **1862**, 15, 161.

30. Goppelsroeder, F., *Compt. Rend. 82*, **1876**, 331, 1392.

31. Dall'Olio, A.; Dascola, Y.; Bocchi, V., *C.R. Hebd. Seances. Acad. Sci., Ser. C.*, **1968**, 267, 433.

32. Diaz, A.F.; Kanazawa, K.K.; Gardini, G.P., *Chem. Commun..*, **1979**, 635.

33. Kanazawa, K.K.; Diaz, A.F.; Geiss, R.H.; Gill, W.D.; Logan, J.A.; Rabolt, J.F.; Street, G.B., *J. Chem. Soc. Chem. Commun..*, **1979**, 854.

34. Kanazawa, K.K.; Diaz, A.F.; Gill, W.D.; Grant, P.M.; Street, G.B.; Gardini, G.P.; Kwak, J.K., *Synth. Metals*, **1979/1980**, 1, 329.

35. Angeli, A., *Gazz. Chim. Ital.*, **1916**, 46, 279.

36. Gardini, G.P., Adv. *Heterocycl. Chem.*, **1973**, 15, 67.

37. Kovacic, P.; Jones, M.B., *Chem. Rev.*, **1987**, 87, 357.

38. Tourillon, G.; Garnier, F., *J. Electroanal. Chem.*, **1982**, 135, 173.

39. Bryce, M.R., *Annu. Rep. Prog. Chem. Sect. B.*, **1985**, 82, 377.

40. Frommer, J.E.; Chance, R.R., in "*Encyclopedia of Polymer Science and Engineering*", Grayson, M.; Krosch-witz, J. (eds.), 2nd edition , Wiley, New York, vol. 5, p.462, **1986**.

41. Diaz, A.F.; Castillo, J.I.; Logan, J.A.; Lee, W-Y., *J. Electroanal. Chem.*, **1982**, 129, 115.

42. Diaz, A.F., *Chem. Scr.*, **1981**, 17, 145.

43. Waltman, R.J.; Bargon, J.; Diaz, A.F., *J. Phys. Chem.*, **1983**, 87, 1459.

44. Diaz, A.F.; Crowley, J.; Bargon, J.; Gardini, G.P.; Torrence, J.B., *J. Electroanal. Chem.*, **1981**, 121, 355.

45. Genies, E.M.; Bidan, G.; Diaz, A.F., *J. Electroanal. Chem.*, **1983**, 149, 101.

46. Bard, A.J.; Ledwith, A., Shine, H.J., *Adv. Phys. Org. Chem.*, **1976**, 12, 155.

47. Hammerich, O.; Parker, V.D., *Adv. Phys. Org. Chem.*, **1984**, 20, 55.

48. Inoue, T.; Yamase, T., *Bull. Chem. Soc, Jpn.*, **1983**, 56, 985.

49. Kossmehl, G.; Chatzitheodorou, G., *Makromol. Chem. Rapid. Commun.*, **1982**, 2, 551.

50. Kossmehl, G.; Chatzitheodorou, G., *Mol. Cryst. Liq. Cryst.*, **1982**, 83, 291.

51. Asavapiriyamont, S.; Chandler, G.K.; Gunawardenu, G.A.; Pletcher, D.J., *J. Electroanal. Chem.*, **1984**, 177, 229.

52. Wei, Y.; Chan, C-C.; Tian, J.; Jang, G-W.; Hsueh, K.F., *Chem. Mater.*, **1991**, 3, 888.

53. Wei, Y.; Tian, J.; Yang, D., *Makromol. Chem., Rapid Commun.*, **1991**, 12, 617.

54. Proceedings of International Conference on Science and Technology of Synthetic Metals, Santa Fe, USA, June 1988, *Synth. Metals*, **1989**, 27-29,

55. Eigen, M.; Kruse, W.; Mass, G.; De Maeyer, L., in Porter, C. (ed.) "*Progress in reaction kinetics*", Pergamon, Oxford, **1964**, vol. 2, p. 284.

56. Debye, P., *Trans. Electrochem. Soc.*, **1942**, 82, 265.

57. Heinze, J.; Hinkelmann, K.; Dietrich, M.; Mortenson, J., *Ber. Bunsenges. Phys. Chem.*, **1985**, 89, 1225.

58. Street, G.; Lindsey, S.E.; Nazzal, A.I.; Wynne, K.J., *Mol. Cryst. Liq. Cryst.*, **1985**, 118, 137.

59. Downard, A.J.; Pletcher, D.J., *J. Electroanal. Chem.*, **1986**, 206, 139.

60. Downard, A.J.; Pletcher, D.J., *J. Electroanal. Chem.*, **1986**, 206, 146.

61. Osa, T.; Yildiz, A.; Kuwana, T., *J. Am. Chem. Soc.*, **1969**, 81, 26.

62. Dietrich, M.; Mortenson, J.; Heinze, J., *J. Chem. Soc. Chem. Commun.*, **1986**, 1131.

63. Wernet, W.; Monkenbusch, M.; Wegner, G., *Makromol. Chem. Rapid. Commun.*, **1984**, 5, 1574.

64. Wernet, W.; Monkenbusch, M.; Wegner, G., *Mol. Cryst. Liq. Cryst.*, **1985**, 118, 193.

65. Tabakubo, M., *Synth. Metals.*, **1987**, 18, 53.

66. Warren, L.F.; Andersen, D.P., *J. Electrochem. Soc.*, **1987**, 134, 101.

67. Waltman, R.J.; Bargon, J., *Tetrahedron.*, **1984**, 40, 3963.

68. Lacroix, J.C.; Diaz, A.F., *J. Electrochem. Soc.*, **1988**, 135, 1457.

69. Roncali,J.; Garnier, F.; Lemaire, M.; Garreau, R, *Synth. Metals.*, **1986**, 15, 323.

70. Salmon, M.; Carbajal, M.E.; Juarez, J.C.; Diaz, A.F.; Rock, M.C., *J. Electrochem. Soc.*, **1984**, 131, 1802.

71. Diaz, A.F.; Castillo, J.I.; Kanazawa, K.K.; Logan, J.A.; Salmon, M.; Fajardo, O., *J. Electroanal. Chem.*, **1982**, 133, 233.

72. Audebert, P.; Bidan, G., *Mol. Cryst. Liq. Cryst.*, **1985**, 118, 187.

73. Diaz, A.F.; Martinez, A.; Kanazawa, K.K.; Salmon, M., *J. Electroanal. Chem.*, **1980**, 130, 181.

74. Skotheim, T.A., *Handbook of Conducting Polymers*, Vol.1, Marcel Dekker, New York, **1986**, Chapters 3.

75. Waltman, R.J.; Diaz, A.F.; Bargon, J., *J. Phys. Chem..*, **1984**, 88, 4343.

76. Waltman, R.J.; Bargon, J., *Can. J. Chem.*, **1984**, 64, 76.

77. Asavapiriyamont, S.; Chandler, G.K.; Gunawardenu, G.A.; Pletcher, D.J., *J. Electroanal. Chem.*, **1984**, 177, 245.

78. Pickup, P.; Osteryoung, R.A., *J. Am. Chem. Soc.*, **1984**, 106, 2294.

79. Hillman, A.R.; Mallen, E.F., *J. Electroanal. Chem.*, **1987**, 220, 351.

80. Thyssen, A.; Borgerding, A.; Schultze, J.W., *Makromol. Chem. Makromol. Symp.*, **1987**, 8, 143.

81. Bard, A.J.; Faulkner, L.R., *Electrochemical Methods*; John Wiley & Sons: New York, 1980.

82. Harrison, J.A.; Thirsk, M.R., in Bard (ed.) "*Electroanalytical chemistry*", **1971**,Marcel Dekker, Inc., New York, vol.5, p. 92.

83. Fleischmann, M.; Thirsk, M.R., in Delahay (ed.) "*Advances in electrochemistry and electrochemical engineering*", **1963**,Wiley-Interscience, New York, vol.3, p. 123.

84. Schultze, J.W.; Lohrengel, M.M.; Rob, D., *Electrochimica Acta*, **1978**, 28, 973.

85. Lang, P.; Chao, F.; Costa, M.; Garnier, F., *Polymer*, **1987**, 28, 668.

86. Christensen, P.A.; Hamnett, A., *Electrochimica Acta*, **1991**, 36, 1263.

87. John, R.; Wallace, G.G., *J. Electroanal. Chem.*, **1991**, 306, 157.

88. Chandler, G.K.; Pletcher, D.J., *Special Reports Electrochemistry*, Vol.10, Royal Society Chemistry, London, **1985**, p.117.

89. Beck, F ; Oberst, M, *J. Electroanal. Chem.*, **1990**, 285, 177.

Chapter 2

Observation of Soluble Electroactive Intermediates During the Anodic Formation of Conducting Polypyrrole Films.

2.1 Introduction.

The formation of electronically conducting polypyrrole films by anodic oxidation in acetonitrile was first reported by Diaz *et al* in 1979 [1]. A large literature has since developed exploring the effect of oxidation conditions such as solvent, electrolyte, additives, functional substituents, and electrode potential on the properties of the polymer [2-12]. The application of these thin conducting films has also been subject to considerable research [12-16]. However, the understanding of the mechanism of polymerization has developed slowly [7,9-12,17-29].

The initial stages of the electropolymerization process is given in Scheme 2.1 below. The first step involves formation of the radical cation (**2**) via oxidation at the electrode surface. Subsequent dimerization via radical-radical coupling then follows forming the doubly charged dihydrodimer (**6**). An alternate pathway involves radical-monomer coupling forming the single charged species (**5**) which must be further oxidized to form species (**6**). Aromatization of the dihydrodimer (**6**) then follows with the formation of bipyrrole (**7**) and the release of two protons in the process. Although there has been considerable controversy regarding the pathway by which oligomer formation occurs, it appears that radical-radical coupling has gained favour in the literature. Chain propagation, shown in bottom of Scheme 2.1 (**8**)-(**11**), then proceeds via oxidation of the oligomeric intermediates which then follow the same reaction scheme.

A version of this chapter has been published. D.E Raymond and D. Jed Harrison, 1990. Journal of Electroanal. Chem., **296**, 269-273.

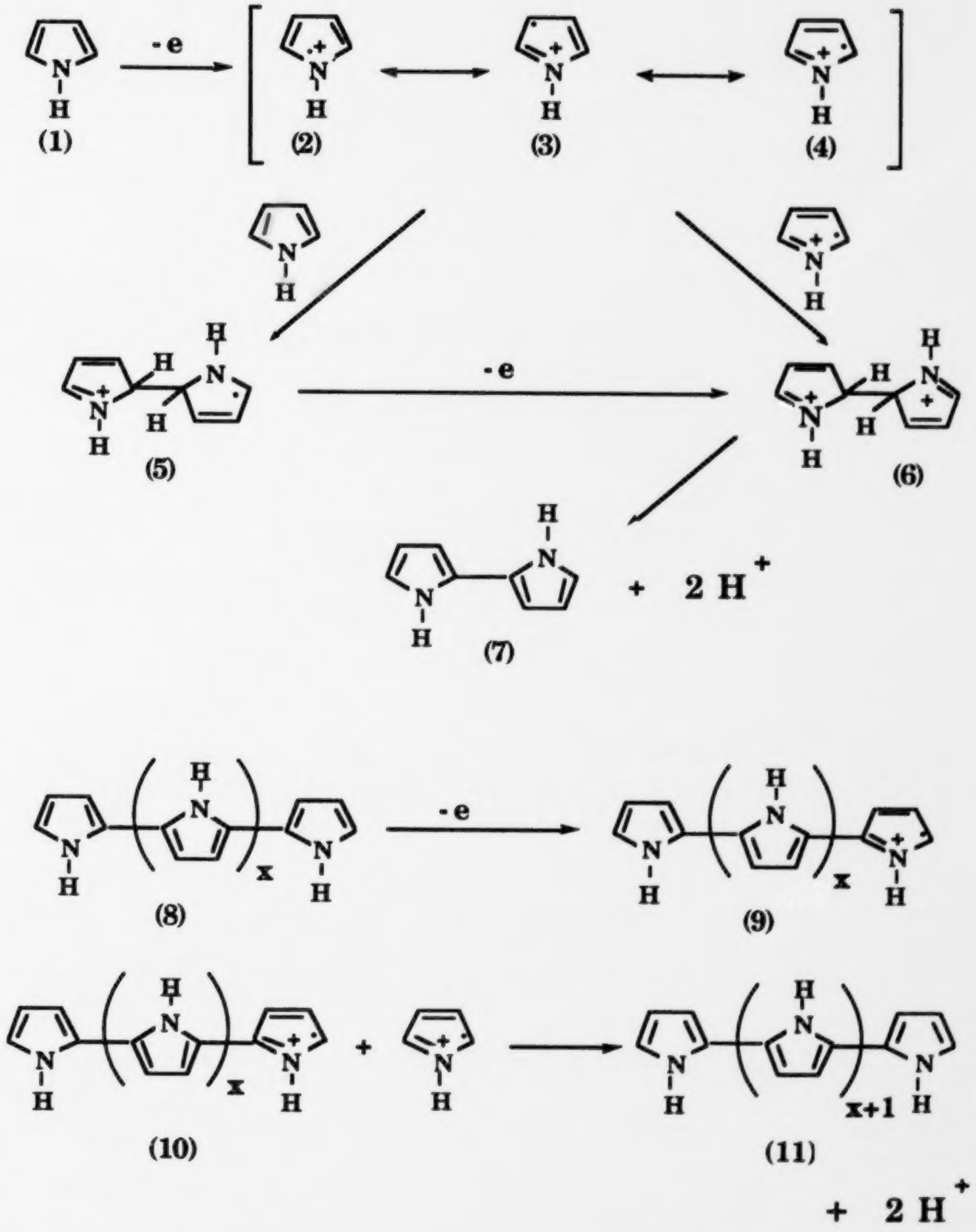
- e
H
(1)
(2)
(3)
(4)
(5)
(6)
(7)
+ 2 H+
(8)
(9)
(10)
(11)
x
x+1

Scheme 2.1 Electropolymerization mechanism

Several authors have concluded that polymer deposition occurs via a three-dimensional nucleation and growth process which involves soluble intermediates [10-13,20,21]. The direct observation or identification of these soluble intermediates has not been reported. Conversely, polymer growth has been said to occur heterogeneously, with growth occurring from the electrode surface outward. [30].

The common single-electrode electrochemical techniques used to analyze intermediates, such as cyclic voltammetry and double potential step chronoamperometry, are not well suited for cases where the product forms an electroactive film on the electrode surface. This limitation is a result of the polymer film being an insulator when in the reduced form. Consequently, in the potential range in which the electrode is covered with an insulating film, soluble intermediates and products cannot be detected electrochemically. Also, the large currents associated with the redox processes of the film can mask other electrochemical processes involving species in the double layer. The use of a dual electrode system, such as the rotating ring-disk electrode (RRDE), can avoid these difficulties by generating polymer film from the monomer at the disk electrode and using the ring electrode to detect soluble products produced. In this way the RRDE overcomes the interferences due to deposition and film redox characteristics.

The rotating ring-disk electrode has been used to evaluate azulene and pyrrole polymerization with only a reduction process at the ring electrode being reported [30,31]. This reduction process was attributed to the protons released during polymerization. In this study a RRDE with a carbon disk and a platinum ring was used to examine the oxidation of pyrrole in dry acetonitrile containing 0.1 *M* $NaClO_4$. An anodic current was observed at the ring during oxidation of pyrrole at the disk which exhibits an extremely low collection efficiency. This ring oxidation current will be shown to be due to oxidation of the dimeric species, bipyrrole. This is the first direct observation of a soluble intermediate formed during electropolymerization of pyrrole that involves a pyrrole moiety.

2.2 Experimental.

2.2.1 Chemicals. HPLC grade CH_3CN (Burdick and Jackson) was distilled over CaH_2. $NaClO_4$ (Fisher Scientific) was vacuum dried at 110 °C and used without further purification. Pyrrole (Aldrich) was vacuum distilled and stored under argon. All solutions were filtered, under argon, through activated alumina (Woelm N-Super I, ICN Nutritional

Biochemicals, Cleveland, Ohio, vacuum dried 250 °C) into the electrochemical cell (under Ar) immediately before use.

2.2.2 Instrumentation. The RRDE (Pine Instruments, Grove City, Pennsylvania) dimensions were r_1=0.2286 (cm), r_2=0.2464 (cm), and r_3=0.2692 (cm), where r_1 is the carbon disk radius, and r_2 and r_3 are the inner and outer platinum ring radii respectively. The RRDE collection efficiency was found to be 0.216 via analysis of ferrocene in 0.1 *M* tetrabutylammonium perchlorate in CH_3CN, which was in agreement with the calculated value of 0.22 [32]. A Pine RDE-4 bipotentiostat was used to control the potentials and sweep the ring, while a PAR 175 programmer was used as a second sweep source for the disk electrode channel. The RRDE was rotated using a Pine MSR rotator, with the speed control periodically calibrated using a Cole-Parmer Model 8211 Phototachometer (Cole-Parmer Instruments Co., Chicago, IL). A Kipp and Zonnen BD91 was used as an x, y, y' recorder. Potentials were measured relative to a saturated sodium chloride calomel electrode (SSCE) isolated with a double junction containing 0.1 *M* $NaClO_4$ in CH_3CN, and CaH_2 powder to consume H_2O derived from the SSCE. A Ag electrode in 0.010 *M* $AgNO_3$ + 0.1 *M* $NaClO_4$ was also used with identical results. A platinum gauze counter-electrode was isolated from the solution using a fine glass frit. The electrochemical cell was a modified Princeton Applied Research (PAR) polarographic electrochemical cell in which the central hole of the cell top was enlarged to accommodate the RRDE.

2.3 Procedures.

2.3.1 RRDE Analysis of Pyrrole.

The general procedure involved rotating the electrode at 3600 rpm, sweeping the disk electrode potential from 0.0 V to 1.2 V vs SSCE at 5 mV/s, while simultaneously cycling the ring electrode potential from 0.30 to 0.70 V vs SSCE at 100 mV/s. Thus, one complete ring cycle was obtained for every ~40 mV swept at the disk. At one point two separate Pine RDE-4 potentiostats were used, with separate reference and counter electrodes, one for the ring and one for the disk, with identical results being obtained. This was done to ensure the low ring currents observed were not a result of cross-talk between the two potentiostat channels of a single RDE-4.

2.3.2 Bipyrrole Electrochemistry.

Cyclic voltammetry and rotating disk (RDE) analysis of a bipyrrole solution in acetonitrile with 0.1 *M* $NaClO_4$ was accomplished at both a platinum disk and the carbon disk of the RRDE described above. The platinum disk had a radius of 0.28 cm. The cyclic voltammetric studies involved sweeping the electrode potential from 0.0 V to 1.2 V at a scan rate of 10 mV/s and 100 mV/s. The observed anodic peak potentials were then used for comparison to literature values. The procedure used in the RDE analysis involved sweeping the disk potential from 0.0 V to 0.75 V at a scan rate of 100 mV/s with the electrode rotated at 3600 rpm.

2.4 Synthesis of Bipyrrole.

The synthetic route was based on the methods of Itahara *et al* [33,34], however modifications were required as discussed below. The synthesis of bipyrrole was a three step route which involved protection of the pyrrole amine group, coupling of the protected monomer and then hydrolysis of the protecting group. The latter step was the most difficult and severely limited the product yield.

2.4.1 Protection of pyrrole amine group with 2,6-dichlorobenzoyl chloride.

This step was straight forward and no complications were encountered. When Itahara *et al.* synthesized bipyrrole they used benzoyl chloride as the protecting group and not the chloro-derivative [33]. However in another unrelated publication the chloro-derivative was used to protect pyrrole [34]. The use of the chloro-derivative became necessary since intra-molecular coupling was encountered during step 2. Protection of pyrrole with benzoyl chloride was accomplished as described below, with similar yields obtained.

To avoid possible coupling at the pyrrole nitrogen it was necessary to protect the pyrrole amine group with 2,6-dichlorobenzoyl chloride. The reaction scheme for this step is shown in Scheme 2.2. To a stirred solution of N,N-dimethylformamide (100 mL) containing 3.5 mL of pyrrole (vacuum distilled) (**1**) under argon, 2.018 g of sodium hydride was added slowly and the pyrrole salt (**2**) was obtained. The solution was then placed in an ice bath and cooled to ~ 0 °C, after which 6.77 mL of 2,6-dichlorobenzoyl chloride (**3**) was added dropwise and the mixture stirred at room temperature for 16 hours under argon. The mixture was then poured into an excess of ice cooled distilled water and the resulting white crystals were recrystallized from ether-hexane with a 75% yield.

Before addition to water the product mixture was analyzed using thin layer chromatography, TLC, (80/20 $CHCl_3$/hexane). The TLC plates were viewed under a UV lamp and indicated complete conversion occurred with only one product formed. The product was identified as 1-(2,6-dichlorobenzoyl)pyrrole (**4**) based on the proton NMR, mass spectral analysis, and the melting point .

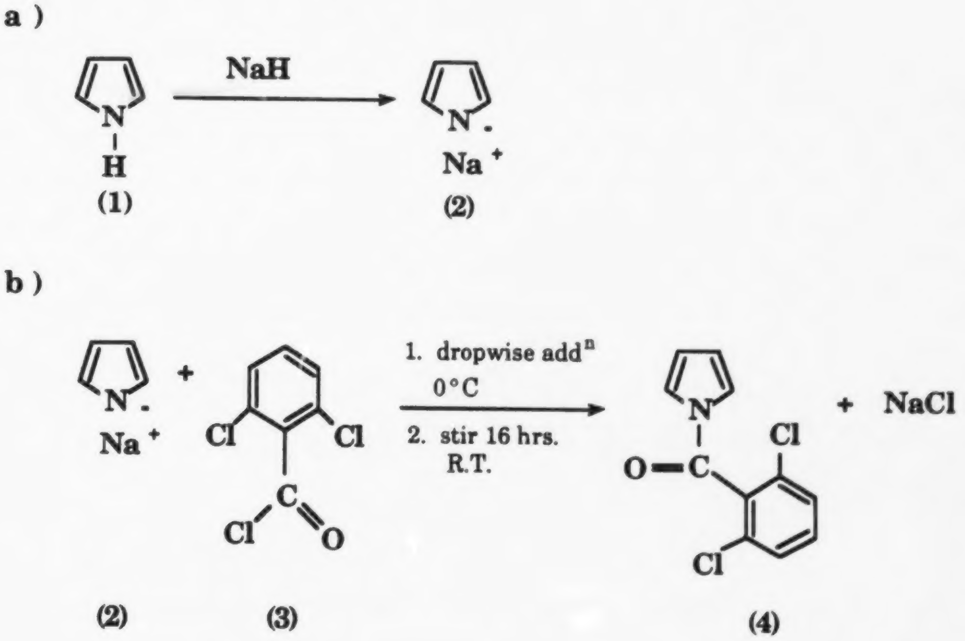

Scheme 2.2 Bipyrrole Synthesis: Protection of pyrrole amine group.

The experimental melting point was 122-123 °C, while the literature melting point [34] for 1-(2,6-dichlorobenzoyl)pyrrole is 121.5-122.5 °C. In Figure 2.1 the proton NMR of 1-(2,6-dichlorobenzoyl)pyrrole in $CDCl_3$ is shown, with the chemical shifts relative to TMS summarized in Table 2.1. The electron impact mass spectrum for 1-(2,6-dichlorobenzoyl)pyrrole is shown in Figure 2.2, with the mass/charge ratio and the likely fragmentation species tabulated in Table 2.2.

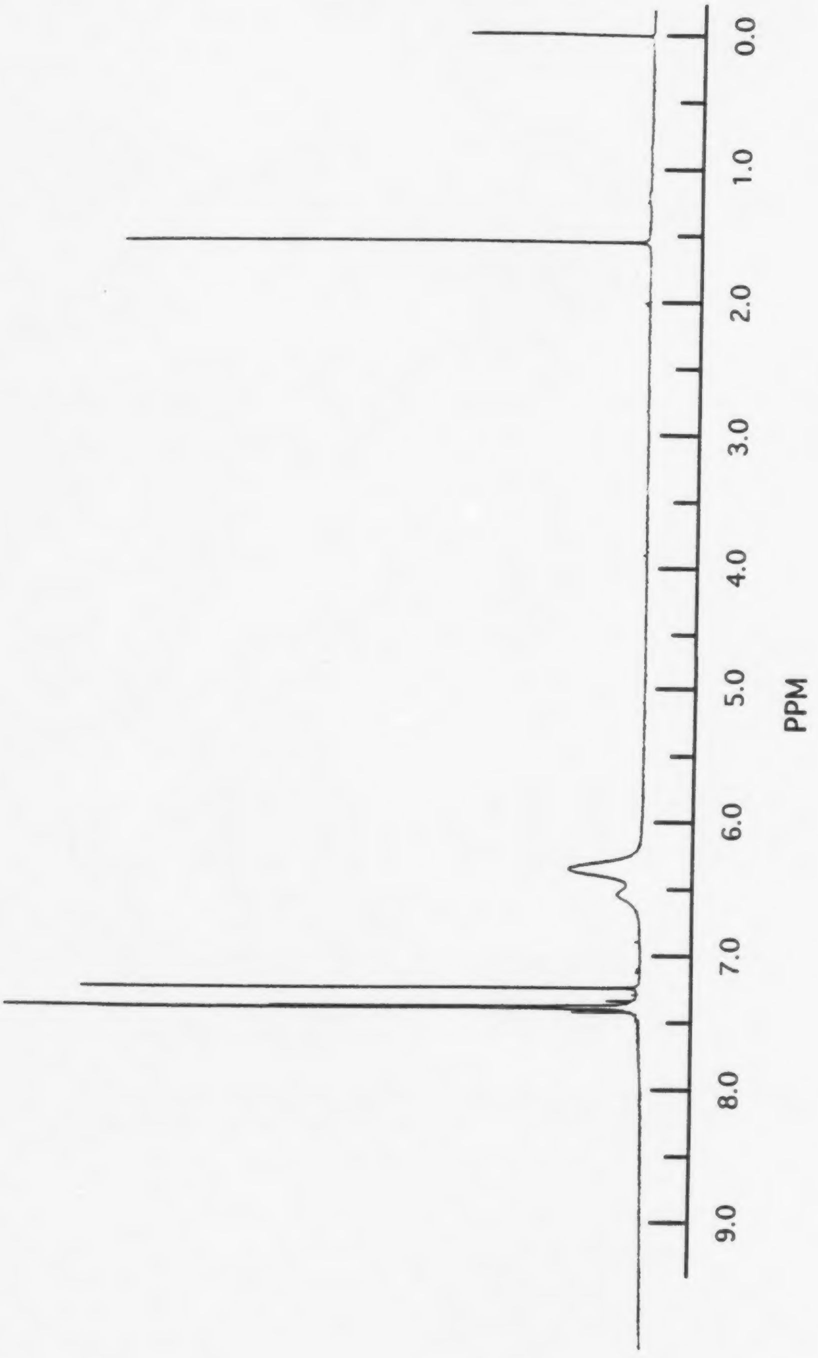

Figure 2.1 Proton NMR of 1-(2,6-dichlorobenzoyl)pyrrole in $CDCl_3$.

	Literature (ref. 34) 60 MHz	Experimental 300 MHz	Proton Type.
Chemical Shift, ppm Relative to TMS	-----	1.55 (singlet)	Solvent Impurity
	6.29	6.35 (broad)	Pyrrole: C-H 3-position
	6.4	6.55 (broad)	Pyrrole: C-H 2-position
	-----	7.25 (singlet)	Solvent $CHCl_3$
	-----	7.45 (multiplet)	Aromatic C-H

Table 2.1 Comparison of the experimental proton NMR ($CDCl_3$) results of 1-(2,6-dichlorobenzoyl)pyrrole to the literature values.

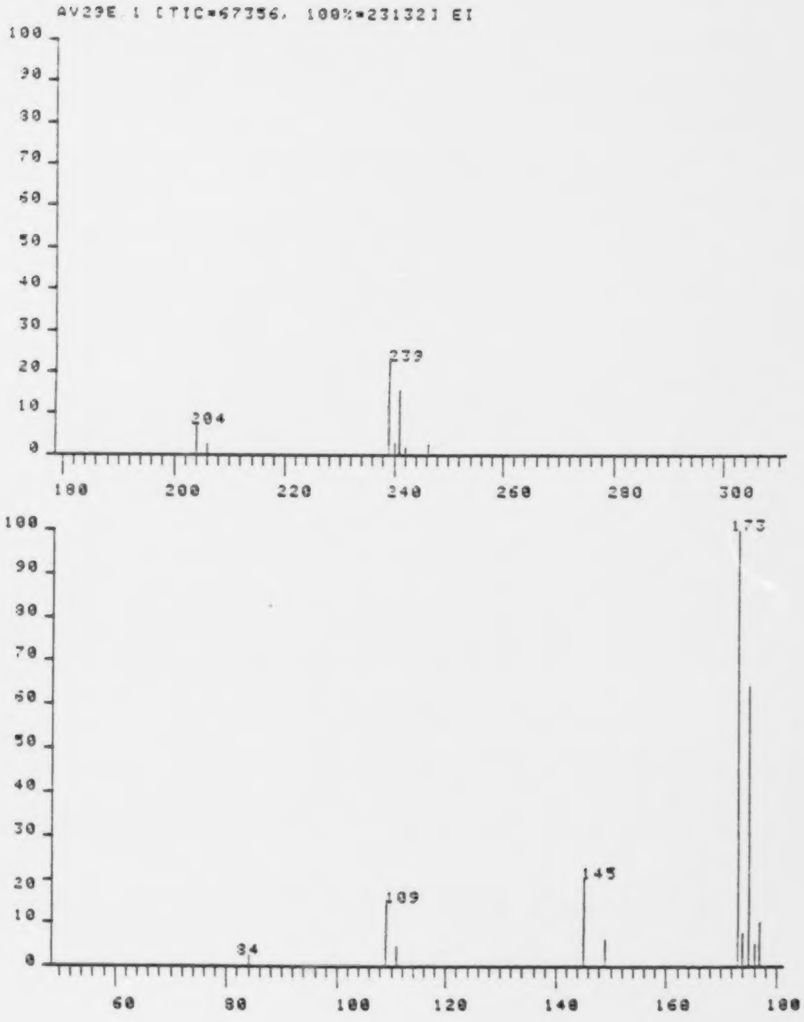

Figure 2.2 Electron impact mass spectrum of 1-(2,6-dichlorobenzoyl)pyrrole.

Mass Value	Empirical Formula
109	C_6H_2Cl
145	$C_6H_3Cl_2$
173 (chlorine isotope pattern)	$C_7H_3OCl_2$: most intense
204	$C_{11}H_7NOCl$
239 (chlorine isotope pattern)	$C_{11}H_7NOCl_2$

Table 2.2 Mass spectral results for 1-(2,6-dichlorobenzoyl)pyrrole

2.4.2 Coupling of 1-(2,6-dichlorobenzoyl)pyrrole using $Pd(OAc)_2$.

Coupling of 1-(2,6-dichlorobenzoyl)pyrrole was not performed by Itahara. The general procedure was followed [34] with modifications to the separation and purification steps. The reaction scheme for this step is shown in Scheme 2.3 below.

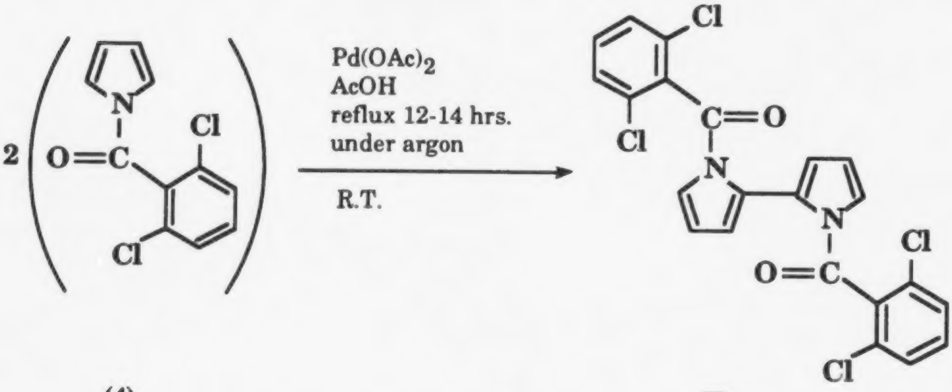

(4) **(5)**

Scheme 2.3 Bipyrrole Synthesis: Coupling of 1-(2,6-dichlorobenzoyl)pyrrole.

An acetic acid (50 mL) solution containing 2.5 g of 1-(2,6-dichlorobenzoyl)pyrrole (**4**) and 1.1688 g of palladium acetate was refluxed under argon for 12-14 hours. The solvent was then removed and the brown residue taken up in chloroform and filtered. Since Pd(0) was generated in this reaction, as observed from the formation of a mirror on the reaction vessel surface, filtration was required to remove possible particulates. TLC analysis (80/20 $CHCl_3$/hexane) of the chloroform solution indicated that starting material and four products were present. The TLC spot with the shortest retention time was found to be the starting material.

The mixture was then separated chromatographically on silica gel (Silica gel 60 Brinkmann Instruments Ltd.) using 80/20 $CHCl_3$/hexane at a flow rate of ~ 0.5 mL/min. The ^1H NMR and electron impact mass spectra identified the second band as protected bipyrrole (**5**) (coupled 1-(2,6-dichlorobenzoyl)pyrrole). The other bands were not identified. The separation step proved to be extremely difficult due to the poor separation encountered with the recommended solvent system [34]. TLC was used to find an appropriate solvent system, and even with this optimized solvent system (80/20 $CHCl_3$/hexane) the flow rate required for adequate separation required anywhere from 7-10 hours. Due to the low yield encountered this reaction was repeated six times in order to accumulate enough protected bipyrrole to carry on to step three.

The work by Itahara involved using benzoyl chloride as the amine protecting group. However, attempts to use this resulted in a significant mixture of products when coupling was carried out. Therefore the chloro-derivative was used as the protecting group to avoid any ring closure as shown in Scheme 2.4.

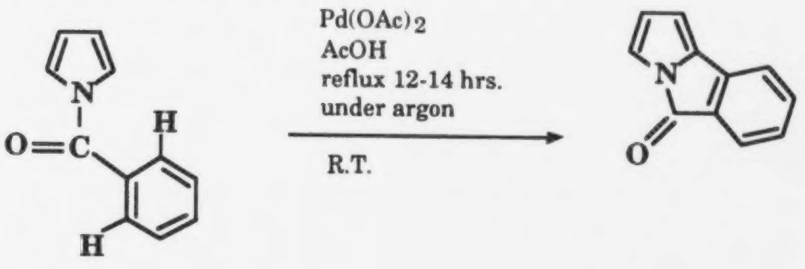

(6) **(7)**

Scheme 2.4 Bipyrrole Synthesis: Intramolecular Coupling of 1-benzoylpyrrole.

The experimental melting point obtained was 196-197 °C, while the literature melting point for coupled 1-(2,6-dichlorobenzoyl)pyrrole was not available. In Figure 2.3 the proton NMR of coupled 1-(2,6-dichlorobenzoyl)pyrrole in $CDCl_3$ is shown, with the chemical shifts relative to TMS summarized in Table 2.3. The electron impact mass spectrum for coupled 1-(2,6-dichlorobenzoyl)pyrrole is shown in Figure 2.4, with the mass/charge ratio and the likely fragmentation species tabulated in Table 2.4.

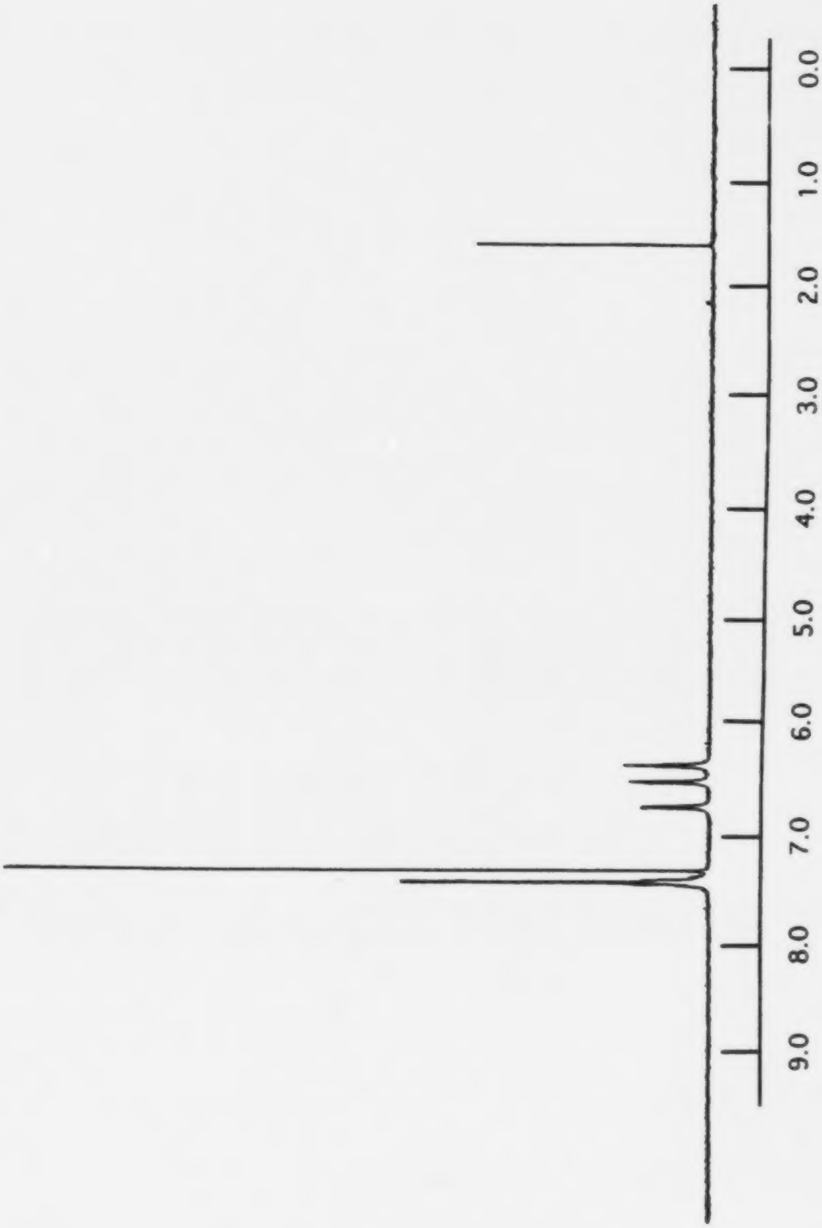

Figure 2.3 Proton NMR of coupled 1-(2,6-dichlorobenzoyl)pyrrole in $CDCl_3$.

	Literature Not Available	Experimental 300 MHz	Proton Type.
Chemical Shift, ppm Relative to TMS	-----	1.65 (singlet)	Solvent Impurity
		6.35 (triplet)	Pyrrole: C-H 4-position
		6.55 (triplet)	Pyrrole: C-H 3-position
		6.80 (triplet)	Pyrrole: C-H 2-position
		7.35 (singlet)	Solvent $CHCl_3$
		7.45 (multiplet)	Aromatic C-H

Table 2.3 Comparison of the experimental proton NMR ($CDCl_3$) results of coupled 1-(2,6-dichlorobenzoyl)pyrrole to the literature values.

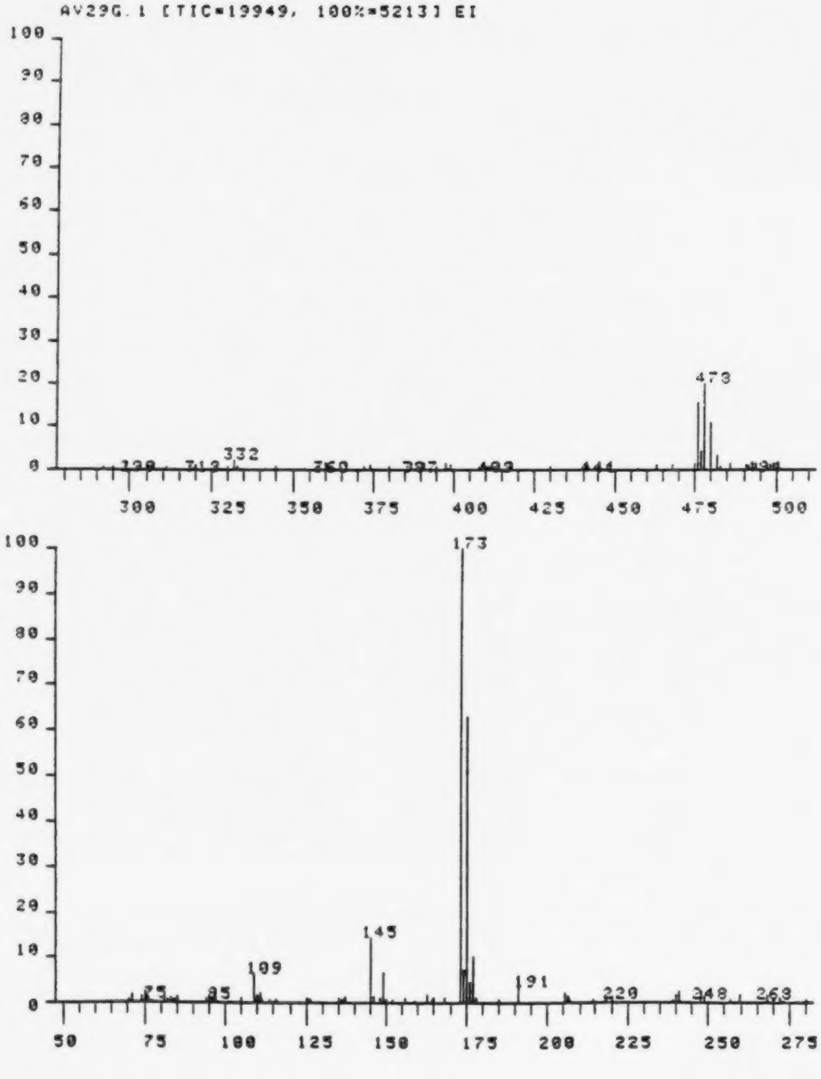

Figure 2.4 Electron impact mass spectrum of 1-(2,6-dichlorobenzoyl)pyrrole.

Mass value	Empirical Formula
109	C_6H_2Cl
145	$C_6H_3Cl_2$
173 (chlorine isotope pattern)	$C_7H_3OCl_2$: most intense
478 (chlorine isotope pattern)	$C_{22}H_{14}N_2O_2Cl_4$

Table 2.4 Mass spectral results for coupled 1-(2,6-dichlorobenzoyl)pyrrole

2.4.3 Step 3: Hydrolysis of the protecting group.

There are two possible approaches to this step, either acid hydrolysis or base hydrolysis. Both methods were attempted and the difficulties encountered will be discussed below.

a) Acid hydrolysis involved using a mixture of MeOH/H_2O/6 N HCl refluxed (60 °C) for 24 hours under argon. The system was purged with argon before addition of protected bipyrrole to avoid oxidation of any bipyrrole formed. The desired product was not isolated from the resulting complex mixture. The recommended procedure involved acid hydrolysis for 6 hours [35], however, when this was attempted no reaction was observed. When the reaction time was extended to 24 hours product formation was observed using TLC. The product mixture was separated on silica gel using 50/50 $CHCl_3$/hexane with no bipyrrole isolated. The products isolated were not identified, however, the NMR spectra obtained showed NH shifts indicating hydrolysis was successful. Presumably the complex mixture formed due to acidic polymerization of bipyrrole.

b) The use of basic conditions to hydrolyze amide functionalities was suggested in a general organic text. The reaction scheme for base hydrolysis is shown in Scheme 2.5. Base hydrolysis involved purging a solution of MeOH and 3 N NaOH with argon and adding 60 mg of protected bipyrrole (**5**). The mixture was refluxed under argon for 7 days and checked daily with TLC until no further increase in bipyrrole was seen. The mixture was then immediately extracted into benzene and a TLC of the product mixture indicated no starting material remained but five products were formed. The products were separated chromatographically on silica gel using 70/30 $CHCl_3$/hexane as eluent. The first band to elute was identified as bipyrrole (**8**) by proton NMR using $CDCl_3$ and deuterated DMSO. The other bands were not identified. The yield of this step was extremely low but sufficient quantities of bipyrrole were obtained to perform the desired electrochemical experiments.

The experimental melting point obtained for bipyrrole was 188-191 °C while the literature melting point [36,37] for bipyrrole is 189-190 °C. In Figure 2.5 the proton NMR of bipyrrole in deuterated chloroform is shown, with the chemical shifts relative to TMS summarized in Table 2.5. In Figure 2.6 the proton NMR of bipyrrole in deuterated dimethyl sulfoxide is shown, with the chemical shifts relative to TMS summarized in Table 2.6. Given in Figure 2.7 are the splitting patterns for the bipyrrole pyrrole protons in both solvents.

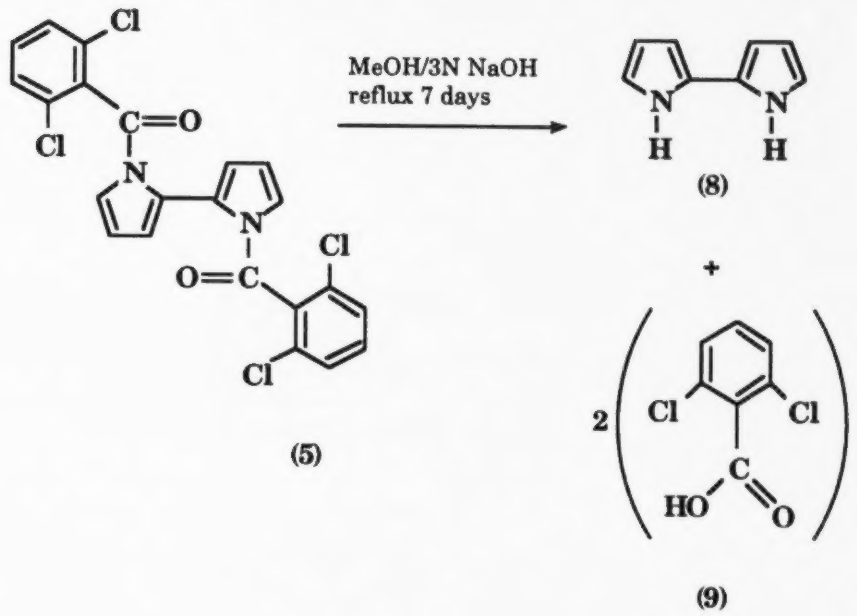
Cl
Cl
C=O
N
N
Cl
O=C
Cl
(5)
MeOH/3N NaOH
reflux 7 days
N
H
N
H
(8)
+
2
Cl
Cl
C
HO
O
(9)

Scheme 2.5 Bipyrrole Synthesis: Hydrolysis of protecting group.

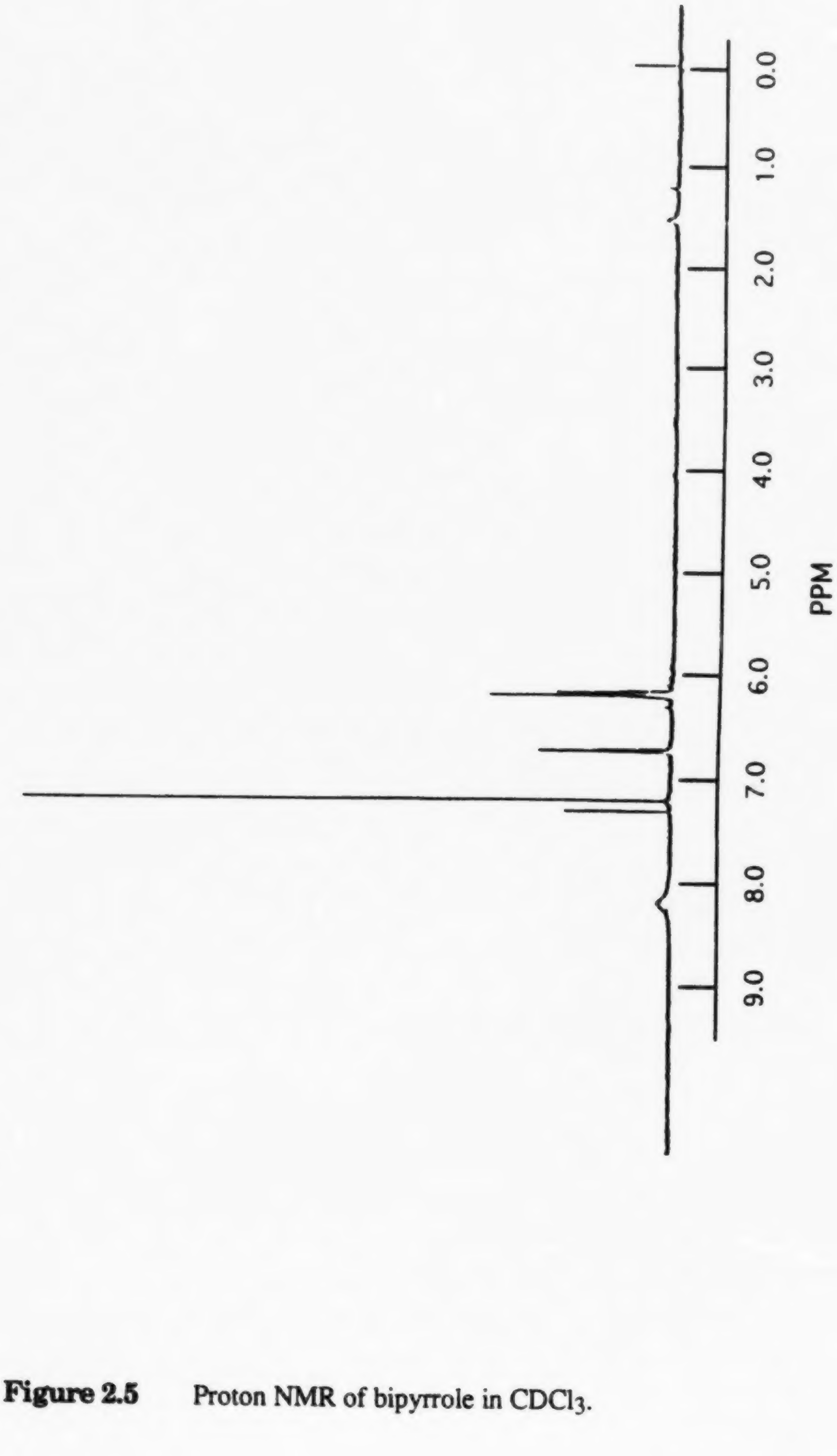

Figure 2.5 Proton NMR of bipyrrole in $CDCl_3$.

	Literature (ref. 36) 60 MHz	Experimental 300 MHz	Proton Type.
Chemical Shift, ppm Relative to TMS	-----	1.55	Solvent Impurity
	6.22	6.18 (multiplet)	Pyrrole: C-H 3-position
	6.66	6.72 (multiplet)	Pyrrole: C-H 2-position
		7.20 (singlet)	Solvent $CHCl_3$
		7.30 (singlet)	Benzene from purification.
		8.18 (broad)	N-H

Table 2.5 Comparison of the experimental proton NMR ($CDCl_3$) results of bipyrrole to the literature values.

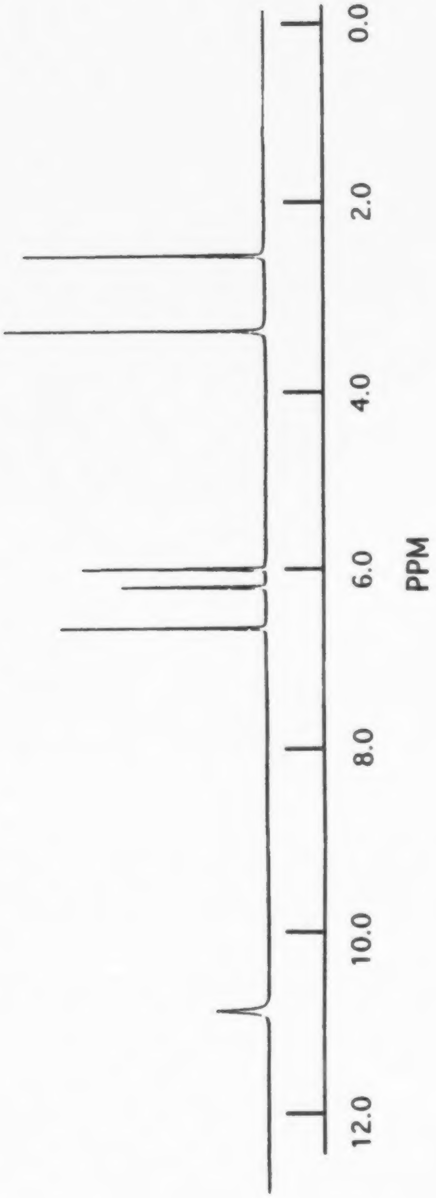

Figure 2.6 Proton NMR of bipyrrole in DMSO-d6.

	Literature (ref. 37) 60 MHz	Experimental 300 MHz	Proton Type.
Chemical Shift, ppm Relative to TMS	-----	2.50 (singlet)	Solvent
		3.30 (singlet)	H_2O in solvent
	6.05	5.99 (multiplet)	Pyrrole: C-H 4,4'-position
	6.26	6.21 (multiplet)	Pyrrole: C-H 3,3'-position
	6.71	6.65 (multiplet)	Pyrrole: C-H 5,5'-position
		10.85 (broad)	N-H

Table 2.6 Comparison of the experimental proton NMR (DMSO-d6) results of bipyrrole to the literature values.

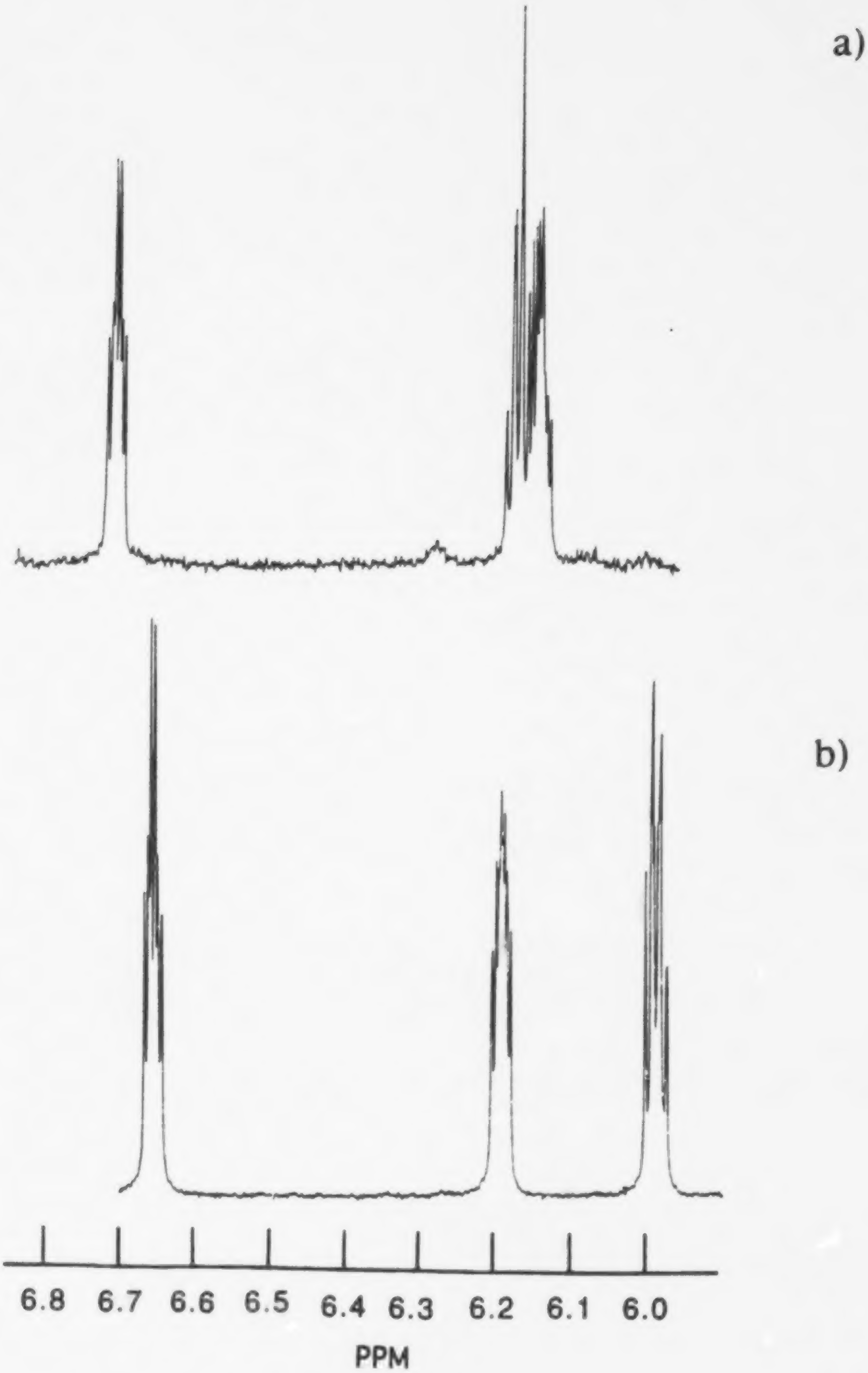

Figure 2.7 Splitting pattern from the proton NMR of bipyrrole in a) $CDCl_3$ and b) DMSO-d6.

2.5 Results and Discussion.

2.5.1 Simultaneous sweeps of the Ring and Disk Potentials.

The ring current versus ring voltage curve obtained from acetonitrile containing 50 m*M* pyrrole and 0.1 *M* $NaClO_4$ during polymerization at the disk is shown in Figure 2.8. The ring potential was cycled between 0.3 V and 0.7 V vs SSCE at 100 mV/s, while simultaneously the disk potential was scanned from 0.0 V to 1.2 V vs SSCE at 5 mV/s. The disk current as a function of disk voltage curve is shown in the inset of Figure 2.8, with pyrrole oxidation at the disk observed to begin at about 0.8 V vs SSCE. No significant current is observed at the ring until the disk potential is about 1.0 V vs SSCE, a potential at which an inflection point is observed in the disk current-voltage curve. Above this disk potential a well-defined oxidation wave develops at the ring as the ring potential is cycled. This ring oxidation wave eventually exhibits a half wave potential, $E_{1/2}$, of 0.55 ± 0.1 V vs SSCE. On the ring oxidation current plateau a collection efficiency (ratio of the ring current to the disk current) of 9×10^{-3} was obtained over a disk potential range of 1.08 to 1.2 V. This value is substantially lower than the expected collection efficiency of 0.216 obtained for a stable intermediate. Therefore, the species observed is either rapidly lost via oxidation at the disk, consumed rapidly in subsequent polymerization steps, or is formed in low yield as a result of a side reaction during the polymerization. The collection efficiency was found to increase in a non-linear fashion as the square root of the rotation rate was increased, indicating that the species observed is not the primary electro-oxidation product. This effect will be discussed in detail in Chapter 5.

Shown in Figure 2.9 are the results of a similar set of experiments in which the ring potential was cycled cathodically from 0.3 to -1.2 V vs SSCE at 500 mV/s, while the disk potential was simultaneously scanned from 0.0 to 1.2 V vs SSCE at 10 mV/s. A reduction current is observed at the ring electrode immediately upon oxidation of pyrrole at the disk. The half wave potential, $E_{1/2}$, of the ring reduction wave was -0.27 V vs SSCE for the forward scan to negative potentials. However, the $E_{1/2}$ is dependent on the sweep direction due to the hysteresis observed. An identical set of experiments was performed, but with the ring and disk potential scan rates at 100 mV/s and 5 mV/s respectively. In this situation the large ring reduction current observed had an $E_{1/2}$ of -0.08 V vs SSCE. This $E_{1/2}$ value is in agreement with the value reported by Bruckenstein and Sharkey [30] for the reduction of protons released during oxidation of azulene and pyrrole. The observed cathodic shift in $E_{1/2}$ at increasing scan rates may reflect homogeneous kinetics

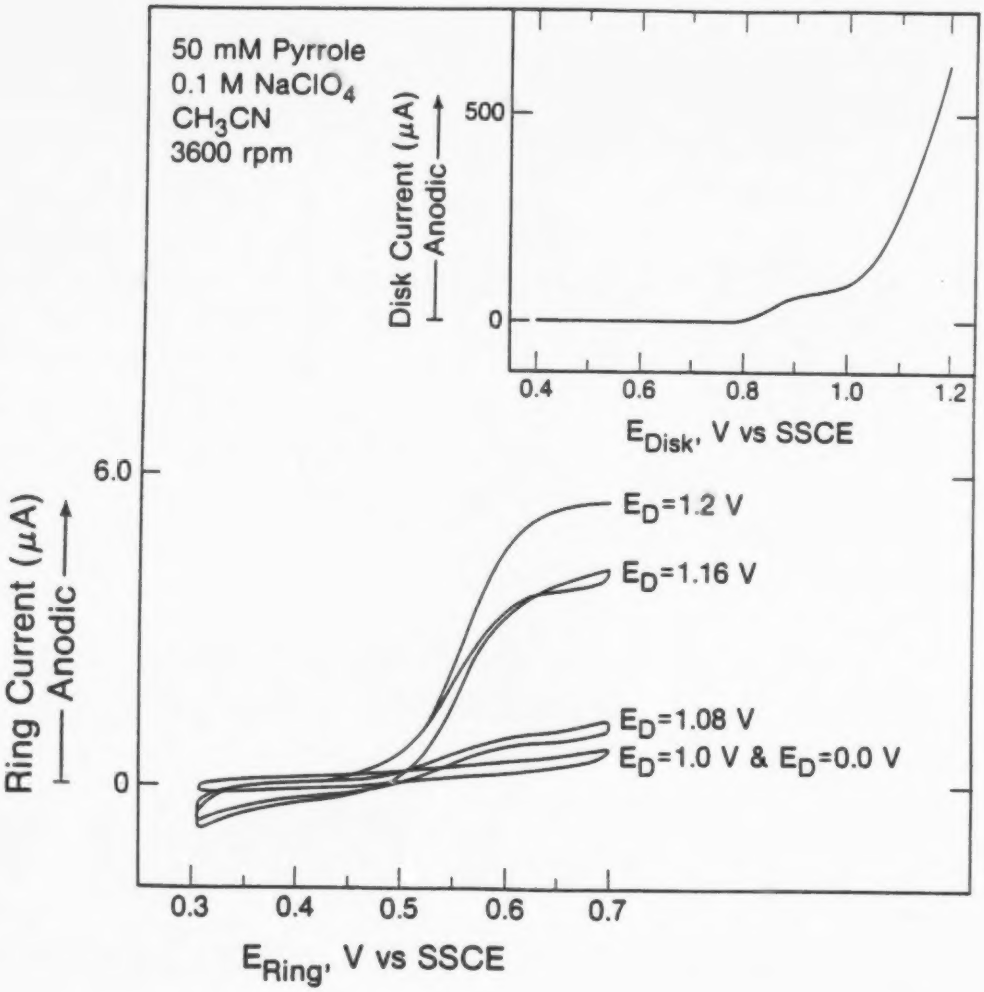

Figure 2.8 The Pt ring electrode current is shown as a function of the ring potential (100 mV/s,3600 rpm) at several values of the disk potential, E_D (± 20 mV, since the disk was also swept at 5 mV/s). The inset shows the disk electrode current for pyrrole oxidation versus disk potential (5 mV/s,3600 rpm).

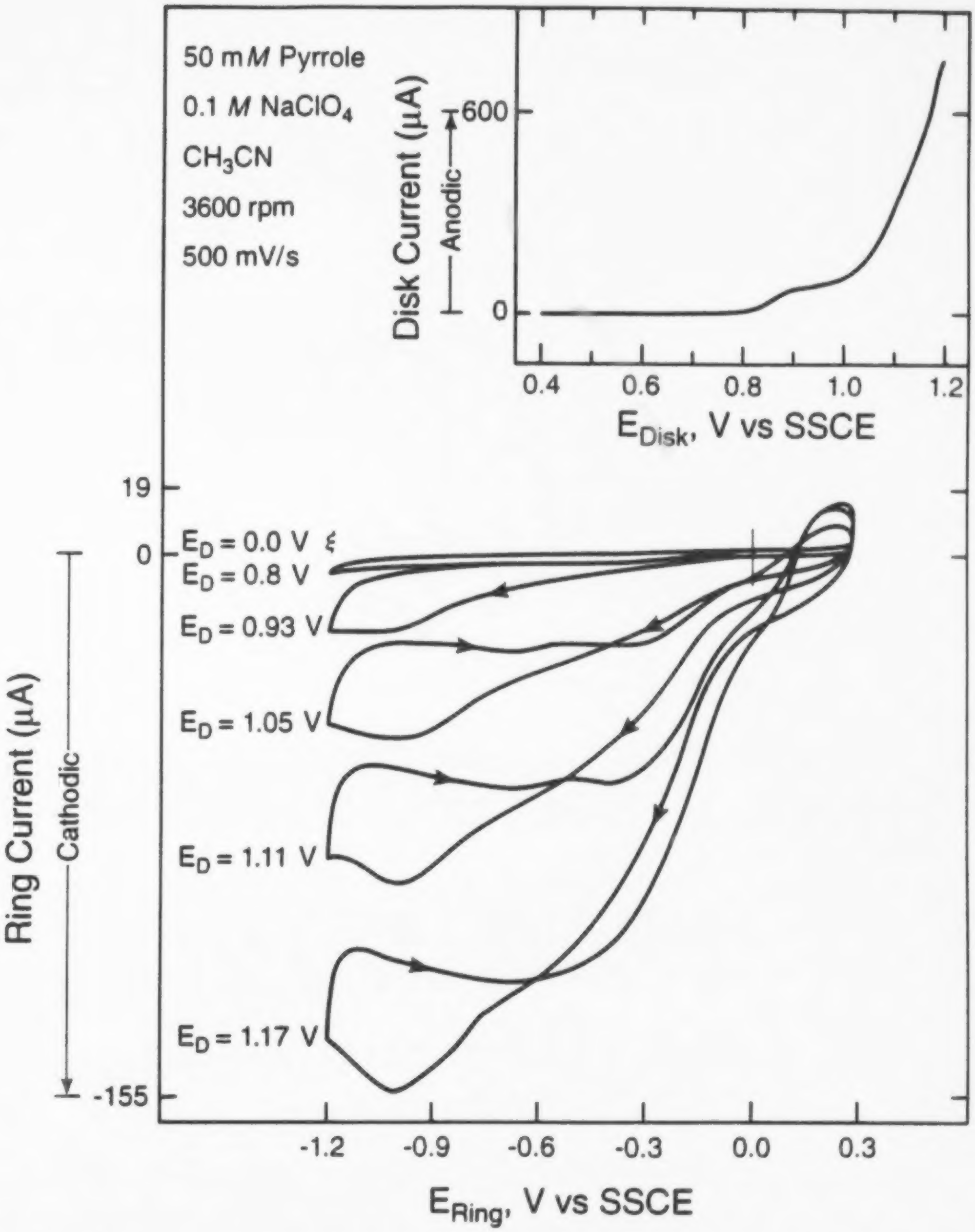

Figure 2.9 The Pt ring electrode current is shown as a function of the ring potential (500 mV/s,3600 rpm) at several values of the disk potential, E_D (± 20 mV, since the disk was also swept at 10 mV/s). The inset shows the disk electrode current for pyrrole oxidation versus disk potential (10 mV/s,3600 rpm).

involved during proton generation. On the current plateau the collection efficiency for the reduction current obtained at both scan rates was 0.216, indicating the product is stable as it should for H^+. The small reduction current near +0.5 V vs SSCE in Figure 2.8 has been determined to be due to pyrrole radical cations [38], as discussed in chapter 3.

2.5.2 Observation of Hydrogen Oxidation during Polymerization of Pyrrole.

Figure 2.10 shows a cyclic voltammogram obtained at a motionless platinum disk electrode during reduction of 10 m*M* $HClO_4$ in acetonitrile containing 0.1 *M* $NaClO_4$. The ring potential was scanned between 0.6 V and -0.6 V vs SSCE at 500 mV/s. A proton reduction peak is clearly observed at -0.14 V vs SSCE, while a hydrogen oxidation peak is seen at 0.3 V SSCE. When the electrode is rotated (not shown) the hydrogen oxidation peak is observed but the magnitude has decreased. Identical experiments with 10 m*M* $HClO_4$ in acetonitrile containing 0.1 *M* $TBABF_4$ gave the same general shape as in Figure 2.10, however, the proton reduction and hydrogen oxidation peak potentials were shifted cathodically to -1.2 V and -0.5 V vs SSCE respectively. This is not unexpected since HBF_4 is a weaker acid in acetonitrile than $HClO_4$. These results again indicate that the ring reduction process observed is due to proton reduction.

In Figure 2.9 a ring oxidation peak is observed at a ring potential of about 0.2 V vs SSCE during the polymerization of pyrrole at the disk. This current is most likely due to oxidation of hydrogen which formed during the reduction of protons at the ring, as indicated by Figure 2.10. Perchloric acid is one of the strongest acids known in acetonitrile, so that in the presence of the ClO_4^- anion there will be significant free H^+. HBF_4 is a much weaker acid, and the use of $TBABF_4$ electrolyte should significantly shift the proton equilibrium. Experiments identical to those shown in Figure 2.9 indicate a large cathodic shift from -0.27 (in 0.1 *M* $NaClO_4$) to -0.9 V (in 0.1 *M* $TBABF_4$) vs SSCE in the H^+ reduction current at the ring, consistent with identification of this as a H_2 evolution reaction. This result clearly shows a significant difference in the local pH in the electrode diffusion layer depending on the choice of electrolyte.

2.5.3 Bipyrrole Electrochemistry.

The cyclic voltammetric peak potential for bipyrrole in acetonitrile was reported to be 0.51 V vs SSCE [9]. This suggests that the ring oxidation current observed in Figure 2.8 is due to bipyrrole. Bipyrrole was synthesized according to the literature methods [33-

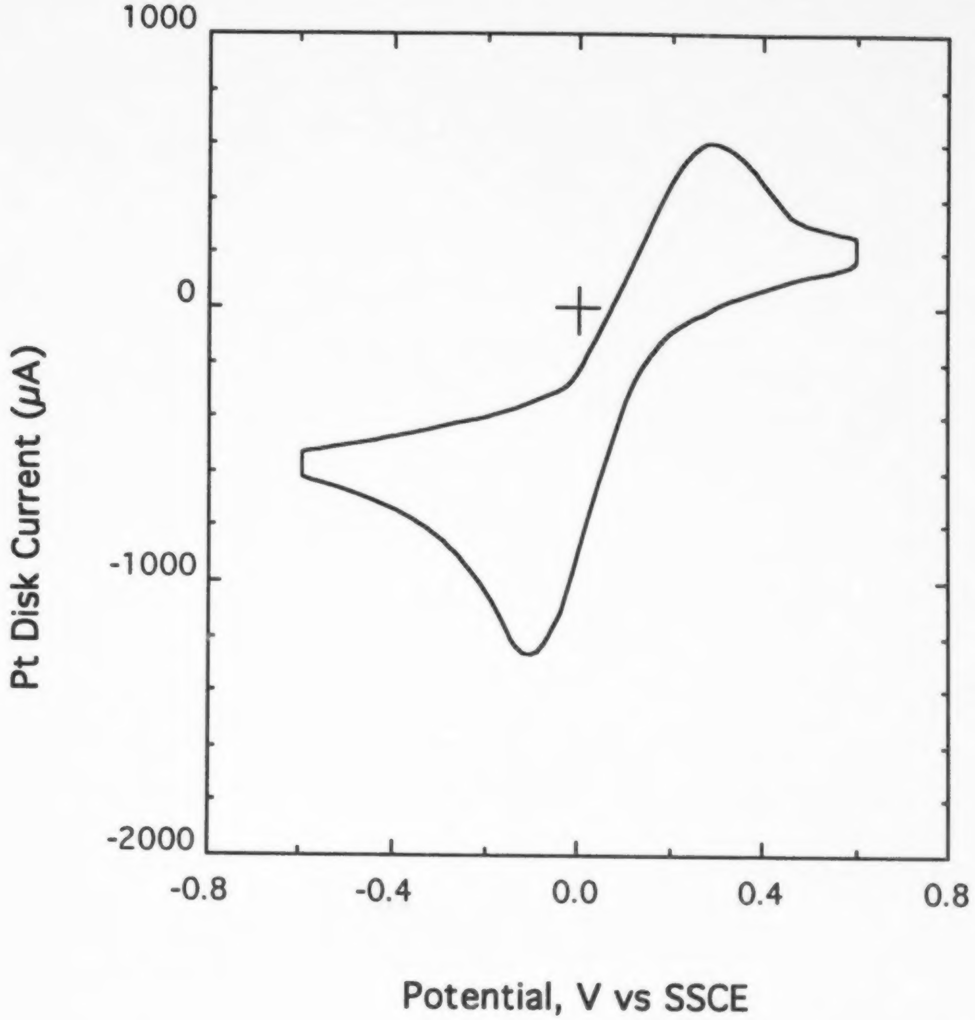

Figure 2.10 Cyclic voltammogram of 10 m*M* $HClO_4$ in CH_3CN containing 0.1 *M* $NaClO_4$. Obtained using a Pt disk electrode at a scan rate of 500 mV/s.

35] and its current-voltage curve was obtained (Figure 2.11) at a platinum disk electrode rotated at 3600 rpm and a potential scan rate of 100 mV/s. An oxidation wave was obtained with a half wave potential, $E_{1/2}$ of 0.55 V vs SSCE, identical to that observed in Figure 2.8. When the electrode was not rotated a cyclic voltammetric peak potential of 0.52. V vs SSCE was obtained. A previously unreported second oxidation step was also observed with a half wave potential, $E_{1/2}$, of 1.15 V vs SSCE as seen in Figure 2.12a. Comparison of the half wave potentials obtained from Figures 2.8 and 2.11 suggest that the species observed is bipyrrole.

Formation of conducting polypyrrole films by electro-oxidation of 2,2'-bipyrrole solutions was initially reported not to occur [9]. However, conducting polybipyrrole films have been deposited [10] and the morphology shown to be dependent on the deposition solvent. Given in Figure 2.12b are the cyclic voltammograms (CV) of polybipyrrole films deposited from acetonitrile containing 0.03 m*M* bipyrrole. After deposition the films were rinsed thoroughly and the CV's obtained in an aqueous solution containing 0.1 *M* $NaClO_4$ (blank). In the figure 1 indicates a clean electrode (Pt) surface, 2 is the CV obtained when the deposition potential was limited to the first oxidation plateau for bipyrrole, and 3 is the CV for the deposition potential at the second oxidation plateau. An identical CV as 3 was obtained when the deposition potential was maintained at the first oxidation plateau for the same length of time as that required to scan to the second oxidation plateau and back. This indicates that polymer deposition can occur at the potential of the first oxidation plateau.

Figure 2.13 compares cyclic voltammograms of both polypyrrole and polybipyrrole films obtained in a 0.1 *M* $NaClO_4$ aqueous solution. Figure 2.13a shows a CV of polypyrrole formed by oxidation in acetonitrile containing 50 m*M* pyrrole and 0.1 *M* $NaClO_4$. There is a broad wave with a peak potential, E_p, at about -0.05 V vs SSCE, and a small shoulder appears at about -0.4 V to -0.35 V. When lower pyrrole concentrations are used the main peak shifts positively, and the shoulder decreases or disappears. Figure 2.13b again shows a CV of polybipyrrole formed by oxidation in acetonitrile containing 0.03 m*M* bipyrrole and 0.1 *M* $NaClO_4$. The peak is sharper than for polypyrrole and the E_p is shifted to -0.35 V, suggesting that these are the same redox centers as observed in the shoulder of polypyrrole. It is likely that the more reactive pyrrole radical cation leads to a larger distribution of branched and other structures than does oxidized bipyrrole, leading to a larger distribution of redox potentials in the polymer. This is consistent with the decreased reactivity of oxidized bipyrrole towards nucleophilic attack as suggested by its

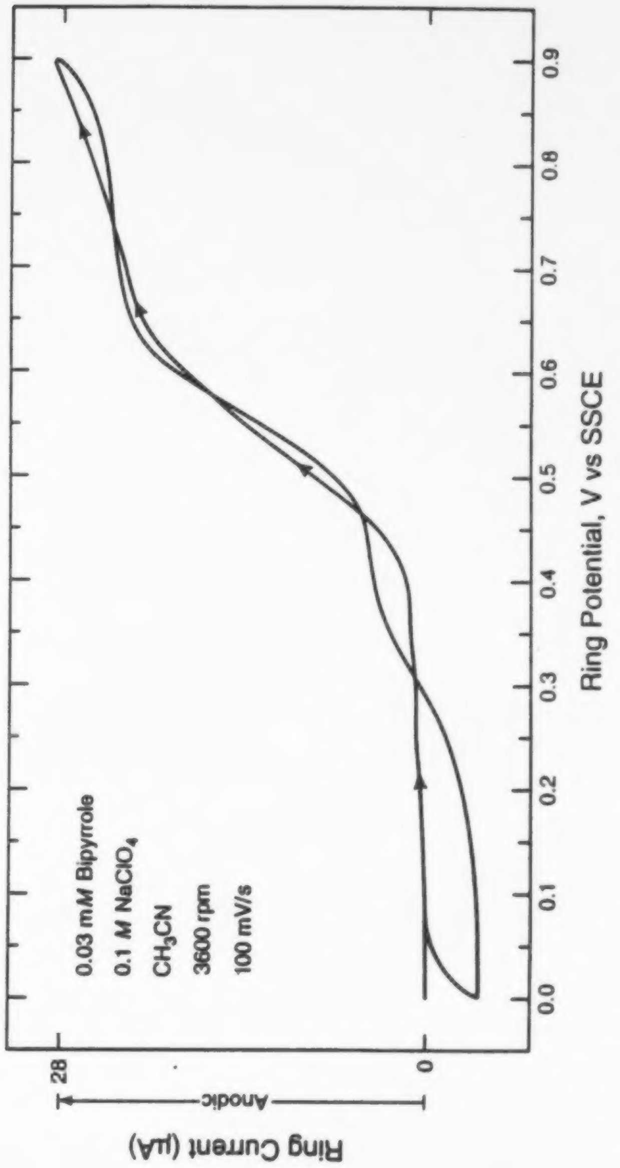

Figure 2.11 The Pt ring electrode current is shown as a function of the ring potential (100 mV/s,3600 rpm) for the first oxidation wave of 0.03 m*M* bipyrrole and 0.1 *M* $NaClO_4$ in acetonitrile.

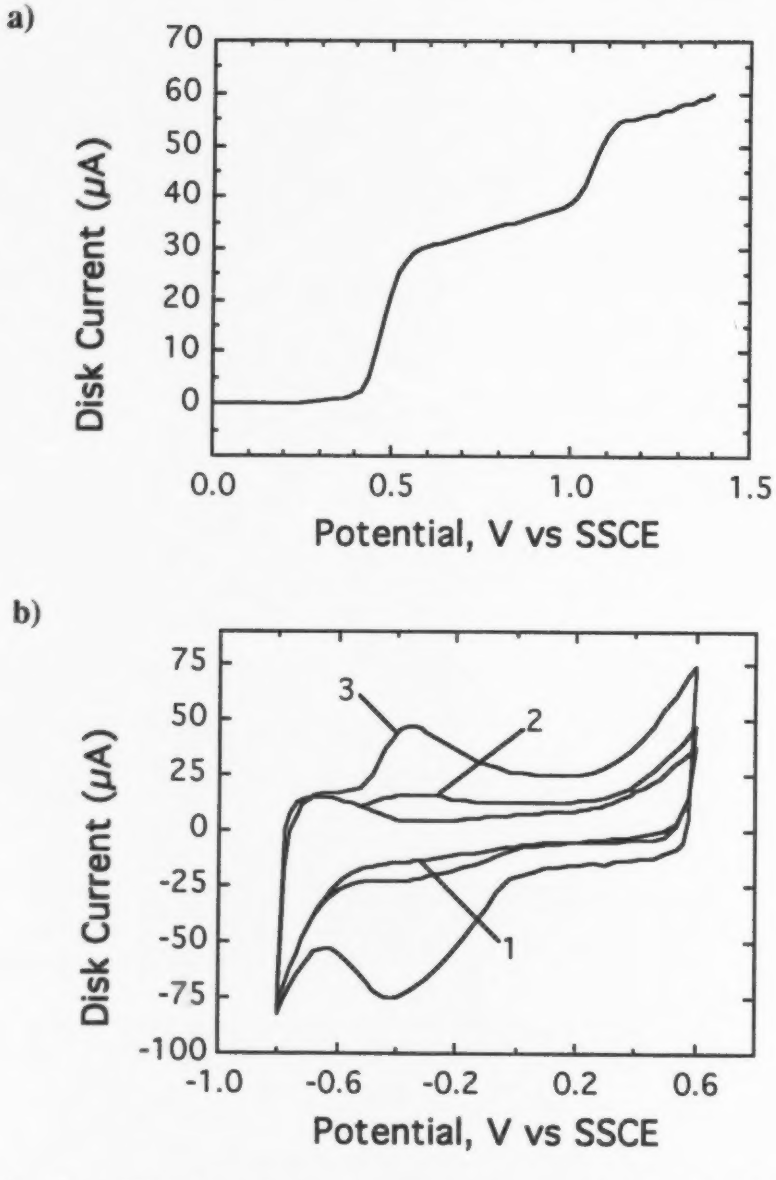

Figure 2.12 a) The Pt ring electrode current-voltage curve (10 mV/s, 4500 rpm) for the oxidation of 0.03 m*M* bipyrrole in acetonitrile containing 0.1 *M* $NaClO_4$.

b) Cyclic voltammograms of deposited polybipyrrole obtained at various deposition potentials.

1. blank.
2. first oxidation plateau: 1 deposition cycle.
3. second oxidation plateau: 1 deposition cycles.

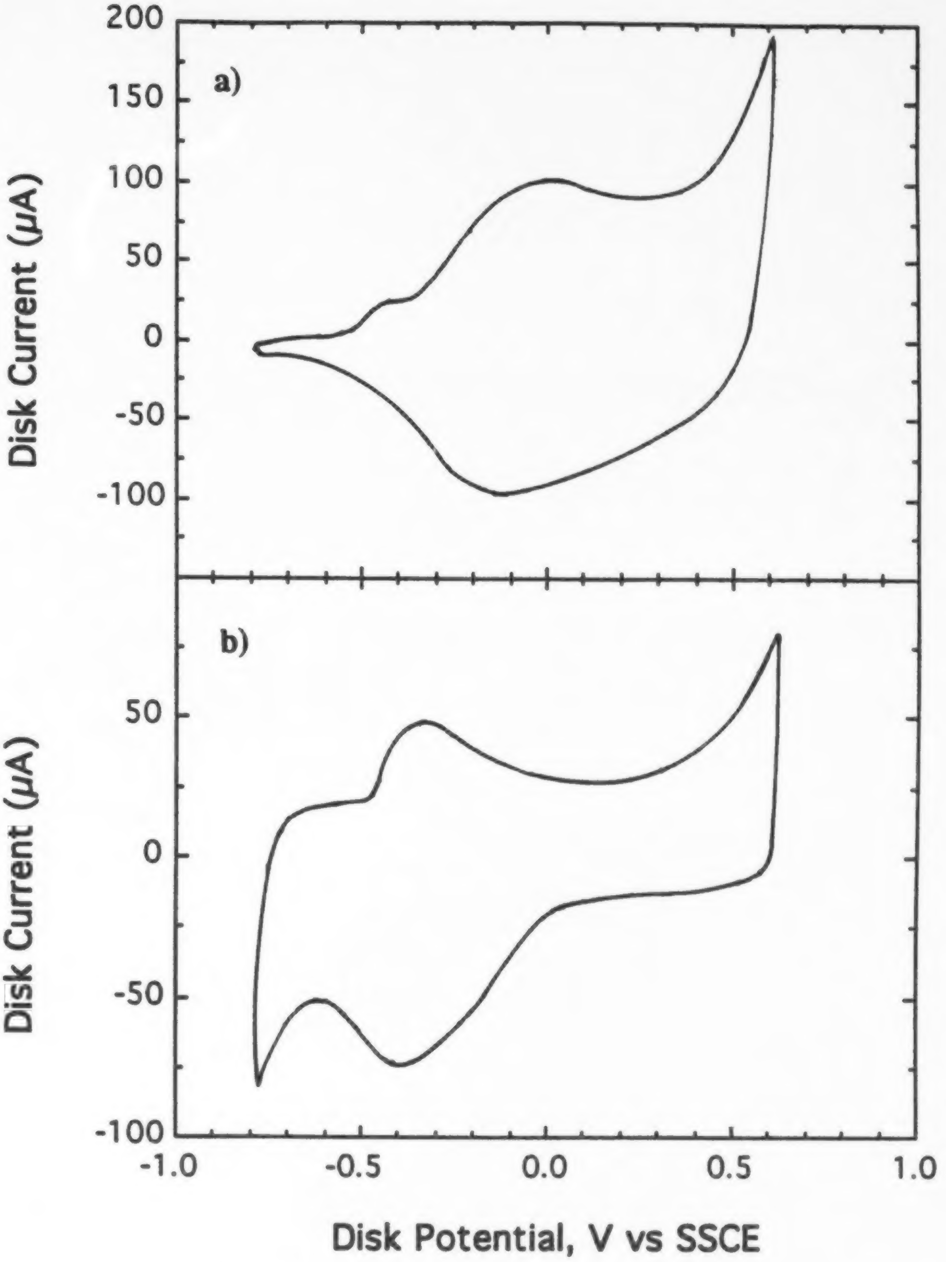

Figure 2.13 Comparison of cyclic voltammograms of (a) polypyrrole and (b) polybipyrrole obtained in aqueous 0.1 *M* $NaClO_4$ after deposition from acetonitrile solution.

pH dependence (discussed below). These effects could account for the increased conductivity of polybipyrrole compared to polypyrrole when it is initially prepared [10].

2.5.4 Effect of Added Pyridine.

Morse et al. [7] have shown that addition of pyridine or 2,6-di-t-butyl pyridine changes the profile and reduces the magnitude of pyrrole oxidation currents, but the onset potential remains unchanged. We found that addition of 100 m*M* pyridine or 100 m*M* 2,6-di-t-butyl pyridine to a 50 m*M* pyrrole solution (Figure 2.14) did not change the onset potential or the half wave potential for the oxidation of the product observed at the ring electrode. The ring current-ring voltage curves were obtained under identical conditions as for Figure 2.8. Similarly, the addition of either base to a bipyrrole solution did not change the onset potential for bipyrrole oxidation, or the half wave potential of the first wave, as seen in Figure 2.15. However, the $E_{1/2}$ of the second wave was shifted cathodically upon addition of base, changing the current-voltage curve from an apparent two, 1 e^- process process to a one, 2 e^- process. Without base added the two waves observed probably correspond to the successive formation of the radical cation and the dication. The shift in the $E_{1/2}$ of the second wave upon addition of base indicates that the second wave is pH dependent. This may reflect the deprotonation of the bipyrrole radical cation prior to further oxidation, or the subsequent deprotonation of the bipyrrole dication. The appearance of a further oxidation peak at about 1.0 V vs SSCE in curve b) of Figure 2.15 and the apparent increase in the number of electrons under basic conditions is more puzzling, but was not investigated in detail. In the case of pyrrole the failure of base to promote a reaction that involves loss of protons has been attributed to nucleophilic attack of the base on pyrrole oxidation products [7]. Consequently, the increase in current flow for bipyrrole under the same conditions indicates that nucleophilic attack either does not occur, or that if it does it generates electroactive products. This shows that base can promote the reaction, as would be predicted by the polymerization mechanism. It is also possible that the increased current is due to further oxidation of the polymer film deposited.

The addition of 100 m*M* pyridine or 100 m*M* 2,6-di-t-butyl pyridine to a 50 m*M* pyrrole solution did change the onset potential and the half wave potential for the reduction of protons, as shown in Figure 2.16. The proton reduction half wave potential shifted cathodically to about -0.6 vs SSCE, while the hydrogen oxidation peak potential shifted to about -0.5 V vs SSCE. This behavior is not unexpected and further demonstrates that the

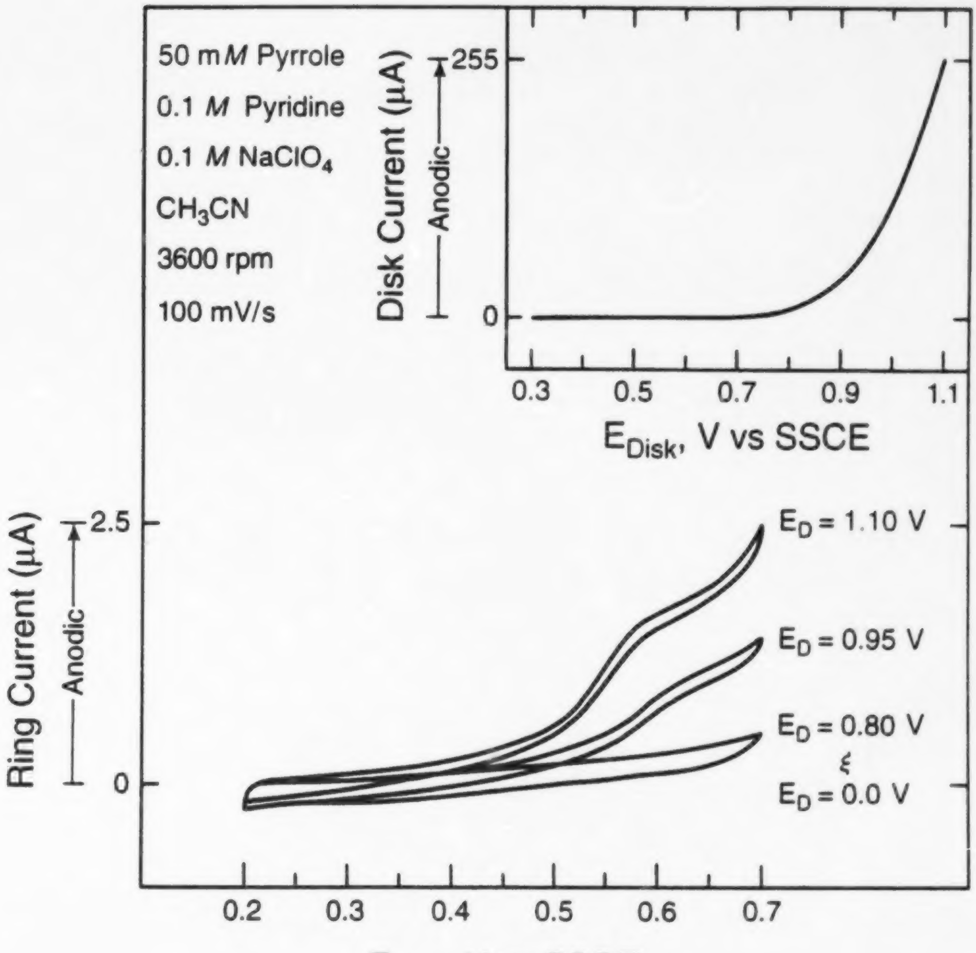

Figure 2.14 The Pt ring electrode current is shown as a function of the ring potential (100 mV/s,3600 rpm) at several values of the disk potential, E_D (± 20 mV, since the disk was also swept at 5 mV/s). The inset shows the disk electrode current for pyrrole oxidation versus disk potential (5 mV/s,3600 rpm). Solution contained 100 m*M* pyridine.

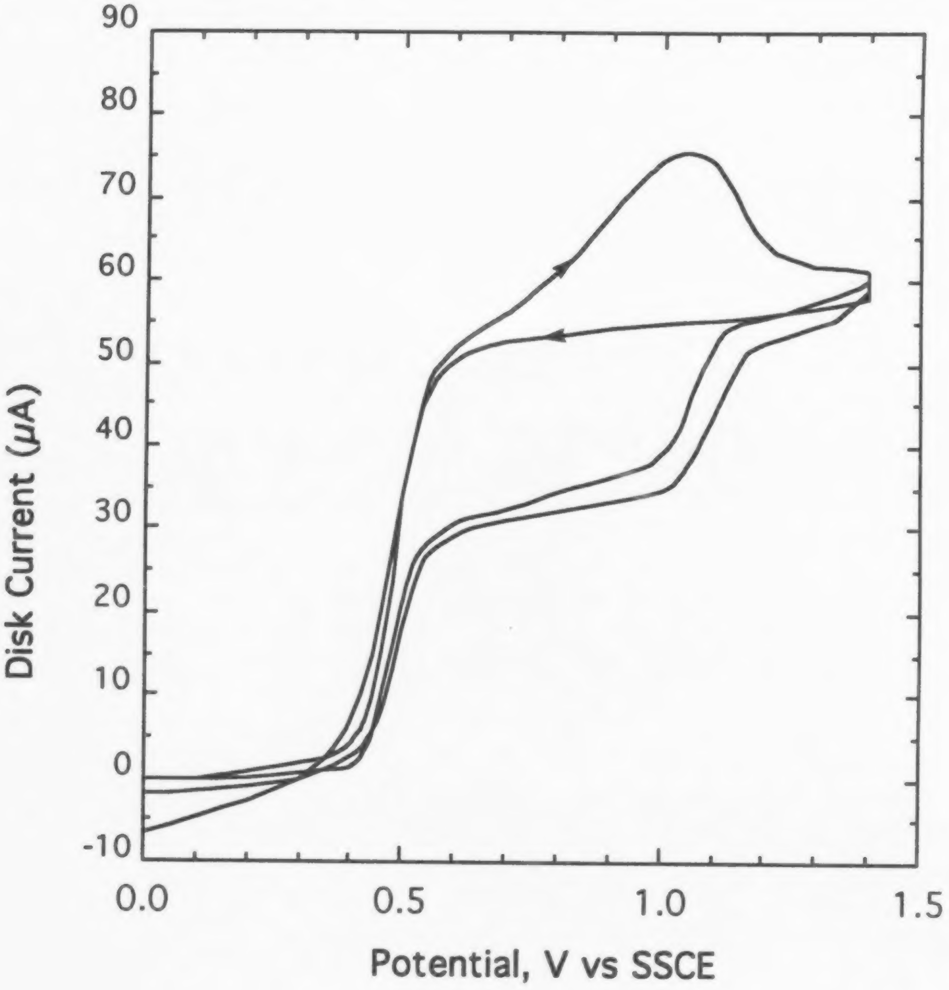

Figure 2.15 The Pt ring electrode current-voltage curve (10 mV/s, 4500 rpm) for the oxidation of 0.03 m*M* bipyrrole in acetonitrile containing 0.1 *M* $NaClO_4$ with added pyridine (arrows) and without added pyridine.

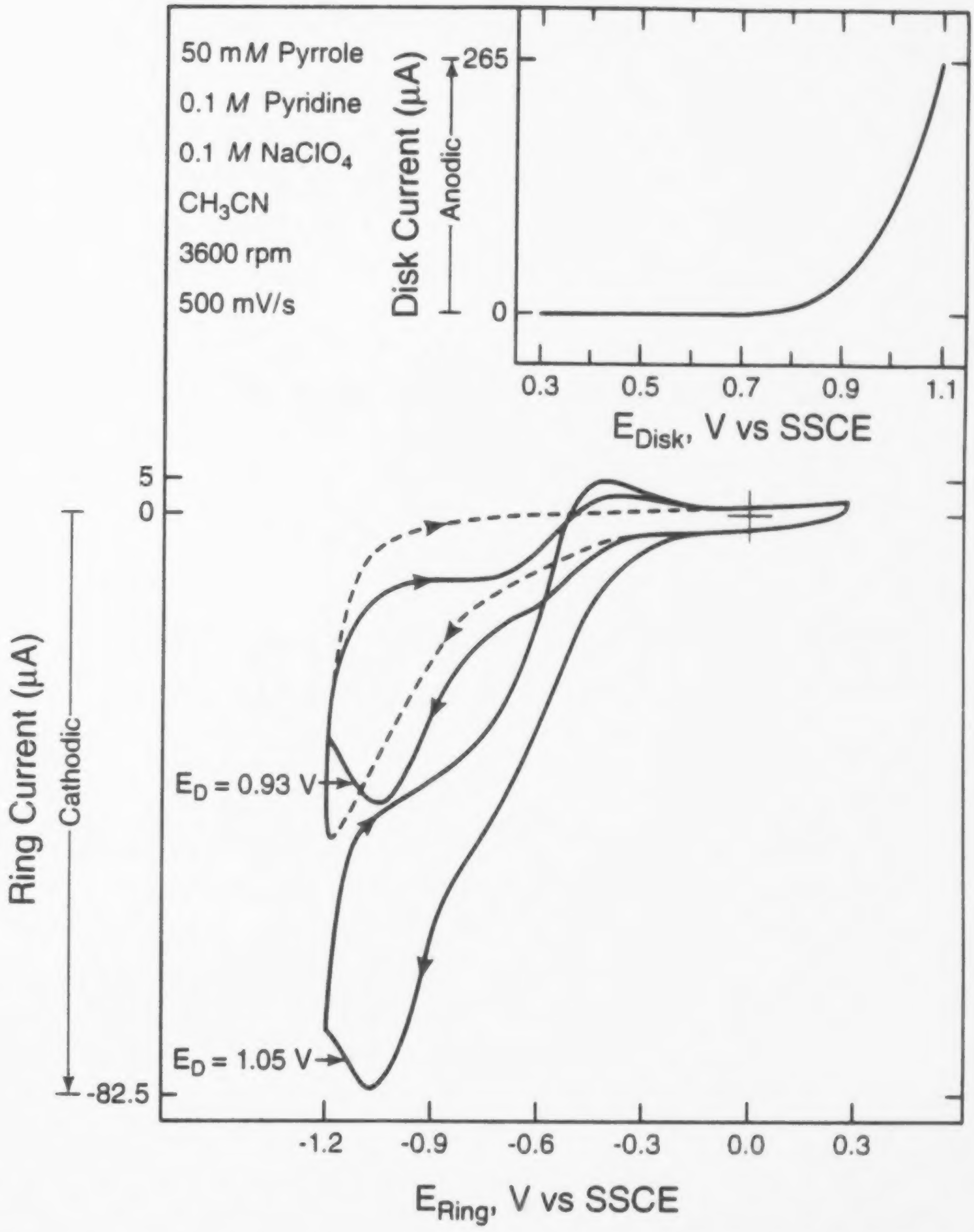

Figure 2.16 The Pt ring electrode current is shown as a function of the ring potential (500 mV/s,3600 rpm) at several values of the disk potential, E$_D$ (± 20 mV, since the disk was also swept at 10 mV/s). The inset shows the disk electrode current for pyrrole oxidation versus disk potential (10 mV/s,3600 rpm). Solution contained 100 mM pyridine.

reduction process at negative potentials is due to proton reduction. Also, since the results obtained were the same for both pyridine and 2,6-di-t-butyl pyridine, the observed effects must be due to deprotonation processes and not nucleophilic attack, as the sterically hindered 2,6-di-t-butyl pyridine would be unable to undergo the latter [7].

There are several products obtained during the oxidation pyrrole that might be expected to be observed at the ring electrode including the primary radical cation, secondary products such as bipyrrole or higher oligomers, pyrrl-pyrrole adducts in various protonated states and protons [11,17,20,21]. For many of these, both a reductive and an oxidative current would be expected. However, only an anodic current is definitely observed at ring potentials greater than 0.5 V vs SSCE, while a cathodic current is obtained at potentials more negative than -0.3 V vs SSCE. As stated the cathodic current has been attributed to proton reduction [30]. Meanwhile, the close agreement of the $E_{1/2}$ values for the observed anodic current and bipyrrole obtained under the same conditions, and the fact that both give a first wave with an $E_{1/2}$ independent of pH provides a compelling argument for the identification of the intermediate as bipyrrole.

2.6 Conclusions.

Direct observation of bipyrrole as a soluble intermediate in the electropolymerization of pyrrole is consistent with the mechanistic conclusions deduced from indirect evidence. It is noteworthy that bipyrrole is not observed until the oxidation current at the disk reaches the inflection point at +1.0 V. In chapter 5 we evaluate the ring collection efficiency as a function of rotation speed to gain further insight onto the potential dependence observed. The bipyrrole formed is obviously not a primary reaction product and the pathway to its formation involves a number of chemical and electrochemical steps that can be expected to lead to a complex dependence on rotation rate. The low collection efficiency for this stable species indicates that it is either rapidly lost via oxidation at the disk, consumed rapidly in the subsequent polymerization steps, or that it is formed in low yield as a result of a side reaction during the polymerization. The fact that bipyrrole can be oxidized to form conducting films contrary to an earlier report, indicates that chain formation is not limited to oligomer or oxidized oligomer coupling with oxidized pyrrole monomer, and that coupling of oligomers in solution followed by precipitation represents a viable mechanism. Finally, the ability to observe a soluble intermediate using the RRDE creates an opportunity to develop an increased understanding of the polymerization process. The conditions of polymerization are likely to affect the yield of bipyrrole at the ring electrode, providing a means to probe the factors influencing physical and chemical properties of the polymer.

2.7 References.

1. Diaz, A.F.; Kanazawa, K.K.; Gardini, G.P., *Chem. Commun.*, **1979**, 635.

2. Diaz, A.F.; Martinez, A.; Kanazawa, K.K., *J. Electroanal. Chem.*, **1981**, 130,181.

3. Penner, R.M.; Martin, C.R., *J. Electrochem. Soc.*, **1986**, 133, 2206.

4. Nagasubramanian, G.; Distefano, S., Moacanin, J., *J. Electrochem. Soc.*, **1986**,133, 305.

5. Warren, L.F.; Anderson, P.J., *J. Electrochem. Soc.*, **1987**, 134, 101.

6. Naoi, K.; Osuka, T., *J. Electrochem. Soc.*, **1987**, 134, 2479.

7. Morse, N.J.; Rosseinsky, D.R.; Mortimer, R.J.; Walton, D.J., *J. Electroanal. Chem.*, **1988**, 255, 119.

8. Vork, F.T.A.; Janssen, L.J.J., *Electrochimica Acta*, **1988**, 33, 1513.

9. Diaz, A.F.; Crowley, J.; Bargon, J.; Gardini, G.P.; Torrence, J.B., *J. Electroanal. Chem.*, **1981**, 121, 355.

10 Lindenberger, H., Schafer-Siebert, D., Roth, S., and Hanack, M., *Synth. Metals*, **1987**, 18, 37.

11. Asavapiriyamont, S.; Chandler, G.K.; Gunawardenu, G.A.; Pletcher, D.J., *J. Electroanal. Chem.*, **1984**, 177, 229.

12. Downard, A.J.; Pletcher, D.J., *J. Electroanal. Chem.*, **1986**, 206, 139.

13. Chandler, G.K.; Pletcher, D.J., *Special Reports Electrochemistry*, Vol.10, Royal Society Chemistry, London, **1985**, p.117.

14. Miller, L.L.; Zinger, B.; Zhou, Q.X., *J. Am. Chem. Soc.*, **1987**, 109, 2267.

15. Josowicz, M.; Janata, J.; Ashley, K.; Pons, S., *Anal. Chem.*, **1987**, 59,253.

16. Noufi, R.; Tench, D.; Warren, L.F., *J. Electroanal. Chem.*, **1981**, 128, 2596.

17. Imana, M.; Waller, *J., Anal. Chem.*, **1986**, 58, 2979.

18. Otero, T.F.; Tejada, R.; Elola, A.S., *Polymer*, **1987**, 28, 651.

19. Zotti, G.; Cattarin, S.; Comisso, N., *J. Electroanal. Chem.*, **1987**, 235, 259.

20. Noftle, R.E.; Pletcher, D.J., *J. Electroanal. Chem.*, **1987**, 227, 229.

21. Marcos, M.L.; Rodriguez, I.; Gonzalez-Velasco, J., *Electrochimica Acta*, **1987**, 32, 1453.

22. Baker, C.K.; Reynolds, J.R., *J. Electroanal. Chem.*, **1988**, 251, 307.

23. Genies, E.M.; Bidan, G.; Diaz, A.F., *J. Electroanal. Chem.*, **1983**, 149, 101.

24. Waltman, R.J.; Bargon, *J., Tetrahedron*, **1984**, 40, 3963.

25. Baker, C.K.; Reynolds, J.R., *Polymer Prepr.*, **1987**, 28, 284.

26. Christensen, P.A.; Hamnett, A., *Electrochimica Acta*, **1991**, 36, 1263.

27. Raymond, D.E.; Harrison, D.J., *J. Electroanal. Chem.*, **1990**, 296, 269.

28. John, R.; Wallace, G.G., *J. Electroanal. Chem.*, **1991**, 306, 157.

29. Rosseinsky, D.R.; Morse, N.J.; Slade, R.C.T; Hix, G.B.; Mortimer, R.J.; Walton, D.J., *Electrochimica Acta*, **1991**, 36, 733.

30. Beck, F ; Oberst, M, *J. Electroanal. Chem.*, **1990**, 285, 177.

31. Bruckenstein, S.; Sharkey, J.W., *J. Electroanal. Chem.*, **1988**, 241, 211.

32. Bard, A.J.; Faulkner, L.R., *Electrochemical Methods*; John Wiley & Sons: New York, 1980.

33. Itahara, T.; *J. Org. Chem.*, **1985**, 50, 5272.

34. Itahara, T.; Kawalski, K.; Ouseto, F., *Bull. Chem. Soc. Jpn.*, **1984**, 57, 3488.

35. Itahara, T.; Kawalski, K.; Ouseto, F., *J.C.S. Chem. Comm.*, **1980**, 49.

36. Rapoport, H.; Castagnioli, N, *J. Am. Chem. Soc.*, **1962**, 84, 2178.

37 Farnier, M.; Soth, S.; Fournari, P., *Can. J. Chem.*, **1976**, 54, 1083.

38. Raymond, D.E.; Harrison, D.J., *Submitted for Publication*, **1992**.

Chapter 3

Observation of Pyrrole Radical Cations as Transient Intermediates During the Anodic Formation of Conducting Polypyrrole Films.

3.1 Introduction.

The formation of conducting polymers derived from the electropolymerization of heterocyclic monomers, such as pyrrole, have been extensively studied over the past decade. While attention has focussed on the physical, chemical, electronic, and electrochemical properties of these conducting films [1-17], research on the mechanism of electropolymerization has only recently become a main focus of study [10,12,18-26].

The mechanism of electropolymerization of heterocyclic monomers, shown in scheme 1.1 of chapter 1, is regarded to be an $E(CE)_n$ type process with the first step being the formation of the radical cation via monomer oxidation. Of the resonance forms of the delocalized radical cation it has been found that the highest spin density occurs at the α-position [21], consequently (4) is the most stable resonance form. Coupling at the α-position via radical-radical coupling occurs because of the lower energy of this transition state. Radical-monomer coupling is said not to occur because of the potential dependence and lack of copolymer formation during copolymerization of pyrrole with other substituted pyrroles [19]. Also, the energy barrier calculated for radical-monomer coupling has been

---

A version of this chapter has been submitted for publication. D.E Raymond and D. Jed Harrison, 1993. Journal of Electroanal. Chem..

shown to be larger than that for radical-radical coupling [27]. After radical-radical coupling two protons are expelled from the hydrodimer, resulting in the formation of a neutral dimer, with the return to aromaticity being the driving force for this step. Chain propagation results via oxidation of the neutral dimer to form the dimer radical cation, which then reacts with other monomeric, dimeric or oligomeric radical cations. This process repeats itself until chain growth is terminated. However, the location of the polymerization processes relative to the solution/electrode interface, and whether the mechanism accounts for nucleation and three-dimensional growth still remains controversial.

It was suggested in early studies [11,13] that neutral monomer adsorption onto the electrode surface occurs prior to oxidation, and the subsequent polymerization then occurs on the electrode surface via scheme 3.1. However, more recent studies using *in-situ* differential ellipsometry [23,28], rotating ring-disk electrodes (RRDE) [24,29], and microelectrodes [25] have supported the hypothesis that the first step in polymer deposition involves solution polymerization with subsequent precipitation of oligomers onto the electrode surface. These studies all confirm the presence of soluble intermediates prior to polymer formation, including the identification of the bipyrrole moiety. The coulombic efficiency of the electropolymerization process has been found to be less than 100%. This loss in efficiency is attributed in part to the transport of soluble intermediates away from the electrode surface, as well as effects due to the monomer concentration and electrolyte type [19].

It is thought that once the oligomers attain a critical length in solution they precipitate or electro-precipitate (facilitated by further oxidation) onto certain sites on the electrode and further polymer growth ensues. The growth is considered to be a nucleation/growth process similar to the electrodeposition of metals [11,13,18,30,31]. This is evidenced by the "nucleation loops" obtained in cyclic voltammetric studies [11,13,18,29,31] and the rising current-time (I-t) curves observed with chronoamperometry [11,13,18,30,31]. Recently, a study involving *in-situ* differential ellipsometry [23] concluded that once above a critical length the oligomers precipitate onto active sites and grow homogeneously by addition to the free end of the polymer chain. The electric field at the end of the chain is the driving force for this growth process, assuming the polymer chain is able to extend freely into solution. After these chains on the electrode surface reach a length such that the potential drop along their length precludes further growth, the polymer is said to "fill in" via nucleation and growth on the remaining exposed electrode surface, with additional growth on the original chains resulting from grafting at the β-positions. Eventually the whole surface is covered and the film continues to grow outward.

The nucleation loops and I-t transient behavior imply that an increase in active electrode surface area is occurring. However it has been pointed out [11,30,32] that addition of a monomer to the growing end of a polymer chain does not increase the electrode area because the process is uni-dimensional. Furthermore, if this type of growth was present then dendritic growth along the potential field toward the counter electrode should occur, however this is contrary to experimental findings [11]. The studies utilizing the unique mass transport behavior characteristic of microelectrodes [25] concluded that polymer growth on the electrodes, after initial solution polymerization and precipitation, resulted from "continual electroprecipitation". That is, further growth resulting in nuclei expansion occurs by precipitation of oligomers on top of already formed nuclei. However, the addition of monomeric species to polymer chain ends was not excluded as a parallel process. The former process was said to be responsible for the bulk of the polymer growth resulting in an increase in electroactive surface area, and hence to rising current transients.

In this study the rotating ring-disk electrode (RRDE) was used to examine the initial processes involved in electropolymerization of pyrrole. Previous work with the RRDE demonstrated the presence of bipyrrole during the anodic formation of polypyrrole at the disk electrode [24]. In this work further evidence that supports the solution polymerization/precipitation theory, as well as the observation of reducible pyrrole species at the ring electrode, will be presented.

3.2 Experimental.

3.2.1 Chemicals. Pyrrole (Aldrich) was vacuum distilled and stored under argon. HPLC grade acetonitrile (Burdick and Jackson) was distilled over calcium hydride prior to use. Sodium perchlorate (Fisher Scientific), and tetrabutylammonium tetrafluoroborate (Southwestern Analytical Chemicals) were used (without further purification) after being dried under vacuum at 110 °C. Pyrrole solutions were prepared by dilution of a freshly prepared 50 m*M* pyrrole solution in acetonitrile. All solutions were filtered through activated alumina (Woelm N-Super I, ICN Nutritional Biochemicals, Cleveland, Ohio, vacuum dried at 250 °C) immediately before use.

3.2.2 Instrumentation. A Pine RDE-4 bipotentiostat and MSR rotator were used for the ring-disk experiments. Data was recorded on a Kipp and Zonen BD91 x,y,y' recorder equipped with a time base. The RRDE dimensions were r_1=0.2286 cm, r_2=0.2464 cm, and r_3=0.2692 cm, where r_1 is the disk radius, and r_2 and r_3 are the inner and outer ring radii respectively. The collection efficiency calculated [33] using the electrode dimensions was 0.216, while the value obtained experimentally using aqueous 1.0 m*M* $K_3Fe(CN)_6$ in 0.1 *M* KCl was 0.22. The RRDE was polished before each run using a series of 3 µm alumina, 1 µm alumina, and 0.3 µm alumina, and was thoroughly rinsed with dry acetonitrile. The kinematic viscosity was obtained using a calibrated viscometer (Cannon Instrument Co.)

3.3 Procedures.

3.3.1 Study of Ring Reduction Transient Time Dependence.

The procedure used for all analyses was essentially the same. The RRDE was rotated at 4500 rpm while the disk potential was swept at 10 mV/s from 0.0 V to a desired maximum limit and then held constant. Throughout this procedure the ring potential was maintained at various constant values. However, in general, a ring potential of 0.65 V was used. All potentials were against the saturated sodium calomel (SSCE) reference electrode, which was isolated using a double junction containing electrolyte solution and calcium hydride powder to consume any water derived from the SSCE. A platinum gauze counter electrode was also isolated using a fine glass frit. For time dependent studies the recorder time base was 5 s/cm and the disk potential was swept at 10 mV/s to a preset constant value.

3.3.2 Acid Addition at the RRDE using Luggin type capillary.

The perchloric acid solution was prepared by dilution of a 0.1 M stock solution in dry acetonitrile prepared from concentrated perchloric acid (70%). Water in the stock solution was removed by addition of the appropriate amount of acetic anhydride and letting stand for 24 hours. The acid addition apparatus was essentially a Luggin capillary equipped with a large reservoir. The capillary tip inner diameter was approximately 0.5 mm. The apparatus was purged with nitrogen before the acid solution was added, and the solution itself was then purged. The tip of the apparatus was placed as close as possible to the center of the disk electrode. The acid solution mixed with the electrolyte solution on the way to the disk electrode during electrode rotation at 4500 rpm. No potential was applied to the disk while the ring was maintained at 0.65 V. Experiments showed a 2% decrease in the disk current occurred when the apparatus was in place and contained only electrolyte, indicating minimal disruption of the flow profile to the disk.

3.3.3 Evaluation of Diffusion Coefficients using the Taylor Dispersion Method

In the Taylor dispersion method a long open tubular column filled with solvent moving slowly under laminar flow conditions was used [41]. A sharp plug of sample was injected and allowed to disperse in the column. The resulting peak shape exhibited a variance that can be used to calculate the diffusion coefficient of the sample via the Golay equation (1).

$$\sigma_t^2 = \frac{r^2 t}{24D_m} \quad (1)$$

where r is the open tube inner radius, t is the elution time, D_m is the diffusion coefficient, and σ_t is the variance of the peak.

The experimental apparatus was borrowed from a graduate laboratory course in chromatography and used without modification. The sample was dissolved in acetonitrile containing 0.1 *M* $NaClO_4$. A variable wavelength UV/VIS detector was set at the wavelength of maximum absorbance. The open tube was 2 m long and had an inner diameter of 0.08 cm. The tube was placed inside a Tygon tube which was attached to a constant temperature bath maintained at 25 °C. Solvent was pumped at 0.8 mL/min and the sample injected via a slider injector. The data was acquired using an IBM PC and the variance was obtained from method of moments analysis via a program written in ASYST (MacMillan).

3.4 Results and Discussion.

A typical RRDE current-voltage curve obtained from the polymerization of a 0.1 m*M* pyrrole solution with 0.1 *M* $NaClO_4$ as electrolyte is shown in Figure 3.1. The results were obtained at a rotation rate of 4500 rpm, and the behavior shown is characteristic of all rotation rates studied. The significant ring electrode features at a constant ring potential of 0.65 V *vs* SSCE are the reduction spike at a disk potential near 1.0 V and the oxidation peak near 1.3 V. We have shown that the anodic current can be attributed to bipyrrole oxidation, and that at 0.65 V the ring is poised on the current plateau for this species. The initial ring reduction spike may be due to various species generated during the first stages of pyrrole oxidation at the disk electrode, with possible candidates being either monomeric or oligomeric radical cations, free radicals formed via radical cation deprotonation, protonated pyrrole, or protons released during polymerization. It is also possible that the products observed at the ring are due to oxidative decomposition of the polypyrrole film rather than intermediates generated during polymerization. Each of these possibilities is considered below, and we argue that the spike is due to a pyrrole derived radical species, most likely the primary radical cation.

3.4.1 Candidates for the Reducible Intermediate.

It is known that pyrrole can be chemically polymerized upon addition of an acid [35]. It is precisely this problem of acid catalyzed polymerization that has made evaluation of the pK_a of protonated pyrrole difficult [36,37]. Acidic polymerization involves formation of a pyrrole trimer which consists of a saturated pyrrolidinine ring between two unsaturated moieties. When this species is the dominant product a non-conducting, or at least minimally conducting powder results. Since protons are released during the electropolymerization process, generating a concentration similar to that of pyrrole itself, it is likely that protonation of pyrrole occurs, thus leading to loss of monomer via formation of the pyrrole trimer. This side reaction may manifest itself as either a loss in coulombic efficiency for conducting polypyrrole formation, or as decreased film conductivity.

If protonated pyrrole forms in significant quantities and it is reducible, then it may be observable at the ring electrode. An apparatus was constructed such that an acidic solution could be added directly at the center of the rotating disk electrode. No potential was applied at the disk, but the ring potential was maintained at 0.65 V and the current response at the ring electrode was then monitored. Addition of a 10 m*M* $HClO_4$ dry,

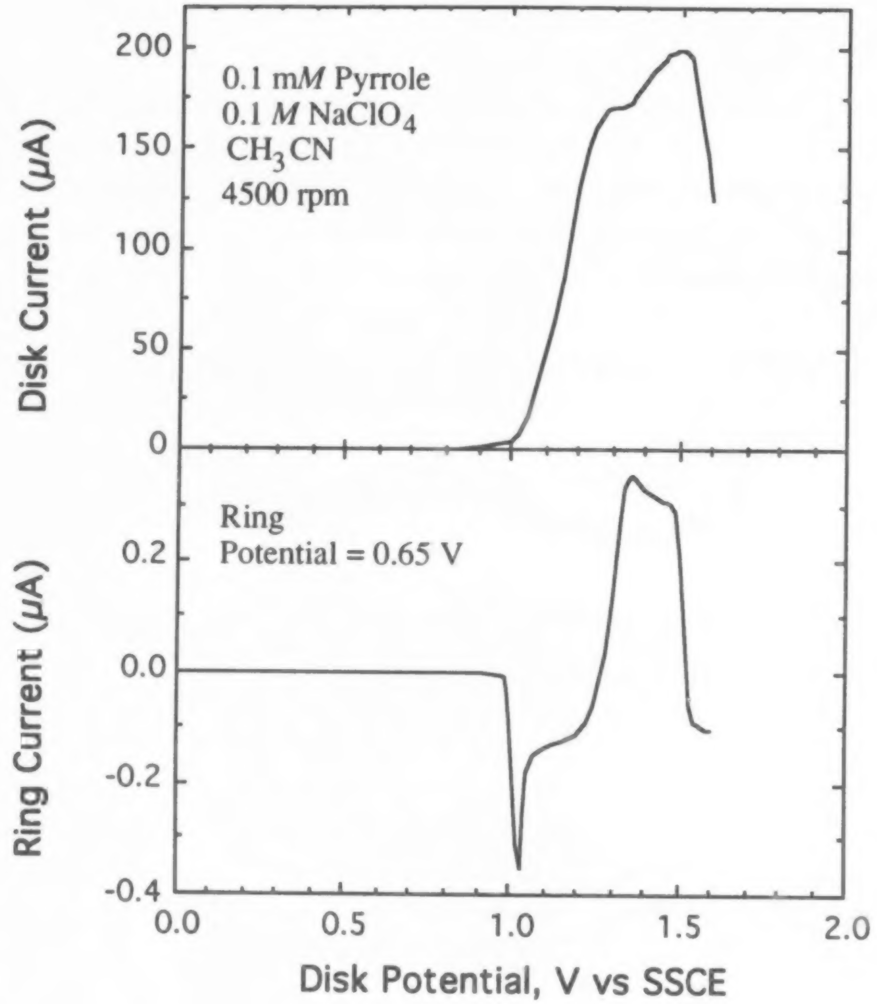

Figure 3.1 Typical RRDE current-voltage curve obtained from the polymerization of a 0.1 m*M* pyrrole solution with 0.1 *M* $NaClO_4$ as electrolyte. Rotation rate of 4500 rpm. Ring potential of 0.65 V vs SSCE. Disk potential scanned 0.0 V to 1.6 V.

CH_3CN solution to a 0.1 m*M* pyrrole solution, both with 0.1 *M* $NaClO_4$ or 0.1 *M* $TBABF_4$ as electrolyte, immediately gave a reductive current spike at the ring. Conversely, a positive current spike of equal magnitude was observed when addition was terminated. These spikes were determined to be due to changes in the ionic strength at the electrode since the same behavior was observed when a 0.1 *M* $NaClO_4$ solution was added to a 0.1 *M* $TBABF_4$ solution. No other features were observed in the ring current. This result indicates that either protonated pyrrole is not formed under these conditions or it is not electroactive, and that the same can be said for any reaction products of the acid polymerization process. Importantly, it also demonstrates that proton reduction is not observed at the ring potential used. We conclude that the initial ring reduction spike in Figure 3.1 is not due to protons, protonated pyrrole, or its reaction products.

To determine whether polypyrrole oxidation products were observed at the ring, a polypyrrole electrode was studied in a blank 0.1 *M* $NaClO_4$ solution. The disk electrode was first coated with polypyrrole, rinsed, placed in a blank solution, and then rotated at 4500 rpm while the disk potential was swept from 0.0 V to 1.6 V. The ring potential was again maintained at 0.65 V. The resulting disk current indicated that polymer degradation occurs above a disk potential near 1.5 V. There was no significant ring current until the disk potential reached 1.5 V, after which a small reduction current was observed. This result demonstrates that the ring current observed in Figure 3.1 is not due to polymer degradation products. It also shows that once polymer degradation occurs at the disk the yield of this species declines substantially. Clearly, the inactivation of the polymer accounts for the peak shaped nature of the disk and ring currents at high disk potentials.

In combination, the experiments described above indicate that pyrrole derived radical species arising during the electropolymerization process are the most probable source of the ring reduction current. Whether radical cations or free radicals are the species causing the ring reduction spike will depend upon whether deprotonation occurs before or after radical-radical coupling. Both intermediates result in bipyrrole formation, therefore it may not be possible to discern which is present. In addition, the above experiments do not clarify whether it is the primary oxidation product, the pyrrole radical cation, or a subsequent product that is observed. A study of the potential and time dependence of the cathodic ring current was undertaken to gain insight into these issues.

3.4.2 Ring Current Potential Dependence.

It has previously been shown that at negative potentials proton reduction at the ring is observed due to H^+ released during pyrrole oxidation [38]. We found that with the ring potential at 0.0 V a large reduction was obtained when pyrrole was oxidized at the disk. This reduction is most likely due to protons, but at a potential significantly on the foot of the current-voltage curve for this process [38]. The dependence of the ring current on ring potential is shown in Figures 3.2 and 3.3 for ring potentials ranging from 0.2 V to 1.1 V. The ring potential was held constant at these potentials while the disk potential was swept from 0.0 V to 1.6 V (10 mV/s) and the RRDE was rotated (4500 rpm). The surface of the ring electrode was checked for polymer coverage both visually and by cyclic voltammetry in an aqueous solution of 0.1 *M* $NaClO_4$. Below a ring potential of 1.1 V, and above the potential for the oxidation of bipyrrole, cyclic voltammetry showed only traces of polymer deposition on the ring. This is consistent with the behavior observed for bipyrrole and pyrrole [24]. Only above a ring potential of 1.1 V did significant polymer deposition occur on the ring. The increasing anodic current observed in Figure 3.3 is attributed initially to the oxidation of bipyrrole above 0.4 V, and then also to pyrrole at 0.75 V and greater (oxidation of pyrrole at Pt and C always shows a small "foot" beginning about 0.75 to 0.8 V).

Proton reduction at the positive ring potentials indicated in Figures 3.2 and 3.3 is ruled out, except for 0.2 V, based on the $HClO_4$ addition experiments. The magnitude of the reduction current decreased as the ring potential increased, and the reduction current spike did not totally disappear until a potential of 1.1 V. This potential coincides with the onset of significant pyrrole oxidation at the ring. However, it is also the recently reported standard potential for the single electron, reversible, oxidation of pyrrole calculated on the basis of rapid cyclic voltammetric studies [39]. The E° value was given [39] relative to a Ag wire psuedo-reference electrode which, in our measurements, is at -0.243 V vs the SSCE, giving a value of about 1.1 V vs SSCE for pyrrole. Based on this comparison the reduction current observed at ring potentials from 0.45 V to 1.0 V vs SSCE is most likely due to the primary oxidation product, the pyrrole radical cation.

The average lifetime reported [39] for the pyrrole radical cation in the rapid scan, microelectrode study is 30 μs, while at the rotation rate used the average transit time from the edge of the disk to the inner edge of the ring is 3 ms. Assuming a radical-radical coupling mechanism the reaction will be a second order process, with the lifetime being concentration dependent, decreasing with increasing concentration. Over the site the radical

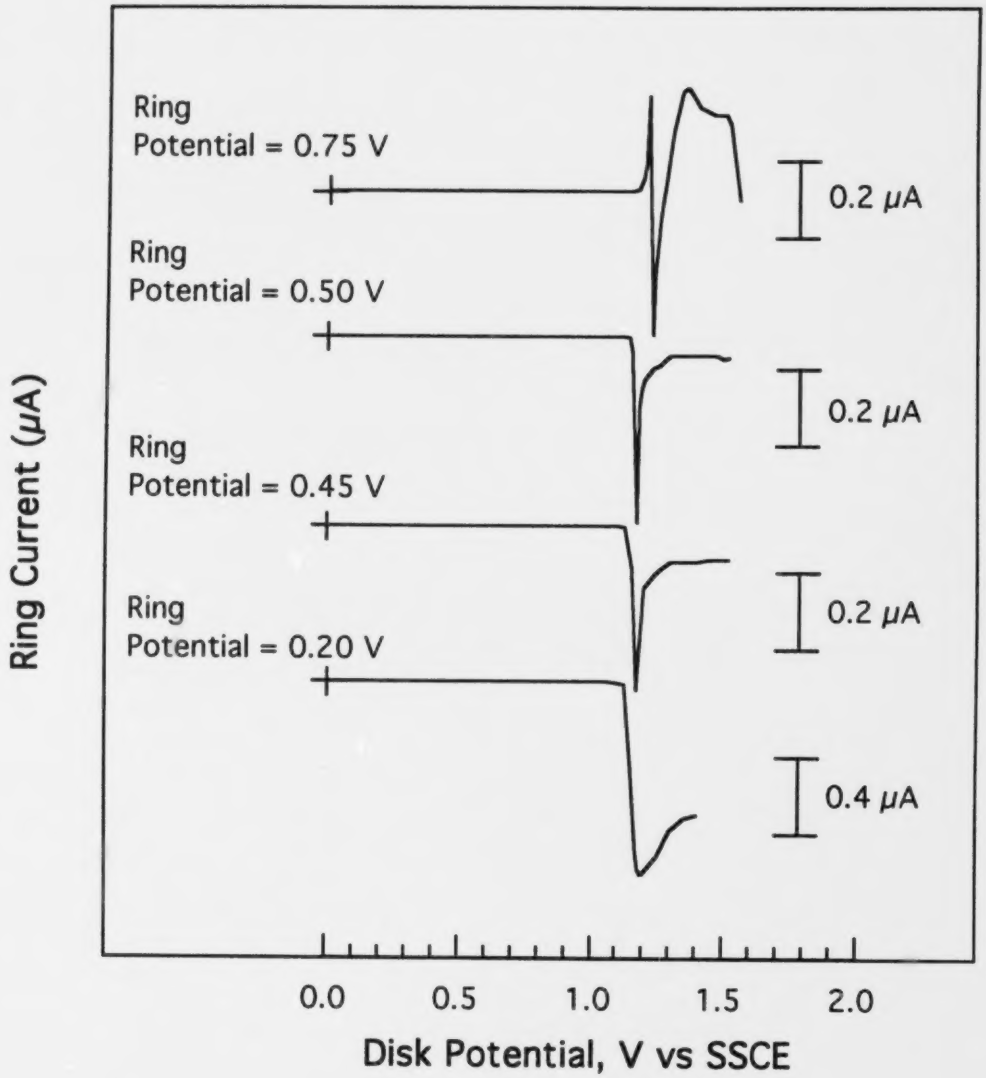

Figure 3.2 Ring current dependence on ring potential obtained from the polymerization of a 0.1 m*M* pyrrole solution with 0.1 *M* $NaClO_4$ as electrolyte. Disk potential scanned 0.0 V to 1.6 V. Rotation rate of 4500 rpm.

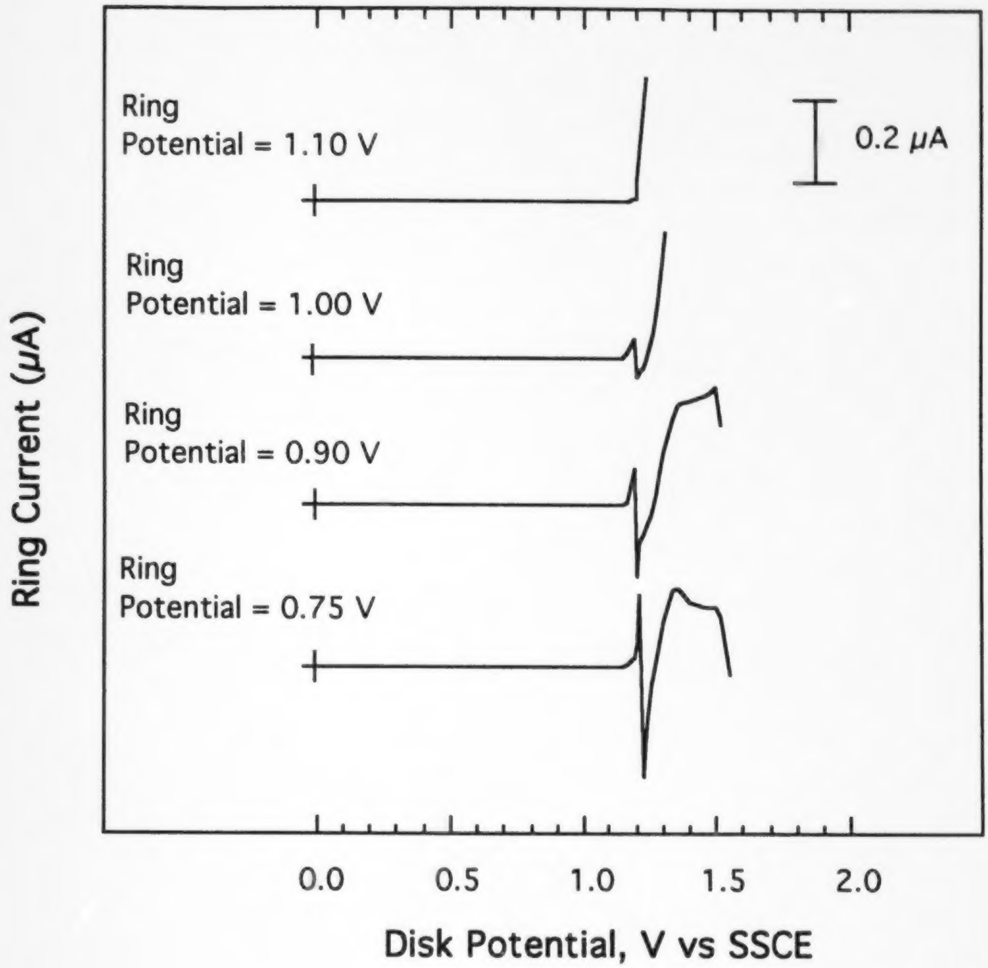

Figure 3.3 Ring current dependence on ring potential obtained from the polymerization of a 0.1 m*M* pyrrole solution with 0.1 *M* $NaClO_4$ as electrolyte. Disk potential scanned 0.0 V to 1.6 V. Rotation rate of 4500 rpm.

is generated (disk or microelectrode) its concentration will be relatively high, as will the concentration of other products with which it can react, such as oxidized higher oligomers. However, at low concentrations the lifetime will be increased. This situation may well be true in the gap between the ring and the disk, since only the outer annulus of radical generated at the disk may escape into the solution volume of the gap, which is radially expanding, and no further electro-oxidation products are generated in this region. If this is the case then the possibility of observing the pyrrole radical cation is greater (*vide infra*).

3.4.3 Time Dependence of Ring and Disk Currents.

The early stages of electrocrystallization are often studied by measuring the current response to a controlled potential perturbation of an electrode. Based on the rising current transients obtained from chronoamperometric studies the electrodeposition of pyrrole has been described as a three dimensional nucleation and growth process [11,13,18,29-31]. Transient behavior is suggested by the ring reduction spike in Figure 3.1, so a study of the current-time behavior of the spike at the RRDE may determine whether this phenomenon is associated with the kinetics of nucleation and growth. In the experiments described below the disk potential was swept at 10 mV/s to a desired maximum value, and then maintained at this value while the current-time behavior at the disk and ring was followed. The ring was potentiostated at 0.65 V during this process to allow both oxidizable and reducible products to be observed. The experiments involved a potential sweep to the maximum disk potential, whereas chronoamperometry usually involves a potential step. Potential step experiments were carried out to verify that the potential sweep method gave identical results. This proved to be so, with the exception that the potential step method gives an initial capacitive current spike.

In Figure 3.4 the results obtained with a maximum disk potential of 1.15 V and a constant ring potential of 0.65 V are shown. The experimental conditions used were identical to those in Figure 3.1. This data is typical of that obtained for maximum disk potentials between 1.13 V and 1.20 V. Pyrrole oxidation at the disk electrode was initiated during the potential sweep (potential ramp at bottom of Figure 3.4), as evidenced by the slow rise in anodic disk current. As in Figure 3.1 there is a sudden rapid rise in the disk current near a disk potential of 1.13 V. Above this potential the disk current began to plateau. The disk potential was held constant once it reached 1.15 V, but the disk current

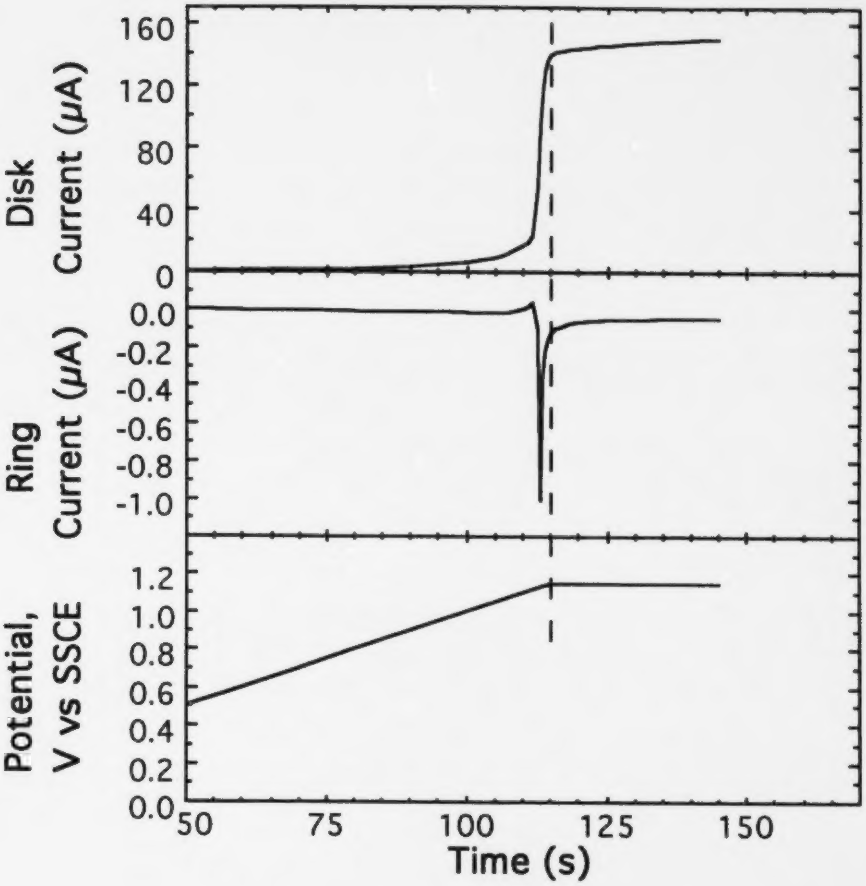

Figure 3.4 Ring reduction transient analysis during the polymerization of a 0.1 m*M* pyrrole solution with 0.1 *M* $NaClO_4$ as electrolyte. Ring potential held at 0.65 V vs SSCE. Rotation rate of 4500 rpm. Maximum disk potential applied was 1.15 V vs SSCE, as indicated by the dashed line.

continued to increase slowly. The current at the ring during the potential sweep was similar to that in Figure 3.1. A small oxidation current appeared at the ring, concurrent with the anodic current onset at the disk. The large ring reduction spike observed coincided with the rapid increase in disk current. The reduction spike decayed rapidly even while the disk potential continued to be swept, and when the potential became constant it continued to decay to a small, constant cathodic current. This behavior contrasts with that in Figure 3.1, in which anodic current is observed at the ring. However, this depends on the maximum potential at which the disk is held, and above a disk potential of about 1.20 V an anodic current plateau is observed at the ring, after the initial reduction spike.

Figure 3.5 demonstrates that significant changes were observed when the maximum disk potential was reduced to 1.125 V, and similar results were obtained at 1.120 V. During the disk potential sweep the disk current began as a slowly rising anodic current, as observed in Figure 3.4. However, the disk potential was held constant before the rapid rise in current occurred, and the disk current remained at a constant, relatively low value for a period of time. After this period a rapid rise in current was observed, indicating that the increase results from a time dependent phenomenon which is most probably related to the kinetics of the polymer nucleation process. Figure 3.5 also shows the ring current during the disk potential sweep. The ring current shows a small anodic current once the disk oxidation onsets, but no ring reduction spike during the disk potential sweep. The ring oxidation current decreased slowly once the disk potential was held constant, until a large reduction spike was observed. This spike again coincided with the rapid increase in disk oxidation current, and it then decayed to a small, constant cathodic value as in Figure 3.4. This important result shows that the ring reduction spike is indeed a transient event and that it is associated with the nucleation of the polymer, being observed only when there is a sudden change in the rate of pyrrole oxidation.

When the maximum disk potential excursion was less than 1.120 V, the initial disk oxidation current was still observed to rise slowly during the potential sweep (not shown). Once the potential became constant a nearly constant disk current was observed for about 40 seconds. It then slowly increased threefold during the next two minutes. A sudden, large increase in disk current was not seen. The ring current changed only a small amount from its initial baseline value during these gradual processes, so that it was difficult to resolve any effects. These results indicate that while the sudden rise in disk current, and the ring reduction spike are a time dependent phenomenon, they are also potential dependent, requiring a threshold potential of about 1.12 V to be induced.

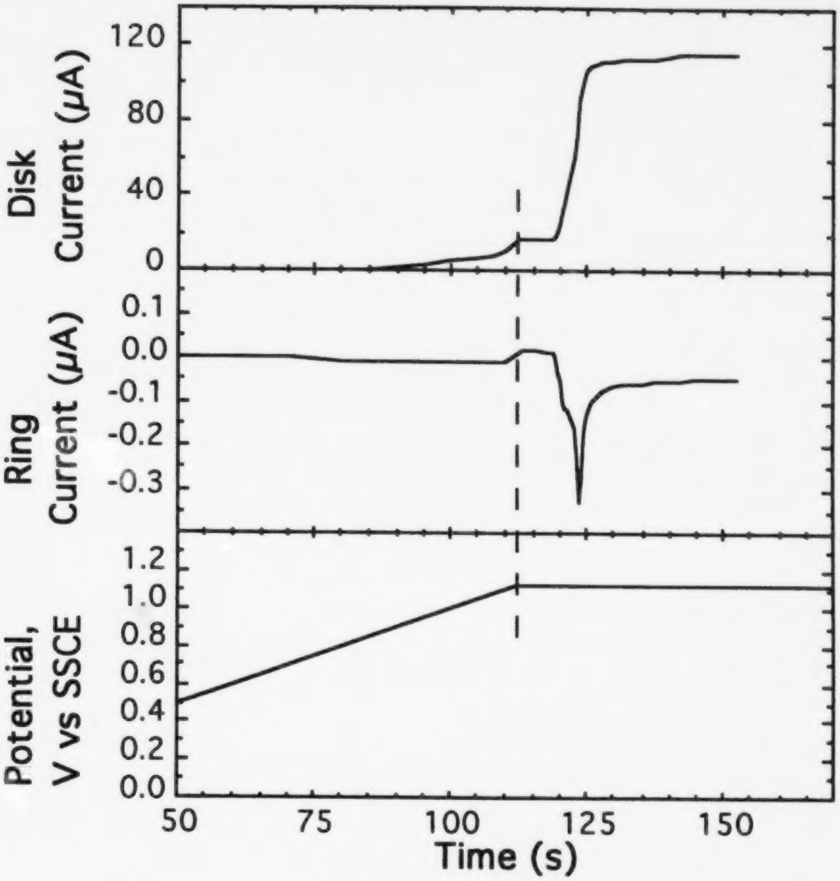

Figure 3.5 Ring reduction transient analysis during the polymerization of a 0.1 m*M* pyrrole solution with 0.1 *M* $NaClO_4$ as electrolyte. Ring potential held at 0.65 V vs SSCE. Rotation rate of 4500 rpm.Maximum disk potential applied was 1.125 V vs SSCE, as indicated by the dashed line.

3.4.4 Evidence for the role of Solution Species in Polymer Deposition.

The data shown in Figures 3.4 and Figure 3.5 provide strong evidence for an activation and/or nucleation period for the formation of active sites on the electrode. The process of three dimensional nucleation and growth involves an initial delay or induction period, followed by three dimensional growth at a rate determined by the rate of incorporation of new atoms at the active site and/or the rate of mass transport to the nuclei. However, the processes observed in Figures 3.4 and 3.5 can not be strictly defined in this way and instead should be regarded as the formation of electroactive sites in increasing numbers. Pyrrole oxidation is facile at these active sites and a fraction of the product is soluble and not incorporated at the active site, as discussed below.

In Figure 3.5 the initial constant disk current when the electrode is held at 1.125 V can be considered as an induction period during which there are presumably only a few locations on the surface at which significant pyrrole oxidation is occurring. The local concentration of radical cation is apparently high enough to form pyrrole dimer, and some of this reaches the ring electrode without further reaction as indicated by the ring oxidation current during this period. Eventually sufficient active sites are created by the deposition of oligomers (electro-precipitation) that the oxidation rate increases rapidly, as seen by the sudden rapid increase in the disk current. It then becomes limited by available surface area and the mass transport rate, since the disk current dependence on rotation rate obeys the Levich equation when the disk potential is 1.35 V or greater (at these low pyrrole concentrations). The length of the activation period decreased as the maximum disk potential increased, indicating the sudden increase in current is an activation barrier controlled phenomenon. This explains why no induction period was observed in Figure 3.4, since at sufficiently high disk potential formation of active sites occurs very rapidly.

The above data is consistent with three dimensional growth on the surface, however, evidence for the role of precipitation of soluble intermediates comes from visual inspection of the polypyrrole coating on the disk. Figure 3.6 shows the surface of a rotated platinum disk electrode obtained by stopping the experiment just after the rapid increase in disk current has occurred. The photograph was obtained when the disk potential was held at 1.125 V, and identical patterns were obtained at potentials between 1.12 and 1.15 V. Similar results were obtained at the carbon disk of the RRDE, but a platinum electrode provided better contrast in the photo. It was important that the experiment be terminated within a few seconds of the initial rise in the disk current to obtain such patterns. When the

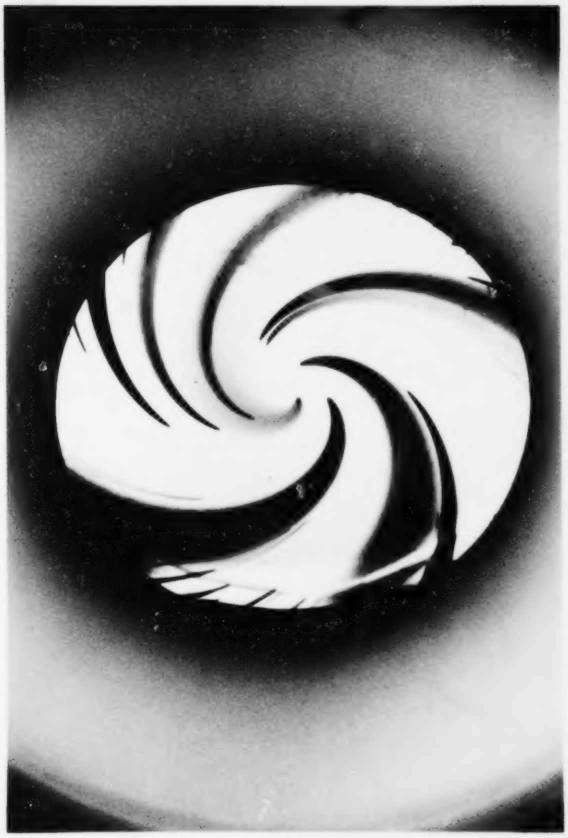

Figure 3.6 Photograph of Pt RDE surface taken after experiment was terminated during the rapid rise in disk current. Solution contained 0.1 m*M* pyrrole in acetonitrile with 0.1 *M* $NaClO_4$ as electrolyte. Maximum disk potential was 1.125 V vs SSCE. Rotation rate was 4500 rpm.

disk surface was examined 40 s after the rapid current rise the whole surface was covered with polymer.

The polymer coverage pattern in Figure 3.6 clearly resembles the hydrodynamic flow patterns at a rotating disk [40]. The photograph shows that polymer deposition begins at a point, and, analogous to the burning Chernobyl nuclear reactor, discharges a plume of intermediates that react and then precipitate back onto the electrode surface blackening all in its path.. This precipitation process presumably involves further oxidation (and oligomerization) at the surface, since the photograph shows there is no visible polymer deposition on the teflon shroud surrounding the active electrode. The areas within the deposited polymer region must themselves be active relative to the surrounding bare electrode, and consequently each "active site" within the area generates its own plume, so that the polymer fills in. When these plumes reach the edge of the disk they pass over the gap region to the ring electrode where the intermediates may be detected. The ring reduction spike is most likely due to this surge in the generation of radicals. Once the disk current reaches steady state the entire surface becomes coated with polypyrrole and is active for pyrrole oxidation. At this stage the radical concentration is sufficiently high that dimerization and further reactions leading to polymer deposition will occur at a high rate while the radical is in the vicinity of the disk. Essentially only the radical and bipyrrole generated in an outer annulus of the disk will escape further reaction and reach the ring electrode, consistent with the rather low collection efficiencies observed (9×10^{-3} compared to the theoretical value of 0.216).

3.4.5 Effect of Electrolyte.

It is known that the electrolyte can have a significant effect on the morphology of the polypyrrole formed [1-17]. Consequently, identical experiments were performed using 0.1 *M* $TBABF_4$ as electrolyte to determine the effect on the intermediates we have observed. Identical behavior to that shown in Figures 3.1, 3.4 and 3.5 was observed, except that the processes were anodically shifted by 0.1 V. We have found that this shift is due to the different junction potential that develops relative to the SSCE reference electrode in this supporting electrolyte. This effect does not appear to be well recognized in the literature. However, the induction period observed was much shorter with $TBABF_4$ than with $NaClO_4$, suggesting that nucleation occurs more rapidly, or with lower activation barrier with this electrolyte.

3.4.6 Effect of Radical Dimerization on Kinetics.

The above interpretation is consistent with the observations presented. However, one might expect that during the rapid rise in disk current a monotonic increase in the cathodic ring current to a steady state value would be observed. It is possible the transient behavior seen may be explained by the concentration dependence of the kinetics of the dimerization reaction. The dimerization rate will increase as the square of the radical cation concentration, leading to a much greater consumption of this species as the rate of pyrrole oxidation and the active electrode area increases at the disk. Consequently, the ring current for the radical would rise as it begins to be produced at a greater rate, and then fall again when its concentration becomes sufficiently large for the dimerization reaction to dominate. This suggests that the ring reduction current transient should be a function of the concentration of pyrrole. Since the production of the radical over the disk will increase with pyrrole concentration, the yield of radical relative to dimer at the ring should decrease with increasing pyrrole concentration. Figure 3.7 shows that this is indeed the case. This trend was observed for both the ratio of the transient current to bipyrrole current, and the ratio of the steady state reduction plateau current, obtained after the transient, to the bipyrrole current.

To further support the hypothesis that the transient behavior of the ring reduction current is due to the coupling of the radical cation a simple calculation was performed. It was assumed that the radical generated at the disk actually originates from an annulus just within the disk radius and that the amount of radical can be described by the Koutecky-Levich equation. The initial radical concentration before subsequent reactions could then be estimated as a function of potential. It was then allowed to react "in the gap" via the reaction scheme given in the appendix. This scheme considers radical-radical coupling of all radicals generated, and also steps which regenerate monomer via electron transfer reactions between primary radical cation and neutral oligomers. The average transit time from the disk edge to the inner ring edge was calculated and used as the reaction time [41]. The reactions at the ring were taken as,

$$M^{\cdot +} + e^- \longrightarrow M$$
$$M_2 \longrightarrow M_2^{\cdot +} + e^-$$

where M is pyrrole, $M^{\cdot +}$ is the pyrrole radical cation, M_2 is bipyrrole, and $M_2^{\cdot +}$ is the bipyrrole radical cation. Further details for the calculation are given in the appendix.

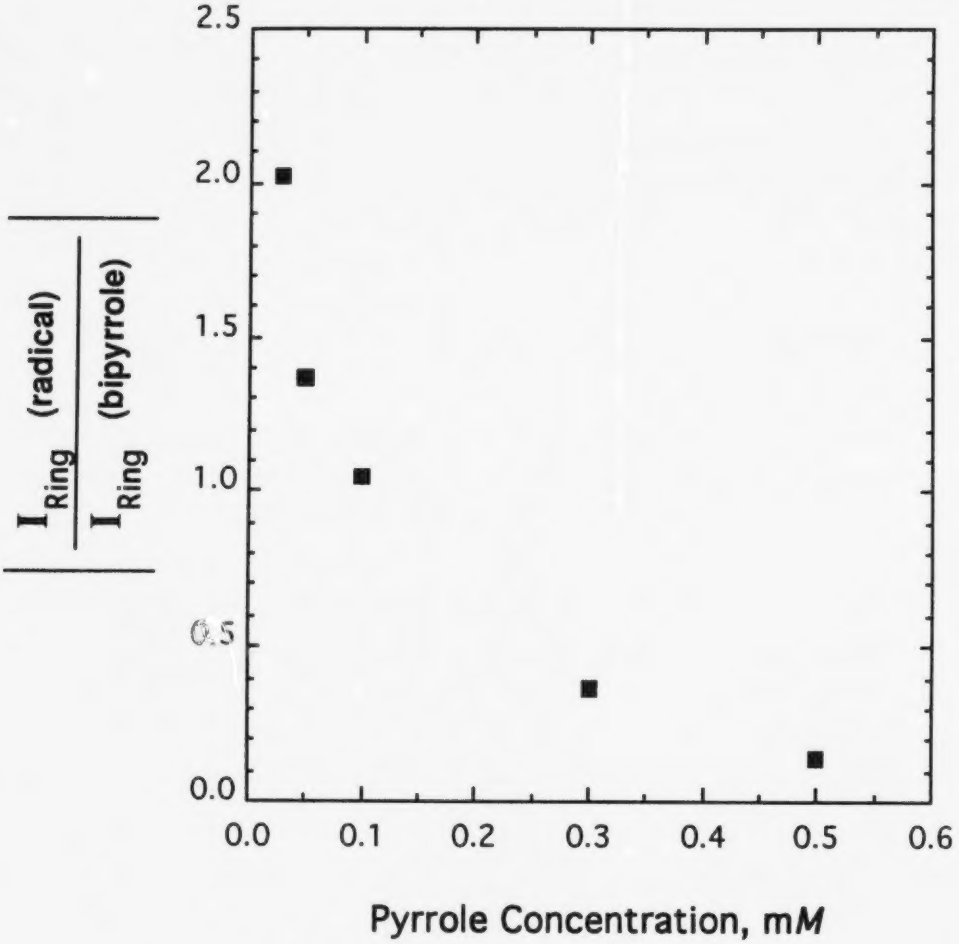

Figure 3.7 Ratio of reduction current to bipyrrole oxidation current (absolute value) versus pyrrole concentrations. Ring potential held at 0.65 V vs SSCE. Disk potential scanned from 0.0 V to 1.6 V vs SSCE. Rotation rate of 4500 rpm.

The calculations required diffusion coefficients for several species. Values for ferrocene, pyrrole, bipyrrole and 2,5-dimethyl pyrrole were measured using the Taylor dispersion method. This method is independent of the difficulties associated with electrochemical measurements of diffusion coefficients for species giving irreversible, complex electrode reactions. Ferrocene was used to compare the method with the value obtained from a Levich plot at a rotating disk. The ratio between these values was used to "correct" the values for the other species obtained by Taylor dispersion, and are given in Table 3.1. For the calculations the pyrrole radical cation was assumed to have the same diffusion coefficient as pyrrole.

The results of the calculations for 0.1 m*M* pyrrole, a rotation rate of 4500 rpm, and a 1.6 μm thick annulus are shown in Figure 3.8. The top of Figure 3.8 shows the experimental current-voltage curves for the ring electrode obtained from a 0.1 m*M* pyrrole solution in acetonitrile. The rotation rate was 4500 rpm and the ring potential was 0.65 V vs SSCE, a potential where both radical cation and bipyrrole are observable. Included in the top of Figure 3.8 is the calculated ring current-voltage curve for the sum of the radical cation and dimer currents. The bottom of Figure 3.8 shows the experimental current-voltage curves for the ring electrode at a ring potential of 0.45 V vs SSCE, a potential where only the radical is observable, as well as the calculated radical cation current.

When the calculated curves are compared to the experimental curves only the general characteristic behavior is seen. The steady state currents for both the radical cation and bipyrrole are obtained and transient behavior for the radical is observed for both calculated curves. However, the sharp spike is not reproduced since the discontinuity in the radical cation concentration incurred by the activation process cannot be accurately modelled by the calculations. However, the calculations do demonstrate that apparently transient behavior is consistent with a non-linear dependence on the radical cation concentration arising from a radical-radical coupling process.

In order to match the experimental steady state dimer and radical cation currents to the calculated values the outer annulus of the disk generating species observed at the ring was taken as only 1.6 μm thick. This indicates that species are escaping from an extremely small area of the disk and that most of the species formed in the disk region are consumed. This also clarifies why the experimental collection efficiencies obtained are significantly smaller than the theoretical value, for instance 9 x 10^{-3} versus 0.216. The rate constants used in the reaction scheme were 1 x 10^{8} liters/mole-sec for all steps, indicating that the solution reactions are close to diffusion controlled overall. This assumption that all steps

Measurement Technique	1 m*M* : Ferrocene (cm^2/s) ± 5%	1 m*M* : Pyrrole (cm^2/s) ± 3%	1 m*M* : Bipyrrole (cm^2/s) ± 5%	1 m*M* : 2,5-DMP (c) (cm^2/s) ± 3%
Taylor Dispersion	2.50×10^{-5}	3.60×10^{-5}	2.58×10^{-5}	2.49×10^{-5}
Electrochemical	2.64×10^{-5} (a)	3.80×10^{-5} (b)	2.72×10^{-5} (b)	2.63×10^{-5} (b)

(a) value obtained using RRDE with 0.1 *M* $NaClO_4$ as electrolyte.

(b) values obtained by multiplying Taylor dispersion value by the ratio of Taylor dispersion to Electrochemical value obtained for ferrocene.

(c) 2,5-Dimethylpyrrole

Table 3.1: Diffusion Coefficients obtained via Taylor Dispersion method.

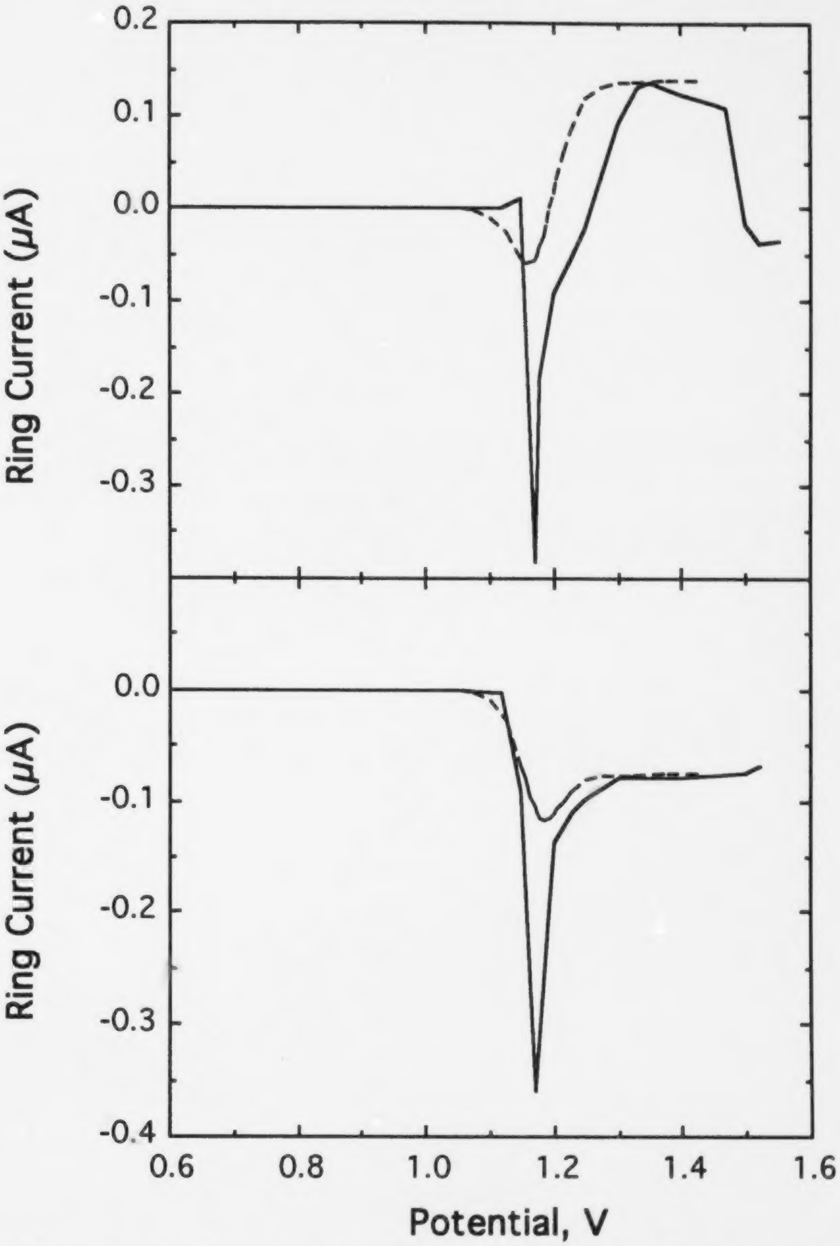

Figure 3.8 Results from calculations for 0.1 m*M* pyrrole solution. Rotation rate of 4500 rpm, 1.6 μm thick annulus and a rate constant of 1 x 10^8 liters/mole-sec.

Top (—) Experimental results with $E_{ring} = 0.65$ V.
(----) Calculated curve for the sum of radical cation and bipyrrole currents.

Bottom (—) Experimental results with $E_{ring} = 0.45$ V.
(----) Calculated curve for the radical cation current only.

proceed at the same rate is obviously a gross estimation, however we lack information to differentiate the various reaction rates. If the rate constants were decreased to 5 x 10^7 liters/mole-sec the annulus thickness increased to 5 μm, however the match with the radical cation current was poorer. Finally when the rate constants were taken as 1 x 10^7 liters/mole-sec the annulus thickness increased to 8 μm and no match with the radical cation current was possible. These kinetic calculations are clearly only a rough approximate of the reaction process.

3.5 Conclusions.

In this work evidence of direct observation of the primary reaction product in pyrrole electropolymerization, the pyrrole radical or radical cation was obtained. Observation of this species is very useful in evaluating the steps involved in polymer film deposition. Since the first observation that the deposition of polypyrrole is analogous to nucleation and three dimensional growth of metals on foreign substrates, the process by which polypyrrole deposition occurs has been the source of controversy and speculation. This study has demonstrated it is not a true three dimensional nucleation and growth process, but rather occurs via solution phase polymerization with subsequent electro-precipitation of oligomers. The process requires the stepwise oxidation of oligomers, and in this sense is stoichiometric rather than chain-like in propagation. These conclusions are evidenced by the coincidence of the rapid growth in current with a pulse of soluble radical product formation at the end of the induction period. Further, the distribution of polymer coating on the electrode at this stage is not random, as would be expected for true three dimensional growth, but shows a pattern attributable to the hydrodynamic flow of solution species formed by oxidation at an active surface site. However, this process is very similar to three dimensional nucleation, in that active surface sites must be formed, and this process is potential, time and electrolyte dependent.

It was also found that a rather crude kinetic model based on radical-radical coupling will generate a peak-shaped ring current/ disk voltage curve for the pyrrole radical species. This supports, but clearly does not prove the radical coupling polymerization model. Importantly, for this model to match the observed data rate constants of 10^7 to 10^8 liter/mol-sec are required. This means that the observation of pyrrole radical species at a ring electrode is feasible, and is not inconsistent with the generally held observation that this species reacts rapidly. While further kinetic analysis of the data is required, the direct observation of the primary reaction products, pyrrole radical and bipyrrole, should open a new window on the effects of solution conditions on polymer formation.

3.6 References.

1. Skotheim, T.A., *Handbook of Conducting Polymers*, Vol.1, Marcel Dekker, New York, **1986**, Chapters 3,8,9.
2. Diaz, A.F.; Kanazawa, K.K.; Gardini, G.P., *Chem. Commun.*, **1979**, 635.
3. Diaz, A.F.; Martinez, A.; Kanazawa, K.K., *J. Electroanal. Chem.*, **1981**, 130,181.
4. Penner, R.M.; Martin, C.R., *J. Electrochem. Soc.*, **1986**, 133, 2206.
5. Nagasubramanian, G.; Distefano, S., Moacanin, J., *J. Electrochem. Soc.*, **1986**,1 33, 305.
6. Warren, L.F.; Anderson, P.J., *J. Electrochem. Soc.*, **1987**, 134, 101.
7. Naoi, K.; Osuka, T., *J. Electrochem. Soc.*, **1987**, 134, 2479.
8. Morse, N.J.; Rosseinsky, D.R.; Mortimer, R.J.; Walton, D.J., *J. Electroanal. Chem.*, **1988**, 255, 119.
9. Vork, F.T.A.; Janssen, L.J.J., *Electrochimica Acta*, **1988**, 33, 513.
10. Diaz, A.F.; Crowley, J.; Bargon, J.; Gardini, G.P.; Torrence, J.B., *J. Electroanal. Chem.*, **1981**, 121, 355.
11. Asavapiriyamont, S.; Chandler, G.K.; Gunawardenu, G.A.; Pletcher, D.J., *J. Electroanal. Chem.*, **1984**, 177, 229.
12. Downard, A.J.; Pletcher, D.J., *J. Electroanal. Chem.*, **1986**, 206, 139.
13. Chandler, G.K.; Pletcher, D.J., *Special Reports Electrochemistry*, Vol.10, Royal Society Chemistry, London, **1985**, p.117.
14. Miller, L.L.; Zinger, B.; Zhou, Q.X., *J. Am. Chem. Soc.*, **1987**, 109, 2267.
15. Josowicz, M.; Janata, J.; Ashley, K.; Pons, S., *Anal. Chem.*, **1987**, 59,253.
16. Noufi, R.; Tench, D.; Warren, L.F., *J. Electroanal. Chem.*, **1981**, 128, 2596.
17. Imana, M.; Waller, *J., Anal. Chem.*, **1986**, 58, 2979.
18. Otero, T.F.; Tejada, R.; Elola, A.S., *Polymer*, **1987**, 28, 651.
19. Baker, C.K.; Reynolds, J.R., *J. Electroanal. Chem.*, **1988**, 251, 307.
20. Genies, E.M.; Bidan, G.; Diaz, A.F., *J. Electroanal. Chem.*, **1983**, 149, 101.
21. Waltman, R.J.; Bargon, *J., Tetrahedron*, **1984**, 40, 3963.
22. Baker, C.K.; Reynolds, J.R., *Polymer Prepr.*, **1987**, 28, 284.

23. Christensen, P.A.; Hamnett, A., *Electrochimica Acta*, **1991**, 36, 1263.

24. Raymond, D.E.; Harrison, D.J., *J. Electroanal. Chem.*, **1990**, 296, 269.

25. John, R.; Wallace, G.G., *J. Electroanal. Chem.*, **1991**, 306, 157.

26. Rosseinsky, D.R.; Morse, N.J.; Slade, R.C.T; Hix, G.B.; Mortimer, R.J.; Walton, D.J., *Electrochimica Acta*, **1991**, 36, 733.

27. Takakubo, M., *J. Electroanal. Chem.*, **1989**, 258, 303.

28. Lang, P.; Chao, F.; Costa, M.; Garnier, F., *Polymer*, **1987**, 28, 668.

29. Tanaka, K.; Shichiri, T.; Wang, S.; Yamabe, T., *Synth. Metals*, **1988**, 24, 203.

30. Noftle, R.E.; Pletcher, D.J., *J. Electroanal. Chem.*, **1987**, 227, 229.

31. Otero, T.F.; de Larreta-Azelair, E., *Polymer*, **1988**, 29, 1522.

32. Hillman, A.R.; Mallen, E.F., *J. Electroanal. Chem.*, **1987**, 220, 351.

33. Albery, W.J.; Hitchman, M.L., "*Ring-Disk Electrodes*", Oxford University Press, London, **1971**, Chapter 3, p.22.

34. Cussler, E.L., "*Diffusion: Mass transfer in fluid systems.*", Cambridge University Press, New York, **1984**, p. 89.

35. Potts, H.A.; Smith, G.F., *J. Chem. Soc.* **1957,** 4018.

36. Chiang, Y.; Whipple, E.B., *J. Am. Chem. Soc.*, **1963**, 85, 2763.

37. Naqvi, N.; Fernando, Q., *J. Org. Chem.*, **1960**, 25, 5551.

38. Bruckenstein, S.; Sharkey, J.W., *J. Electroanal. Chem.*, **1988**, 241, 211.

39. Andrieux, C.P.; Audebert, P.; Hapiot, P.; Saveant, J.M., *J. Am. Chem. Soc.*, **1990**, 112, 2439.

40. Levich, V.G., "*Physicochemical Hydrodynamics*", Prentice-Hall, New Jersey, **1962**, Chapter 2, p.66.

41. Bruckenstein, S.; Feldman, G.A., *J. Electroanal. Chem.*, **1965**, 9, 395.

42. Albery, W., J.; Bruckenstein, S., *Trans. Faraday Soc.* ,**1966**, 62, 1920.

43. Filinovskii, V., Yu., *Elektrokhimiya*, **1987**, 23, 1219.

44. Filinovsky, V., Yu.; Kadija, I., V.; Nicolic, B., Z.; Nakic, M., B., *J. Electroanal. Chem.*, **1974**, 54, 39.

Chapter 4

SpectroElectrochemical Investigation of the Electropolymerization of Pyrrole.

4.1 Introduction.

Various electrochemical techniques such as chronoamperometry, at both macro- and microelectrodes [1-5], cyclic voltammetry at normal and rapid scan rates [3-10], and the rotating ring-disk electrode system [11-14] have been used to investigate the electropolymerization mechanism of pyrrole. From these analyses it has been interpreted that the polymerization process involves the formation of soluble oligomeric species via a radical-radical coupling mechanism. The use of spectroscopic methods as a probe for the polymerization mechanism by direct detection of these intermediates has been limited [15,16], although numerous studies have been reported in which infra-red and UV/VIS spectroscopy were used to investigate the polymer film properties [9,10,17-19]. In the UV/VIS study the possible presence of oligomeric species was reported, however the identity of these species was not given. In the present study UV/VIS was used to monitor the electropolymerization of pyrrole in the presence of various electrolytes ($NaClO_4$, TBAP and $TBABF_4$) and solvents, (acetonitrile and propylene carbonate). The observation of oligomeric species and protonated pyrrole will be presented.

A version of this chapter has been submitted for publication. D.E Raymond and D. Jed Harrison, 1992. Journal of Electroanal. Chem.

4.2 Experimental.

4.2.1 Chemicals. HPLC grade CH_3CN (Burdick and Jackson) was distilled over CaH_2 prior to use. Propylene carbonate, PC, (Eastman Organic Chemicals) was vacuum distilled four times with the middle fraction being retained from each distillation. Purity of both solvents was demonstrated by their respective UV spectra. $NaClO_4$ (Fisher Scientific), TBAP (Southwestern Analytical Chemicals) and $TBABF_4$ (Southwestern Analytical Chemicals) were vacuum dried and used without further purification. Pyrrole (Aldrich) was vacuum distilled and stored under argon.

4.2.2 Spectroelectrochemical cell. The thin layer spectroelectrochemical cell, shown in Figure 4.1, was constructed using two quartz microscope slides which were sealed together with epoxy (Clear-Hysol). The space between the slides was maintained at 2 mm using spacers made from glass microscope slides. Also sealed between the slides was a Pt gauze counter electrode. The top of the cell remained open so the working and reference electrodes could be easily removed. A thin Pt wire was coiled and served as the working electrode, while a silver wire served as the pseudo-reference electrode. Solutions of pyrrole were introduced into the top of the cell using a pipette. The whole assembly was then sealed at the top using parafilm and the solution contained was purged for 5 minutes with nitrogen. The cell was placed in a Hewlett-Packard UV-vis photodiode array spectrometer and the spectra recorded according to the procedure described below.

4.3 Procedures.

4.3.1 Spectroelectrochemical Analysis.

To ensure that a proper reference was available reference spectra of a solution containing only electrolyte with and without electrodes in the cell were obtained before the spectra of the electrolyzed pyrrole solution were taken. The potential dependence and time dependence of the species generated during the polymerization of pyrrole were investigated as outlined below. In these experiments 50 m*M* pyrrole solutions in acetonitrile with either $NaClO_4$, TBAP, or $TBABF_4$ as electrolyte were used, while only TBAP and $TBABF_4$ were used in propylene carbonate. All solutions were prepared immediately before use to minimize atmospheric water uptake.

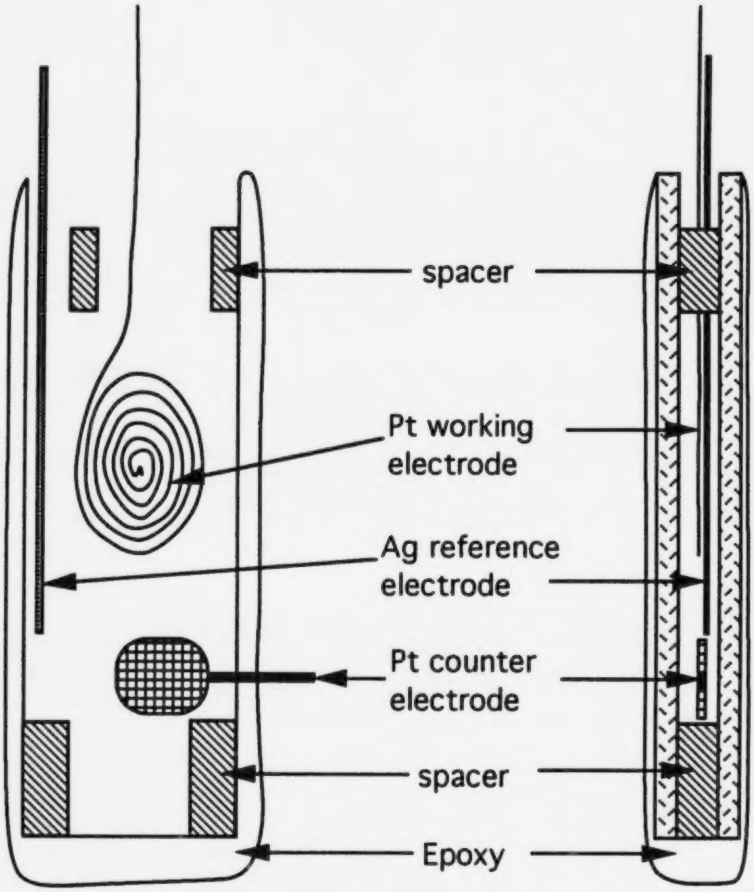
spacer
Pt working electrode
Ag reference electrode
Pt counter electrode
spacer
Epoxy

Figure 4.1 Schematic of the Spectroelectrochemical cell.

A. Potential Dependence Study.

The pyrrole solution was placed in the cell and purged with nitrogen for 5 minutes. The cell was then sealed and oriented in the spectrometer such that the light path was directly through the center of the coiled working electrode. The working electrode potential was applied for 30 seconds and a spectrum was then taken immediately after the potential was stepped back to 0.0 V. The magnitude of the applied potentials ranged from 0.0 V to 0.85 V vs Ag(s). Spectra were taken both with the working electrode in and out of the light path. The potentials of the Ag (s) pseudo reference electrode versus an SCE in different solvent systems are given in Table 4.1. The values were obtained after a 30 second electrolysis of 50 mM pyrrole in the appropriate solvent system.

B. Time Dependence Study.

The pyrrole solution was placed in the cell and purged with nitrogen for 5 minutes. The cell was then sealed and oriented in the spectrometer such that the light path was directly through the center of the coiled working electrode. The working electrode was stepped from 0.0 V to 0.8 V vs Ag (s) for 30 seconds and a spectrum was immediately taken after the potential was stepped back to 0.0 V. Spectra were again taken 5 minutes and 10 minutes later. Spectra were taken with the working electrode both in and out of the light path.

4.3.2. Acidic Polymerization of Pyrrole.

An acetonitrile solution containing 1.0 m*M* pyrrole and 0.1 *M* $NaClO_4$ as electrolyte was introduced into the spectroelectrochemical cell and purged for 5 minutes. The cell, without electrodes, was sealed at the top with parafilm and the UV-VIS spectrum was taken. After the spectrum was acquired 50 µL of 0.1% v/v $HClO_4$ in acetonitrile containing 0.1 *M* $NaClO_4$, was added to the cell and the spectrum taken immediately. The $HClO_4$ solution was prepared from 20 mL of concentrated $HClO_4$ from which the water was removed by addition of an appropriate amount of acetic anhydride. A spectrum was then taken every 30 seconds for the first 5 minutes, then every 15 minutes thereafter for one hour.

Solvent System	Potential vs SCE
0.1 *M* $NaClO_4$/ CH_3CN	0.006 V
0.1 *M* $TBABF_4$/ CH_3CN	-0.024 V
0.1 *M* $TBAClO_4$/ CH_3CN	-0.045 V
0.1 *M* $TBABF_4$/ PC	-0.056 V
0.1 *M* $TBAClO_4$/ PC	-0.020 V

Table 4.1: Potential of the Ag (s) pseudo reference electrode versus the saturated calomel electrode in the various solvent systems studied.

4.4 Results and Discussion.

4.4.1 Potential and Time Dependent Spectra.

The potential dependent and time dependent spectra obtained during electropolymerization of 50 m*M* pyrrole in acetonitrile containing 0.1 *M* $NaClO_4$ are shown in Figures 4.2 and 4.3 respectively. In Figure 4.2 each spectrum was obtained 30 seconds after the application of the indicated applied potentials. Figure 4.3 shows the progression over 0.5 to 10 minutes after the application of a potential of 0.80 V Ag for 30 seconds. In both Figures 4.2 and 4.3 absorbance peaks are observed at wavelengths of 242, 336, 437 and 500 nm. It is clear that the absorbance at these wavelengths increases as the potential is increased. However, as the time after electrolysis increases the absorbance at 242 nm is seen to decrease while the other values remain essentially constant. If the species at 242 nm were a precursor for the species absorbing at longer wavelengths, then, as the absorbance at 242 nm decreased increases at 336, 437 and 500 nm should be observed. This behaviour was not seen, indicating the species at 242 nm is not a precursor.

The polymer is known to absorb between 400 nm and 800 nm [15,20] and may contribute to the absorbance observed. Figure 4.4 is the spectrum obtained from the same solution as above, but with the working electrode removed from the light beam path after electrolysis. Care was taken not to introduce air into the cell, or disturb the cell position in the process. Absorbance peaks are clearly observed at 242, 277, 330, 432 and 500 nm, indicating the presence of solution species. Also, the species observed are quite stable since the spectrum was acquired several minutes after electrolysis, and are most likely neutral reaction products. The absorbance peaks at 336 and 437 nm in Figures 4.2 and 4.3 have shifted to 330 and 432 nm in Figure 4.4. This suggests that the polymer is contributing to the absorbance observed in Figures 4.2 and 4.3, resulting in slightly broadened peaks.

4.4.2 Bipyrrole and Terpyrrole Spectra.

The species responsible for the absorbance peaks between 300 nm and 500 nm reported by Genies *et al* [15] were identified only as oxidized pyrrole oligomers produced as intermediates. To aid in assigning the peaks observed the spectra of possible species were obtained for comparison to the above figures. The spectrum of synthesized bipyrrole, taken in acetonitrile containing 0.1 *M* $NaClO_4$, is shown in Figure 4.5. A peak maximum

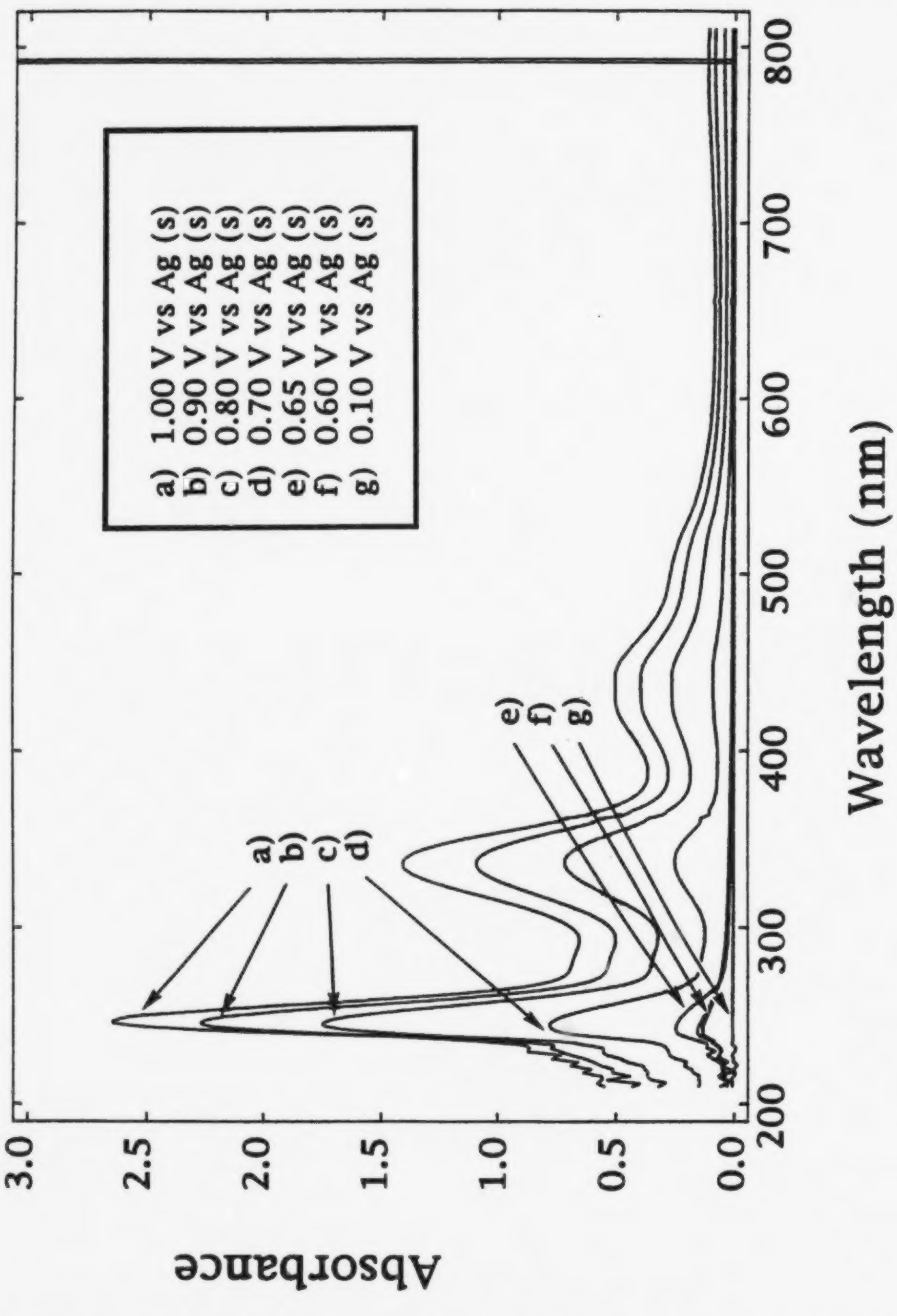

Figure 4.2 Potential dependent spectra obtained in acetonitrile containing 50 m*M* pyrrole and 0.1 *M* $NaClO_4$ as electrolyte. Spectra taken 30 second after electrolysis at the indicated applied potentials. The working electrode was in the path of the spectrometer light beam while the spectra were taken.

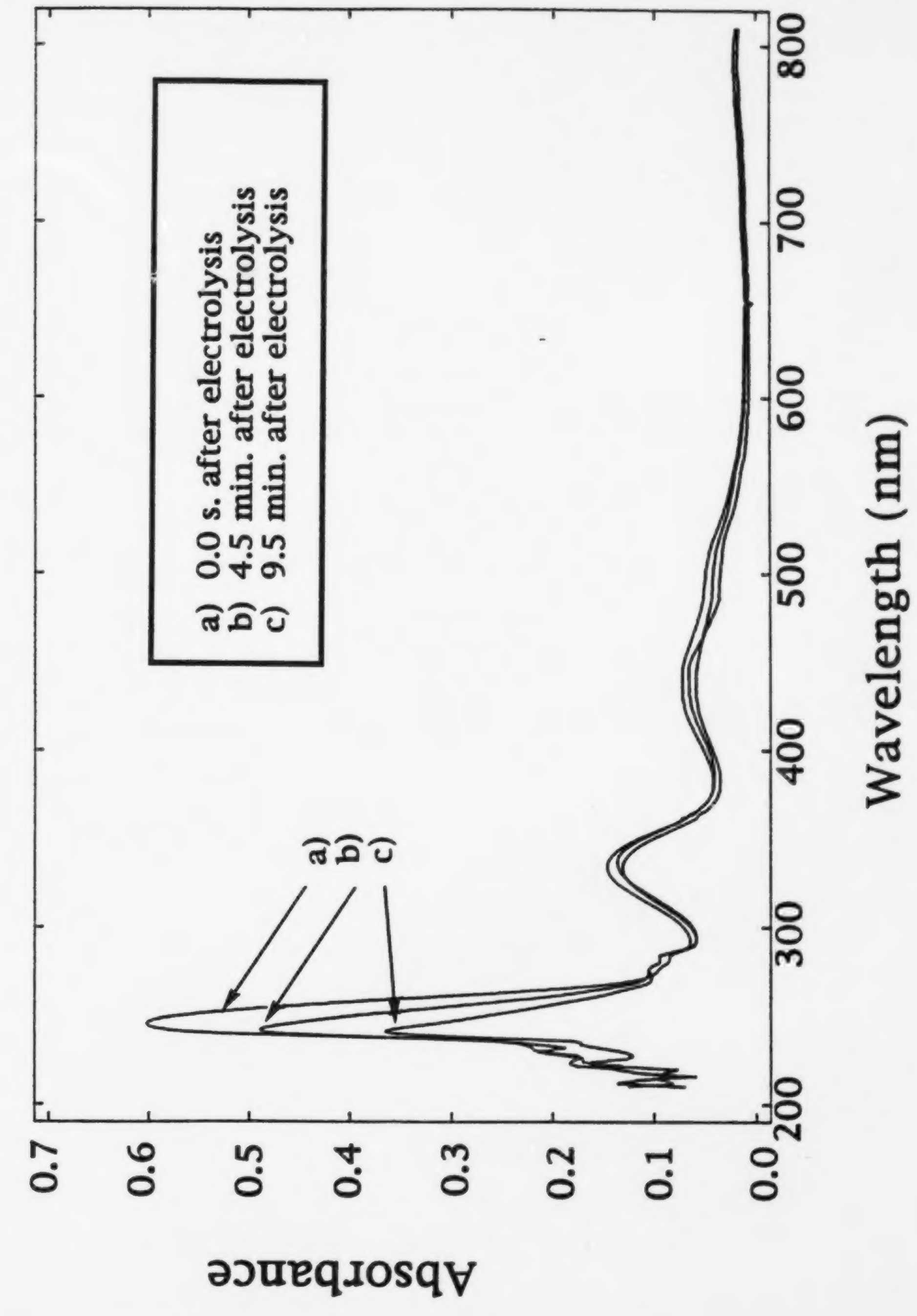

Figure 4.3 Time dependent spectra obtained in acetonitrile containing 50 m*M* pyrrole and 0.1 *M* $NaClO_4$ as electrolyte. The time after electrolysis the spectra were acquired is given. The working electrode was in the path of the spectrometer light beam while the spectra were taken.

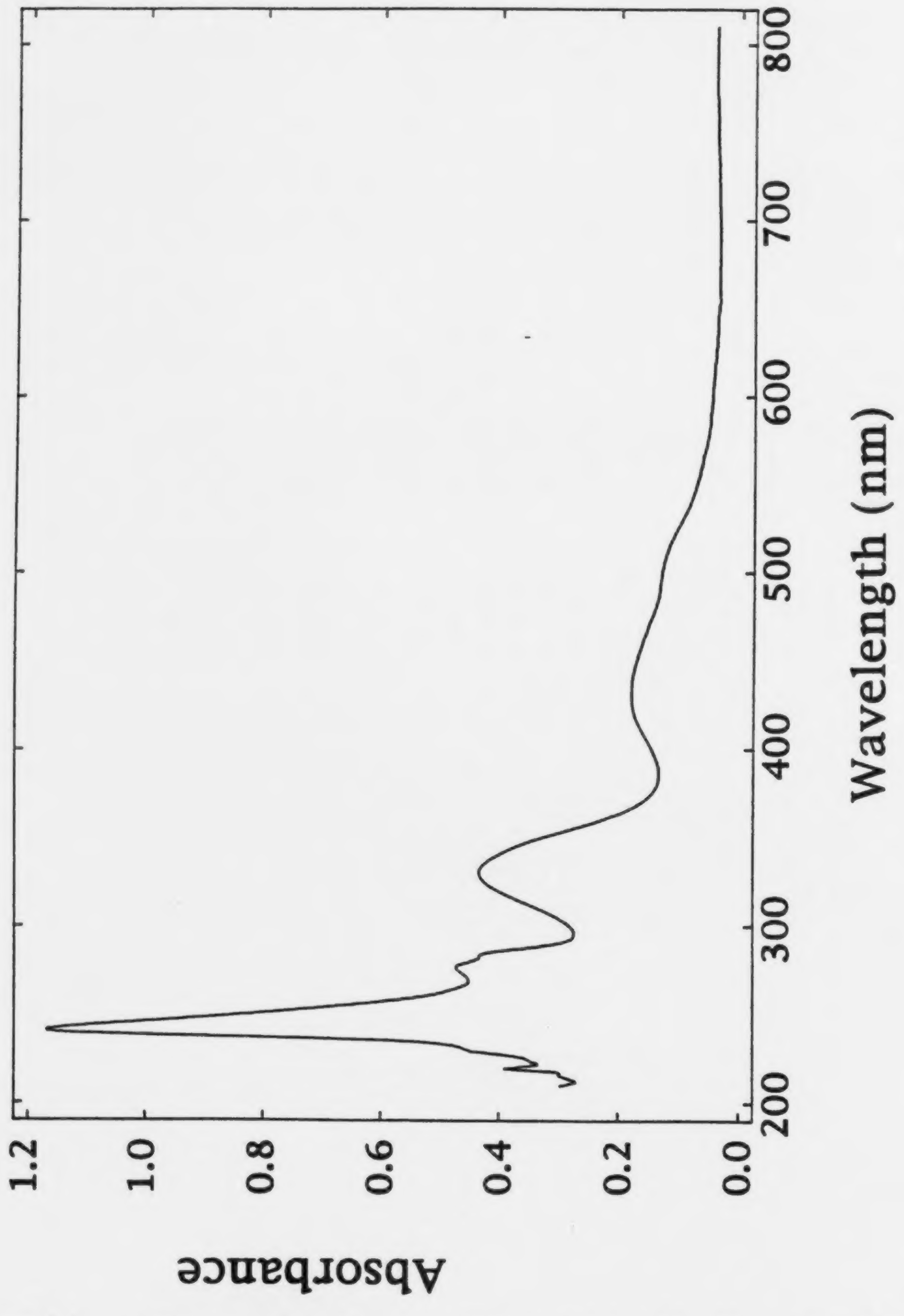

Figure 4.4 Spectrum obtained in acetonitrile containing 50 m*M* pyrrole and 0.1 *M* $NaClO_4$ as electrolyte. The spectrum was taken after electrolysis with the working electrode out of the path of the spectrometer light beam.

of 277 nm is observed with a small shoulder at 285 nm, and agrees very well with the peak at 277 nm in Figure 4.4. This is consistent with the rotating ring-disk study which identified bipyrrole as a solution phase intermediate [14]. Its presence in solution also shows that a reasonable amount does escape the electrode reaction/diffusion layer.

The spectrum of bipyrrole has been reported in methanol [20,24] as having an absorbance peak maximum at 286 nm, while the spectrum of terpyrrole in methanol has an absorbance peak maximum at 345 nm [20,26]. This corresponds to a 9 nm bathochromic shift for bipyrrole relative to the value obtained in acetonitrile. The absorbance spectrum of bipyrrole in acetonitrile containing 0.1 *M* $NaClO_4$ is shown in Figure 4.5. If the same shift is assumed for terpyrrole then an absorbance should occur at about 336 nm in acetonitrile, whereas Figure 4.4 shows a peak at 330 nm and assignment of this peak as terpyrrole is equivocal. However, data for other conjugated oligomeric species formed from thiophene or benzene [20] show that there is significant curvature in a plot of peak absorbance wavelength (λ_{max}) versus the number of monomer units, as illustrated in Figure 4.6. Plotting the λ_{max} values obtained from Figure 4.4 against an assumed number of pyrrole units as in Figure 4.6 strongly suggests that the peak at 330 nm is due to terpyrrole. Linear extrapolation of the pyrrole values measured in methanol [20], as shown by the dashed line in Figure 4.6, suggest an assignment of the peaks at 432 nm and 500 nm to quaterpyrrole and quinquepyrrole could be made. This is not completely convincing though, since curvature in the extrapolation is expected based on other systems studied. Recently, the λ_{max} of the stable radical cation of the α-coupled trimer of 3-methylthiophene was obtained using UV/VIS spectroelectrochemistry and reported to be 550 nm [27]. Identification of the radical cation was obtained from comparison of the λ_{max} to literature values. It is possible that the absorbances observed at longer wavelengths are due to stable radical cations of higher oligomers or complexes of such radicals with neutral oligomers [28], but the spectra of such species are not available. However, stability of such species over several minutes in a solution at room temperature that was only partially protected from air and near an electrode held at 0.0 V vs Ag seems unlikely.

Pyrrole and bipyrrole were copolymerized in acetonitrile containing 0.1 *M* $NaClO_4$. A potential of 0.6 V vs Ag was initially used as it was anticipated that pyrrole was electro-inactive at this potential. A spectrum was acquired 30 seconds after the application of the potential with only an absorbance peak at 336 nm observed. This is the same wavelength maximum observed during pyrrole oxidation when the electrode remains in the optical path, and is most probably due to terpyrrole. Cyclic voltammetric experiments within the

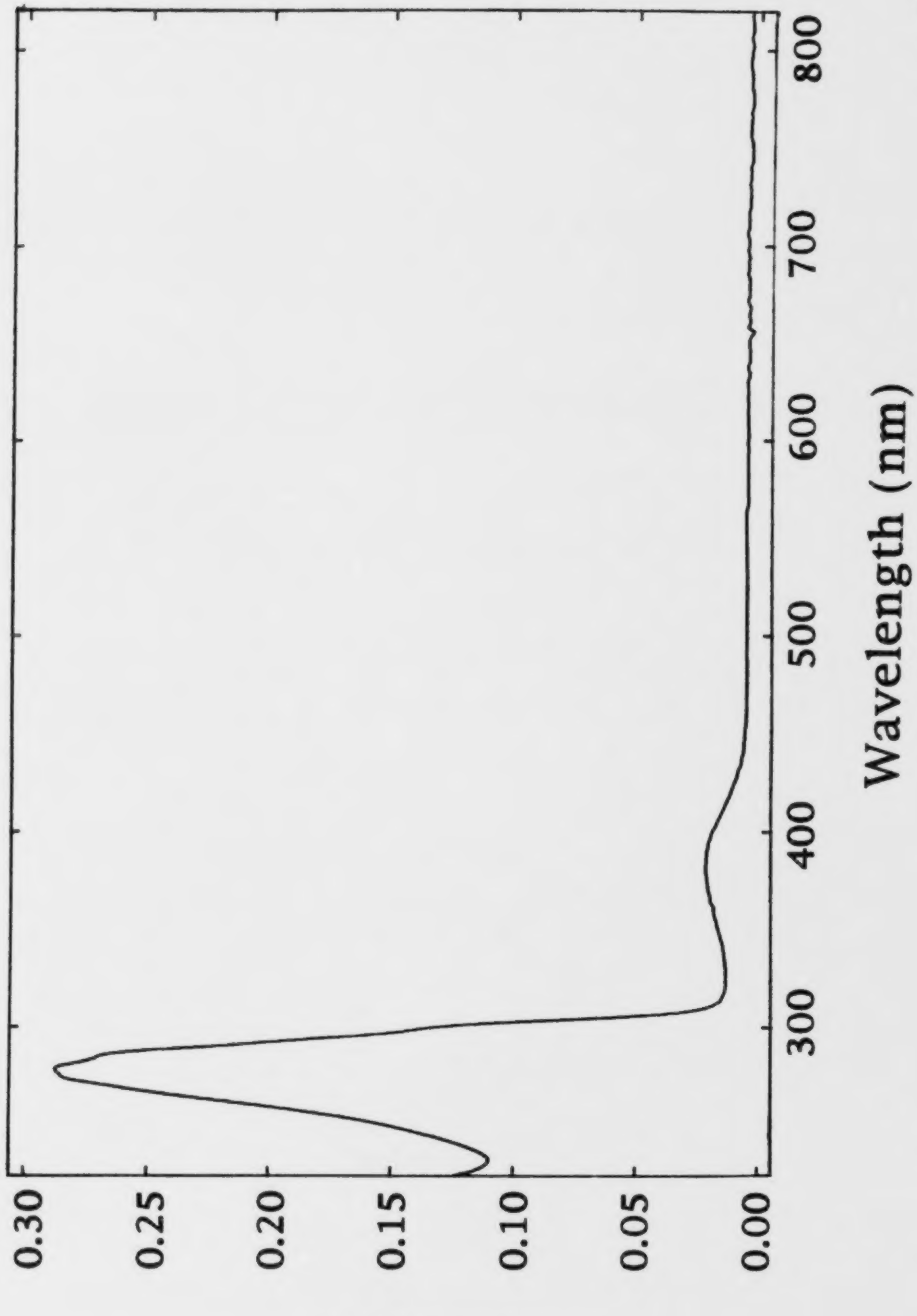

Figure 4.5 Spectrum of bipyrrole in acetonitrile containing 0.1 *M* $NaClO_4$ as electrolyte. Spectrum was taken in spectroelectrochemical cell without electrodes.

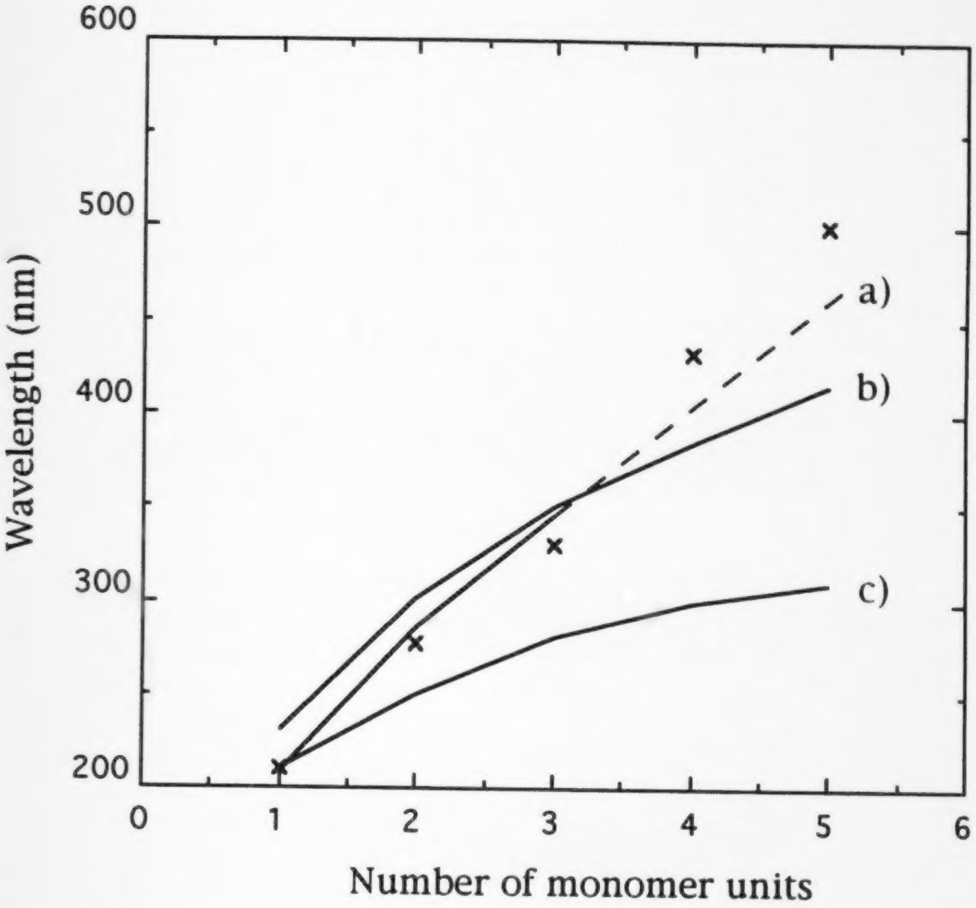

Figure 4.6 Plot of Absorbance versus λ_{max} for (a) pyrrole, (b) thiophene, (c) benzene and their respective oligomers in CH_3OH (ref. 20). Crosses are experimental results for pyrrole and oligomers obtained in CH_3CN, without correction for the effect of solvent on λ_{max}. The dashed line is an extrapolation of the pyrrole data from reference 6.

spectroelectrochemical cell indicated that pyrrole oxidation actually began at approximately 0.5 V vs Ag. Thus, the formation of terpyrrole in the mixture could have occurred from coupling of pyrrole and bipyrrole radical cations. The absence of higher oligomers may be a result of the small concentration of pyrrole radicals generated at the potential used. When the potential was increased to 1.0 V vs Ag the observed spectrum was identical to that shown in Figure 4.2. Also, after removal of the working electrode the copolymerization spectrum was similar to Figure 4.4, but with no observation of the bipyrrole peak at 277 nm. The is because the reference spectrum of the mixture contained bipyrrole.

4.4.3 Acid Polymerization Spectra.

Pyrrole is a weak base that undergoes proton exchange at all four carbon atoms and nitrogen under mildly acidic conditions. Direct evidence for protonation at the 2-position has been obtained by ^{1}H NMR spectroscopy in acidic media [22], which also found that protonation at the 3-position in unsubstituted pyrrole does not readily occur [23]. The pK_a obtained for protonation at the 2-position is -3.8, whereas that for the 3-position has been estimated as -5.9 [22]. Direct determination of the pK_a for protonation on the nitrogen atom has not been possible, but calculations based on N-protonation studies of carbazole lead to an estimation of -10 [29]. This implies that at equilibrium protonation at the 3-position is 1% of that at the 2-position, while protonation at the nitrogen is 1 million times less. This is consistent with the well-known predominance of pyrroles for electrophilic attack at the 2-position and is supported by simple theoretical arguments regarding the relative stabilities of the protonated species, shown below. C-protonation at the 2-position of the pyrrole ring produces resonance stabilized pyrrolenine **(1a)** in which the positive charge may be delocalized over four atoms **(1a-1c)**, whereas protonation at the 3-position yields pyrrolenine **(2a)** in which the charge is delocalized over only two atoms **(2a-2b)**. Therefore, pyrrolenine **(1)** is the more thermodynamically stable protonated species.

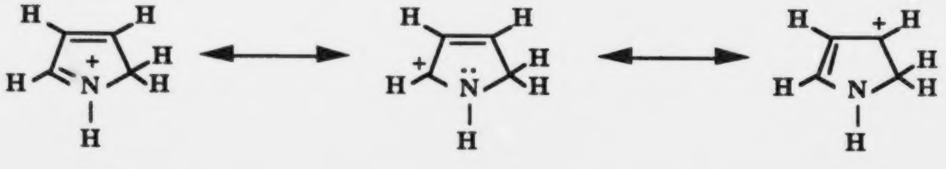

(1a) **(1b)** **(1c)**

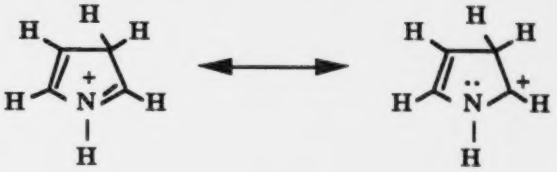

(2a) (2b)

It has been known for nearly a century that pyrrole can undergo oligomerization under acidic conditions and ultimately form intractable polymers [30,31]. Pyrrole forms a trimer [21] on treatment with dry HCl in ether, or on brief contact with 6 M HCl. The mechanism of formation of the trimer is shown in scheme 4.1. The formation of the trimer is presumably by way of initial nucleophilic attack of a neutral pyrrole molecule **(1)** on the 3-protonated form of pyrrole **(2)**. The resulting intermediate dipyrrole derivative **(3)** then aromatizes to give the dipyrrole derivative **(4)**, which is subsequently protonated at the 3-position **(5)**. Further attack by another molecule of pyrrole then affords the trimer **(7)**. The unexpected involvement of 3-pyrrolenine has been attributed to its greater electrophilic reactivity than the more abundant 2-pyrrolenine, and although 2-protonation of pyrrole is favoured thermodynamically, kinetic protonation of the 3-position is more rapid [22].

The trimer **(7)** can be obtained only under carefully controlled conditions and, when treated with acid under anaerobic conditions [32], undergoes further polymerization to form colorless materials. A possible side reaction competing with the formation of trimer is the reaction forming 2,2'-(1'-pyrrolinyl)pyrrole, shown in scheme 4.2. This process involves initial nucleophilic attack of a neutral pyrrole molecule **(1)** on the 2-protonated form of pyrrole **(8)** rather than the 3-protonated form. The resulting intermediate dipyrrole derivative **(9)** then aromatizes to give the dipyrrole derivative **(10)**. This species is subsequently protonated at the remaining 3-positions to yield 2,2'-(1'-pyrrolinyl)pyrrole **(11)**.

The ^{1}H NMR studies of protonation of pyrrole have also been complemented and supported by UV spectral investigations [22,33,34]. Pyrrole, for example, absorbs at λ_{max} 205 nm in aqueous solution, whereas the conjugate acid corresponding to 2-protonation, absorbs at 241 nm in 7.6 M H_2SO_4. The value for the conjugate acid corresponding to 3-protonation at unsubstituted pyrrole was not given. Meanwhile, 2,2'-(1'-pyrrolinyl)pyrrole was found to absorb at 324 nm in methanol [25]. The trimer **(7)** consists of a saturated pyrrole ring separating two unsaturated moieties, consequently, due

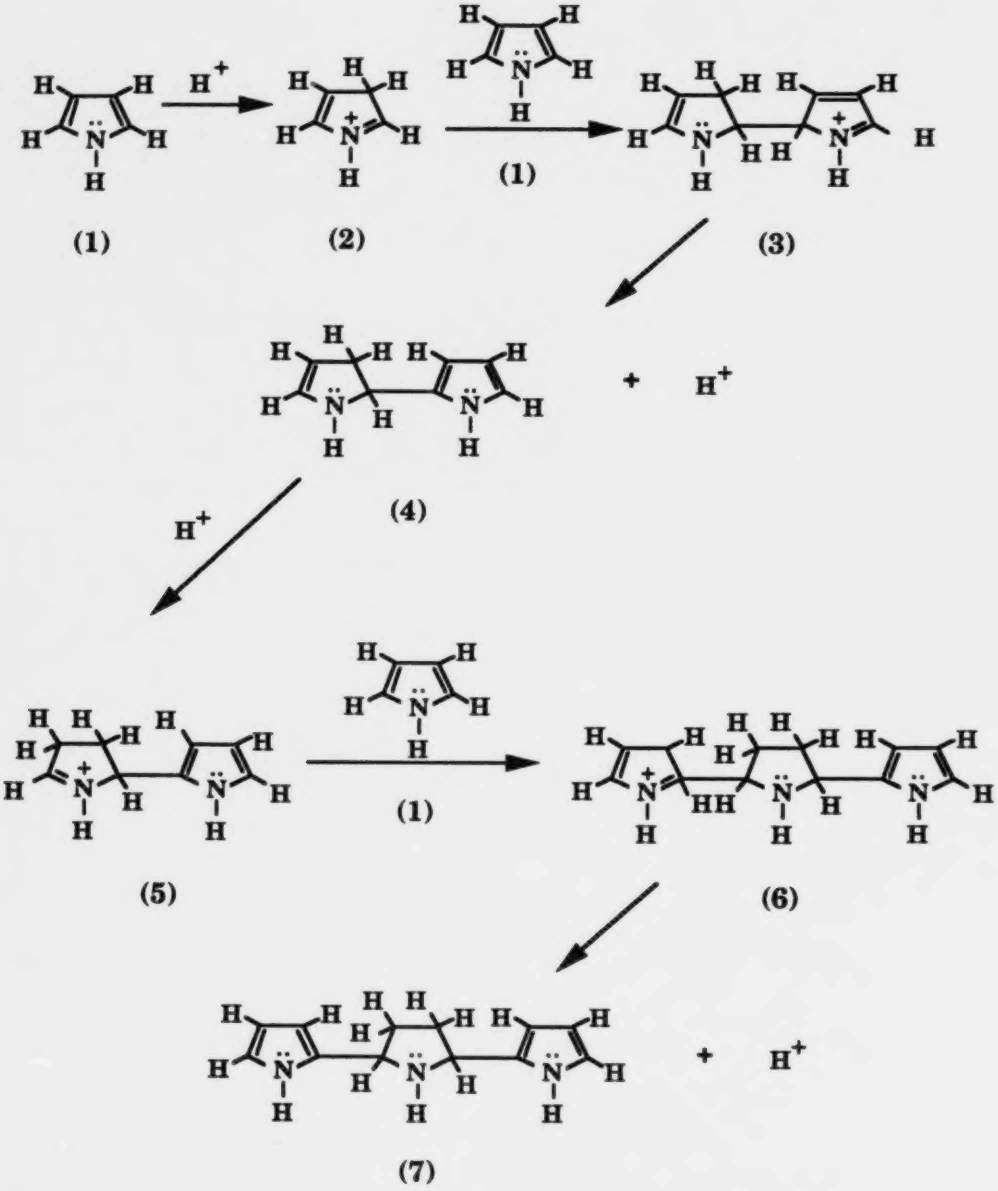
H$^+$
(1)
(2)
(1)
(3)
+ H$^+$
(4)
H$^+$
(1)
(5)
(6)
+ H$^+$
(7)

Scheme 4.1 Acidic polymerization: formation of pyrrole trimer.

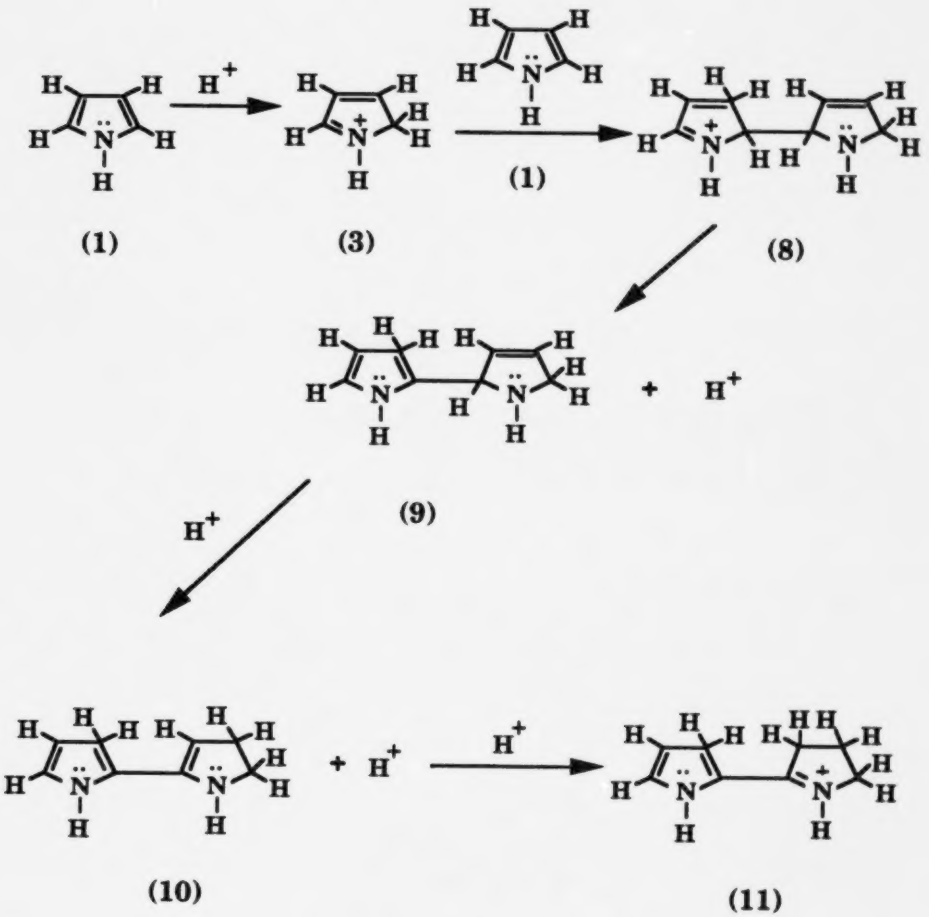
(1)
(3)
(1)
(8)
(9)
(10)
(11)
H⁺

Scheme 4.2 Formation of 2,2'-(1'-pyrrolinyl)pyrrole.

to the loss of conjugation this molecule has an absorption maximum similar to pyrrole, with a reported value of 204 nm [21].

Protons are known to be released during the electropolymerization of pyrrole [12-14] at a concentration similar to the pyrrole bulk concentration. Therefore the formation of protonated pyrrole, trimer and 2,2'-(1'-pyrrolinyl)pyrrole is possible. Also, since conditions used are essentially anaerobic further polymerization of the trimer may occur. To investigate whether protonated pyrrole is present during electropolymerization, dry perchloric acid was added to a purged acetonitrile solution containing 1.0 m*M* pyrrole and 0.1 *M* $NaClO_4$. After addition of the acid the absorbance spectrum was immediately taken with two absorbance peaks being observed at 244 nm and 321 nm. The spectrum obtained 30 minutes after addition of the acid is shown in Figure 4.7. The peaks at 244 nm and 321 nm are likely due to protonated pyrrole and 2,2'-(1'-pyrrolinyl)pyrrole respectively. The absorbance of pyrrole in the reference makes the observation of the trimer impossible. The peak at 244 nm has apparent shoulders which may be the result of further polymerization of the trimer and other species..

The acidic polymerization of pyrrole was monitored as a function of time. The plot of the absorbance for both protonated pyrrole and 2,2'-(1'-pyrrolinyl)pyrrole versus time is given in Figure 4.8. The slight variation in absorbance for protonated pyrrole is likely due to instrumental drift. Meanwhile, the absorbance for 2,2'-(1'-pyrrolinyl)pyrrole increased continuously for the period investigated, but exhibits two linear regions in the absorbance versus time plot. Acidic polymerization of pyrrole is a catalytic process and therefore it is not unreasonable that the absorbance for protonated pyrrole remains essentially constant until the concentration of pyrrole is significantly diminished. The change in the absorbance for 2,2'-(1'-pyrrolinyl)pyrrole after 2.5 minutes is probably due to the competing side reaction forming more favourable product, the trimer. The peak at 242 nm in Figure 4.4 may also be protonated pyrrole, although the slight wavelength shift of 2 nm suggests the presence of a different species. The possibility of an ion pair of the radical cation and the anion ClO_4^- is unlikely due to the unstable nature of the radical cation and that the spectrum given in Figure 4.4 was obtained several minutes after the applied potential was removed. The results obtained from electropolymerization of pyrrole in acetonitrile containing 0.1 *M* $NaClO_4$ and the literature values are summarized in Table 4.2. Identical experiments were performed with different electrolytes and solvent. Figure 4.9 shows the spectrum obtained in propylene carbonate containing 0.25 *M* TBAP as electrolyte. The results obtained from the propylene carbonate and other acetonitrile

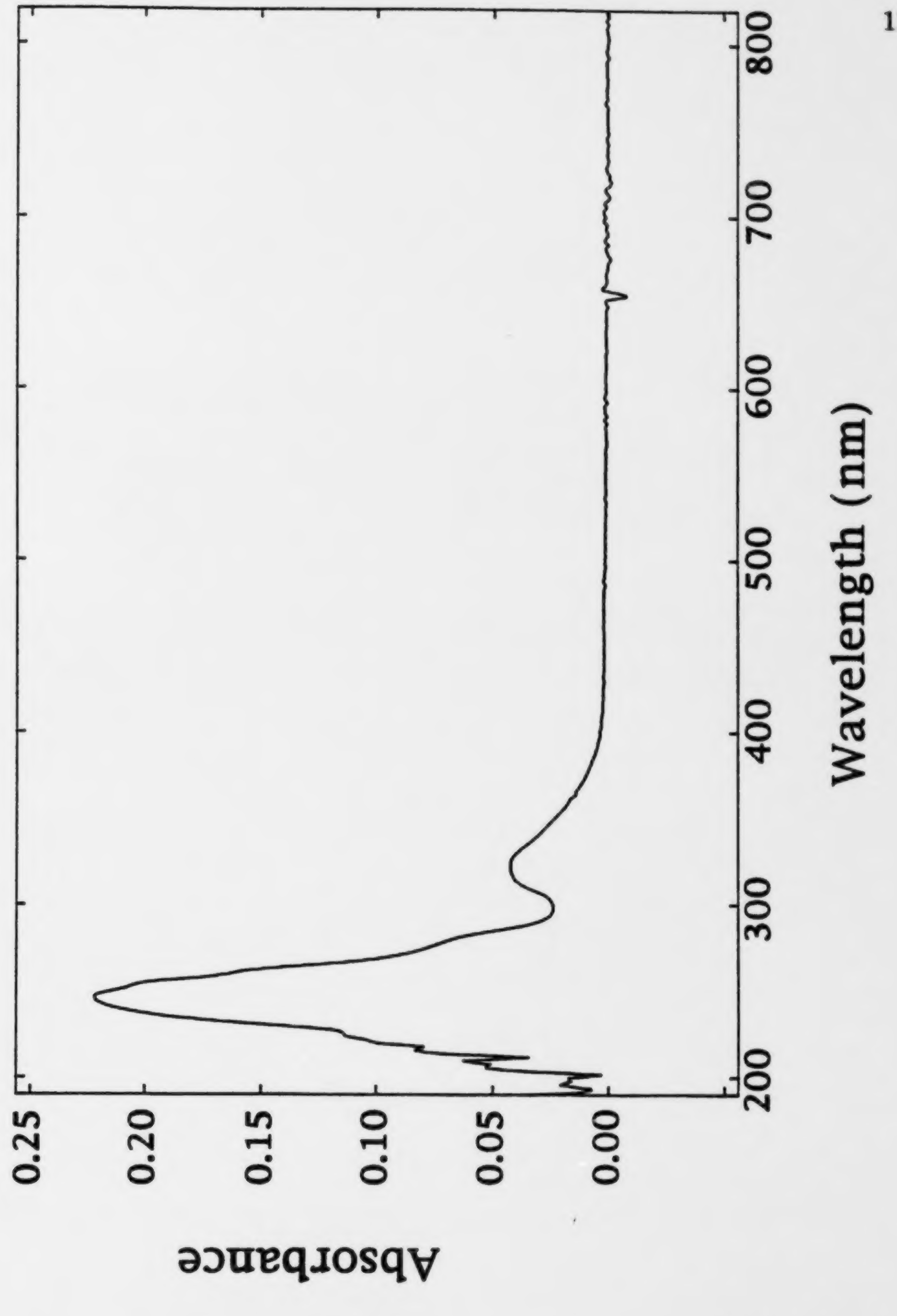

Figure 4.7 Spectrum obtained during acid polymerization. Acquired 30 minutes after addition of $HClO_4$ to 1 m*M* pyrrole in acetonitrile containing 0.1 *M* $NaClO_4$ as electrolyte. Spectrum was taken in spectroelectrochemical cell without electrodes.

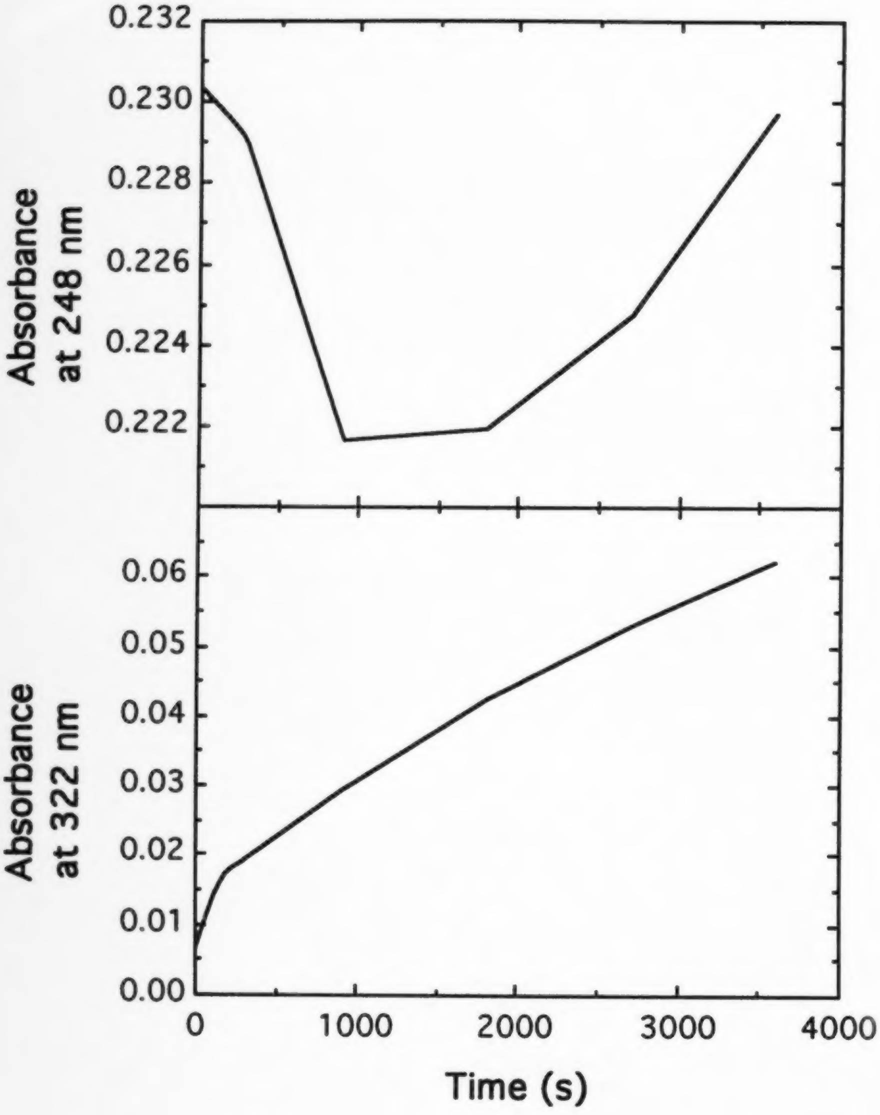

Figure 4.8 Plot of Absorbance versus Time for protonated pyrrole (top) and protonated bipyrrole (bottom).

Species	λ_{max} (nm)					
	Literature.		Experimental. No Electrolysis.		Value in Acetonitrile [d]	Experimental. Electrodes removed after Electrolysis.
	MeOH (a)	H_2SO_4 (b)	MeOH	CH_3CN		
Pyrrole	208	-----	210	210		-----
Bipyrrole	285	-----	286	277		277
Terpyrrole	345	-----	-----	-----	336	330
Quaterpyrrole [e]	-----	-----	-----	-----		432
Quinque-pyrrole [e]	-----	-----	-----	-----		500
Protonated pyrrole	-----	241	244 [c]	-----		242
2,2'-(1-pyrrolinyl)pyrrole	324	-----	321 [c]	-----		-----

a) Methanol: References 20, 25, and 26.
b) 7.6 *M* Sulphuric acid (aq.): Reference 22
c) Acidic polymerization in acetonitrile.
d) Estimated using 9 nm hypsochromic shift observed with bipyrrole.
e) The experimental peaks are only tentatively assigned to these wavelengths.

Table 4.2 Summary of spectral data obtained for electropolymerization of 50 m*M* pyrrole in acetonitrile with 0.1 *M* $NaClO_4$ as electrolyte.

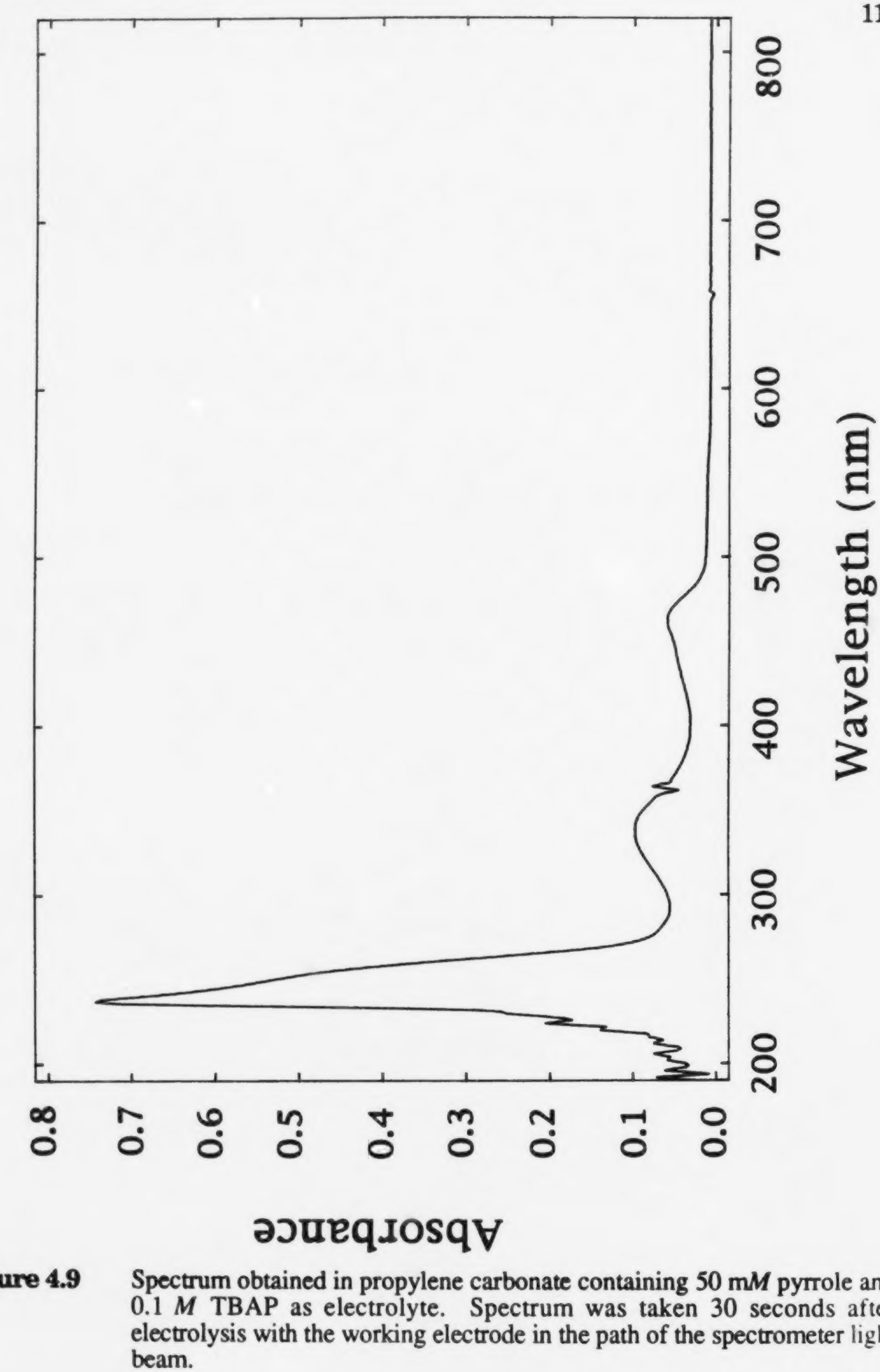

Figure 4.9 Spectrum obtained in propylene carbonate containing 50 m*M* pyrrole and 0.1 *M* TBAP as electrolyte. Spectrum was taken 30 seconds after electrolysis with the working electrode in the path of the spectrometer light beam.

systems and are summarized in Table 4.3. The same characteristic UV/VIS spectra were obtained in the various solvent systems, but the wavelength values are shifted due to the change in solvent.

4.5 Conclusions.

The spectroscopic evidence clearly shows that bipyrrole is formed in solution during the anodic polymerization of pyrrole. This result is supported by the electrochemical evidence for the presence of bipyrrole given in chapter 2. A fraction of this species is free to diffuse away from the disk and build up a measurable solution concentration. The exact role of the bipyrrole formed in the overall mechanism is not identified by these experiments. However, direct observation of the intermediate allows for kinetic studies with the RRDE through the rotation rate dependence of the current, as will be discussed in chapter 5.

The other species identified, the pyrrole radical cation (which is discussed in chapter 3) protons, and protonated pyrrole, also provide routes to probe the polymerization reaction. The spectroelectrochemical results strongly suggest that protonated pyrrole is formed during electropolymerization in acetonitrile. Since the acid products are non-conductive their presence should degrade film conductivity if incorporated in the film. This suggests that the use of basic species during pyrrole polymerization should improve the polymer properties, if the tendency for nucleophilic reactions leading to other reaction products can be avoided. The basicity of BF_4^- relative to ClO_4^- may be one of the reasons for some of the preferred properties of BF_4^- as an electrolyte during pyrrole anodization in acetonitrile.

Solvent System	Experimental λ_{max} (nm) After electrolysis; electrodes removed.	Species
Acetonitrile / TBABF$_4$ a)	242 277 330 432	Protonated pyrrole Bipyrrole Terpyrrole Quaterpyrrole (c)
Acetonitrile / TBAP b)	242 277 330 432	Protonated pyrrole Bipyrrole Terpyrrole Quaterpyrrole (c)
Propylene Carbonate / TBABF$_4$ a)	238 273 328 462	Protonated pyrrole Bipyrrole Terpyrrole Quaterpyrrole (c)
Propylene Carbonate / TBAP b)	238 273 328 462	Protonated pyrrole Bipyrrole Terpyrrole Quaterpyrrole (c)

(a) Tetrabutylammonium tetrafluoroborate

(b) Tetrabutylammonium perchlorate

(c) The experimental peak is only tentatively assigned to this wavelength.

Table 4.3 Summary of spectral data for 50 m*M* pyrrole in various electrolytes and solvents.

4.5 References

1. John, R.; Wallace, G.G., *J. Electroanal. Chem.*, **1991**, 306, 157.
2. Downard, A.J.; Pletcher, D.J., *J. Electroanal. Chem.*, **1986**, 206, 139.
3. Asavapiriyamont, S.; Chandler, G.K.; Gunawardenu, G.A.; Pletcher, D.J., *J. Electroanal. Chem.*, **1984**, 177, 229.
4. Otero, T.F.; Tejada, R.; Elola, A.S., *Polymer*, **1987**, 28, 651.
5. Zotti, G.; Cattarin, S.; Comisso, N., *J. Electroanal. Chem.*, **1987**, 235, 259.
6. Andrieux, C.P.; Audebert, P.; Hapiot, P.; Saveant, J.M., *J. Am. Chem. Soc.*, **1990**, 112, 2439.
7. Marcos, M.L.; Rodriguez, I.; Gonzalez-Velasco, *Electrochimica Acta*, **1987**, 32, 1453.
8. Diaz, A.F.; Martinez, A.; Kanazawa, K.K., *J. Electroanal. Chem.*, **1981**, 130,181.
9. Morse, N.J.; Rosseinsky, D.R.; Mortimer, R.J.; Walton, D.J., *J. Electroanal. Chem.*, **1988**, 255, 119.
10. Rosseinsky, D.R.; Morse, N.J.; Slade, R.C.T; Hix, G.B.; Mortimer, R.J.; Walton, D.J., *Electrochimica Acta*, **1991**, 36, 733.
11. Beck, F ; Oberst, M, *J. Electroanal. Chem.*, **1990**, 285, 177.
12. Beck, F ; Oberst, M; Jansen, R., *Electrochimica Acta*, **1990**, 35, 1841.
13. Bruckenstein, S.; Sharkey, J.W., *J. Electroanal. Chem.*, **1988**, 241, 211.
14. Raymond, D.E.; Harrison, D.J., *J. Electroanal. Chem.*, **1990**, 296, 269.
15. Genies, E.M.; Bidan, G.; Diaz, A.F., *J. Electroanal. Chem.*, **1983**, 149,101.
16. Christensen, P.A.; Hamnett, A., *Electrochimica Acta*, **1991**, 36, 1263.
17. Beck, F ; Braun, P.; Oberst, M, *Ber. Bunsenges. Phys. Chem.* ,**1987**, 91, 967.
18. Yakushi, K.; Lauchlan, L.J.; Clarke, T.C.; Street, G.B., *J. Chem. Phys.*, **1983**,79, 4774.
19. Scott, J.C.; Brédas, J.L.; Yakushi, K.; Pflunger, P.; Street, G.B., *Synth. Metals*, **1984**, 9, 165.
20. Diaz, A.F.; Crowley, J.; Bargon, J.; Gardini, G.P.; Torrence, J.B., *J. Electroanal. Chem.*, **1981**, 121, 355.

21. Potts, H.A.; Smith, G.F., *J. Chem. Soc..*, **1957**, 4018.

22. Chiang, Y.; Whipple, E.B., *J. Am. Chem. Soc.*, **1963**, 85, 2763.22.

23. Chiang, Y.; Whipple, E.B., *J. Am. Chem. Soc.*, **1963**, 85, 26.

23. Naqvi, N.; Fernando, Q., *J. Org. Chem.*, **1960**, 25, 5551.

24. Rapoport, H.; Holden, K.G., *J. Am. Chem. Soc.*, **1962**, 84, 635.

25. Rapoport, H.; Castagnioli, N, *J. Am. Chem. Soc.*, **1962**, 84, 2178.

26. Rapoport, H.; Castagnioli, N, Holden, K.G, *J. Org. Chem.*, **1964**, 29, 883.

27. Hoier, S.N.; Park, Su-Moon, *Private Communication.*

28. Hill, M.G.; Penneau J-F; Zinger, B.; Mann, K.R.; Miller, L., *Chem. Mater.*, **1992**, 4, 1106.

29. Jones, R. A. (Ed.), *Pyrroles: The Synthesis and the Physical and Chemical Aspects of the Pyrrole Ring.*, John Wiley and Sons, New York, **1990**, Chapter 3, p. 305.

30. Dennstedt, M.; Zimmerman, J., *Ber. Dtsch. Chem. Ges.*, **1888**, 21, 1478.

31. Dennstedt, M.; Voigtlander, F., *Ber. Dtsch. Chem. Ges.*, **1894**, 27, 478.

32. Smith, G.F., *Adv. Heterocycl. Chem.*,**1963**, 2, 287.

33. Bullock, E., *Can. J. Chem.*,**1958**, 36, 1686.

34. Abraham, R. J.; Bullock, E.; Mitra, S., *Can. J. Chem.*,**1959**, 37, 1859.

Chapter 5

Analysis of Pyrrole Polymerization using Standard Rotating Ring-Disk Electrode Kinetic Theory and Digital Simulation.

5.1 Introduction.

The rotating ring-disk electrode, RRDE, was developed primarily to study the kinetics of electrode processes involving the formation of unstable intermediates [1]. The method initially proved useful in the mechanistic investigation of the cathodic reduction of oxygen [2]. The theory and application of the rotating ring-disk to both heterogeneous electrode kinetics and first and second order homogeneous processes has been described [3]. The RRDE has shown itself to be a very useful technique in electrochemical studies, even for complicated mechanisms involving parallel reaction paths [3,4], dimerizations [5-8] and the observation of isomerization resulting from parallel higher-order reactions [9]. However extension of this powerful technique to other complicated simultaneous reactions, such as polymerizations, have been limited [10-12]. This is mainly due to the reaction routes having more than one pure simple reaction step. In particular, the application of the RRDE to the analysis or pyrrole polymerization has been minimal [13-17].

Approximate analytical solutions of the differential equations describing first and second order homogeneous kinetics at the rotating ring-disk electrode have been described [18-20]. Meanwhile, the complexity of the mathematics associated with the calculation of analytical solutions for dimerization and complex higher order reaction mechanisms have necessitated the development of digital simulation techniques. Digital simulation methods (iterative finite difference calculations) were originally pioneered in the electrochemical field by Feldberg [21, 22] and since then have been extensively used [3-10]. The technique has been successfully applied to solution of boundary value problems describing electrochemical systems, especially those for which calculation of closed form analytical solutions are not possible or are inconvenient to evaluate, e.g. dimerization reactions [9]. The values of the rate constants obtained via digital simulation have compared very well to those obtained by non-electrochemical methods [3].

In this chapter the RRDE theory for first and second order homogeneous kinetics was used to evaluate the kinetics of pyrrole polymerization. However, due to the lack of a closed form analytical solution for polymerization, numerical analysis by a finite difference technique was used to obtain an overall polymerization rate constant. The polymerization of pyrrole in acetonitrile and propylene carbonate, containing either tetrabutylammonium perchlorate (TBAP), tetrabutylammonium tetrafluoroborate ($TBABF_4$), or sodium perchlorate ($NaClO_4$) as electrolyte, was investigated. For the purpose of comparison the analysis was applied to three assumed reaction schemes; radical-radical coupling, radical-monomer coupling and comproportionation.

5.2 Rotating Ring-Disk Theory.

5.2.1 The RRDE Collection Efficiency.

In the simplest sense the disk electrode can be regarded as the source from which a constant flux of intermediates is generated and the disk current is a measure of this flux. If the ring electrode is set at a potential such that all the intermediates that reach it are consumed, then the ring current is a measure of the quantity of intermediates "collected" at the ring electrode. Thus, the "collection efficiency" is defined as the ratio of the ring current, I_R to the disk current, I_D, and is given in Equation 5.2.1.

(5.2.1)

$$N_0 = -\frac{I_R}{I_D}$$

The collection efficiency is always less than unity due to the loss of intermediate species by diffusion into the bulk solution. The negative sign is due to the current flow being in opposite directions.

The theoretical value of the collection efficiency is a function of the electrode geometry and can be calculated using Equation 5.2.2.

(5.2.2) $$N_0 = 1 - F\left(\frac{\alpha}{\beta}\right) + \beta^{\frac{2}{3}}\left[1-F(\alpha)\right] - \left(1+\alpha+\beta\right)^{\frac{2}{3}}\left[1-F\left(\frac{\alpha}{\beta}\right)\left(1+\alpha+\beta\right)\right]$$

The collection efficiency and Equations 5.2.1 and 5.2.2 are discussed in the introductory chapter with α, β and the function, $F(x)$, described by Equations 1.2.4 and 1.2.5 (pp.8 and 9).

5.2.2 First Order Homogeneous Kinetics.

In this case the electrochemically generated intermediate is considered to decompose on its way from the disk to the ring by first order kinetics, as shown in the scheme below. This may be a genuine unimolecular reaction, or it may be a pseudo-first order situation in which the intermediate reacts with solvent, or any other species whose concentration is much larger than that of the intermediate.

$$\begin{array}{lll} \text{DISK} & A \pm n_D e^- \xrightarrow{\qquad} & B \\ \text{SOLUTION} & B \xrightarrow{\quad k_f \quad} & \text{Products} \\ \text{RING} & B \pm n_R e^- \xrightarrow{\qquad} & A \end{array}$$

The concentration profile of the intermediate B for a first order kinetic reaction has been described [3]. For the pseudo-first order case where B is reacting with species C the analysis is the same, and the rate constant is given as $k_f = k'[C]$. The presence of a homogeneous reaction manifests as a change in the collection efficiency. That is, for a given rotation rate, as the rate of the reaction increases (larger k_f) less of species B reaches the ring and the kinetic collection efficiency, N_k, is correspondingly lower.

The differential equation describing radial, axial and diffusional transport of B to the RRDE under steady state conditions, along with the kinetic contribution, is given in Equation 5.2.3.

(5.2.3) $$D_b\frac{\delta^2 b}{\delta z^2} - v_r\frac{\delta b}{\delta r} - v_z\frac{\delta b}{\delta z} - k_f b = 0$$

This equation has been solved for thin-gap thin-ring electrodes only. The reason for the restriction is that in order to solve the equation for the ring and gap regions the axial term needed to be neglected [3]. This was said to be justified for the given geometry, since for very short radial distances the concentration profile in the gap and ring regions is not affected by axial convection.

The closed form expression derived for thin gap and thin ring electrodes is given in Equation 5.2.4.

$$\ln N_\kappa - \ln N_0 = -a\kappa + b - \ln\left[1 + \frac{1}{(\kappa + c)}\right] \tag{5.2.4}$$

The coefficients a, b and c are parameters dependent on the electrode geometry, and have been tabulated for common radius ratios in the publication by Albery and Hitchman [3]. N_0 is the theoretical collection efficiency calculated for the thin-gap thin-ring electrode using Equation 5.2.2. The most important feature of Equation 5.2.4 is the rate parameter, κ. This parameter is defined by Equation 5.2.5.

$$\kappa = \left(\frac{k_f}{D}\right)^{\frac{1}{2}}\left(\frac{D}{C}\right)^{\frac{1}{3}} \tag{5.2.5}$$

with

$$C = 0.51\ \omega^{\frac{3}{2}}\nu^{\frac{-1}{2}}$$

Here k_f is the first order rate constant, ω is the angular velocity, and ν is the kinematic viscosity. D is the diffusion coefficient of the intermediate species (B) generated at the disk electrode and is generally taken as the value for the parent molecule (A). Equation 5.2.4 was derived assuming that κ is greater than 1, while for κ less than 1 a more complicated expression was obtained [3]. It is evident from Equation 5.2.4 that N_κ depends solely on the geometric parameters of the electrode and the dimensionless rate parameter, κ. Therefore, a plot of N_κ as a function of κ, for a defined electrode geometry, will generate a first order working curve, from which the experimental collection efficiency values can be used to obtain "experimental" values for the rate parameter, κ. These "experimental" rate values are then used to determine the first order rate constant, k_f, by plotting κ^2 versus ω^{-1} as described by Equation 5.2.5. The slope of this plot is proportional to k_f.

5.2.3 Second Order Homogeneous Kinetics.

The theory of second order reactions in the gap of a RRDE between a reactant generated at the disk and an electro-inactive substrate in solution was described by Albery and Hitchman [3] and is sometimes referred to as diffusion layer titration theory. The reaction scheme is shown below.

$$\begin{array}{lll} \text{DISK} & A \pm n_D e^- \longrightarrow & B \\ \text{SOLUTION} & B + C \xrightarrow{k_s} & \text{Products} \\ \text{RING} & B \pm n_R e^- \longrightarrow & A \end{array}$$

The differential equations describing radial, axial and diffusional transport of species B and C to the RRDE under steady state conditions, along with the kinetic contribution, are given in Equations 5.2.6 and 5.2.7, respectively.

(5.2.6)

$$D_b \frac{\delta^2 b}{\delta z^2} - v_r \frac{\delta b}{\delta r} - v_z \frac{\delta b}{\delta z} - k_s bc = 0$$

(5.2.7)

$$D_c \frac{\delta^2 c}{\delta z^2} - v_r \frac{\delta c}{\delta r} - v_z \frac{\delta c}{\delta z} - k_s bc = 0$$

Approximate closed form solutions for the ring current and the kinetic collection efficiency have been obtained by solving Equations 5.2.6 and 5.2.7 using the method of moments [3]. In order to solve the equations three assumptions were made. First, that the reaction is fast enough that the axial convection term could be neglected. Second, that the ring is wide enough to collect all intermediates reaching it, and the third assumption is that the concentration profiles are symmetric at the reaction boundary. The approximate analytical solution for the kinetic collection efficiency is given in Equation 5.2.8, while that for the ring current is given by Equation 5.2.9.

(5.2.8) $$N_\kappa = \frac{0.339\, r_2^2 D^{1/3} [1 - F(\alpha)]}{r_1^2 \nu^{1/3} k_s} \frac{\omega}{C^*}$$

(5.2.9) $$I_{R,\kappa} = 0.21\, \pi\, r_2^2\, n\, F\, D\, \omega^{3/2}\, \nu^{-1/2}\, k_s^{-1}$$

$F(\alpha)$ is the function described in the introductory chapter (p.9) with α replacing x, k_s is the second order rate constant, ω is the angular velocity, ν is the kinematic viscosity, F is the Faraday, r_1 is the disk electrode radius and r_2 is the inner radius of the ring electrode. D is the diffusion coefficient of the intermediate species (B) generated at the disk electrode and is generally taken as the value for the parent molecule (A). The second order rate constant, k_s, can be obtained from plots of either N_κ versus ω/C^* or from $I_{R,\kappa}$ versus $\omega^{3/2}$. The values of N_κ and $I_{R,\kappa}$ are obtained using the mass transport limiting current values for the disk and ring electrodes.

Diffusion layer titration theory [3] is identical to that above, however, the values for the kinetic collection efficiency and the kinetic ring current are obtained using galvanostatic conditions rather than potentiometric. A biamperometric plot of ring current versus disk current is obtained by monitoring the ring current at a fixed potential and scanning the disk current. The resulting titration curve has four characteristic regions which are identified in Figure 5.2.1 as regions A, B, C,and D. In region A, prior to the "endpoint", the generated reactant B has reacted completely with species C and no ring current is observed. At higher disk currents a point is reached where the flux of B from the disk just equals the transport limited flux of C to the disk. This point is called the critical disk current, μ, and the ring current remains zero at this point. As the disk current is increased further the solution in the gap becomes dominated by B, and when the disk current is sufficiently large such that the B dominated zone has reached the inside edge of the ring, a ring current is observed. This point is denoted as region B and the disk current at this point is called the kinetic disk current which is given by Equation 5.2.10.

(5.2.10) $$I_{D,\kappa} = \frac{\mu}{1-F(\alpha)}$$

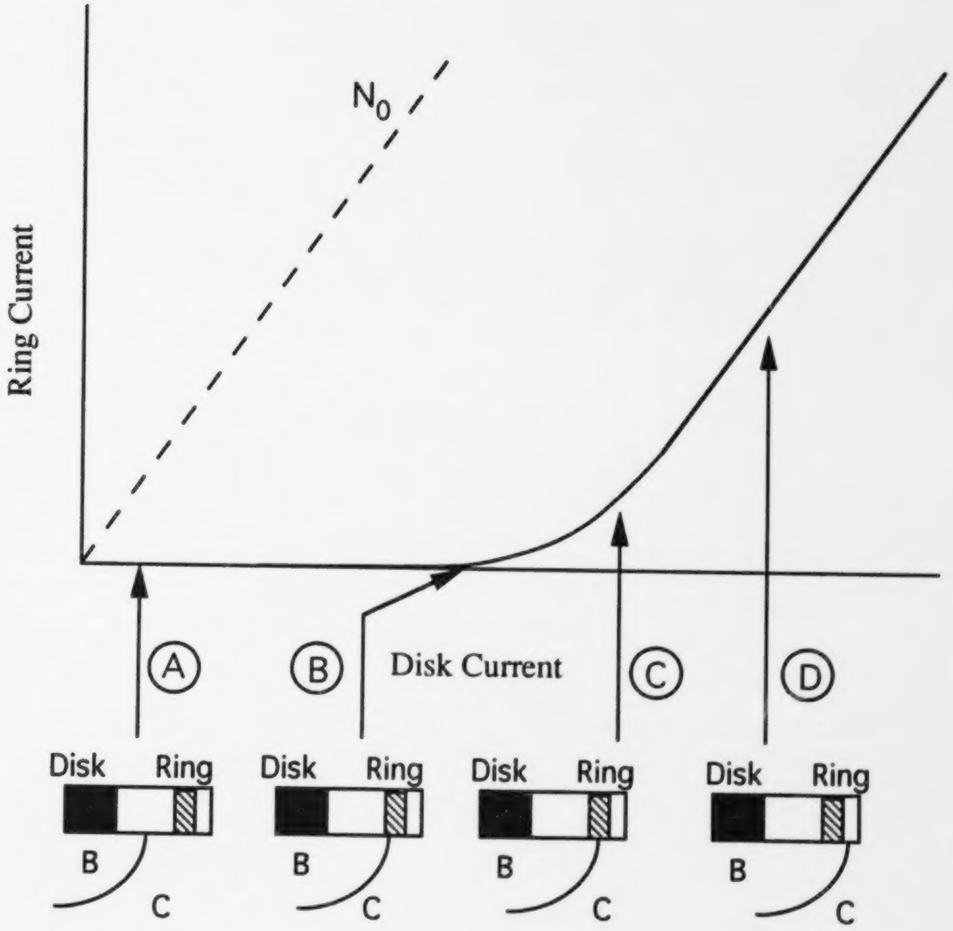
Ring Current
N_0
Disk Current
A
B
C
D
Disk
Ring
B
C

Figure 5.2.1: Schematic of reaction zones and corresponding diffusion layer titration curve (solid line). The dashed line shows the curve observed for a stable system.

where α and $F(\alpha)$ are given in chapter 1 (p.8 and 9).

In region C the reaction zone has moved across the ring and an increase in the ring current occurs. When the reaction zone has moved completely across the ring, and for any further increases in disk current, a simple linear relation occurs between I_R and I_D (region D), given in Equation 5.2.11.

$$I_R = N_0 I_D - \mu\beta^{2/3} \qquad (5.2.11)$$

By extrapolation of the linear portion of the titration curve to zero ring current (I_R=0, Equation 5.2.11), μ can be calculated from Equation 5.2.12.

$$\mu = \frac{N_0 I_D}{\beta^{2/3}} \qquad (5.2.12)$$

where I_D is the disk current obtained at zero ring current, N_0 is the theoretical collection efficiency, and β is a geometric parameter defined in chapter 1 (p.8).

Titration curves are obtained at various rotation rates and concentration of species C. Using the value of μ and Equation 5.2.11 I_{DK} can be calculated and used to locate its corresponding kinetic ring current, I_{RK}, on the titration curve. These two values are then used to calculate the kinetic collection efficiency, N_K, (the ratio of the kinetic ring current to the kinetic disk current). The resulting values of N_K and I_{RK} are then used to determine the second order rate constant, k_s, using either Equations 5.2.8 or 5.2.9.

5.2.4 Digital Simulation via Finite Difference.

Digital simulation is a method used to model a given physical system. In electrochemistry it is transport problems that are commonly simulated. The basic equation solved is the diffusion equation (Equation 5.2.13) relating concentration , c, to time, t, and distance, x, from the electrode surface, given the diffusion coefficient. This is Fick's second law of diffusion, and is a partial second-order differential equation of parabolic type.

(5.2.13)
$$\frac{\delta c}{\delta t} = D\frac{\delta^2 c}{\delta x^2}$$

This is only a portion of the actual equations needed to be solved numerically, as it is necessary to consider solution convection and chemical reactions. In addition to diffusion these complications cause concentration changes and may make the equation unsolvable analytically. Therefore, numerical analysis may be the only method to obtain numbers from such equations. The numerical technique most often used in electrochemistry is that of finite differences, although other methods such as orthogonal collocation have been used. The following section provides a brief introduction to the method of finite difference analysis.

The basis of numerical analysis by finite difference is to take the differential equations describing the system in question and approximating it as a series of finite difference equations which can then be solved by simple arithmetic. In the literature of this field this process is referred to as discretization. The process is easier to view pictorially and is illustrated at the top of Figure 5.2.2. Consider a curve y(t) in which the first derivative dy/dt is known, and that the curve has been generated up to point L at t_1. However, the value at the next point M is required at $t_2 = t_1 + \delta t$. Since dy/dt is known at L (tangent drawn) we can move along it to t_2 and call this M at $y(t_2)$. If δt is small enough this is a reasonable approximation. A better approximation would be if the slope of the chord between L and M was known and it was used instead. This latter method is in fact done. The methods involved in approximating the differential equations are shown in the middle of Figure 5.2.2. Shown are three equidistant points, P_{i-1}, P_i and P_{i+1} with corresponding x and y values, and the first and second derivatives at P_i are required. Let $h = x_{i+1} - x_i = x_i - x_{i-1}$. The first derivative is the slope of the tangent at P_i, which can be found using three methods.

1. Forward difference. $\left(\frac{dy}{dx}\right)_{for} \approx \frac{y_{i+1} - y_i}{h}$ Slope of chord $P_i - P_{i+1}$

2. Backward difference. $\left(\frac{dy}{dx}\right)_{back} \approx \frac{y_i - y_{i-1}}{h}$ Slope of chord $P_{i-1} - P_i$

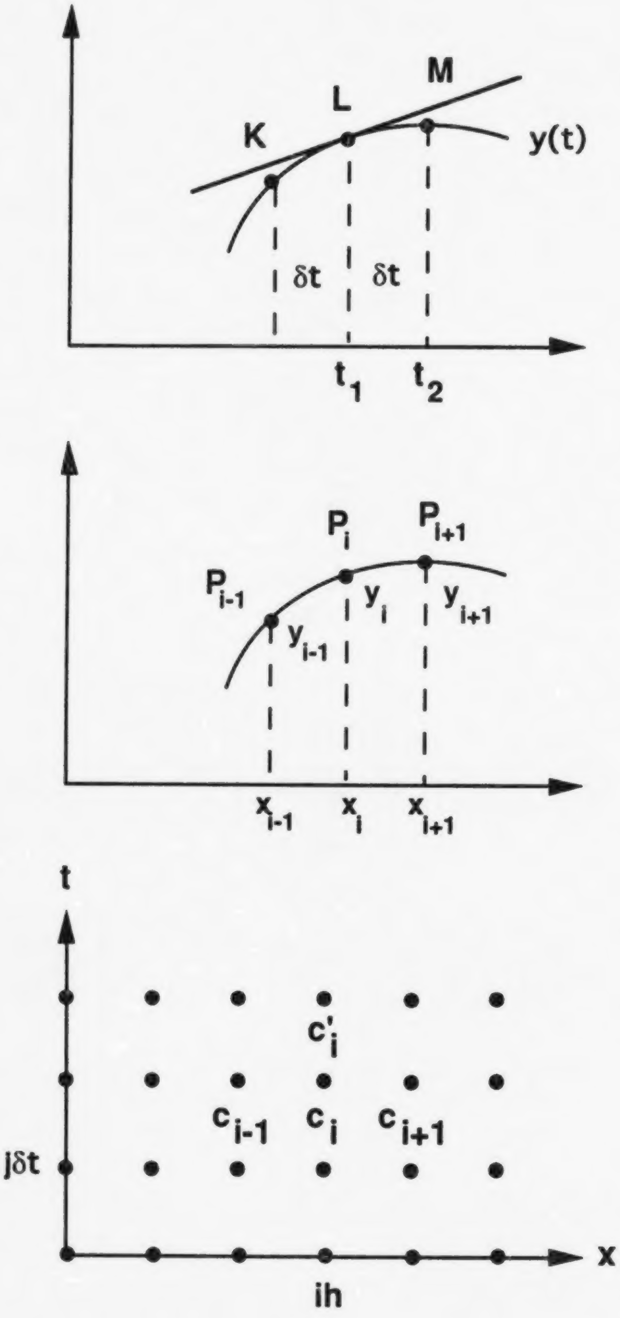
M
L
K
y(t)
δt
δt
t_1
t_2
P_i
P_{i+1}
P_{i-1}
y_i
y_{i+1}
y_{i-1}
x_{i-1}
x_i
x_{i+1}
t
c'_i
c_{i-1}
c_i
c_{i+1}
jδt
x
ih

Figure 5.2.2: Schematic of the methodology of finite difference analysis.

3. Central difference. $\left(\frac{dy}{dx}\right)_{cent} \approx \frac{y_{i+1} - y_{i-1}}{2h}$ Slope of chord $P_{i-1} - P_{i+1}$

The central difference method is the most satisfactory on average, although any of the discretization methods can be used.

The second derivative is the rate of change of slope at P_i. There are two slopes about P_i, the forward and backward differences approximating the first derivatives, and the change in slope takes place over the interval h. Thus the formula is

$$\frac{d^2y}{dx^2} = \frac{\left(\frac{dy}{dx}\right)_{for} - \left(\frac{dy}{dx}\right)_{back}}{h} = \frac{1}{h}\left(\frac{y_{i+1} - y_i}{h} - \frac{y_i - y_{i-1}}{h}\right)$$

therefore;

$$\frac{d^2y}{dx^2} = \frac{1}{h^2}\left(y_{i-1} - 2y_i + y_{i+1}\right)$$

These expressions are then used to obtain a finite difference equation, as demonstrated below for Fick's second law of diffusion in one dimension (Equation 5.2.13). The unknown variable c is a function of two variables t and x and is shown schematically in the bottom of Figure 5.2.2. In the figure c is sampled at a grid of points in the (x,t) plane spaced at distances h apart in the x-direction, and δt in the t-direction. The index j is given to t (i.e. $t = j\delta t$), while the index i is given to x ($x = ih$). Assume that all c values for all x up to time $j\delta t$ are known and the next row in time is required at $(j+1)\delta t$. The trio of points c_{i-1}, c_i and c_{i+1} are used to obtain c_i' via discretization of Equation 5.2.13. The left-hand side is a first time-derivative and applying a forward difference to it the following expression is obtained.

$$\frac{\delta c}{\delta t} \approx \frac{c_i' - c_i}{\delta t}$$

The right-hand side is the second derivative which becomes:

$$\frac{\delta^2 c}{\delta x^2} \approx \frac{1}{h^2}\left(c_{i-1} - 2c_i + c_{i+1}\right)$$

Putting these together results in:

$$c_i' = c_i + \frac{D\delta t}{h^2}\left(c_{i-1} - 2c_i + c_{i+1}\right)$$

These expressions are fine for positions away from the electrode, but for the space right next to the electrode the non diffusion-derived c_0 value is required. This concentration value is obtained from the boundary conditions applied to the particular system being simulated.

The basic differential equation describing transport of a species of concentration c from the bulk of solution to the surface of a rotating disk electrode under steady state conditions was given on page 7 of the introductory chapter (Equation 1.2.1). A concentration change at any point can be brought about by diffusion, described by the left-hand side, or by convection, described by the right-hand side. The differential equation describing transport to a rotating ring-disk electrode, RRDE, is given in Equation 5.2.14. This equation is identical to Equation 1.2.1 except for the added effect of first order reaction kinetics.

(5.2.14)
$$D\left(\frac{\delta^2 c}{\delta r^2} + \frac{\delta c}{r\delta r} + \frac{\delta^2 c}{\delta z^2}\right) = v_r\frac{\delta c}{\delta r} - v_z\frac{\delta c}{\delta z} - k_f c$$

To apply the finite difference technique to the RRDE, the system must be divided into three zones characterized by the geometry of the system. The first zone is the region of the disk electrode, the second zone is the region of the insulating gap, and the third zone is the region of the ring electrode. Each zone has its own set of boundary conditions. The discretization of the RRDE is shown in Figure 5.2.3. Discretization normal to the surface comprises $i_{max,d}$ layers of equal thickness, Δz, over the disk, and $i_{max,gr}$ layers of equal thickness, Δz, over the gap and ring where $i_{max,gr} \leq i_{max,d}$. Above the disk there are no radial concentration gradients, thus no radial discretization is required. The disk is uniformly accessible and is therefore considered to be only one radial element. Radial concentration gradients begin at the edge of the disk/gap boundary, therefore, discretization

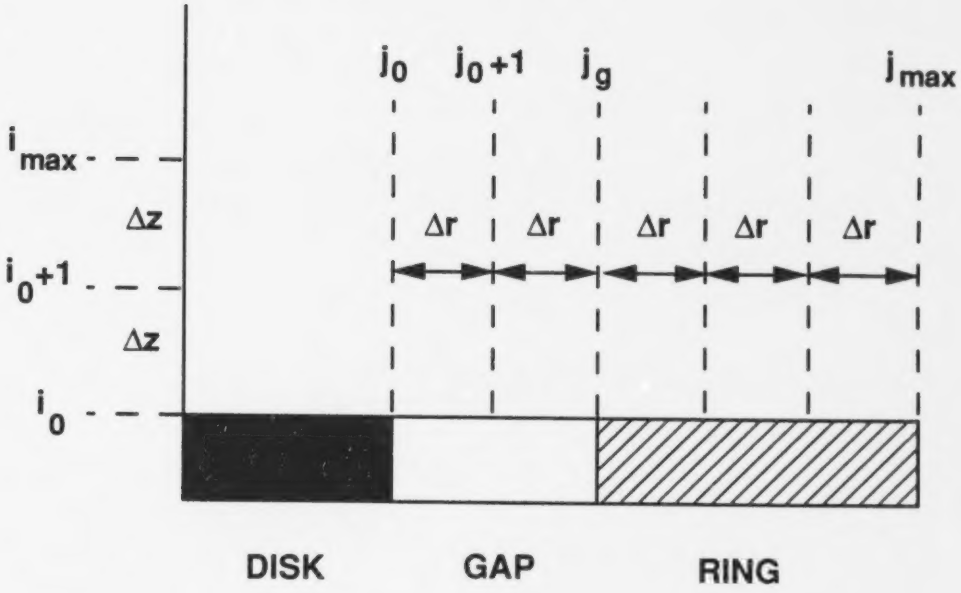
j_0
j_0+1
j_g
j_{max}
i_{max}
Δz
i_0+1
Δz
i_0
Δr
Δr
Δr
Δr
Δr
DISK
GAP
RING

Figure 5.2.3: RRDE discretization.

begins at the edge of the disk, at radius $r_1 = j_0\Delta r$. There are j_{max} concentric boundaries at $j_0\Delta r$, $(j_0+1)\Delta r$, $(j_0+2)\Delta r$, ...$(j_0+j_g)\Delta r$, ...$(j_0+j_{max})\Delta r$, where j_g is the outermost element of the gap. The finite difference equations and boundary conditions employed in the simulation used to analyze complex electrode reactions at the RRDE are given in the publication describing the algorithm used [23,24]. The polymerization of pyrrole is analyzed here using these algorithms.

5.3 Experimental.

5.3.1 Chemicals.

Pyrrole (Aldrich) was vacuum distilled and stored under argon. HPLC grade acetonitrile (Burdick and Jackson) was distilled over calcium hydride prior to use. Propylene carbonate (Eastman Organic Chemicals) was vacuum distilled four times with the middle fraction being retained from each distillation. Purity of both solvents was demonstrated by their respective UV spectra. Sodium perchlorate, $NaClO_4$, (Fisher Scientific), tetrabutylammonium perchlorate, TBAP, (Southwestern Analytical Chemicals) and tetrabutylammonium tetrafluoroborate, $TBABF_4$, (Southwestern Analytical Chemicals) were vacuum dried (110°C) and used without further purification. Pyrrole solutions were obtained by dilution of a freshly prepared 50 m*M* pyrrole solution. All solutions were filtered, under argon, through activated alumina (Woelm N-Super I, ICN Nutritional Biochemicals, Cleveland, Ohio, vacuum dried at 250 °C) into the electrochemical cell (under Ar) immediately before use.

5.3.2 Instrumentation.

A Pine RDE-4 bipotentiostat and MSR rotator were used for the ring-disk experiments. Data was recorded on a Kipp and Zonen BD91 x,y,y' recorder. The RRDE dimensions were r_1=0.2286 cm, r_2=0.2464 cm, and r_3=0.2692 cm, where r_1 is the disk radius, and r_2 and r_3 are the inner and outer ring radii respectively. The collection efficiency calculated [3] using the electrode dimensions was 0.216, while the value obtained experimentally using aqueous 1.0 m*M* $K_3Fe(CN)_6$ in 0.1 *M* KCl was 0.22. The RRDE was polished before each run using a series of 3 μm alumina, 1 μm alumina, and 0.3 μm alumina, and was thoroughly rinsed with dry acetonitrile. The kinematic viscosity was obtained using a calibrated viscometer (Cannon Instrument Co.)

5.4 Results and Discussion.

5.4.1 Evaluation of "n" and the reaction order using the RDE.

The mass transport limited current obtained at a rotating disk electrode, RDE, is described by the Levich equation [25], (Equation 5.4.1) which V.G Levich obtained by solving Equation 1.2.1 (chapter 1, p.7).

$$I_D = 0.6205\ nFAD^{2/3}\nu^{-1/6}\ \omega^{1/2}\ C^* \tag{5.4.1}$$

Here n is the number of electrons involved in the electrochemical step, F is the Faraday, A is the electrode area, D is the diffusion coefficient of the bulk species, ν is the kinetic viscosity of the solution, ω is the angular velocity and C^* is the concentration of the bulk species in m*M* if the current is in μA. A plot of limiting current against the square root of the angular velocity, i.e. I_D vs $\omega^{1/2}$, should yield a straight line with a zero intercept. However, non-linear plots are often obtained as a result of kinetic limitations due to slow electron transfer at the electrode surface. When this is the case the Koutecky-Levich equation, Equation 5.4.2, is used.

$$\frac{1}{I_D} = \frac{1}{A} + \frac{1}{B\omega^{1/2}} \tag{5.4.2}$$

where:

$$A = nFC^*k'\exp[nF\eta/RT] \qquad \text{(y-intercept)}$$

$$B = 0.6205\ nFAD^{2/3}\nu^{-1/6}C^* \qquad \text{(slope)}$$

Thus, a plot of $1/I_D$ versus $1/(\omega^{1/2}C^*)$ should be linear with a slope proportional to the diffusion coefficient if the number of electrons is known, or vise versa. The y-intercept is proportional to the electron transfer rate, k', at the electrode surface. If the limiting current is used in the plot this implies that the overpotential, η, is large and therefore the electron transfer is very fast and a near zero intercept is observed.

Figure 5.4.1a shows the Levich plot obtained for various concentrations of pyrrole in acetonitrile with 0.1 *M* $NaClO_4$ as electrolyte, while the corresponding

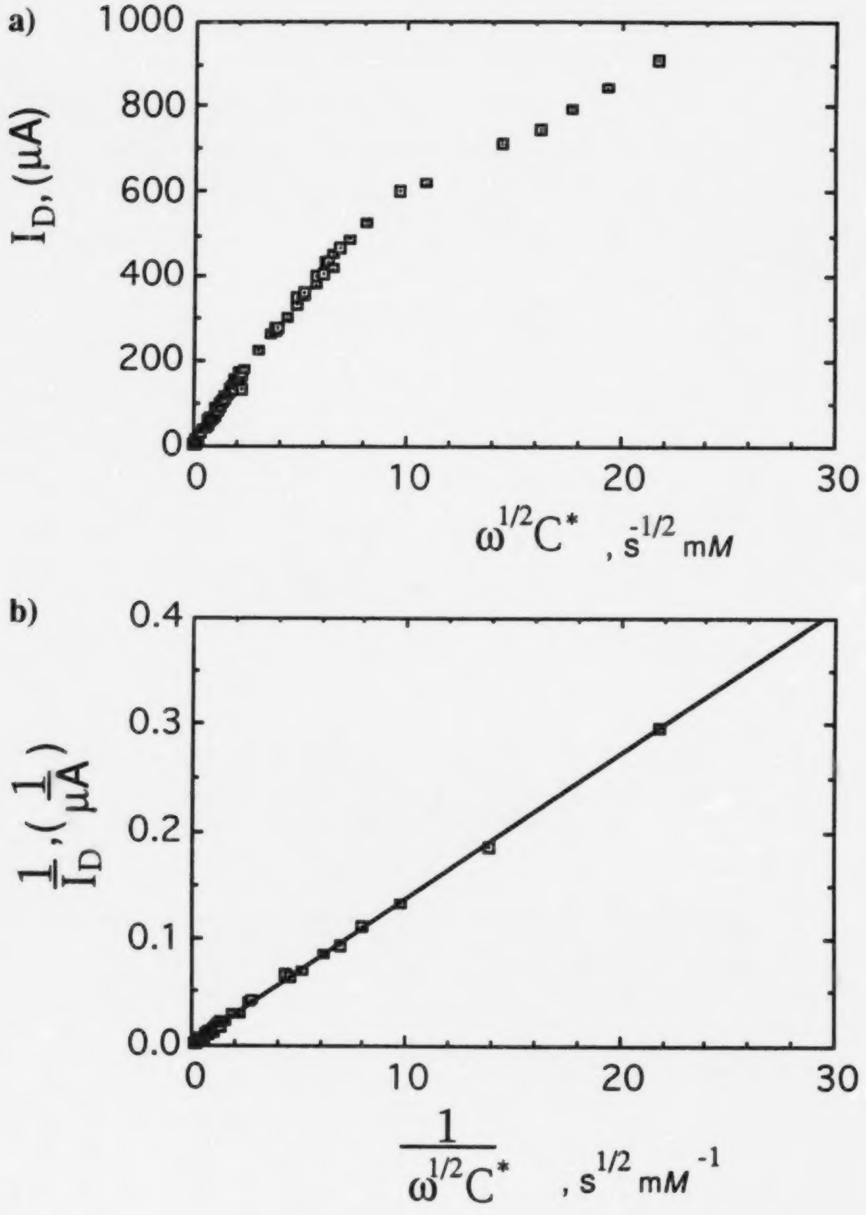

Figure 5.4.1: a) Cumulative Levich plot for various concentrations of pyrrole in acetonitrile containing 0.1 *M* $NaClO_4$. (0.01 to 3.0 m*M*)

b) Cumulative Koutecky-Levich plot for various concentrations of pyrrole in acetonitrile containing 0.1 *M* $NaClO_4$.

Koutecky-Levich plot is given in Figure 5.4.1b. At concentration 3 mM the Levich plot became non-linear, and the non-linear portion of Figure 5.4.1a reflects high concentration rather than high rotation rate at all concentrations. Identical plots for $TBABF_4$ in acetonitrile are given in Figure 5.4.2. The presence of a larger kinetic effect than that observed for $NaClO_4$ is clearly observed. This effect will be discussed later. Not given are the plots obtained for TBAP in acetonitrile and for TBAP and $NaClO_4$ in propylene carbonate, as the plots are similar to those in Figure 5.4.1 but with varying slopes which reflect the different solvent systems used. The number of electrons involved in the polymerization of pyrrole in the different solvent systems can be calculated from the equation for the slope (Equation 5.4.2), provided the values of the electrode area, the kinematic viscosity and the diffusion coefficient are known. The electrode area and kinematic viscosity were readily available, while the diffusion coefficient for pyrrole in acetonitrile was not. Electrochemical methods are generally used to obtain diffusion coefficients, however, since these methods require a prior knowledge of the number of electrons, the value of which we are calculating, it was necessary to use a non-electrochemical technique. A diffusion coefficient of 3.8×10^{-5} cm^2/s for pyrrole in acetonitrile containing 0.1 *M* $NaClO_4$ was obtained using a Taylor Dispersion technique described in Chapter 3. This value was used to calculate the values for "n" in the various solvent systems given in Table 5.4.1.

The values of "n" reported in the literature are summarized in Table 5.4.2. The apparent stoichiometry for film formation in acetonitrile is in the range of 2.17 to 2.7 faraday/mol of monomer, while in propylene carbonate the apparent stoichiometry varies from 1.7 to 1.84. The stoichiometry for the polymerization reaction includes the stoichiometry for the formation of the polymer chain, which is 2 electrons/molecule in the case of pyrrole, plus the charge associated with the oxidation of the polymer. The majority of the values were obtained either by elemental analysis or by coulometric measurements, although electrochemical quartz crystal microbalance (QCM) measurements have also been used [27-29]. These measurement techniques may produce different results for identical solvent systems, for instance elementary analysis cannot distinguish any additional solvent contribution, while coulometry also includes the capacitive charging effects. The QCM was demonstrated to have measured the incorporation of solvent into the polymer film, resulting in significantly lower apparent values of n for propylene carbonate compared to values obtained coulometrically.

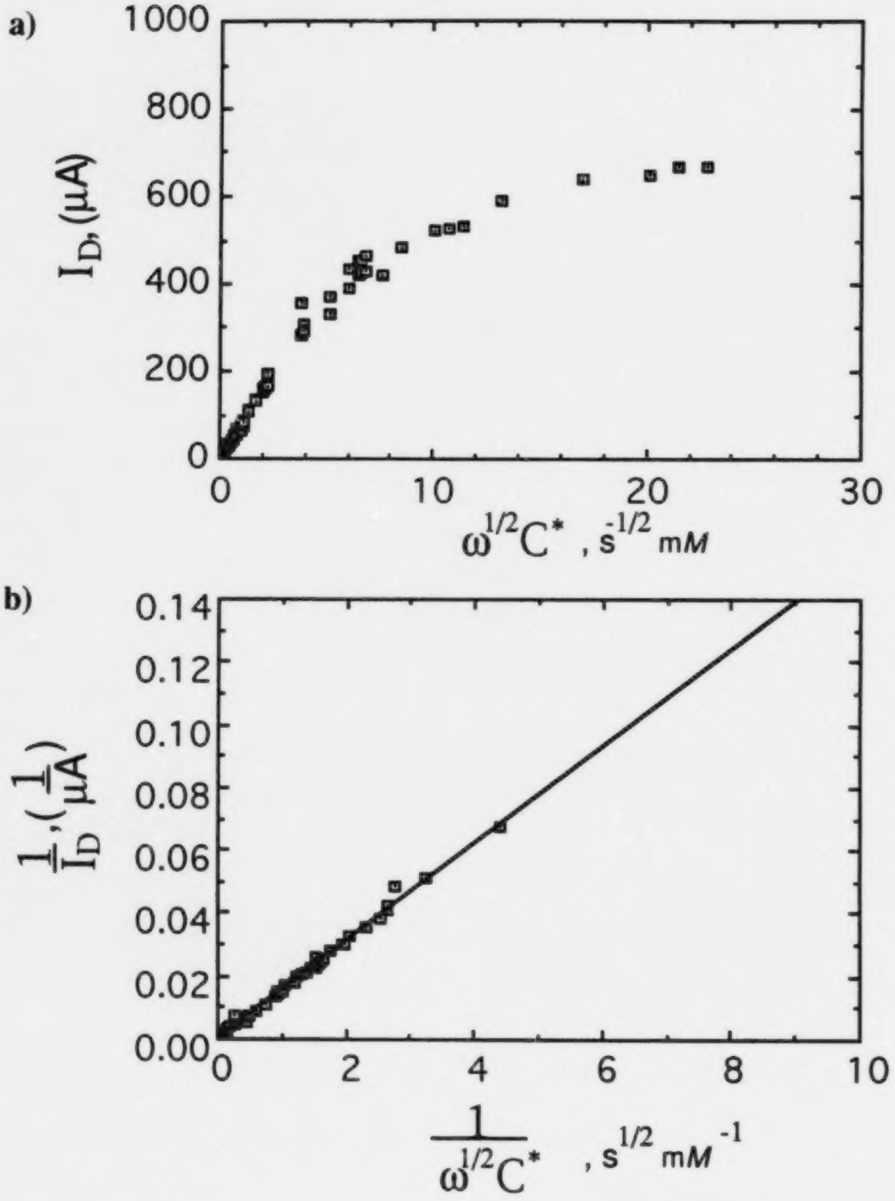

Figure 5.4.2: a) Cumulative Levich plot for various concentrations of pyrrole in acetonitrile containing 0.1 M TBABF$_4$. (0.03 to 3.0 m*M*)

b) Cumulative Koutecky-Levich plot for various concentrations of pyrrole in acetonitrile containing 0.1 M TBABF$_4$.

Solvent System	Koutecky-Levich Slope ($s^{1/2}$-mM /μA) ± 10 %	n (a)
0.1 M $NaClO_4$ / AN	1.4×10^{-2}	2.7
0.1 M $TBABF_4$/AN	1.6×10^{-2}	2.3
0.1 M TBAP / AN	1.6×10^{-2}	2.3
0.25 M TBAP / PC	5.7×10^{-2}	0.8
0.20 M $NaClO_4$ / PC	5.0×10^{-2}	1.0

(a) calculated based on $D_{pyrrole} = 3.8 \times 10^{-5}$ cm^2/s for all solvent systems.

Table 5.4.1: Summary of the values of "n" obtained for polymerization of pyrrole in various solvent systems.

Solvent System	n	References
$TBABF_4$ / AN	2.25 - 2.32	28
$TBAClO_4$ / AN	2.30 - 2.33	28
$NaNO_3$ / H_2O	2.6 - 2.7	29
$TBABF_4$ / AN	1.77	27
$LiClO_4$ / AN	2.17	27
$TBABF_4$ / PC	1.84	27
$LiClO_4$ / PC	1.70	27

Table 5.4.2: Summary of literature values of "n" obtained for polymerization of pyrrole in various solvent systems.

The values of "n" obtained using the RRDE for the various electrolytes in acetonitrile (Table 5.4.1) are similar to those given in Table 5.4.2, while a large discrepancy is observed for propylene carbonate. The degree of polymerization of pyrrole is known to be solvent and electrolyte dependent [26]. This is also shown in Table 5.4.2, in which the value of "n" varies from 2.3 to 2.7 in acetonitrile, while in propylene carbonate it varies from 0.8 to 1.0. However, the value of the diffusion coefficient is dependent on the solvent (and electrolyte) used, therefore it is not realistic to assume that the diffusion coefficient for pyrrole is the same in both acetonitrile and propylene carbonate. Propylene carbonate is a more viscous solvent than acetonitrile, and therefore the diffusion coefficient for pyrrole should be smaller in this solvent. It is this change in diffusion coefficient that causes the significant difference in the values of "n" calculated for propylene carbonate (Table 5.4.2).

The diffusion coefficient of pyrrole in propylene carbonate was not obtained using the Taylor dispersion method. The diffusion coefficient can only be estimated by assuming the number of electrons is the same as that obtained in acetonitrile, by using the literature value of "n" from Table 5.4.1, or by applying the Stokes-Einstein equation (Equation 5.4.3). The Stokes-Einstein equation demonstrates that the diffusion coefficient, D, is inversely proportional to the solvent viscosity, η, and the solvation radius, a. The constant

$$D = \frac{kT}{6\pi\eta a} \tag{5.4.3}$$

k is the Boltzmann constant and T is the absolute temperature (K). The diffusion coefficient of pyrrole in propylene carbonate was calculated by multiplying the value of D in acetonitrile by the ratio of the viscosity of acetonitrile to the viscosity of propylene carbonate. The solvation radius, a, was assumed to be the same in both solvents. The diffusion coefficient of pyrrole in propylene carbonate was also calculated using the various value of "n" from the literature given in Table 5.4.2. Given in Table 5.4.3 are the values of D in propylene carbonate calculated from our observed Koutecky-Levich slopes and the literature values of "n" used. The value of D estimated from the Stokes-Einstein relationship and the value of "n" this leads to is also given. The estimated values of n and D can be seen to vary by a factor of 2. The preferred values are n = 2.3 to 2.7 and D = 8 x 10^{-6} cm2/s. This is because n obtained by QCM analysis is recognized to be low due to solvent incorporation. Further, the value of 3.35 obtained from the Stokes-Einstein

Method Used	Solvent System	Koutecky-Levich Slope ($s^{1/2}$-mM/μA) ± 10%	n (method used)	Diffusion Coefficient (cm^2/s)
Koutecky-Levich	0.25 M TBAP PC	5.7×10^{-2}	(coul.) 2.3 [(a)]	7.9×10^{-6}
Koutecky-Levich	0.20 M $NaClO_4$ PC	5.0×10^{-2}	(coul.) 2.7[(b)]	8.0×10^{-6}
Koutecky-Levich	0.25 M TBAP PC	5.7×10^{-2}	(QCM) 1.8[(c)]	1.1×10^{-5}
Koutecky-Levich	0.20 M $NaClO_4$ PC	5.0×10^{-2}	(QCM) 1.7[(c)]	1.4×10^{-5}
Stokes-Einstein	0.25 M TBAP PC	5.7×10^{-2}	(calc.) 3.0[(d)]	5.2×10^{-6}
Stokes-Einstein	0.20 M $NaClO_4$ PC	5.0×10^{-2}	(calc.) 3.5[(d)]	5.2×10^{-6}

(a) value from reference 29, used to calculate D

(b) value from reference 28, used to calculate D

(c) value from reference 27, used to calculate D

(d) D calculated from D in acetonitrile using Stokes-Einstein relationship, and this value was used to calculate n from the Koutecky-Levich slope.

Table 5.4.3: Summary of calculated diffusion coefficients and values of n for pyrrole in propylene carbonate.

corrected value is unreasonably high, and the accuracy of the Stokes-Einstien relationship is not that satisfactory.

The efficiency of the polymerization process was reported to be dependent on the concentration of pyrrole in solution [26]. The dependence of the rate of polymerization on monomer concentration, or the order of reaction, can be studied from the slopes of log I vs log [pyrrole] plots [26]. The order of reaction has been studied by several researchers in this way with conflicting results. Reaction orders of 0 [27, 28], 1 [29, 30] and 1.5 [31] have been obtained with respect to pyrrole concentration, while a 0.5 pH order dependence was obtained in the case of polymerization on ITO glass. The current-voltage curve for the oxidation of pyrrole at the disk electrode is given in chapter 3 (Figure 3.1) and shows that two waves are observed at 1.3 V and 1.5 V vs SSCE. Plots of log I vs log [pyrrole] were constructed for TBAP, $TBABF_4$ and $NaClO_4$ in acetonitrile for the first mass transport limited current plateau and the value of the slope in each case was approximately one. However, it has been pointed out [26] that in obtaining the reaction order from log I vs log [pyrrole] plots the inefficiency due to loss of soluble oligomers to the bulk solution is unaccounted for. Also, the inability to separate the charge passed due to radical cation formation from that due to polymer doping and capacitive charging is not possible. The use of QCM technique was stated to have avoided these difficulties [26], and a reaction order of 2 was obtained for the polymerization of pyrrole confirming that the the coupling process is second order. The authors ascribed this to coupling of the radical cation species, but did not consider the other possible second order reactions.

5.4.2 Kinetic Analysis of Pyrrole Polymerization at the RRDE.

We have shown that bipyrrole is formed during the electropolymerization of pyrrole [13]. The collection efficiency obtained from monitoring bipyrrole at the ring electrode was significantly smaller than the theoretical value, and exhibited an unusual rotation rate dependence. Given in Figure 5.4.3 is the dependence of the collection efficiency on the square root of the angular velocity for various concentrations of pyrrole in acetonitrile containing 0.1 *M* $NaClO_4$ and 0.1 *M* $TBABF_4$. Both electrolytes in acetonitrile give the same rotation rate dependence, however, with 0.1 *M* $NaClO_4$ the collection efficiency is observed to decrease as the concentration of pyrrole increases up to a value of 0.3 m*M*, while the opposite behaviour is obtained with 0.1 *M* $TBABF_4$. In Figure 5.4.4 the plots of the ring current versus $\omega^{1/2}$ for various concentrations of pyrrole in acetonitrile containing

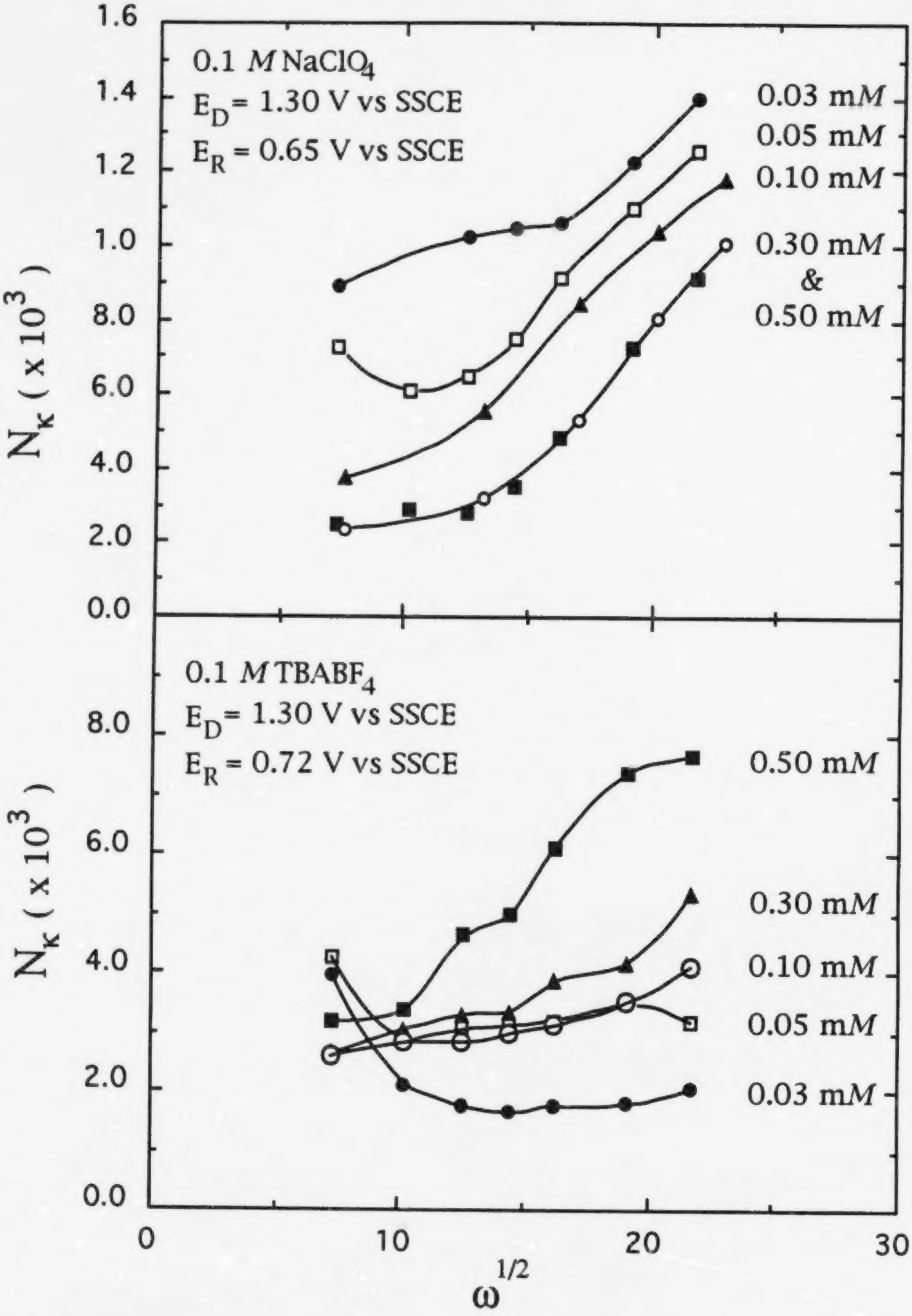

Figure 5.4.3: Dependence of the collection efficiency on $\omega^{1/2}$ for various concentrations of pyrrole in acetonitrile containing either 0.1 *M* $NaClO_4$ or 0.1 *M* $TBABF_4$.

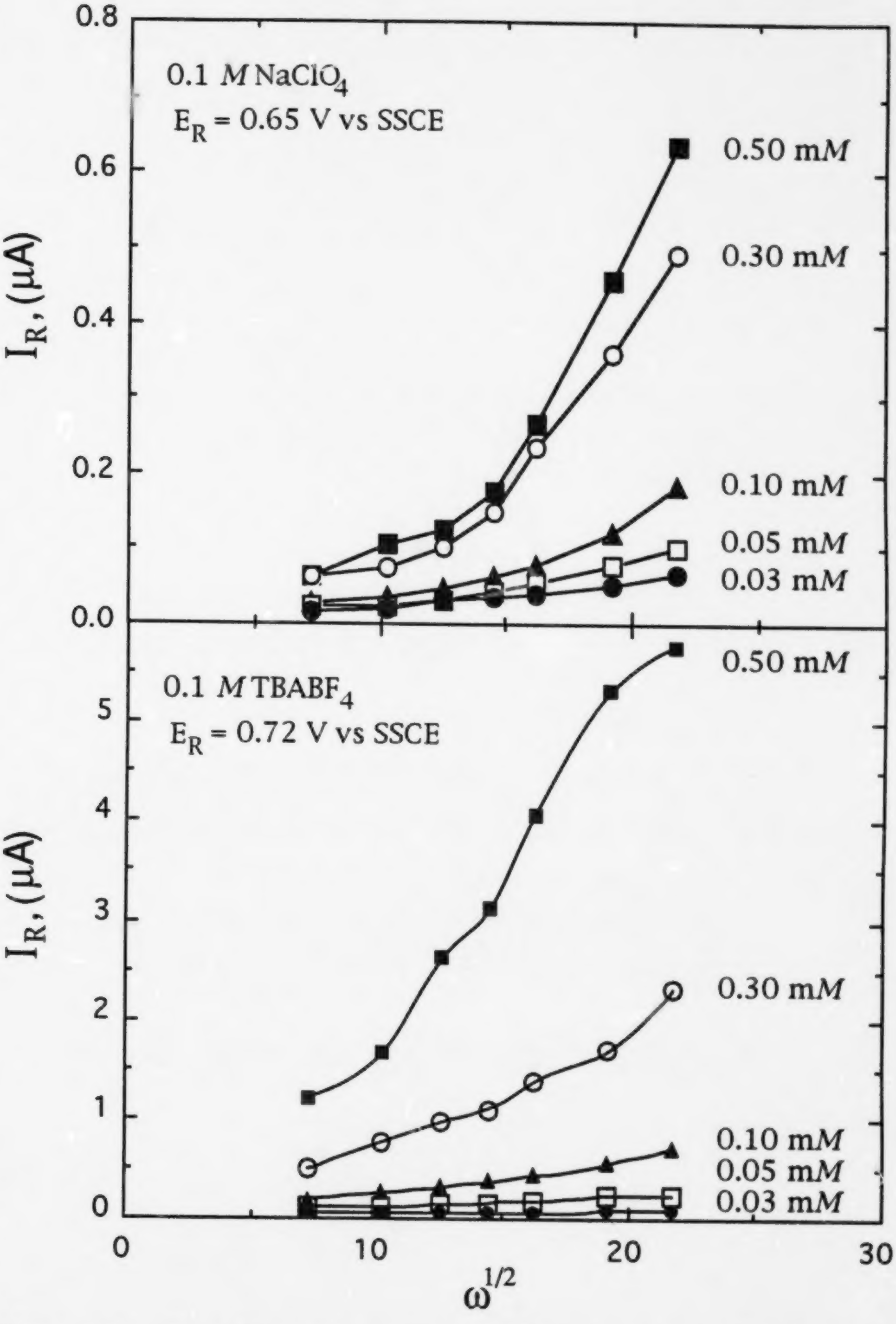

Figure 5.4.4: Dependence of ring current on $\omega^{1/2}$ for various concentrations of pyrrole in acetonitrile containing either 0.1 M NaClO$_4$ or 0.1 M TBABF$_4$.

0.1 *M* $NaClO_4$ and 0.1 *M* $TBABF_4$ are given. These plots show that as the pyrrole concentration increases the ring current increases for both electrolytes. However, there is a much faster increase for $TBABF_4$, as reflected in the different trends shown for the collection efficiencies. It is interesting that the yield of bipyrrole is much greater in $TBABF_4$ than in $NaClO_4$, and that the collection efficiency increases with pyrrole concentration in $TBABF_4$, while in $NaClO_4$ it decreases. Similar differences were observed between TBAP and $TBABF_4$.

The collection efficiency obtained for stable intermediates should exhibit no rotation rate dependence, while for uncomplicated reactions a linear dependence should be observed. Clearly the formation and loss of bipyrrole during the electropolymerization of pyrrole is more complicated. This dependence was investigated using the first and second order kinetic theory for the RRDE described earlier. The analytical expressions for first and second order kinetics were derived [3] assuming that the ring electrode detected the product of the initial electron transfer at the disk. Unfortunately, no expressions exist for the situation in which the ring electrode monitors the product from a chemical reaction of the initial species generated at the disk, whether it occurs via first or second order kinetics. It is likely that bipyrrole is consumed by homogeneous reactions, either by first or second order kinetics and, assuming the formation of bipyrrole is extremely fast, it seemed possible to analyze the bipyrrole current as if it were the primary product. The reaction scheme describing this situation is shown below.

$$\begin{array}{llll}
\text{DISK} & M - n_D e^- \longrightarrow M^{\cdot +} & & \\
\text{SOLUTION} & 2\,M^{\cdot +} \xrightarrow{k_d} M_2 & & \textbf{(fast)} \\
 & M_2 \xrightarrow{k} \text{Products} & & \\
\text{RING} & M_2 - n_R e^- \longrightarrow M_2^{\cdot +} & &
\end{array}$$

M is pyrrole, $M^{\cdot +}$ is the pyrrole radical cation, M_2 is bipyrrole, and $M_2^{\cdot +}$ is the bipyrrole radical cation. K_d is the rate constant for the rapid formation of bipyrrole, while k is the rate constant with an order to be determined.

5.4.2-1 First Order Kinetic Analysis.

The first order working curve calculated using Equation 5.2.4 for $\kappa \geq 1$ and with the specific RRDE geometry is shown in Figure 5.4.5. The experimental collection efficiencies for polymerization of pyrrole in acetonitrile and propylene carbonate, with either $NaClO_4$, TBAP, or $TBABF_4$ as electrolyte, were used to obtain corresponding values for the kinetic parameter, κ, (Equation 5.2.5) from the working curve. A plot of κ^2 versus ω^{-1} for 0.1 m*M* pyrrole in acetonitrile containing 0.1 *M* $NaClO_4$ is given in Figure 5.4.6. The relationship observed is characteristic of all concentrations of pyrrole investigated in this solvent system. Included in Figure 5.4.6 are the kinetic plots obtained for 0.1m*M* pyrrole in acetonitrile with 0.1 *M* $TBABF_4$, and in propylene carbonate with 0.1 *M* $NaClO_4$. It is apparent that there is a considerable difference between electrolytes in the same solvent, while a change of solvent alters the behaviour completely. The plot of κ^2 versus ω^{-1} should be linear with a zero intercept. This relationship is not observed for either solvent and therefore, the rotation rate dependence of bipyrrole current is not first order in nature. The reaction kinetics of bipyrrole with other species were then analyzed according to standard second order RRDE theory.

5.4.2-2 Second Order Kinetic Analysis.

The polymerization of pyrrole was investigated using both potentiometric and galvanostatic conditions. The theory for both methods is identical and, although the acquisition of the kinetic collection efficiencies is different, both yield similar results. The kinetic collection efficiencies and kinetic ring currents were used in Equations 5.2.8 and 5.2.9, respectively, to obtain the second order rate constant. This rate constant is for the reactions of bipyrrole following its formation. The plots corresponding to Equations 5.2.8 and 5.2.9 obtained from various pyrrole concentrations in acetonitrile containing $NaClO_4$ are shown in Figures 5.4.7 and 5.4.8. The plots are linear with near zero intercepts, however, the theory predicts that for plots of N_κ versus ω/C^* the data should all lie on one line. Theory is obeyed for pyrrole concentrations from 0.01 m*M* to 0.05 m*M*, but for larger concentrations deviation is observed. Identical plots for 0.1 *M* $TBABF_4$ in acetonitrile are given in Figures 5.4.9 and 5.4.10. These plots deviate from theory more significantly than for 0.1 *M* $NaClO_4$. Therefore, the assumption that analysis of bipyrrole using typical second order kinetic analysis methods is invalid.

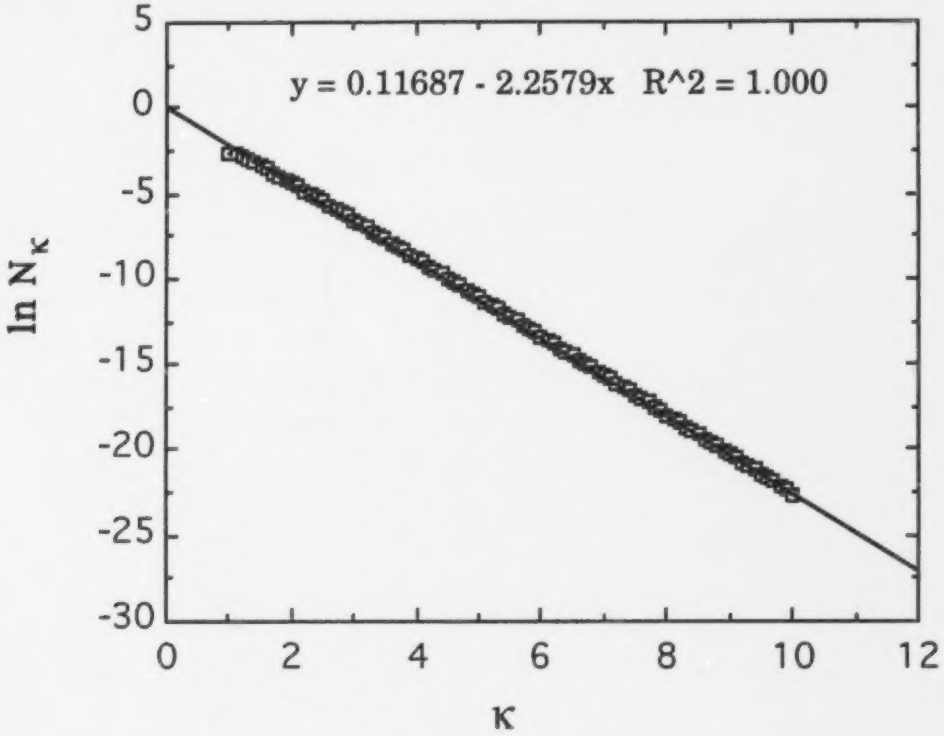

Figure 5.4.5: RRDE First Order Working Curve.

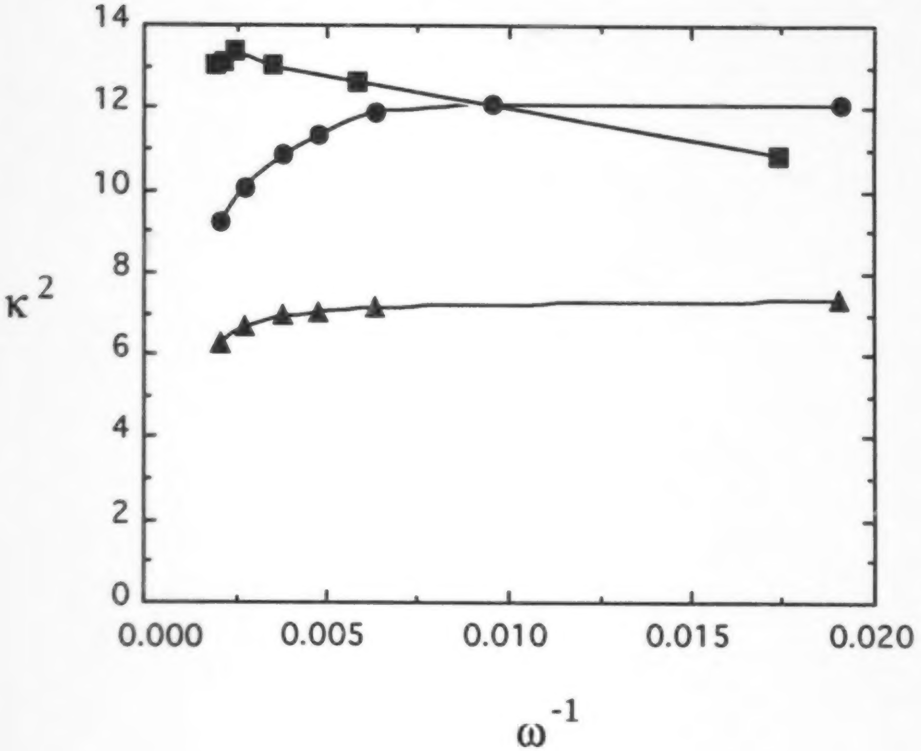

Figure 5.4.6: First order kinetic plot for 0.1 m*M* pyrrole with 0.1 *M* NaClO4 in acetonitrile (circles) and with 0.1 *M* $NaClO_4$ in propylene carbonate (squares). Triangles are for 0.1 m*M* pyrrole with 0.1 *M* $TBABF_4$ in acetonitrile

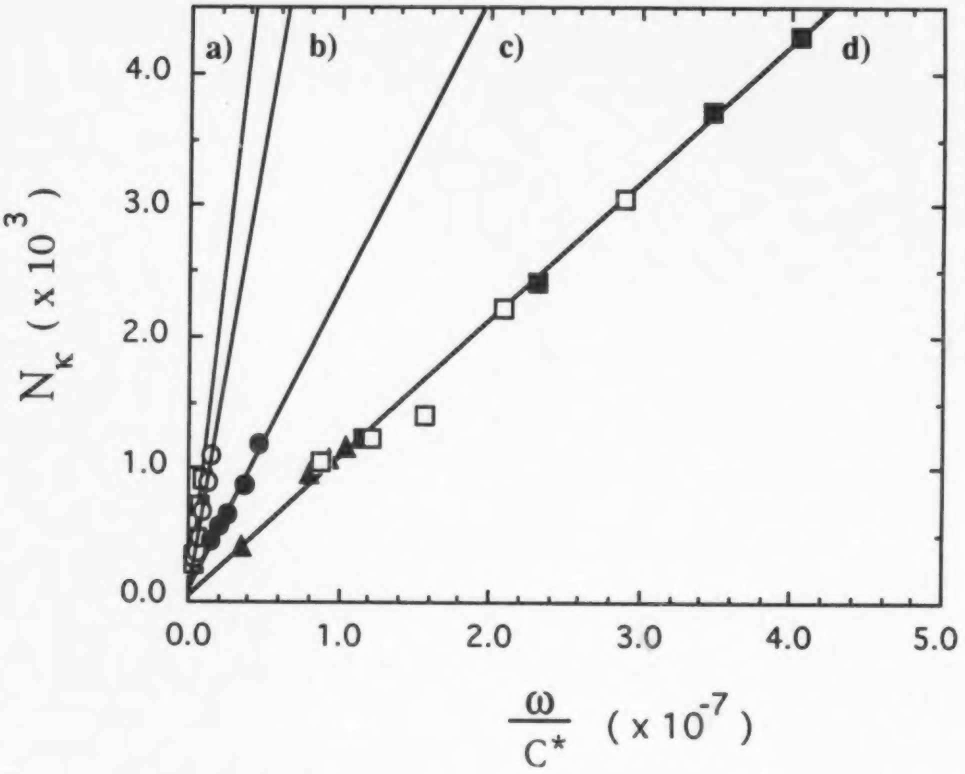

Figure 5.4.7: Second order plot: Kinetic collection efficiency versus ω/C* for various concentrations of pyrrole in acetonitrile containing 0.1 *M* $NaClO_4$.

a). 0.50 m*M*
b). 0.30 m*M*
c). 0.10 m*M*
d). 0.05 m*M*, 0.03 m*M* , and 0.01 m*M*

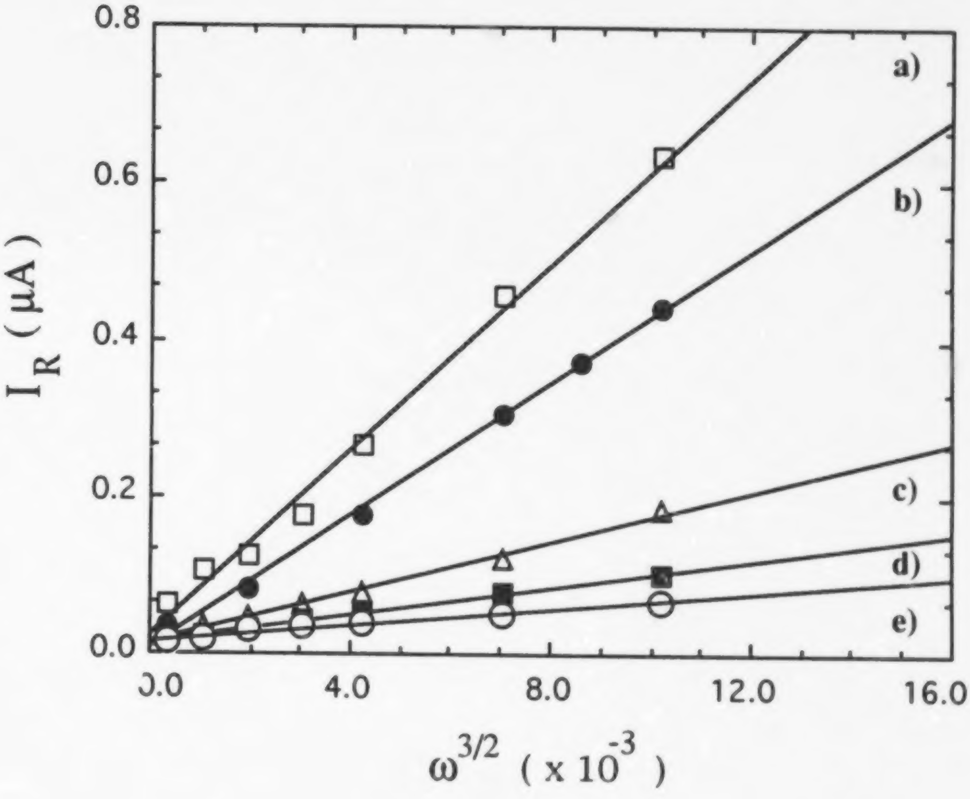

Figure 5.4.8: Second order plot: Ring (bipyrrole) current versus $\omega^{3/2}$ for various concentrations of pyrrole in acetonitrile containing 0.1 *M* $NaClO_4$.

a).	0.50 m*M*
b).	0.30 m*M*
c).	0.10 m*M*
d).	0.05 m*M*
e).	0.03 m*M*

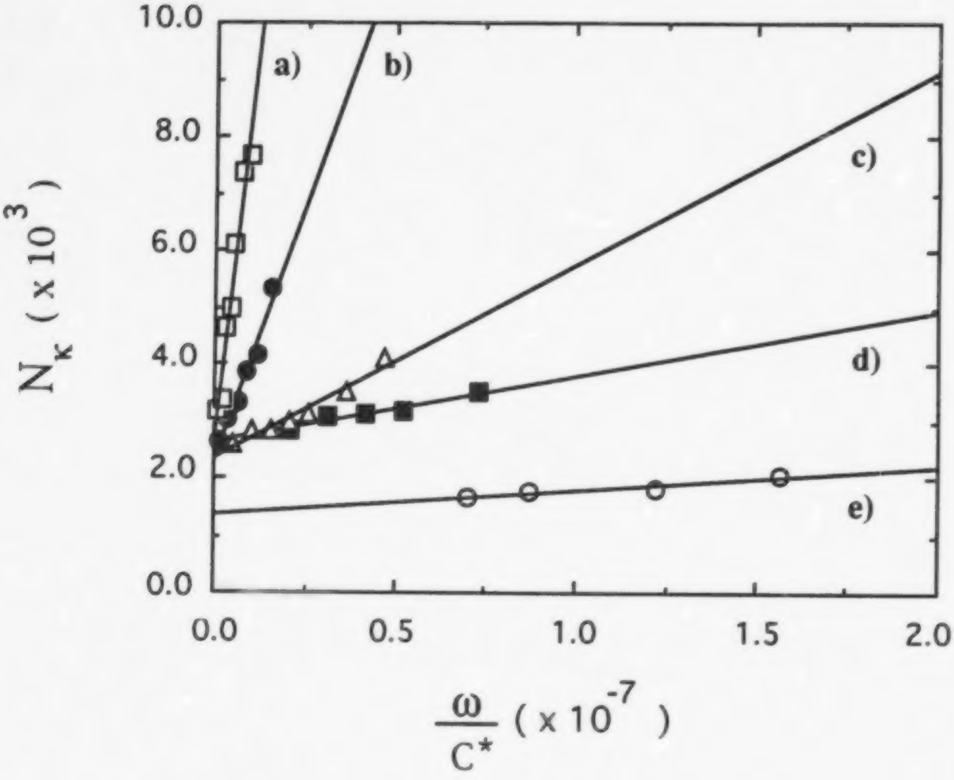

Figure 5.4.9: Second order plot: Kinetic collection efficiency versus ω/C* for various concentrations of pyrrole in acetonitrile containing 0.1 *M* TBABF$_4$.

a). 0.50 m*M*
b). 0.30 m*M*
c). 0.10 m*M*
d). 0.05 m*M*
e). 0.03 m*M*

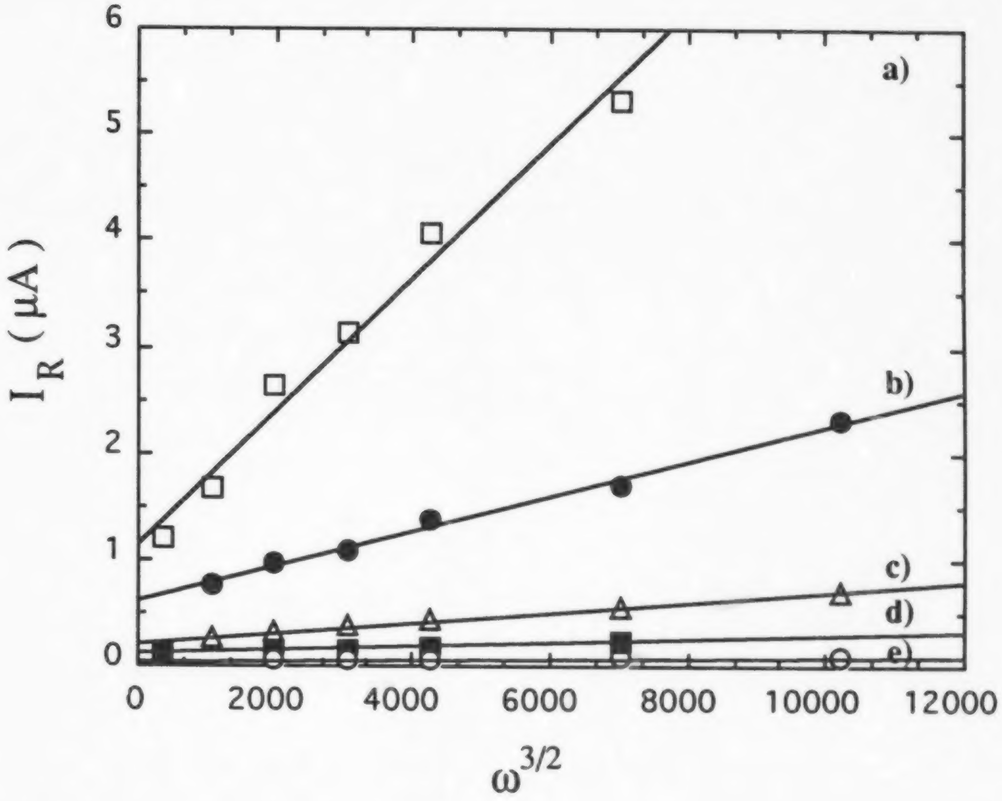

Figure 5.4.10: Second order plot: Ring (bipyrrole) current versus $\omega^{3/2}$ for various concentrations of pyrrole in acetonitrile containing 0.1 *M* TBABF$_4$.

a). 0.50 m*M*
b). 0.30 m*M*
c). 0.10 m*M*
d). 0.05 m*M*
e). 0.03 m*M*

It is useful to calculate values of the second order rate constants from the slopes of the various plots, as it indicates the magnitude of the rate observed. Table 5.4.4 lists the values of the second order rate constants obtained from various pyrrole concentrations in acetonitrile with 0.1 *M* $NaClO_4$, while Table 5.4.5 and Table 5.4.6 contain the values obtained with 0.1 *M* $TBABF_4$ and 0.1 *M* TBAP, respectively. The values of the rate constants for $NaClO_4$ were obtained from a number of replicate runs resulting in a standard deviation of ±13% and ±12% for the N_k versus ω/C^* and I_{Rk} versus $\omega^{3/2}$ plots, respectively. These standard deviations are assumed to be the same for TBAP and $TBABF_4$, as replicate runs for these electrolytes were not carried out. The magnitude of the second order rate constant in acetonitrile containing perchlorate anions ranges from 3.0 x 10^7 liters/mole-sec to 1.5 x 10^9 liters/mole-sec, while for the tetrabutylammonium tetrafluoroborate anion the range is an order of magnitude less. The top of Figure 5.4.11 shows the rate constants obtained with perchlorate anion electrolyte in acetonitrile versus the concentration of pyrrole. The rate constants obtained from the collection efficiency data and the ring current data are used in the figure. The data show an inverse dependence of the rate constant on the concentration of pyrrole, as demonstrated in the bottom of Figure 5.4.11. The identical plots for various pyrrole concentrations in acetonitrile with 0.1 *M* $TBABF_4$ are given in Figure 5.4.12. A different relationship is observed between the second order rate constant and the pyrrole concentration and was found to correspond to an inverse square dependence.

The standard RRDE second order kinetic theory (Equation 5.2.8) predicts that one common line should be obtained from a plot of N_K versus ω/C^* for various bulk concentrations investigated. In Figures 5.4.7 and 5.4.9 an individual line is obtained for each concentration of pyrrole used. This demonstrates that deviations from theory occur when analyzing the polymerization of pyrrole in acetonitrile containing $NaClO_4$ or $TBABF_4$. Similarly, it is anticipated that if the theory is correct then the rate constants obtained should exhibit no concentration dependence. The $1/C^*$ and $1/C^{*2}$ concentration dependence of the rate constant shown in Figures 5.4.11 and 5.4.12, respectively, further demonstrates that using the standard RRDE second order kinetic theory is inappropriate. This result is not entirely surprising since the theory was developed assuming a second order reaction between two different species and not a dimerization process. Also, the rate of formation of bipyrrole was not considered in the above analysis, a process undoubtedly significant for kinetic analysis of pyrrole polymerization. This process is incorporated in the digital simulation approach discussed below.

	Second order rate constant , k_2. (liters/mole-sec)	
Pyrrole Concentration. m*M*	Plot of N_κ versus ω/C^* ± 13%	Plot of $I_{R,\kappa}$ versus $\omega^{3/2}$ ± 12%
0.01	1.45×10^9	1.48×10^8
0.03	1.02×10^9	1.14×10^9
0.05	3.75×10^8	6.41×10^8
0.10	1.90×10^8	3.36×10^8
0.30	6.10×10^7	1.27×10^8
0.50	3.77×10^7	7.41×10^7

Table 5.4.4: Second order rate constants obtained for various pyrrole concentrations in acetonitrile containing 0.1 *M* $NaClO_4$.

	Second order rate constant, k_2. (liters/mole-sec)	
Pyrrole Concentration. m*M*	Plot of N_κ versus ω/C ± 13%	Plot of $I_{R,\kappa}$ versus $\omega^{3/2}$ ± 12%
0.01	--------------------	--------------------
0.03	9.68×10^8	1.02×10^9
0.05	3.48×10^8	2.71×10^8
0.10	1.17×10^8	9.78×10^7
0.30	2.24×10^7	2.87×10^7
0.50	5.62×10^6	8.45×10^7

Table 5.4.5: Second order rate constants obtained for various pyrrole concentrations in acetonitrile containing 0.1 *M* $TBABF_4$.

	Second order rate constant , k_2. (liters/mole-sec)	
Pyrrole Concentration. m*M*	Plot of N_κ versus ω/C^* ± 13%	Plot of $I_{R,\kappa}$ versus $\omega^{3/2}$ ± 12%
0.01	--------------------	--------------------
0.03	9.23×10^8	1.08×10^9
0.05	5.91×10^8	7.26×10^8
0.10	1.92×10^8	3.01×10^8
0.30	6.39×10^7	1.19×10^8
0.50	5.63×10^7	1.05×10^8

Table 5.4.6: Second order rate constants obtained for various pyrrole concentrations in acetonitrile containing 0.1 *M* TBAP.

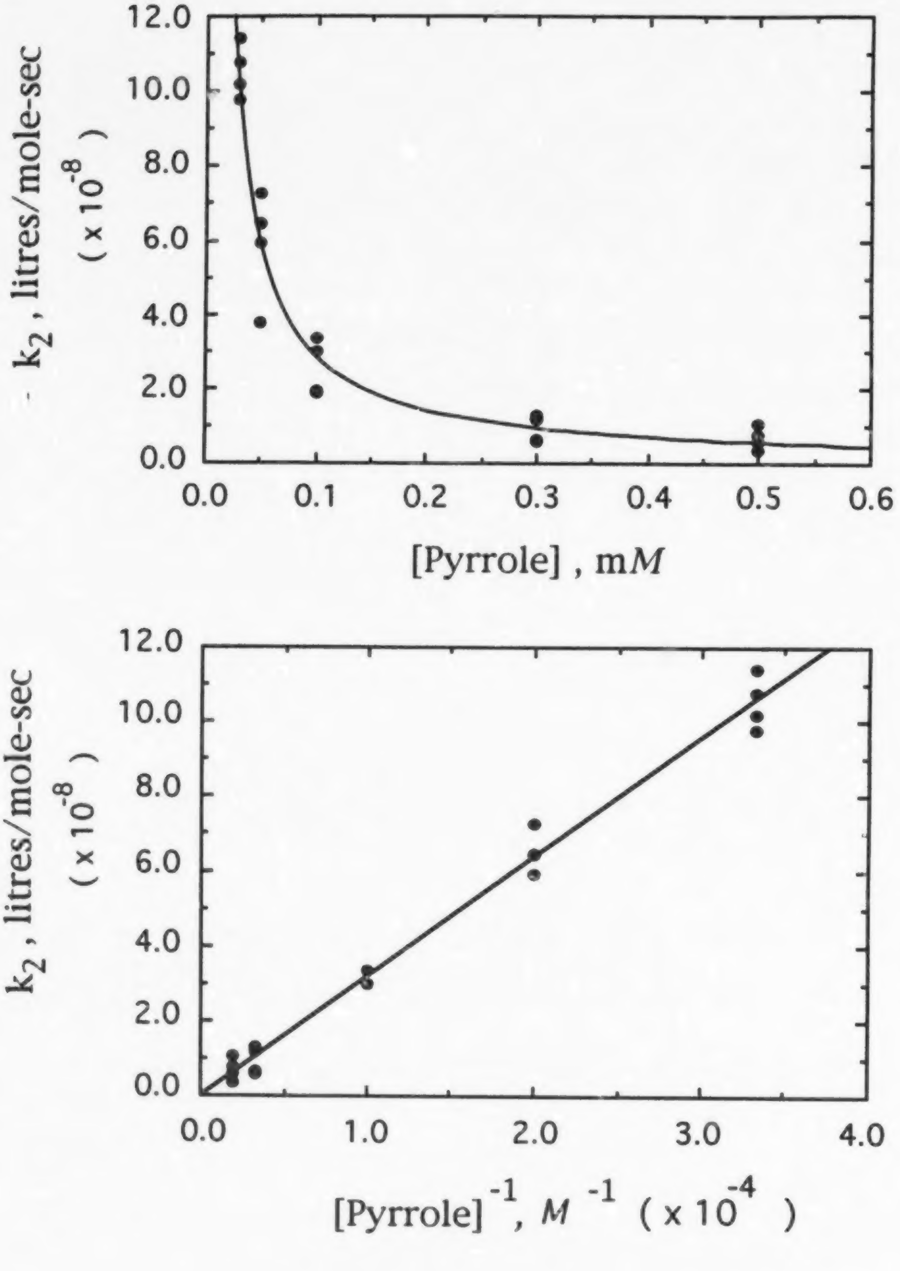

Figure 5.4.11: Second order rate constant as a function of pyrrole concentration in acetonitrile containing 0.1 *M* $NaClO_4$ and 0.1 *M* TBAP.

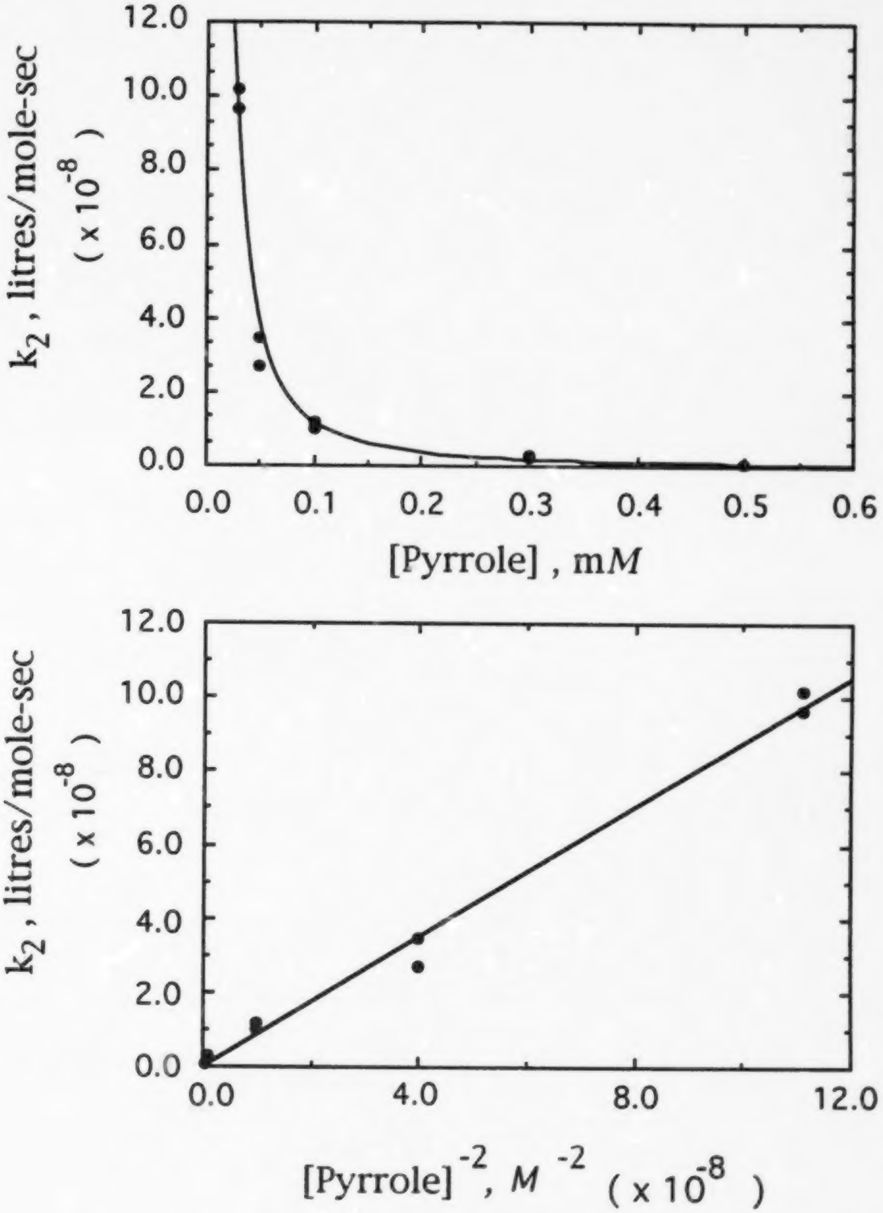

Figure 5.4.12: Second order rate constant as a function of pyrrole concentration in acetonitrile containing 0.1 *M* $TBABF_4$.

5.4.2-3 Digital Simulation: Finite Difference Analysis.

Digital simulation techniques have been applied to the determination of rate parameters for complicated electrochemical processes [5]. In those analyses the diffusion coefficients of all species present were assumed to be equal. The ability to investigate situations in which the reacting species diffuse at very different rates was one of the primary reasons for the development of the algorithm of Feldberg *et al* [23]. The digital simulation program, written in Professional Fortran, describing the algorithm [23] was obtained indirectly from Feldberg and used after modification to incorporate the appropriate homogeneous kinetic scheme. The program is given in the appendix indicating the modified subroutines. The reaction schemes used will be discussed below. The algorithm was used to calculate simulated collection efficiency as a function of the dimensionless rate parameter, Q_k. This kinetic parameter corresponds to a rate constant used in the simulation as seen in Equation 5.4.4,

$$Q_k = \frac{kC^{*}\nu^{1/3}}{(0.51)^{2/3}\omega D^{1/3}} \tag{5.4.4}$$

where k is the reaction rate constant, v is the kinematic viscosity, ω is the angular velocity, C* is the bulk concentration, and D is the diffusion coefficient of the bulk species. In the program it was possible to choose a different kinetic parameter for each step in the reaction scheme.

The simulation required the diffusion coefficients for the various species involved in the reaction scheme. The largest diffusion coefficient entered was normalized to the dimensionless value of 0.4 and the others were scaled with respect to this value. The value of 0.4 is the maximum value allowable in the program, as larger values result in simulation errors. To ensure that the simulation does not oscillate during explicit finite difference analysis, a stability factor is used [39]. This factor limits the value available for the dimensionless diffusion coefficient. To overcome this limitation implicit finite difference techniques have been developed [39], but were not used in this analysis. The bipyrrole dimensionless diffusion coefficient was obtained by multiplying the dimensionless pyrrole value by the ratio of the actual diffusion coefficient of bipyrrole and pyrrole. The diffusion coefficients for pyrrole and bipyrrole obtained from Taylor dispersion were 3.8×10^{-5} cm^2/s and 2.7×10^{-5} cm^2/s, respectively. This resulted in dimensionless values of 0.4 and dimensionless values of 0.4 and 0.28 being assigned to pyrrole and bipyrrole. To obtain the values for the larger oligomers a linear extrapolation of the plot of dimensionless diffusion coefficient versus the number of monomer units was used. With this method the dimensionless diffusion coefficients for terpyrrole and quatrepyrrole were found to be 0.17 and 0.053, respectively. Further extrapolation resulted in negative dimensionless diffusion coefficient values, therefore 0.053 was used for the remaining higher oligomers. Finally, the dimensionless diffusion coefficients for the radical cations were assumed to be equal to their respective parent species.

As discussed in chapter 3 the electropolymerization of pyrrole is thought to occur via solution phase polymerization. For pyrrole to polymerize the monomer must be oxidized in solution, forming the radical cation as the primary product. All the reaction schemes assumed in the digital simulation for the solution phase polymerization of pyrrole involved this oxidation process, however, the propagation steps were either radical-radical coupling, radical-monomer coupling, or a comproportionation process involving the bipyrrole dication. The latter scheme incorporates radical-radical coupling as the propagation process. During the simulation all reaction steps described in the various reaction schemes were assumed to have the same value of Q_k, and the protons generated during polymerization are not explicitly mentioned. The first steps in the radical-radical coupling mechanism are:

$$\begin{aligned}
2M^{\cdot +} &\xrightarrow{k_p} M_2 \\
M_2 + M^{\cdot +} &\longrightarrow M_2^{\cdot +} + M \\
M_2^{\cdot +} + M^{\cdot +} &\longrightarrow M_3 \\
2M_2^{\cdot +} &\longrightarrow M_4
\end{aligned}$$

The steps then cascade as described in Figure 5.4.13. The first steps in the radical-monomer coupling mechanism are:

DISK

$$\begin{array}{l} M - n_D e^- \longrightarrow M^{\cdot +} \\ M_2 - n_D e^- \longrightarrow M_2^{\cdot +} \\ M_3 - n_D e^- \longrightarrow M_3^{\cdot +} \\ M_4 - n_D e^- \longrightarrow M_4^{\cdot +} \\ M_5 - n_D e^- \longrightarrow M_5^{\cdot +} \end{array}$$

RING

$$M_2 - n_R e^- \longrightarrow M_2^{\cdot +}$$

SOLUTION

$$\begin{array}{rcl} 2M^{\cdot +} & \xrightarrow{k_p} & M_2 \\ M_2 + M^{\cdot +} & \longrightarrow & M_2^{\cdot +} + M \\ 2M_2^{\cdot +} & \longrightarrow & M_4 \\ M_2^{\cdot +} + M^{\cdot +} & \longrightarrow & M_3 \\ M_3 + M^{\cdot +} & \longrightarrow & M_3^{\cdot +} + M \\ M_3^{\cdot +} + M^{\cdot +} & \longrightarrow & M_4 \\ M_3^{\cdot +} + M_2^{\cdot +} & \longrightarrow & M_5 \\ M_4 + M^{\cdot +} & \longrightarrow & M_4^{\cdot +} + M \\ M_4^{\cdot +} + M^{\cdot +} & \longrightarrow & M_5 \\ M_4^{\cdot +} + M_2^{\cdot +} & \longrightarrow & M_6 \\ M_4^{\cdot +} + M_3^{\cdot +} & \longrightarrow & M_7 \end{array}$$

Figure 5.4.13: Radical-radical coupling scheme used in digital simulation.

$$\begin{aligned}
M + M^{\cdot +} &\xrightarrow{k_p} M{-}M^{\cdot +}\\
M{-}M^{\cdot +} + M^{\cdot +} &\longrightarrow M_2 + M\\
M_2 + M^{\cdot +} &\longrightarrow M_2{-}M^{\cdot +}\\
M_2^{\cdot +} + M &\longrightarrow M_2{-}M^{\cdot +}\\
M_2{-}M^{\cdot +} + M^{\cdot +} &\longrightarrow M_3 + M\\
M_2{-}M^{\cdot +} + M_2^{\cdot +} &\longrightarrow M_3 + M_2
\end{aligned}$$

The steps then cascade as described in Figure 5.4.14. The steps in the comproportionation/radical-radical coupling mechanism are:

$$\begin{aligned}
2M^{\cdot +} &\xrightarrow{k_p} M_2\\
M_2^{2+} + M &\longrightarrow M_2^{\cdot +} + M^{\cdot +}\\
M_2 + M^{\cdot +} &\longrightarrow M_2^{\cdot +} + M\\
M_2^{\cdot +} + M^{\cdot +} &\longrightarrow M_3\\
2M_2^{\cdot +} &\longrightarrow M_4
\end{aligned}$$

This reaction scheme is described in Figure 5.4.15. In these schemes M corresponds to monomer (pyrrole), $M^{\cdot +}$ is the pyrrole radical cation, M_2 is bipyrrole, $M_2^{\cdot +}$ is the bipyrrole radical cation, M_2^{2+} is the bipyrrole dication, M_n-$M^{\cdot +}$ is the radical monomer couple, M_3 is terpyrrole and M_4 is quatrepyrrole.

Working curves for each assumed mechanism were constructed by plotting the simulated collection efficiencies against the dimensionless kinetic parameter. The curves were subsequently used to evaluate the rate constant, k, from the experimental collection efficiencies at each electrode rotation rate, ω, by plotting the value of Q_k obtained from the experimental data versus ω^{-1}. The slope of the resulting plot is proportional to the rate constant, k, as shown in Equation 5.4.4. Figure 5.4.16 shows a plot of Q_k versus C^*/ω for various concentrations of pyrrole in acetonitrile containing 0.1 *M* $NaClO_4$. Equation 5.4.4 indicates that a plot of Q_k versus C^*/ω should be one common line. This is observed in Figure 5.4.16 for concentrations of pyrrole less than and equal to 0.1 m*M*. The plots at larger concentrations are linear with similar slopes, but are shifted along the C*/w axis.

DISK

$$
\begin{aligned}
M - n_D e^- &\longrightarrow M^{\cdot+}\\
M{-}M^{\cdot+} - n_D e^- &\longrightarrow M_2\\
M_2 - n_D e^- &\longrightarrow M_2^{\cdot+}\\
M_2{-}M^{\cdot+} - n_D e^- &\longrightarrow M_3\\
M_3 - n_D e^- &\longrightarrow M_3^{\cdot+}\\
M_3{-}M^{\cdot+} - n_D e^- &\longrightarrow M_4\\
M_4 - n_D e^- &\longrightarrow M_4^{\cdot+}\\
M_4{-}M^{\cdot+} - n_D e^- &\longrightarrow M_5\\
M_5 - n_D e^- &\longrightarrow M_5^{\cdot+}
\end{aligned}
$$

RING

$$M_2 - n_D e^- \longrightarrow M_2^{\cdot+}$$

SOLUTION

$$
\begin{aligned}
M + M^{\cdot+} &\xrightarrow{k_p} M{-}M^{\cdot+}\\
M{-}M^{\cdot+} + M^{\cdot+} &\longrightarrow M_2 + M\\
M_2 + M^{\cdot+} &\longrightarrow M_2{-}M^{\cdot+}\\
M_2^{\cdot+} + M &\longrightarrow M_2{-}M^{\cdot+}\\
M_2{-}M^{\cdot+} + M^{\cdot+} &\longrightarrow M_3 + M\\
M_2{-}M^{\cdot+} + M_2^{\cdot+} &\longrightarrow M_3 + M_2\\
M_3 + M^{\cdot+} &\longrightarrow M_3{-}M^{\cdot+}\\
M_3^{\cdot+} + M &\longrightarrow M_3{-}M^{\cdot+}\\
M_3{-}M^{\cdot+} + M^{\cdot+} &\longrightarrow M_4 + M\\
M_3{-}M^{\cdot+} + M_2^{\cdot+} &\longrightarrow M_4 + M_2\\
M_3{-}M^{\cdot+} + M_3^{\cdot+} &\longrightarrow M_4 + M_3\\
M_4 + M^{\cdot+} &\longrightarrow M_4{-}M^{\cdot+}\\
M_4^{\cdot+} + M &\longrightarrow M_4{-}M^{\cdot+}\\
M_4{-}M^{\cdot+} + M^{\cdot+} &\longrightarrow M_5 + M\\
M_4{-}M^{\cdot+} + M_2^{\cdot+} &\longrightarrow M_5 + M_2\\
M_4{-}M^{\cdot+} + M_3^{\cdot+} &\longrightarrow M_5 + M_3\\
M_4{-}M^{\cdot+} + M_4^{\cdot+} &\longrightarrow M_5 + M_4
\end{aligned}
$$

Figure 5.4.14: Radical-monomer coupling scheme used in digital simulation.

DISK

$$M - n_D e^- \longrightarrow M^{\cdot +}$$

$$M_2 - n_D e^- \longrightarrow M_2^{2+}$$

$$M_2^{\cdot +} - n_D e^- \longrightarrow M_2^{2+}$$

$$M_3 - n_D e^- \longrightarrow M_3^{2+}$$

RING

$$M_2 - n_R e^- \longrightarrow M_2^{\cdot +}$$

SOLUTION

$$2M^{\cdot +} \xrightarrow{k_p} M_2$$

$$M_2^{2+} + M \longrightarrow M_2^{\cdot +} + M^{\cdot +}$$

$$M_2 + M^{\cdot +} \longrightarrow M_2^{\cdot +} + M$$

$$M_2^{\cdot +} + M^{\cdot +} \longrightarrow M_3$$

$$2M_2^{\cdot +} \longrightarrow M_4$$

Figure 5.4.15: Comproportionation with radical-radical coupling scheme used in digital simulation.

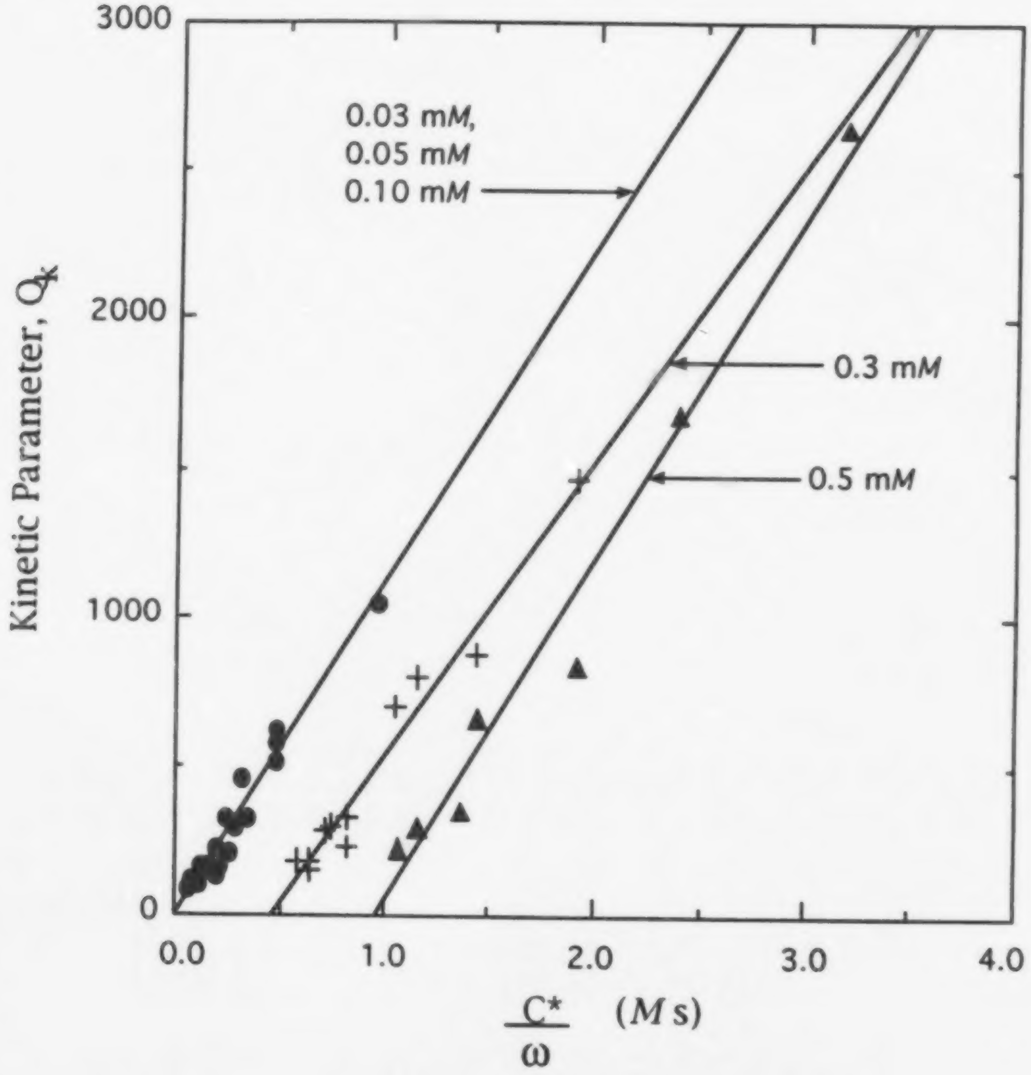

Figure 5.4.16: Plot of dimensionless rate parameter (obtained from experimental collection efficiencies) versus C*/ω for various concentrations of pyrrole in acetonitrile containing 0.1 *M* $NaClO_4$.

Similar plots for acetonitrile containing 0.1 *M* $TBABF_4$ are shown in Figure 5.4.17. In this electrolyte the kinetic plots for all concentrations of pyrrole are linear but exhibit differing slopes and intercepts. This deviation from theory suggests that the mechanisms assumed in this electrolyte system are inappropriate.

Figure 5.4.18 demonstrates the effect on the working curve as the number of polymerization steps increases during simulation of the radical-radical coupling scheme. In this plot the logarithm of the kinetic parameter is used for clarity. The largest working curve in Figure 5.4.18 was obtained by considering only the formation of a dimer, which subsequently is oxidized at the disk and does not react in solution. It can be seen that a significant decrease in the magnitude of the simulated collection efficiency occurs as the number of steps in the propagation process increases from the formation of the dimer to the formation and solution reaction of the trimer. Also, a shift in the peak toward smaller Q_k values is observed. The same trend occurs for further increases in the number of propagation steps, but to a much lesser degree.

An important feature of the working curves not generally observed [5] is that for small kinetic parameters the simulated collection efficiency drops toward zero. More commonly the primary electrochemical species generated at the disk electrode is monitored at the ring electrode. This results in the collection efficiency for stable intermediate species (theoretical collection efficiency) being obtained at a Q_k of zero, and as the value of Qk increases the collection efficiency decreases [5,24]. Equation 5.4.4 indicates that as Q_k increases the value of ω decreases and the rate constant increases. These two factors cause the collection efficiency for the primary species to decrease as Q_k is increased. That is, as the rate of reaction increases less of the primary radical cation reaches the ring electrode and consequently the collection efficiency decreases. Similarly, as the rotation rate decreases there is more time for the following reaction to occur and again the collection efficiency decreases. In contrast, if the primary species dimerizes to form an electroactive product, and this product is monitored at the ring electrode, then the collection efficiency is zero at a Q_k of zero. This is because with a rate constant of zero the product does not form and the product collection efficiency is zero. It is observed in Figure 5.4.18 that as Q_k increases the collection efficiency increases to a maximum value, and then decreases at larger Q_k. The initial rise is a result of increasing quantities of product being observed at the ring electrode due to increases in the rate constant. The decrease is a result of the decreasing rotation rate. As the rotation rate decreases more time is available for the electroactive product to react at the disk electrode, which results in less product observed at the ring.

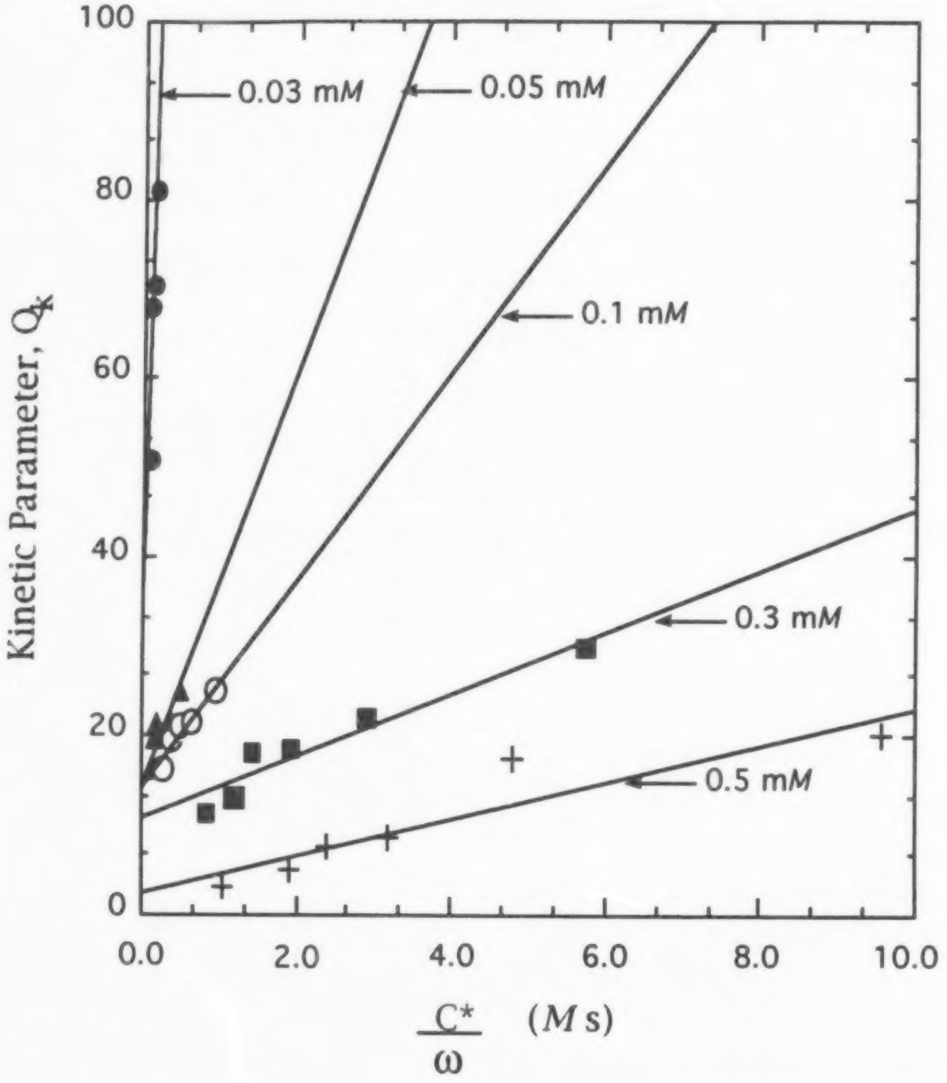

Figure 5.4.17: Plot of dimensionless rate parameter (obtained from experimental collection efficiencies) versus C^*/ω for various concentrations of pyrrole in acetonitrile containing 0.1 *M* $TBABF_4$.

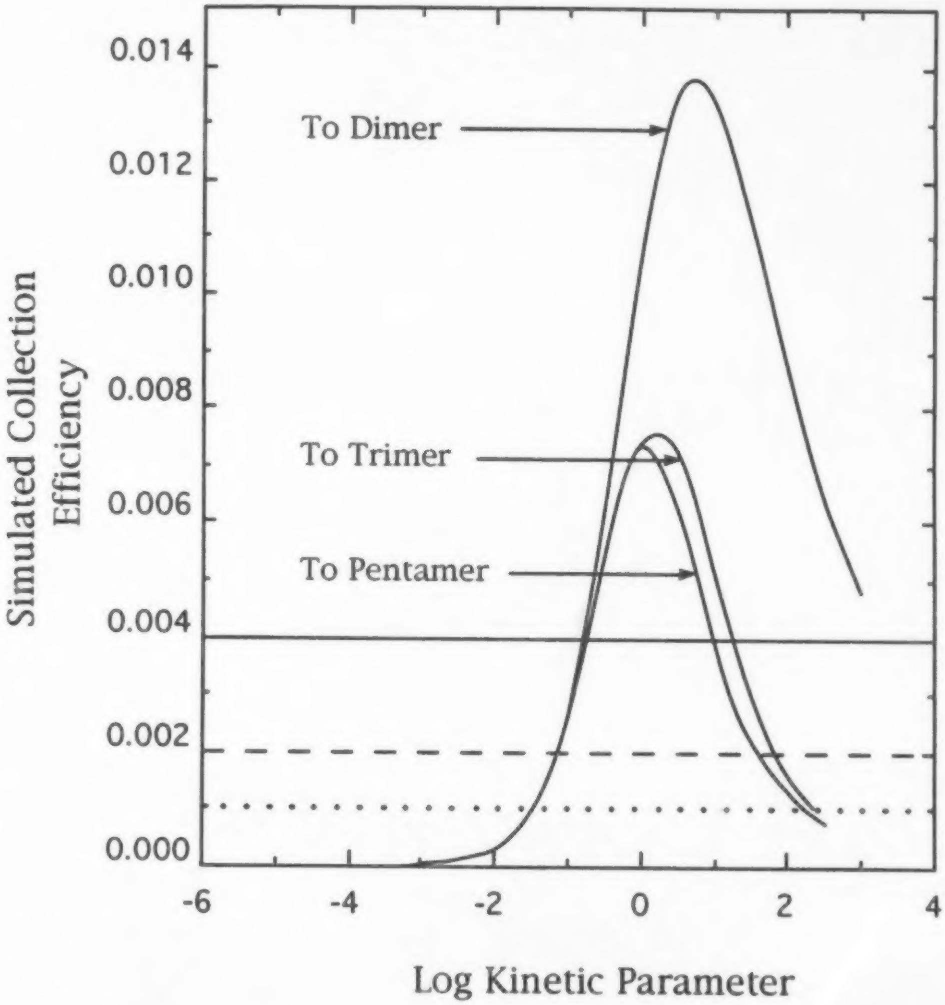

Figure 5.4.18: Set of curves demonstrating the effect the number of polymerization steps has on the working curves for the radical-radical coupling scheme. These curves were obtained using a correction factor of 2.66 (see text p.169). The $NaClO_4$ and TBAP data lies below the dashed line, the $TBABF_4$ data lies below the solid line. The dotted line indicates the data region for propylene carbonate.

Finally, the maximum in collection efficiency is due to the competition between the rate constant and rotation rate effects.

In this study bipyrrole is the species monitored at the ring electrode. Bipyrrole is the product of a chemical reaction involving the primary oxidation product, the radical cation, and is electroactive. Therefore, the working curve shown in Figure 5.4.18 corresponding to just the formation of an electroactive dimer should be sufficient to model this system. However, bipyrrole is also involved in a homogeneous chemical reaction, a process not considered above. The remaining working curves given in Figure 5.4.18 incorporate reaction steps involving the electroactive dimer which results in the formation of the trimer and pentamer. This situation should be a more accurate model of the formation and reaction of bipyrrole. The same general shape is observed for each working curve because of similar competing effects between the rotation rate and the rate of formation of the dimer. The decrease in the maximum collection efficiency is probably due to loss of bipyrrole via homogeneous reactions.

The digital simulation assumes the overall disk and ring electrode reactions are one electron processes and does not consider the variability in the number of electrons involved during the polymerization of pyrrole in different electrolytes (Table 5.4.2). Therefore, only one working curve for each reaction scheme is actually generated. To be able to analyze the data for different electrolyte systems the collection efficiencies from this working curve were divided by the appropriate number of electrons, generating working curves for the specific electrolyte used. The logic behind this approach is described below.

The simulated collection efficiencies were calculated from the dimensionless ring and disk currents, which were related to the respective dimensionless fluxes [23]. This approach assumed that the number of electrons at each electrode were identical. However, if the number of electrons at the ring, n_R, is not equal to the number of electrons at the disk, n_D, then these must be included in the expressions used to calculate the collection efficiency. Equation 5.4.5 shows the dimensioned collection efficiency expression relating the ring and disk fluxes at the electrode surfaces, i.e.z=0.

$$N_0 = \left| - \frac{i_R}{i_D} \right| = \frac{n_R F D_{red} 2\pi \int_{r_2}^{r_3} \left(\frac{\delta C_{red}}{\delta z} \right)_{z=0} r \, dr}{n_D F A_D D_{ox} \left(\frac{\delta C_{ox}}{\delta z} \right)_{z=0}} \quad \textbf{(5.4.5)}$$

The total ring current is the summation of the ring currents obtained from infinitesimal sections of the ring of thickness δr.

The expression for the ring current in Equation 5.4.5 is obtained as δr approaches zero. In these equations D_{red} and D_{ox} are the diffusion coefficients for the reducible and oxidizable species, while C_{red} and C_{ox} are their respective concentrations. F is the faraday, A_D is the disk area, and r2 and r3 are the inner and outer ring radii, respectively. Also, r and z define the radial and axial components of the RRDE. When the number of electrons are assumed to be the same and the diffusion coefficients are unequal, equation 5.4.5 is reduced to Equation 5.4.6. A dimensionless form of this expression was used in the simulation.

(5.4.6)
$$N_0 = \left| -\frac{i_R}{i_D} \right| = \frac{2\pi\, D_{red} \int_{r_2}^{r_3} \left(\frac{\delta C_{red}}{\delta z} \right)_{z=0} r\, dr}{A_D\, D_{ox} \left(\frac{\delta C_{ox}}{\delta z} \right)_{z=0}}$$

If $n_D \neq n_R$ then Equation 5.4.5 must be used instead. For example, if $n_D = 2n_R$ and the diffusion coefficients of the species observed at the ring and disk are different, then the expected collection efficiency is given by Equation 5.4.7.

(5.4.7)
$$N' = \frac{D_{ring}\, 2\pi \int_{r_2}^{r_3} \left(\frac{\delta C_{red}}{\delta z} \right)_{z=0} r\, dr}{2 A_D D_{disk} \left(\frac{\delta C_{ox}}{\delta z} \right)_{z=0}}$$

Inserting Equation 5.4.6 into Equation 5.4.7 yields the relationship (Equation 5.4.8) required to correct the simulated collection efficiencies for the cases when $n_D \neq n_R$. In this equation the diffusion coefficients for pyrrole and bipyrrole are inserted.

(5.4.8)
$$N' = \frac{N_0}{2} \frac{D_{bipyrrole}}{D_{pyrrole}}$$

This indicates that the collection efficiencies obtained from the simulation program must be divided by the number of electrons involved at the disk electrode for the specific electrolyte used (Table 5.4.2).

Figure 5.4.19 shows the working curves calculated for each reaction scheme described in Figures 5.4.13 to 5.4.15 normalized to the largest value of the simulated collection efficiency. The working curves for $NaClO_4$ and TBAP can be obtained by multiplying Figure 5.4.19 by a normalizing factor of 8.6 x 10^{-3}, while for TBABF4 the factor is 9.9 x 10^{-3}. Also shown are the regions (normalized) in which the experimental collection efficiencies for the various electrolytes occur. The curves used to calculate the rate constants for polymerization of pyrrole in acetonitrile containing various electrolytes were corrected for the number of electrons, n, by substituting n from Table 5.4.2 where 2 occurs in Equation 5.4.8. These curves were identical in shape as the normalized curves. For instance the curves in Figure 5.4.18 were obtained using a value of 2.7 for the number of electrons. In Figure 5.4.18 it is evident that the experimental data lies below the dimer curve. Therefore, as indicated in Figure 5.4.19, the working curves corresponding to the reaction progressing to the pentamer were used to obtain the kinetic parameters for radical-radical coupling and radical-monomer coupling, while a curve for the reaction to trimer was used for the comproportionation scheme. The decreasing portion of the working curves were used to obtain the rate information since the plot of experimental N_k against ω^{-1} shows that N_k decreases as ω^{-1} increases, the same behaviour observed for the analogous plot of N_k versus Q_k. Also, evaluation of the rate constants using the rising portion resulted in values significantly smaller than those expected for the polymerization of pyrrole.

The overall polymerization rate constants obtained from the respective working curves for 0.1 *M* $NaClO_4$, 0.1 *M* TBAP and 0.1 *M* $TBABF_4$ in acetonitrile are given in Tables 5.4.7, 5.4.8 and 5.4.9, respectively. The values of the rate constants obtained in $NaClO_4$ were obtained from a number of replicate runs resulting in a standard deviation of 19% (typically N=8 for a given concentration). This standard deviation is assumed to be the same for TBAP and TBABF4, as extensive replicate runs for these electrolytes were not carried out. Plots of the rate constants for the different reaction schemes are given in Figure 5.4.20 as a function of pyrrole concentrations in acetonitrile containing 0.1 *M* $NaClO_4$. Similar plots for the other electrolyte systems are given in Figures 5.4.21 and 5.4.22.

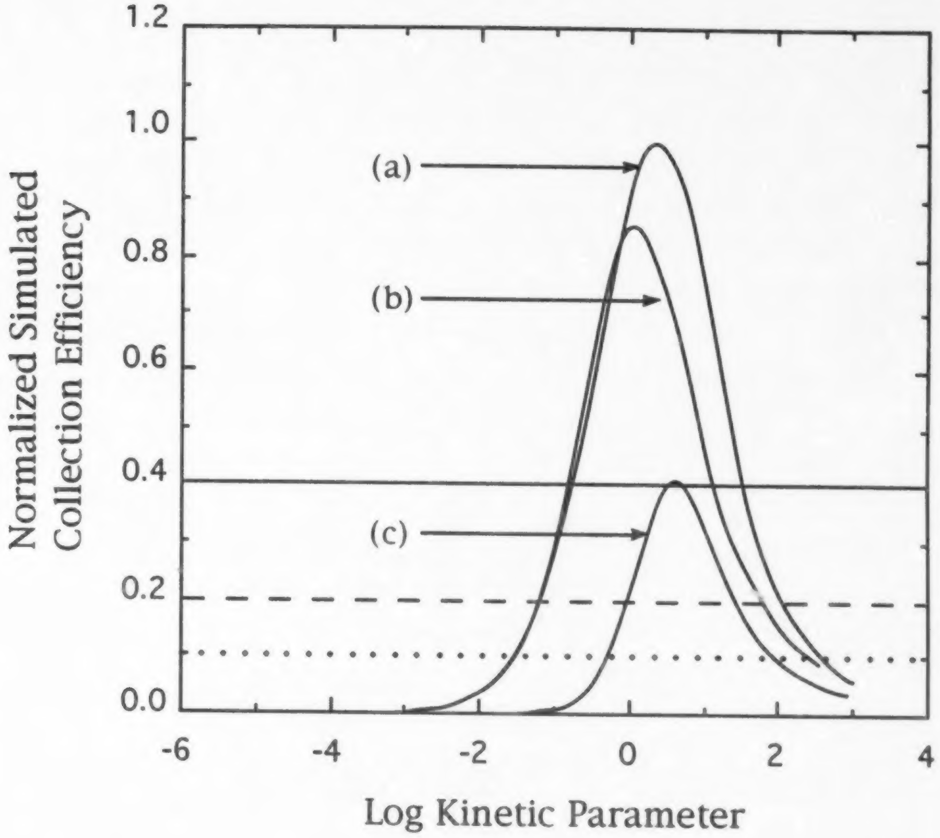

Figure 5.4.19: Normalized working curves used to evaluate pyrrole polymerization in acetonitrile containing 0.1 *M* $NaClO_4$, 0.1 *M* TBAP and 0.1 *M* $TBABF_4$. The $NaClO_4$ and TBAP data lies below the dashed line, the $TBABF_4$ data lies below the solid line. The dotted line indicates the data region for propylene carbonate.

Curve (a) shows comproportionation to the trimer.
Curve (b) shows radical-radical coupling to the pentamer.
Curve (c) shows radical-monomer coupling to the pentamer.

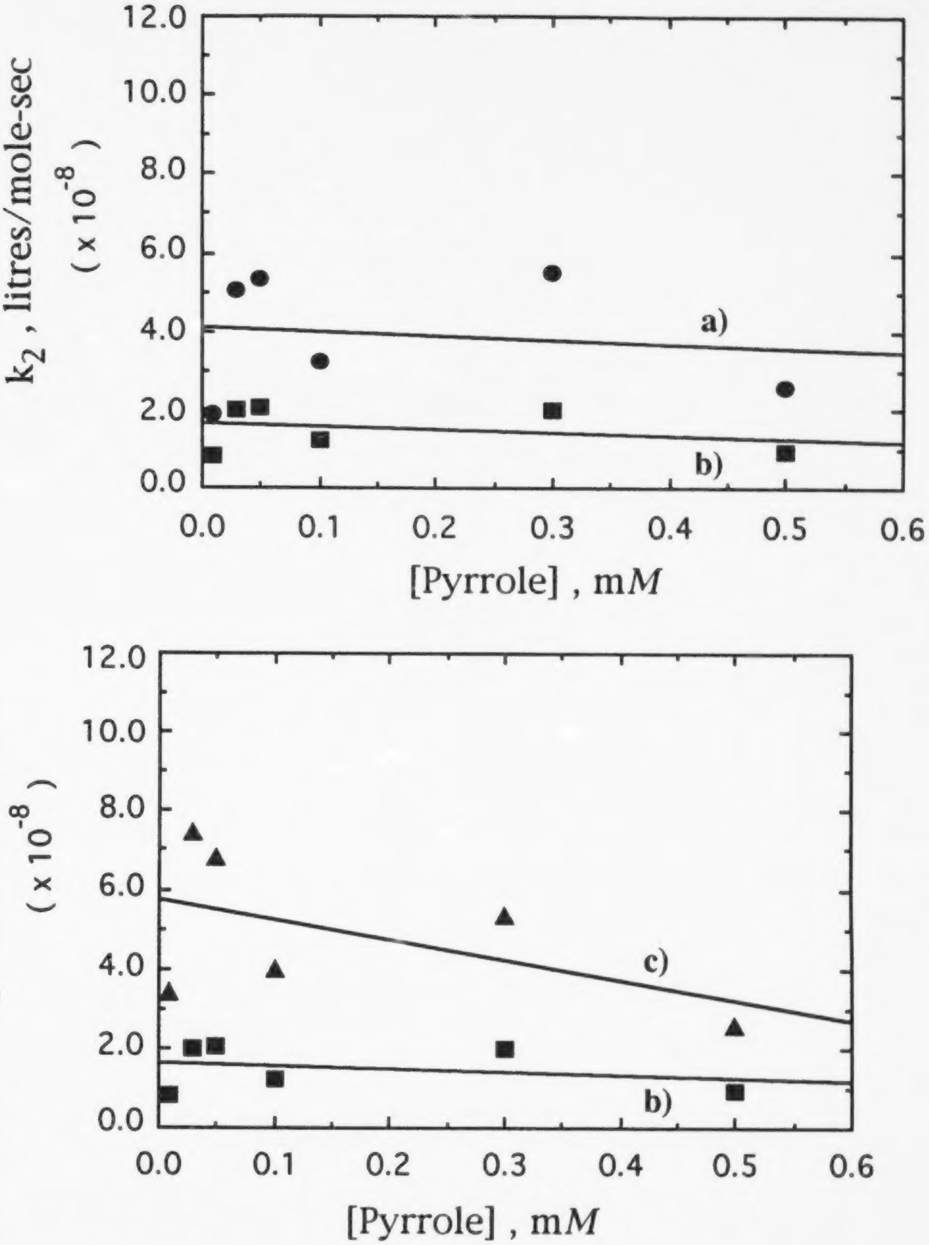

Figure 5.4.20: Dependence of the overall polymerization rate constant on the concentration of pyrrole in acetonitrile and 0.1 M $NaClO_4$.
a). Radical-radical coupling scheme.
b). Radical-monomer coupling scheme.
c). Comproportionation scheme.

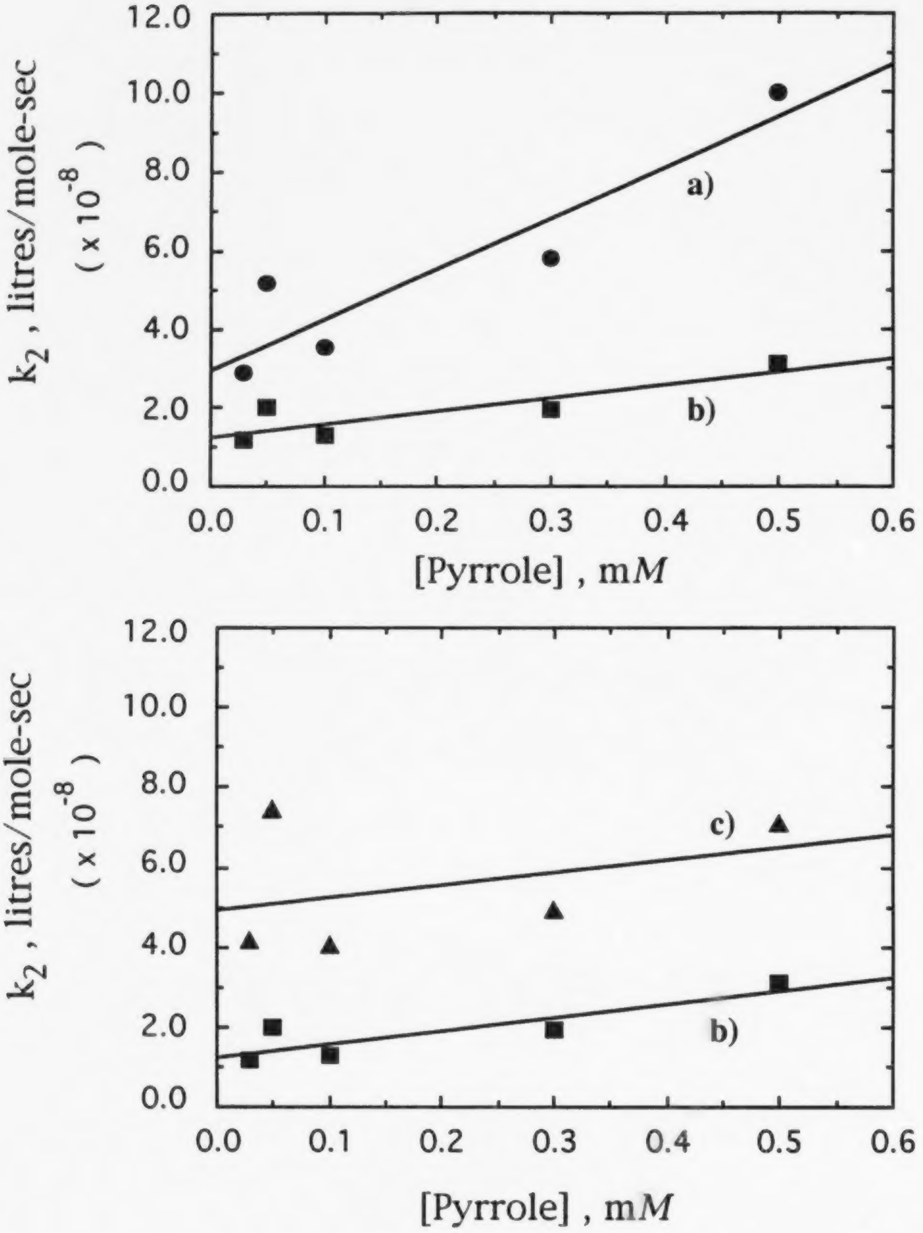

Figure 5.4.21: Dependence of the overall polymerization rate constant on the concentration of pyrrole in acetonitrile and 0.1 M TBAP.
a). Radical-radical coupling scheme.
b). Radical-monomer coupling scheme.
c). Comproportionation scheme.

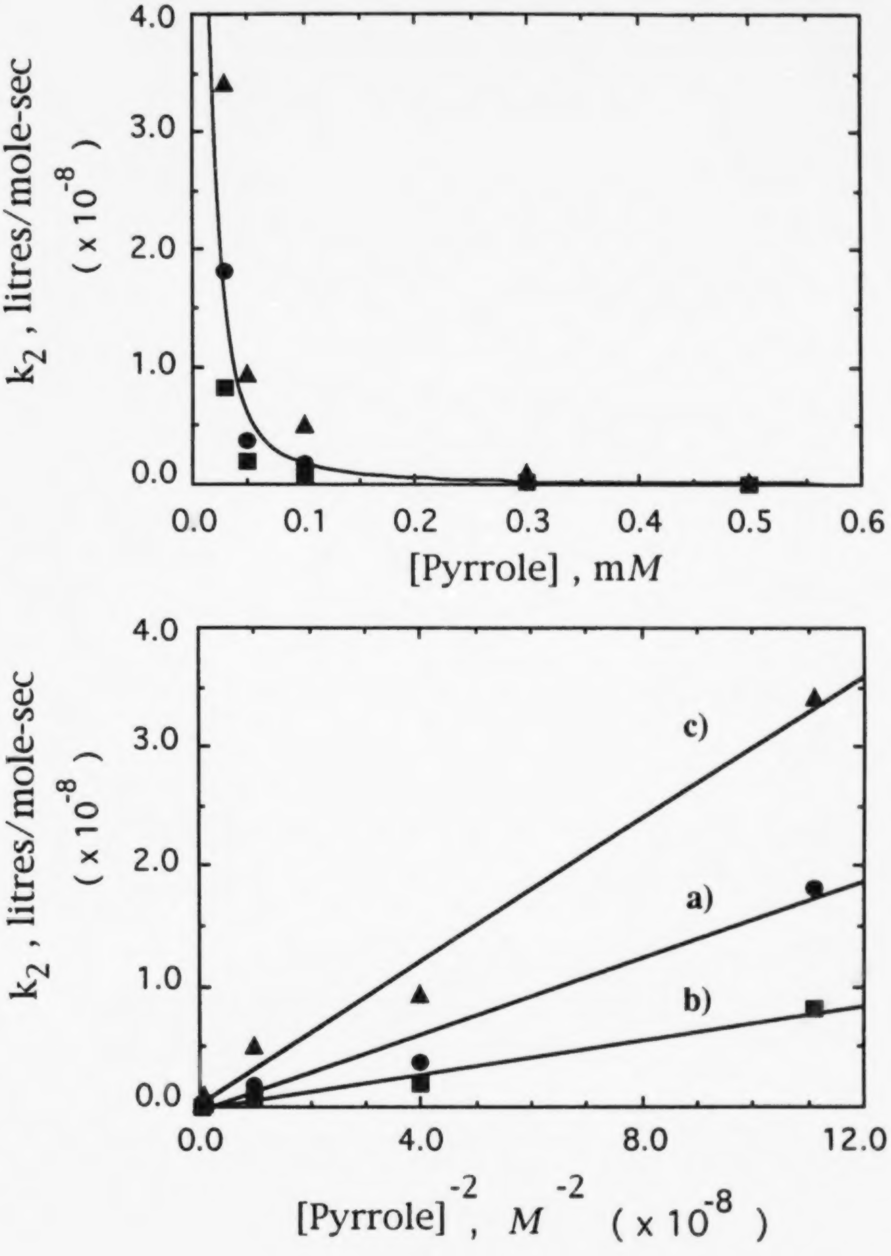

Figure 5.4.22: Dependence of the overall polymerization rate constant on the concentration of pyrrole in acetonitrile and 0.1 M $TBABF_4$.

a). Radical-radical coupling scheme.
b). Radical-monomer coupling scheme.
c). Comproportionation scheme.

The overall rate constant obtained for the polymerization of pyrrole in acetonitrile containing the perchlorate anion is essentially constant as the concentration of pyrrole increases. The rate analysis for systems containing perchlorate anions show no dependence on pyrrole concentration, therefore the average overall rate constants and their associated standard deviations are given in Tables 5.4.7 and 5.4.8. This non-dependence on pyrrole concentration suggests that the assumed reaction schemes used in the simulation are appropriate to describe pyrrole polymerization in these systems.

With the tetrabutylammonium tetrafluoroborate anion the second order rate constant exhibits a dependence on the inverse square of the pyrrole concentration. The values of the rate constants obtained for the various pyrrole concentrations are given in Table 5.4.9. This dependence indicates that the reaction schemes are not accurate representations of the polymerization processes with this electrolyte. This conclusion is demonstrated in Figure 5.4.17 in which the plots of Q_k versus C^*/ω for various concentrations of pyrrole do not lie on a common line. This deviates from the expected behaviour described by Equation 5.4.4. Attempts to find another reasonable reaction scheme to describe the observed inverse square relationship were unsuccessful. It is possible the different electrolyte behaviour reflects a more complicated role of the protons in the polymerization process so that the electrolyte (a stronger base than ClO_4^-), and or protons, must be explicitly involved in the simulation. This aspect of the digital simulation of pyrrole polymerization remains unanswered and requires future work.

	Overall polymerization rate constant , k. (liters/mole-sec) ± 19 %		
Pyrrole Concentration. m*M*	Radical-Radical Coupling. Scheme 1	Radical-Monomer Coupling. Scheme 2	Comproportionation. Scheme 3
0.01	1.9×10^8	8.3×10^7	3.4×10^8
0.03	5.0×10^8	2.0×10^8	7.4×10^8
0.05	5.3×10^8	2.1×10^8	6.8×10^8
0.10	3.2×10^8	1.2×10^8	4.0×10^8
0.30	5.5×10^8	2.0×10^8	5.3×10^8
0.50	2.6×10^8	9.1×10^7	2.6×10^8
Average ± Std Dev	$(4 \pm 1) \times 10^8$	$(1.5 \pm 0.6) \times 10^8$	$(5 \pm 2) \times 10^8$

Table 5.4.7: Overall polymerization rate constants obtained using Finite Difference Method for various pyrrole concentrations in acetonitrile containing 0.1 *M* $NaClO_4$. Different reactions schemes as shown.

	Overall polymerization rate constant , k. (liters/mole-sec) ± 19 %		
Pyrrole Concentration. m*M*	Radical-Radical Coupling. Scheme 1	Radical-Monomer Coupling. Scheme 2	Comproportionation. Scheme 3
0.03	2.9×10^8	1.18×10^8	4.17×10^8
0.05	5.1×10^8	1.97×10^8	7.46×10^8
0.10	3.5×10^8	1.32×10^8	4.06×10^8
0.30	5.8×10^8	1.94×10^8	4.93×10^8
0.50	1.0×10^9	3.13×10^8	7.08×10^8
Average ± Std Dev	$(5 \pm 3) \times 10^8$	$(1.9 \pm 0.8) \times 10^8$	$(5 \pm 2) \times 10^8$

Table 5.4.8: Overall polymerization rate constants obtained using Finite Difference Method for various pyrrole concentrations in acetonitrile containing 0.1 *M* TBAP. Different reactions schemes as shown.

	Overall polymerization rate constant , k. (liters/mole-sec) ± 19 %		
Pyrrole Concentration. m*M*	Radical-Radical Coupling. Scheme 1	Radical-Monomer Coupling. Scheme 2	Comproportionation. Scheme 3
0.03	1.81×10^{8}	8.12×10^{7}	3.41×10^{8}
0.05	3.70×10^{7}	1.86×10^{7}	9.37×10^{7}
0.10	1.68×10^{7}	7.85×10^{6}	5.05×10^{7}
0.30	4.06×10^{6}	1.93×10^{6}	8.85×10^{6}
0.50	9.50×10^{5}	4.77×10^{5}	2.38×10^{6}

Table 5.5.9: Overall polymerization rate constants obtained using Finite Difference Method for various pyrrole concentrations in acetonitrile containing 0.1 *M* $TBABF_4$. Different reactions schemes as shown.

5.4.2-4 Discrimination between Reaction Schemes.

It has been previously demonstrated that digital simulation allows the discrimination between coupling reactions involving either the primary species generated at the disk and the parent species, or by dimerization of the primary species [5]. The resulting N_k-Q_k curves were said to accurately describe the reaction kinetics and mass transport effects, and could be used to determine the values of the rate constants provided the mechanism was known. However, the use of these curves to discriminate between mechanisms was impossible since identical curve shapes were obtained. On the other hand the use of disk currents at values below the limiting disk current were shown to be more diagnostic in determining the mechanism among various reaction schemes [5]. In this situation simulations involved evaluation of the simulated collection efficiency at different values of the relative disk current, CONI. This variable is the ratio of the disk current (I_D) at a given potential along the disk current-voltage curve to the limiting disk current ($I_{D,L}$) as shown in Equation 5.4.5.

$$\text{CONI} = \frac{I_D}{I_{D,L}} \qquad \textbf{(5.4.5)}$$

The values of I_D and $I_{D,L}$ were calculated assuming a single value for Q_k, resulting in separate N_k versus CONI curves for each Q_k used. It was observed that for different reaction schemes and Q_k values the N_k versus CONI curves had dramatically different curve shapes. Comparison of experimental N_k versus CONI curves to the simulated curves could then allow assignment of the appropriate mechanism. The experimental data was obtained by stepping the disk potential to various values along the disk current-voltage curve and monitoring the steady state ring and disk currents.

The working curves (Figure 5.4.19) calculated for the three different mechanisms assumed for the polymerization of pyrrole had similar shapes but were shifted along the log Q_k axis depending on the mechanism. This is the same observation as in the literature [5], and therefore, it is not possible to use these curves to distinguish between radical-radical coupling, radical-monomer coupling, or comproportionation. Attempts to analyze the electropolymerization mechanism of pyrrole using the approach of the N_k versus CONI plot were unsuccessful since the data was obtained from potential scan experiments and not at steady state. The deposition process described in chapter 3 causes distortions in the disk current-voltage curves such that the experimental N_k versus CONI plot were meaningless. It would be more appropriate to obtain the data using steady state currents at fixed potentials, however this was not done. The assignment of the mechanism for pyrrole polymerization by digital simulation remains unanswered.

5.4.2-5 Analysis of Pyrrole Polymerization in Propylene Carbonate.

The plots of N_K versus $\omega^{1/2}$ for various concentrations of pyrrole in propylene carbonate containing 0.2 *M* $NaClO_4$ are shown in Figures 5.4.23. In contrast to the increase in N_k with increasing $\omega^{1/2}$ observed in acetonitrile, Figures 5.4.3 and 5.4.4, in propylene carbonate there is a decrease in N_k. Analyzing the data using the standard second order kinetic theory was not possible because of this rotation rate dependence. The plot of N_k versus log ω^{-1} is shown in Figure 5.4.24 and is analogous to plotting N_k versus log Q_k. Opposite behaviour is observed in propylene carbonate compared to acetonitrile, with the value of N_k increases with log ω^{-1} in propylene carbonate while it decreases in acetonitrile. Since the kinetic collection efficiency increased with increasing log ω^{-1} it was anticipated that the propylene carbonate data could be analyzed on the rising portion of the calculated working curves.

Evaluation of the overall polymerization rate constant using the rising portion of the working curve resulted in values substantially lower than anticipated, e.g. 10^3 liters/mole-sec and lower. If these values for the overall polymerization rate constants are appropriate for this solvent system then it is expected that a stable reduction current for the radical cation should be observed. Instead of obtaining this stable current, the transient behaviour discussed in chapter 4 occurred. Therefore, the rate constants obtained are meaningless and it is unreasonable to assume the data can be analyzed appropriately on the rising portion of the working curves. The mechanistic process present in propylene carbonate remains unclear.

5.4.2-6 Effect of Added Water on the Observation of Bipyrrole during the Polymerization of Pyrrole in Acetonitrile.

It was demonstrated that in comparison to polypyrrole films formed in dry acetonitrile, those formed in acetonitrile containing 1% water had smoother morphologies [40]. Also, the addition of higher concentrations (e.g. 25%) lead to loss in tensile strength

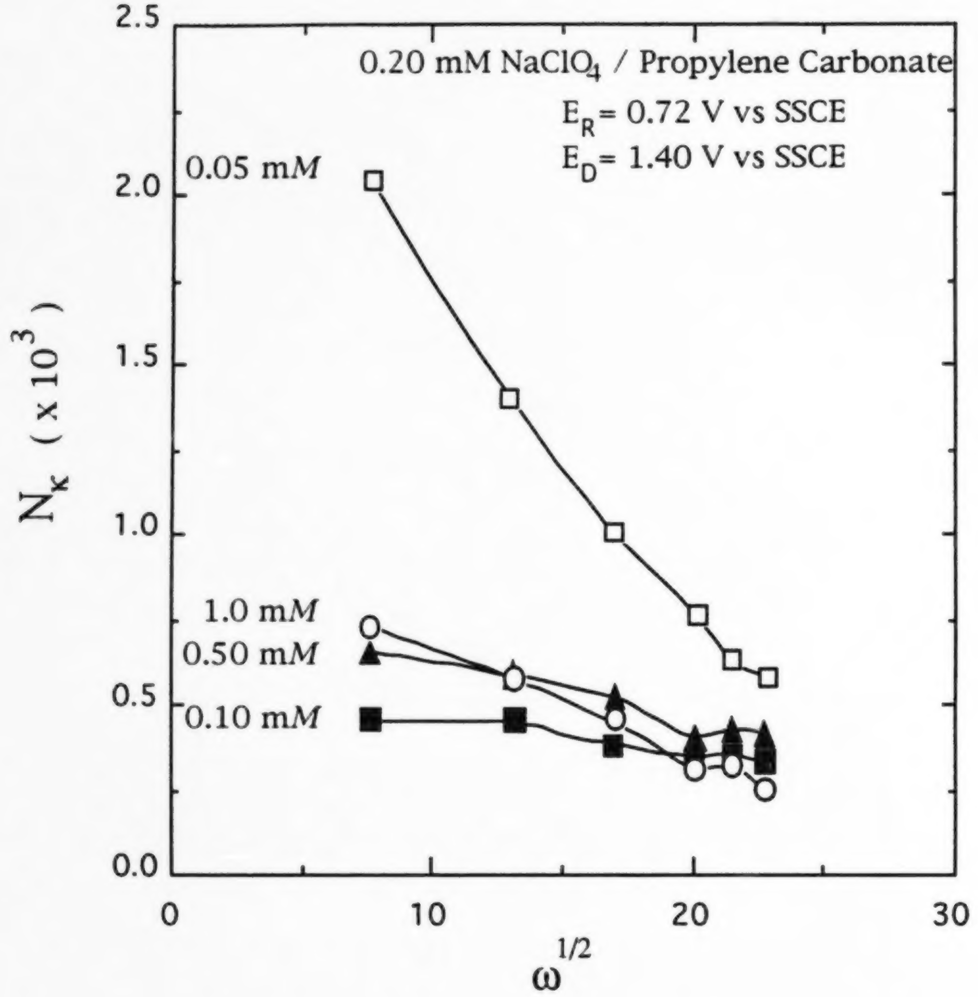

Figure 5.4.23: Plot of the experimental collection efficiency versus $\omega^{1/2}$ obtained during pyrrole polymerization in propylene carbonate containing 0.2 *M* $NaClO_4$.

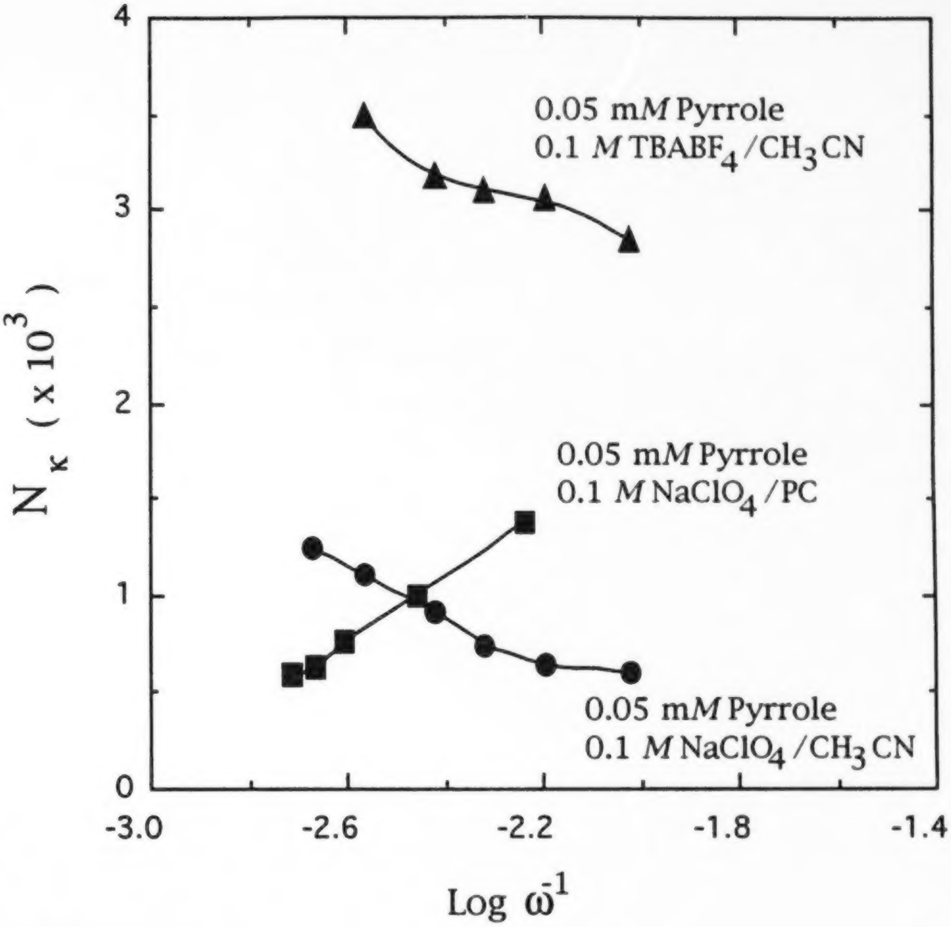

Figure 5.4.24: Plot comparing the experimental collection efficiency versus log ω^{-1} obtained during pyrrole polymerization in propylene carbonate containing 0.1 *M* $NaClO_4$ to the results obtained in acetonitrile containing 0.1 *M* $TBABF_4$ and 0.1 *M* TBAP.

and conductivity [41]. It was anticipated that by monitoring the effect of added water on the yield of bipyrrole some general mechanistic conclusions could be drawn to understand this observation. A preliminary investigation was undertaken and the results are shown in Figure 5.4.25. The top of Figure 5.4.25 shows N_k versus $\omega^{1/2}$ for 0.1 m*M* pyrrole, 0.1 *M* $NaClO_4$ in acetonitrile with various volume percentages of added water. The bottom of Figure 5.4.25 shows N_k versus $\omega^{1/2}$ for 50 m*M* pyrrole, 0.1 *M* $NaClO_4$ in acetonitrile. The percentages of water added correspond to the following concentrations of water: 0.01 % is approximately 5.5 m*M* and 0.1 % is approximately 55 m*M*.

The top of Figure 5.4.25 demonstrates that a dramatic decrease in the yield of bipyrrole occurs when water is added to the solvent, and the yield continues to decrease as the concentration of water is increased. In this situation the initial concentration of the added water immediately exceeded the concentration of pyrrole present. In the bottom of Figure 5.4.25 the effect of increasing the concentration of water for a larger pyrrole concentration (50 m*M*) is shown. This plot demonstrates that a decrease in the yield of bipyrrole occurs when the water concentration equals that of pyrrole. This latter concentration of pyrrole is generally used in the literature to form polypyrrole films which are subsequently tested for conductivity differences. At this point no conclusions can be drawn about the effect of the water on the mechanism of pyrrole polymerization.

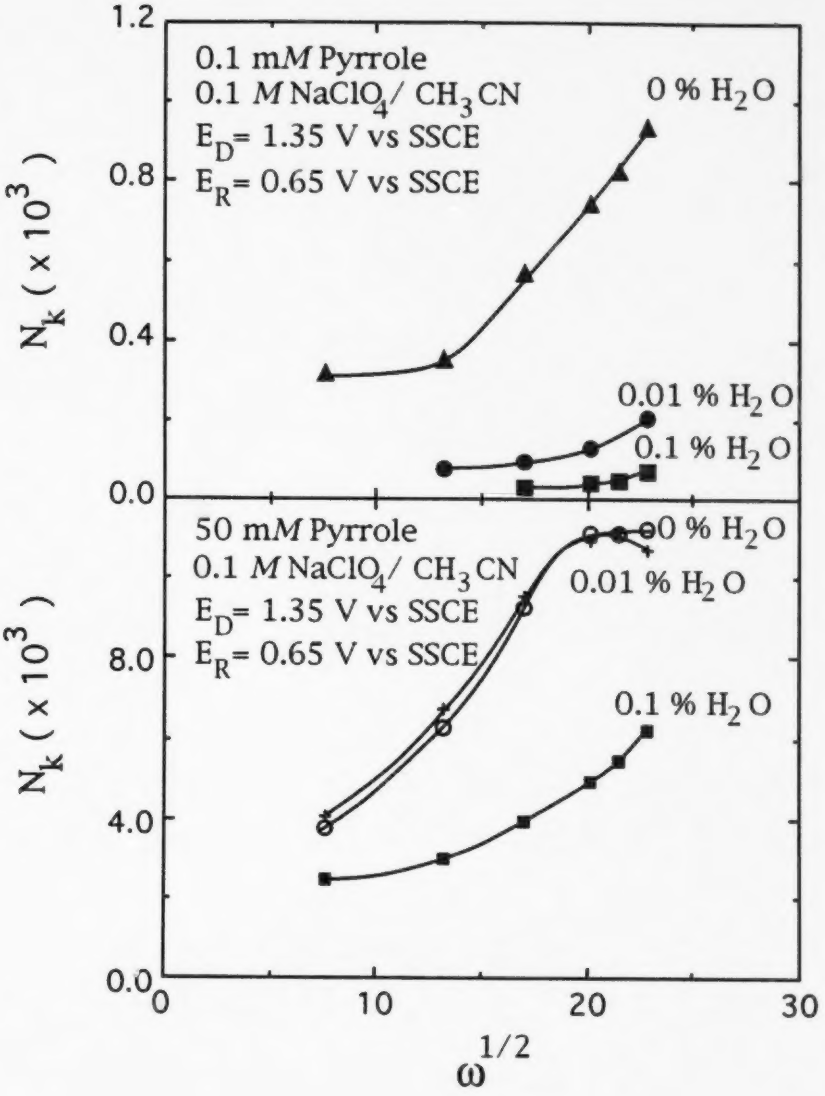

Figure 5.4.25: Plot of experimental collection efficiency versus $\omega^{1/2}$ demonstrating the effect of added water on the yield of bipyrrole during polymerization of pyrrole from 0.1 m*M* pyrrole and 50 m*M* pyrrole in acetonitrile containing 0.1 *M* $NaClO_4$.

5.5 Conclusions.

In this work digital simulation and standard rotating ring-disk electrode (RRDE) kinetic theory, for both first and second order homogeneous processes, were used to evaluate the overall polymerization rate constant for the electropolymerization of pyrrole. These analyses were applied to the evaluation of polymerization in acetonitrile and propylene carbonate containing either $NaClO_4$, $TBABF_4$ or TBAP as electrolyte. Using the standard RRDE kinetic theory it was observed that the polymerization of pyrrole in acetonitrile and propylene carbonate is not a first order process. For acetonitrile containing perchlorate anions the second order kinetic plots of N_k vs ω/C^* were linear for all concentrations of pyrrole investigated. However, the theory predicts that the data should lie on one common line. This behaviour was only observed for concentrations of pyrrole less than and equal to 0.05 m*M*. For acetonitrile with TBABF4 deviations from the theory occurred at all pyrrole concentrations. The magnitude of the observed rates ranged from 10^7 liters/mole-sec to 10^9 liters/mole-sec for acetonitrile with perchlorate anions, while with $TBABF_4$ the range was an order of magnitude less. The second order rate constants obtained using perchlorate anions exhibited an inverse dependence on pyrrole concentration, while with $TBABF_4$ an inverse square dependence was observed. These dependences may only serve to demonstrate that the second order reaction model was not obeyed. The rotation rate dependence of the collection efficiency in propylene carbonate was observed to be the inverse of the behaviour described by the second order kinetic theory, and therefore the rate constants were not evaluated.

Finite difference analysis was used to digitally simulate the expected collection efficiency for the polymerization of pyrrole at the RRDE. The three mechanisms reported in the literature describing electrochemical polymerization processes were used in the simulation. These mechanisms were radical-radical coupling, radical-monomer coupling and comproportionation combined with radical-radical coupling. The radical cation is involved in the propagation process in each mechanism, and for this reason the process can be considered identical for each scheme. The working curves obtained via digital simulation were found to have identical curve shapes, and therefore discrimination between the three assumed reaction mechanisms by this method was ineffective. However, following the procedure of plotting N_k versus CONI with data obtained under steady state conditions may allow possible discrimination.

The overall polymerization rate constants obtained using digital simulation for acetonitrile containing perchlorate anions exhibited no dependence on pyrrole concentration and gave average values of 4.1 x 10^8 liter/mole-sec assuming radical-radical coupling, 5.2 x 10^8 liter/mole-sec assuming comproportionation, and 1.7 x 10^8 liter/mole-sec assuming radical-monomer coupling. This indicates that the polymerization of pyrrole occurs at diffusion limited rates and suggests that the mechanisms assumed with ClO_4^- are appropriate. The overall polymerization rate constants obtained using digital simulation for acetonitrile containing $TBABF_4$ exhibited an inverse square dependence on pyrrole concentration for each mechanism with a range of values from 4.8 x 10^5 liter/mole-sec to 3.4 x 10^8 liter/mole-sec obtained. Clearly this dependence demonstrates that a different process is involved with this electrolyte.

Finally, a preliminary investigation using changes in the magnitude of the collection efficiency upon addition of water to the acetonitrile was undertaken. The effect of added water was found to decrease the yield of bipyrrole at a water concentration comparable to the bulk pyrrole concentration.

5.6 References.

1. a) Frumkin, A.N.; Nekresov, L.N.; Dokl Akad Nauk SSR, **1959**, 126, 115;
   b) Frumkin, A.N.; Nekresov, L.N.; Levich, B.; Ivanov, Yu., *J. Electroanal. Chem*, **1959-1960**, 1, 84.

2. Bagotskii, V.S.; Nekresov, L.N.; Shumilova, N.A., *Usepekhi Khimii*, **1965**, 34, 1697.

3. Albery, W.J.; Hitchman, M.C., *"Ring-Disk Electrodes"*, Oxford Press, London, **1971.**

4. a) Prater, K.B.; Bard, A.J., *J. Electrochem. Soc.*, **1970**, 117, 207, 335.
   b) Prater, K.B.; Bard, A.J., *J. Electrochem. Soc.*, **1970**, 117, 207, 1517.

5. a) Puglisi, V.J.; Bard, A.J., *J. Electrochem Soc.*, **1972**, 119, 829.
   b) Puglisi, V.J.; Bard, A.J., *J. Electrochem Soc.*, **1972**, 119, 833.

6. Puglisi, V.J.; Bard, A.J., *J. Electrochem Soc.*, **1973**, 120, 748.

7. Neubert, B.; Prater, K.B., *J. Electrochem Soc.*, **1974**, 121, 745.

8. Korotov, A.P.; Nekresov, L.N., *Soviet Electrochem.*, **1982**, 18, 35.

9. Yeh, Lun-Shu R.; Bard, A.J., *J. Electrochem. soc.*, **1977**, 124, 189.

10. Yeh, Lun-Shu R., *J. Electroanal Chem.*, **1977**, 84, 159.

11. Funt, B. Lionel; Severs, W.; Glasel, A., *J. Polym. Sci. Polym. Ed.*,**1976**, 14, 2763.

12. Funt, B. Lionel; Verigin, Victor, *Can. J. Chem.*, **1974**, 52, 1642.

13. Raymond, D.E.; Harrison, D. Jed, *J. Electroanal. Chem.*, **1990**, 296, 269.

14. Kras'ko, V.V.; Yakovleva, A.A.; Kozlova, N.V., *Soviet Electrochem.*, **1989**, 25, 947.

15. Beck, F.; Oberst, M.; Jansen, R., *Electrochimica Acta*, **1990**, 35, 1841.

16. Beck. F.; Oberst, M.; *J. Electroanal. Chem.*, **1990**, 285, 177.

17. Bruckenstein, S.; Sharkey, J.W., *J. Electroanal. Chem.*, **1988**, 241, 211.

18. Albery, W.J.; Bruckenstein, S.; Ulstrup.J., *Trans. Faraday. Soc.*, **1966**, 62, 2584.

19. Albery, W.J.; Bruckenstein, S.; Ulstrup.J., *Trans. Faraday. Soc.*, **1969**, 65, 1101.

20. Albery W.J., and Bruckenstein, S., *Trans. Faraday, Soc.*, **1966**, 62, 1946.

21. Feldberg, S.W.; Auerbach, C., *Anal. Chem.*, **1964**, 36, 505.

22. Feldberg, S.W., "*Electroanalytical Chemistry* ",Vol. 3, A.J. Bard, (Ed.), Marcel Dekker, Inc., New York, **1969**.

23. Feldberg, S.W.; Bowers, M.L.; Anson, F.C., *J. Electroanal. Chem.*, **1986**, 215, 11.

24. Bowers, M.L.; Anson, F.C.; Feldberg, S.W., *J. Electroanal. Chem.*, **1987**, 216, 249.

25. Levich, V.G., *Acta. Phys. Chim. URSS.*, **1942**, 11, 257.

26. Baker, C.K.; Reynolds, J.R., *J. Electroanal. Chem.*, **1988**, 251, 307.

27. Prejza, J.; Lundström, I.; Skothein, T., *J. Electrochem. Soc.*, **1982**, 129, 1685.

28. Funt, B.C.; Lowen, S.V., *Synth. Met.*, **1985**, 11, 129.

29. Genies, E.M.; Bidan, G.; Diaz, A.F., *J. Electroanal. Chem.*, **1983,** 149, 101.

30. Zotti, G.; Cattarin, S.; Comisso, N., *J. Electroanal. Chem.*, **1987**, 235, 259.

31. Rodrigues, I.; Marcos, M.L.; Bonzalea-Velasco, *Electrochimica. Acta*, **1987**, 32, 1181.

32. Prater, K.B.; Bard, A.J.; *J. Electrochem. Soc.*, **1970**, 117, 207.

33. Prater, K.B.; Bard, A.J.; *J. Electrochem. Soc.,* **1970**, 117, 335.

34. Prater, K.B.; Bard, A.J.; *J. Electrochem. Soc.*, **1970**, 117, 1517.

35. Skinner, J.F.; Glasel, A.; Hsu, L.; Funt, B.L., *J. Electrochem. Soc.*, **1980**, 27, 315.

36. Salmon, M.; Diaz, A.F.; Logan, A.J.; Drounbi, M.; Bargon, J., *Mol. Cryst. Liq. Cryst.*, **1983**, 83, 1297.

37. Asavapiriyamont, S.; Chandler, G.K.; Gunawardenu, G.A.; Pletcher, D.J., *J. Electroanal. Chem.*, **1984**, 177, 229.

38. Skotheim, Terje A., (Ed.), "*Handbook of Conducting Polymers* ", Chap. 3. **1982**, 1685.

39 Britz, D., "*Digital Simulation in Electrochemistry*", Springer-Verlag, New York, **1981.**

40. Diaz, A.F.; Kanazawa, K.K.; Gardini, G.P., *Chem. Commun.*, **1979**, 635.

41. Diaz, A.F.; Hall, B., *IBM J. Res. Develop.*, **1983**, 27, 342.

Chapter 6

Conclusions.

The morphology and conductivity of polypyrrole has been demonstrated to be very dependent on the polymerization conditions [1]. This behavior has resulted in a variety of empirical methods to obtain the appropriate film with the desired properties. Therefore, one of the principle reasons for investigating the electropolymerization of pyrrole is to obtain mechanistic information such that the film properties can be designed without the need of a set of empirically obtained conditions. The original goal of this thesis work was to use the rotating ring-disk electrode (RRDE) to study how solvent, electrolyte and water affects the polymer properties. However, it became evident that sorting out the RRDE data was not a simple process. The ability to observe and identify key intermediates and to obtain rate information became the new focus of study. The purpose of this concluding chapter is to summarize the contributions obtained and to discuss possible future efforts.

6.1 Summary of Contributions.

The possible presence and involvement of soluble intermediates species in the electropolymerization of pyrrole [2] prompted the investigation into the polymerization process using the RRDE. The studies focussed mainly on polymerization of pyrrole in acetonitrile containing either $NaClO_4$, $TBABF_4$ or TBAP as electrolyte. Studies using propylene carbonate were also undertaken but to a lesser extent. The first direct observation and identification of bipyrrole formed as an intermediate species resulted from this RRDE work. This observation was consistent with conclusions drawn from indirect mechanistic evidence. The collection efficiency for bipyrrole was found to be extremely small and the dependence on the rotation rate was observed to be complex. The low collection efficiency for this stable species indicated bipyrrole was either lost via oxidation at the disk electrode, rapidly consumed in the subsequent polymerization steps, or it was formed in low yield as a result of side reactions. The complex rotation rate dependence demonstrates that bipyrrole is not formed by a primary reaction and the pathway to its formation involves a number of chemical and electrochemical steps. Similar RRDE studies demonstrated the presence of pyrrole radical cations formed as transient intermediates. The data given in the pyrrole radical cation chapter (Chapter 3) demonstrates that solution species are involved and that these species are almost certainly associated with the main polymerization process, not a side reaction. Also, simple calculation indicated that the apparent transient behaviour of the pyrrole radical cations can be the result of the non-linear dependence of the radical cation concentration in a radical-radical coupling process. This supports, but does not prove, the radical coupling model. Finally, the ability to obtain peak shaped ring current/disk voltage curves for the radical cation using a rather crude calculation indicates that the radical is observed at the ring electrode.

Further evidence that bipyrrole is formed during the polymerization of pyrrole was obtained from spectroelectrochemical investigations. These studies also provided evidence for the formation of protonated pyrrole, terpyrrole and possibly quater- and quinquepyrrole. It also became evident that the choice of electrolyte can dramatically affect the local pH in the vicinity of the electrode surface. This evidence indicates the considerable probability that acid polymerization products will form along with electrochemical polymerization products. Since the acid polymerization products are non-conductive their presence should degrade film conductivity. This suggests that the use of basic species during pyrrole polymerization should improve the polymer properties, if the tendency for nucleophilic reactions leading to other reaction products can be avoided. This may be one of the reasons for some of the preferred properties of BF_4^- as an electrolyte during pyrrole anodization in acetonitrile.

The actual process by which polypyrrole films form is a major source of controversy in the literature. One view was that film growth occurs directly on the electrode surface [3], while the other opposite view of solution phase polymerization followed by oligomeric precipitation was presented [4]. The observation of the formation of conducting films by electropolymerization of bipyrrole indicated that chain formation was not limited to reaction of oxidized oligomers with pyrrole radical cation, and that coupling of oligomers in solution followed by precipitation was a viable mechanism. Overwhelming evidence to support this statement was obtained during the study of the pyrrole radical cation. This study demonstrated that the deposition process is not a true three dimensional nucleation and growth process, but rather occurs via solution-phase polymerization with subsequent electro-precipitation of oligomers. The process was also shown to require stepwise oxidation of oligomers, and in this sense is stoichiometric rather than chain-like in propagation. These conclusions were supported by the coincidence of the rapid growth in disk current with the pulse of soluble radical product formed at the end of an induction period. Also, the photograph of the platinum disk electrode surface demonstrated that the distribution of the polymer coating on the electrode at the stage of rapid current growth is not random but shows a pattern attributable to the hydrodynamic flow of solution species formed by oxidation at an active surface. The lack of formation of polymer on the surrounding teflon shroud indicated that an active surface is required for polymer growth to occur and that continual oxidation of species formed is needed.

The investigations using finite difference analysis to digitally simulate the pyrrole polymerization kinetics at the RRDE demonstrated that differentiation between possible mechanisms is not possible. Kinetic analysis of pyrrole polymerization in acetonitrile containing perchlorate anions showed no dependence of the overall rate constant on pyrrole concentration, supporting the reactions schemes assumed for this system. When $TBABF_4$ was used as electrolyte an inverse square dependence of the rate constant was found, which implies a different mechanism must be present. The value of the overall polymerization rate constant obtained with perchlorate anions varied depending on the reaction scheme assumed, but had a value around 4×10^8 liters/mole-sec. A noteworthy comparison with this value is the value of the rate constant required in the crude calculation used to describe the peak shaped ring current/disk voltage curves for the radical cation. The value needed was 1×10^8 liters/mole-sec. Both values indicate that polymerization occurs at near diffusion-limited rates.

6.2 Future Research.

The work described in this thesis has established a firm basis for future evaluations of the affect of polymerization conditions on the formation of polypyrrole. The observation of the key intermediates and the subsequent rate information will be an invaluable tool for this endeavour. The basicity of the electrolyte anion has been demonstrated to be an important factor. Further investigations using a variety of electrolytes would provide the necessary kinetic information required to enable designing films with specific properties.

necessary kinetic information required to enable designing films with specific properties. The tosylate anion has been shown to give excellent conductivities and film morphologies [5], therefore a kinetic study with tetrabutylammonium tosylate would prove interesting. Also, the use of electron microscopy to correlate the kinetic information to film morphology would be very useful. Preliminary investigations into the effect of added water on the yield of bipyrrole indicated that the RRDE can be successfully applied to this problem. A more in depth study and analysis of the data is required.

A thorough RRDE investigation of the polymerization of bipyrrole would help to clarify why terpyrrole, quatrepyrrole and other oligomers are not observed in the pyrrole RRDE study. The reason may be due to the very small quantities of these species that escape the disk electrode region. The electrochemistry of bipyrrole demonstrated that the bipyrrole radical cation is not as reactive as the pyrrole radical cation and this may prove useful in evaluating the propagation process. Investigation of the radical cation reduction current as a function of concentration and rotation rate, as well as electrolyte, should be informative and might allow differentiation between different reaction rates for the different steps involved during propagation.

Finally, further digital simulation work using different mechanisms should be carried out to gain understanding on the role of protons and electrolyte anion in the polymerization process. In light of the BF_4^- data direct involvement of the anion in the reaction scheme may be required.

6.3 References

1. Skotheim, T.A., *Handbook of Conducting Polymers*, Vol.1, Marcel Dekker, New York, **1986**, Chapters 3,8,9.

2. Miller, L.L.; Zinger, B.; Zhou, Q.X., *J. Am. Chem. Soc.*, **1987**, 109, 2267.

3. Beck, F ; Oberst, M, *J. Electroanal. Chem.*, **1990**, 285, 177.

4. Christensen, P.A.; Hamnett, A., *Electrochimica Acta*, **1991**, 36, 1263.

5. Warren, L.F.; Andersen, D.P., *J. Electrochem. Soc.*, **1987**, 134, 101.

Appendix A1: Chapter 3 Ring Current-Voltage Curve Calculations.

A simple model was used to demonstrate the hypothesis that the transient behavior of the ring reduction current could be the result of radical cation coupling. In order to accomplish this, theoretical current-voltage curves for the ring and disk electrodes were calculated for comparison to experimental curves. This calculation was performed in three steps. The Koutecky-Levich equation was used to calculate the initial concentration of radical generated from the outer annulus of the disk. This concentration was then allowed to react for the average time of transit across the disk-ring gap according to a cascade of reaction steps, and the concentration of radical and bipyrrole were calculated. These reactant concentrations were then substituted into the Koutecky-Levich equation for their reaction at the ring, taken into account the geometry of the reacting system.

It is known that the oligomeric intermediates formed during the electropolymerization of pyrrole are electroactive at lower oxidation potentials than the monomer [10], consequently nearly all of the oligomers formed in the disk electrode region must also be consumed there. This should result in only a very small fraction of the intermediates escaping to the ring electrode. Consequently, it was assumed that the oligomers observed must originate from a small outer annulus at the edge of the disk. To analyze the products that escape the disk can be treated as consisting of two regions, the central area and the annulus. The disk can be viewed as a ring-disk system in which no insulating gap is present, and this is encircled by the outer ring, as indicated in Figure 3.9. Mathematically, the RRDE can be treated as a rotating double ring electrode, RDRE, with the outer disk annulus as the inner ring and the ring of the RRDE as the outer ring.

The disk region encompassed by the annulus is still active and therefore consumes much of the bulk pyrrole before it can reach the annulus, shielding it from the total flux of pyrrole. Therefore, the current obtained from the disk annulus (inner ring of the RDRE) will be the current obtained from a shielded ring electrode. However, the non-shielded current must first be calculated, i.e with the disk, excluding the outer annulus, inactive.

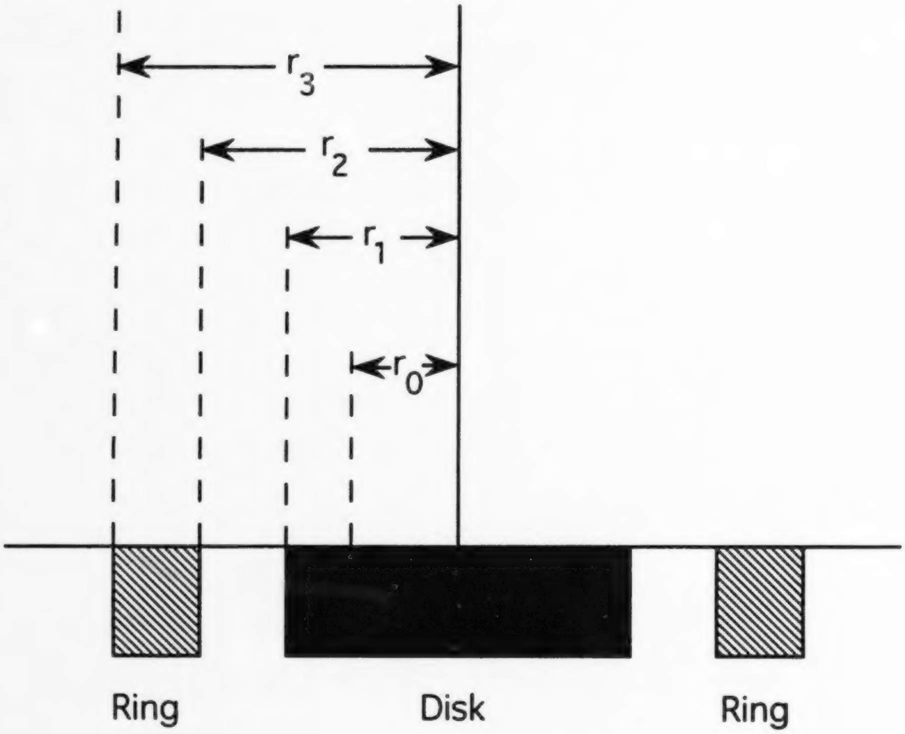
r_3
r_2
r_1
r_0
Ring
Disk
Ring

Figure A1 Schematic of Rotating Ring-Disk Electrode with radial distances applicable to treatment of the outer annulus of the disk as part of a Rotating Double Ring Electrode.

The Koutecky-Levich equation (1) can be used to calculate the total current expected for the oxidation of pyrrole at a single, unshielded, rotating ring electrode, at a specific applied potential.

$$(1).\quad \frac{1}{I_T} = \frac{1}{I_K} + \frac{1}{I_L}$$

with: $$(2).\quad I_K = n\,F\,\pi(r_1^3 - r_0^3)^{\frac{2}{3}} C^* k' e^{\left(\frac{\beta n F (E-E^{\circ'})}{R T}\right)} ;\qquad \text{kinetic current.}$$

$$(3).\quad I_L = 0.62 n F \pi (r_1^3 - r_0^3)^{\frac{2}{3}} D^{\frac{2}{3}} v^{\frac{-1}{6}} w^{\frac{1}{2}} C^* ;\quad \text{mass transport limited current.}$$

where n is the number of electrons, k' is the exchange rate constant (cm/s), F is the Faraday (C/mole electrons), ß is the transfer coefficient, r_1 is the outer annulus radius (cm), r_0 is the inner annulus radius (cm), E-E°' is the overpotential (V), R is the gas constant (J/mole-K), D is the diffusion coefficient (cm^2/s), T is the temperature (K), v is the kinematic viscosity (cm^2/s), ω is the angular velocity (s^{-1}), C^* is the bulk concentration (in I_L calculation (m*M*), in I_K calculation (mole/cm^3)).

The disk current dependence on rotation rate was found to obey the Levich equation (equation (3) with the disk electrode area substituted for the annulus area) when the disk potential was 1.35 V. A value of n = 2.66 for pyrrole oxidation was obtained from the slope of a plot of limiting disk current versus $\omega^{1/2}$, which is similar to values reported in the literature [25]. The number of electrons involved in radical cation reduction and bipyrrole oxidation were both assumed to be one.

Tafel analysis of the experimentally determined kinetic current, I_k, as a function of potential was analyzed to obtain the Tafel parameters **a** and **b** from the Tafel equation ($\log I_k = a + bE$). To obtain I_k as a function of E, Koutecky-Levich plots (I^{-1} vs $\omega^{-1/2}$) were constructed at various potentials along the disk current-voltage curve. The kinetic current, at the specific disk potentials, was obtained from the inverse of the intercept of the Koutecky-Levich plot. The Tafel parameters **a** and **b** were then used in the Koutecky-Levich equation for a rotating disk electrode to calculate the expected disk current-voltage curve. The calculated curve was then visually compared to the experimental disk current-voltage curve. To obtain the best overlap between the experimental and calculated curves parameter **b** was maintained constant while the **a** value was adjusted. Once adequate overlap was achieved the Tafel parameters were then used to calculate the contribution of the kinetic current to the current from the annulus region alone. The Tafel parameter a was normalized to account for the difference in areas.

Equations (1) to (3) give the current from the disk annulus assuming the inner disk was not present. The shielded annulus current was calculated on the basis of the shielding factor and collection efficiency for a no gap system [42], as shown below.

Where: (4) $(1 - N\beta_r^{\frac{-2}{3}})$ Shielding Factor

with (5) $N = 1 + \beta_r^{\frac{2}{3}} - (1 + \beta_r)^{\frac{2}{3}}$ No gap Collection Efficiency

and (6) $\beta_r = (\frac{r_{or}}{r_d})^3 - (\frac{r_{ir}}{r_d})^3$ Geometric factor

In (6) r_{or} is the outer radius of the disk annulus, which is the total disk radius of the RRDE, r_{ir} is the inner radius of the disk annulus and r_d is the inner disk radius. However because there is no gap present $r_{ir} = r_d$, and using the convention defined in Figure 3.9, $r_{or} = r_1$ and $r_d = r_0$, resulting in (6) becoming;

(6a) $\beta_r = (\frac{r_1}{r_0})^3 - 1$

The shielded annulus current was then obtained using equation (7), with the non-shielded current value obtained from (1).

(7). $I_{ann,shielded} = I_{ann,non\text{-}shielded}(1 - N\beta_r^{\frac{-2}{3}})$

Using this shielded annulus current the expected concentration of radical cations initially generated at the outer disk annulus was obtained using equations (1)-(3). This step assumes that the current obtained corresponds to a certain quantity of pyrrole oxidized, and hence to an equal quantity of radical cations generated.

The initial concentration of radical cation was then allowed to react via the reaction scheme shown in scheme 1. The concentration of the various species present after a reaction time, which was equal to the rotation rate dependent transit time between the disk annulus and the ring [39] was then obtained. The average transit time was calculated using equation (8).

$$WT = 43.1\left(\frac{v}{D}\right)^{\frac{1}{3}}\left(\log\frac{r_2}{r_1}\right)^{\frac{2}{3}} \tag{8}$$

where W is the rotation rate, in rev./min.and T is the transit time.

To simulate the reaction of species across the gap according to the scheme a subroutine which integrated the differential equations describing the homogeneous kinetics described in scheme 1 was used.

Scheme 1

$$\begin{aligned}
2M^{\cdot+} &\xrightarrow{k_p} M_2 \\
M_2 + M^{\cdot+} &\longrightarrow M_2^{\cdot+} + M \\
2M_2^{\cdot+} &\longrightarrow M_4 \\
M_2^{\cdot+} + M^{\cdot+} &\longrightarrow M_3 \\
M_3 + M^{\cdot+} &\longrightarrow M_3^{\cdot+} + M \\
M_3^{\cdot+} + M^{\cdot+} &\longrightarrow M_4 \\
M_3^{\cdot+} + M_2^{\cdot+} &\longrightarrow M_5 \\
M_4 + M^{\cdot+} &\longrightarrow M_4^{\cdot+} + M \\
M_4^{\cdot+} + M^{\cdot+} &\longrightarrow M_5 \\
M_4^{\cdot+} + M_2^{\cdot+} &\longrightarrow M_6 \\
M_4^{\cdot+} + M_3^{\cdot+} &\longrightarrow M_7
\end{aligned}$$

where M is pyrrole , $M^{\cdot+}$ is the pyrrole radical cation, M_2 is bipyrrole, $M_2^{\cdot+}$ is the bipyrrole radical cation, M_3 is terpyrrole, $M_3^{\cdot+}$ is the terpyrrole radical cation, M_4 is quaterpyrrole, $M_4^{\cdot+}$ is the quaterpyrrole radical cation, M_5 is quinquepyrrole, M_6 is sexipyrrole, and M_7 is heptipyrrole.

These calculated concentrations must then be modified for the collection efficiency of the ring electrode at which they are detected. Mathematically the system was treated as a rotating double ring electrode, RDRE, rather than a rotating ring-disk electrode. Therefore it was necessary to multiply the concentration values calculated after the reaction period by the theoretical collection efficiency for a RDRE [43,44] given in equation (9).

$$N = \left(\frac{r_3^3-r_2^3}{r_1^3-r_0^3}\right)^{\frac{2}{3}} G\left(\frac{r_1^3-r_0^3}{r_2^3-r_1^3}\right) + G\left(\frac{r_3^3-r_2^3}{r_2^3-r_1^3}\right) - \left(\frac{r_3^3-r_0^3}{r_1^3-r_0^3}\right)^{\frac{2}{3}} G\left(\frac{(r_1^3-r_0^3)(r_3^3-r_2^3)}{(r_3^3-r_0^3)(r_2^3-r_1^3)}\right) \tag{9}$$

with

$$G(x) = \frac{\sqrt{3}}{4\pi} \ln\left(\frac{1+x}{(1+x^{\frac{1}{3}})^3}\right) + \frac{3}{2\pi} \arctan\left(\frac{2x^{\frac{1}{3}}-1}{\sqrt{3}}\right) + \frac{1}{4} \tag{10}$$

where r_0 and r_1 are the inner and outer radii of the inner ring (annulus), while r_2 and r_3 are the inner and outer radii of the outer ring. This equation assumes that the inner ring (annulus) is generating the species which is observed at the outer ring, which is the reason the RDRE formalism is used.

These final concentration values were then used in equation (3) to calculate the individual ring currents for the radical cation and the dimer, with the values for r_2 and r_3 substituted for r_0 and r_1. Also, only equation (3) was used since it was assumed that the potential used to monitor these species resulted in mass transport limited current. The current calculated for just radical cation reduction should correspond to the situation in which the ring electrode is poised at a potential at which only the radical cation is observable. The sum of the two calculated current values should correspond to the situation where both the radical cation and the dimer are observable at the ring potential used. Current for oxidation or reduction of the dimer radical or higher oligomeric species was not considered.

Given in Table A1 are the parameter values used in equations (1)-(3) to obtain the calculated current-voltage curves shown in Figure 3.8. The homogeneous rate constants were all assumed to be equal, since discrimination between the rates of individual steps is unjustified given the available information. The calculated radical cation current and the sum of the calculated radical cation and dimer currents were matched to both the experimental steady state radical cation and bipyrrole currents. For the best match the inner annulus radius used was 0.22844 cm, giving an annulus thickness of only 1.6 μm and an overall rate constant of 1×10^8 liters/mole-sec.

Parameter	Value	Units
F	96487	C/mole electrons
R	8.31415	J/mole-K
T	298	K
v	4.8×10^3	cm^2/s
C*	0.1	m*M*
r_0	0.22860	cm
r_1	0.22844	cm
k'	2×10^{-5}	cm/s
ω	471.2	s^{-1}
D: for pyrrole and pyrrole radical cation.	3.8×10^{-5}	cm^2/s
D: for bipyrrole	2.7×10^{-5}	cm^2/s
n: pyrrole oxidation	2.66	unitless
n: radical cation reduction.	1	unitless
k_n: for all reaction steps.	1×10^8	liters/mole-sec

Table A1: Parameters used in Ring Current Calculations.

Appendix A2: Feldberg's Finite Difference Program

Written in Professional Fortran.
Radical-Radical Coupling Mechanism

```
      real k1,knorm,KR1
      common D(12),Sc,beta,k1,ns,nre,nkin,xj0,jg,jg1,j1,i1,i1gre,
     1 a1(12,0:50,100),a2(12,0:50,100),a9(100),vi2(100),dvi(100),
     1 aj1(50),aj2(50),f(12,0:50),r(50),c(12),KR1
c     OPEN(7,FILE='LPT1')
c     OPEN(2,FILE='A:DANS.DAT')
      write(*,*)'Program RRPENT.FOR:'
      write(*,*)
      write(*,*)' Changes in the program are introduced in three'
      write(*,*)' subroutines:'
      write(*,*)'    1. SUBROUTINE mech '
      write(*,*)'    2. SUBROUTINE surflux( )'
      write(*,*)'    3. SUBROUTINE homkin'
      write(*,*)
      call mech
      write(*,*)
      write(*,*)' NOTES on notation:'
      write(*,*)'   xj0 = disc radius'
      write(*,*)'    jg = value of j for outermost gap element'
      write(*,*)'    j1 = value of j for outermost ring element'
      write(*,*)
      write(*,*)'    Consistent with the paper, j=0 corresponds'
      write(*,*)'      to the disc elements (IBM Professional'
      write(*,*)'      FORTRAN accepts 0 subscripts).'
      write(*,*)
      call levart
  130 write(*,*)
      write(*,*)' There are ',ns,' species. '
      write(*,*)' Input D s (real or D* s) in order (values of D*'
      write(*,*)'    are automatically adjusted so D*(max) = 0.4):'
      read(*,*) (D(n),n=1,ns)
      Dmax=D(1)
      Dmin=D(1)
      Do 150 n=2,ns
        Dmax=amax1(D(n),Dmax)
        Dmin=amin1(D(n),Dmin)
  150   continue
      Do 160 n=1,ns
  160   D(n)=0.4*D(n)/Dmax
      Dmin=0.4*Dmin/Dmax
```

```
Dmax=0.4
write(*,*)
write(*,*)'Input:'
write(*,*)'   Beta (<=0.001)'
write(*,*)'   Sc (Schmidt no. based on D(1))'
write(*,*)'   k* (normalized kinetic parameter)'
write(*,*)'   KR1'
write(*,*)
read(*,*)beta,Sc,knorm,KR1
Pt=D(1)**.333333333*beta**.666666666666
write(*,*)Pt
k1=knorm*Pt+1e-20
k1=k1+1.0e-20
if((nkin.ne.0).and.(k1.ne.0.))then
 if(sqrt(D(nkin)/k1).lt.5)then
   write(*,*)'Sqrt(D(nkin)/k1) =',sqrt(D(nkin)/k1),' is <5.'
   write(*,*)'  Change input: smaller beta or smaller k1'
   goto130
 endif
endif
tout=0.025
dtout=tout
mtmax=100000
delta = (1+(Sc*D(1)/Dmax)**(-.3333333))*(Dmax/beta)**.3333333
deltam= (1+(Sc*D(1)/Dmin)**(-.3333333))*(Dmin/beta)**.3333333
i1m=1+int(3*deltam)
i1=1+int(3*delta)
if(i1m.lt.20)then
write(*,*)' Too few elements for accuracy (i1(min) =',i1m,')'
write(*,*)'    i1(min) is associated with Dmin, .:'
write(*,*)'     Decrease beta.'
goto 130
endif
w=0.620327*D(1)**(2./3.)*(beta/a9(2))**(1./3.)
if (i1.gt.99)then
write(*,*)
write(*,*)'Exceeded index limit: increase index or beta.'
goto 130
endif
write(*,*)'Give r2/r1, r3/r1, and jg (integral number'
write(*,*)'   of gap elements:'
read(*,*)r2,r3,jg
i1gre=1+int(2.5*delta*(r3-1)**.333333333)
if (i1gre.gt.i1)i1gre=i1
write(*,*)'Imax,rde is',i1,' Imax,rrde is',i1gre
```

```
      call subab1(r2,r3)
      xnjprev=100
      mtfin=0
      call subvel
      call initial
c
c
      i1=i1-1
      i1gre=i1gre-1
      do 2000 m=1,mtmax
c
      call subexp0
      call subexp1
      call homkin
c
      tstar=m*Pt
      if(tstar.lt.tout-.01*dtout) go to 2000
      tout=tout+dtout
      write(*,*)'Data from RRPENT.FOR: REAL WORLD
                     PARAMETERS'
      write(*,*)' Sc=',Sc,'    knorm=',knorm
      write(*,*)' r2/r1=',r2,'  r3/r1>',r3
      write(*,*)
      write(*,*)'SIMULATOR PARAMETERS:'
      write(*,*)'D*s=',(D(n),n=1,ns)
      write(*,*)' Beta=',beta,'   k1=',k1
      write(*,*)'  j0=',xj0,'    jg=',jg,'     j1=',j1
      write(*,*)'     imax(rde)=',i1,'     imax(rrde)=',i1gre
      write(*,*)
      write(*,*)' After ',m,' iterations at t*=',tstar
      f01save=f(1,0)
      f03save=f(3,0)
      f05save=f(5,0)
      f07save=f(7,0)
      f09save=f(9,0)
      f011save=f(11,0)
      f012save=f(12,0)
      call surflux(0)
      f01=(f01save+f(1,0))/2
      f03=(f03save+f(3,0))/2
      f05=(f05save+f(5,0))/2
      f07=(f07save+f(7,0))/2
      f09=(f09save+f(9,0))/2
      f011=(f011save+f(11,0))/2
      f012=(f012save+f(12,0))/2
      f0=f01+f03+f05+f07+f09+f011+f012
      write(*,*)' f(1,0)*=',f0/w
      write(*,*)'          j  a(nre,j,1)       a(nre,j,i1gre)
     1 Nab          Nsim'
      xnj=0
      f0a=f0*xj0**2
      write(*,*)0,a1(nre,0,1),a1(nre,0,i1gre)
      do 1900 j=1,j1
      if (j.le.jg)write(*,*)j,a1(nre,j,1),a1(nre,j,i1gre)
      if (j.gt.jg) then
        fjsave=f(nre,j)
        call surflux(j)
        fj=(fjsave+f(nre,j))/2
        xnj=xnj+fj*(2.*(xj0+j)-1.)/f0a
        write(*,*)j,a1(nre,j,1),a1(nre,j,i1gre),r(j),xnj
      endif
1900  continue
      ftest=abs((xnj-xnjprev)/xnjprev)
      write(*,*)ftest
      xnjprev=xnj
      if ((mtfin.eq.0).and.(ftest.le.1e-5)) then
        mtfin=m
        write(*,*)
        write(*,*)mtfin,ftest
        write(*,*)f0/w
c       write(7,*)' PROGRAM RRPENT.FOR'
c       write(7,*)
c       write(7,*)' RADICAL-RADICAL COUPLING WITH
                      REGENERATION'
c       write(7,*)' LAST SPECIES IS THE PENTAMER: '
c       write(7,*)' NO PENTAMER REACTIONS IN SOLUTION'
c       write(7,*)' PENTAMER ONLY OXIDIZED AT DISK
                      ELECTRODE'
c       write(7,*)
c       write(7,*)' Parameters used in calculation'
c       write(7,*)
c       write(7,*)' Beta=',beta,'       Sc=',Sc
c       write(7,*)'  Qk=',knorm,'       k1=',k1
c       write(7,*)'  KR1=',KR1
c       write(7,*)
c       write(7,*)' r2/r2=',r2,'        r3/r3 >',r3
c       write(7,*)
c       write(7,*)' Monomer Diffusion Coefficient.=',D(1)
c       write(7,*)' Monomer Rad. Cat. Diff. Coeff.=',D(2)
c       write(7,*)' Dimer Diffusion Coefficient.=',D(3)
```

```
c       write(7,*)' Dimer Rad. Cat. Diff. Coeff.=',D(4)
c       write(7,*)' Trimer Diffusion Coefficient.=',D(5)
c       write(7,*)' Trimer Rad. Cat. Diff. Coeff.=',D(6)
c       write(7,*)' Tetramer Diff. Coeff.=',D(7)
c       write(7,*)' Tetramer Rad. Cat. Diff. Coeff.=',D(8)
c       write(7,*)' Pentamer Diff. Coeff.=',D(9)
c       write(7,*)
c       write(7,*)' j0=',xj0,'   jg=',jg,'   j1=',j1
c       write(7,*)
c       write(7,*)' imax(rde)=',i1,'     imax(rrde)=',i1gre
c       write(7,*)
c       write(7,*)' After ',m,' iterations at t*= ',tstar
c       write(7,*)
c       write(7,*)' Disk Flux=',f0/w
c       write(7,*)
c       write(7,*)' Radial Ring Flux for Dimer'
c       write(7,*)
c       write(7,*)' j, a(nre,j,1)        a(nre,j,i1gre)'
c       write(7,*)
c       write(7,*)  0,a1(nre,0,1),a1(nre,0,i1gre)
c       do 1910 j=1,j1
c         write(7,*)  j,a1(nre,j,1),a1(nre,j,i1gre)
c 1910    continue
c      write(7,*)
       write(7,*)' Collection Efficiency = ',xnj
c      do 1930 j=0,j1
c      do 1930 i=1,i1
c        write(2,*)i,j,a1(1,j,i),a1(2,j,i),a1(3,j,i)
c1930    continue
c      do 1950 j=0,j1
c      do 1950 i=1,i1
c        write(2,*)i,j,a1(4,j,i),a1(5,j,i)
c1950    continue
       goto 2100
      endif
 2000  continue
 2100  end
c
c     -----------------------------------------------------
c     -----------------------------------------------------
      SUBROUTINE initial
c
c     Initialize concentration and flux values for disc, gap,
c       and ring.
c
```

```
      real k1,knorm,KR1
      common D(12),Sc,beta,k1,ns,nre,nkin,xj0,jg,jg1,j1,i1,i1gre,
     1 a1(12,0:50,100),a2(12,0:50,100),a9(100),vi2(100),dvi(100),
     1 aj1(50),aj2(50),f(12,0:50),r(50),c(12),KR1
c
      do 300 n=1,ns
      do 300 j=0,j1
        f(n,j)=0
      do 300 i=1,i1
        a1(n,j,i)=c(n)
 300  continue
c
      return
      end
c     ---------------------------------------------------------
c
      SUBROUTINE mech
c
c         Subroutine to define mechanistic parameters.
c
      real k1,knorm,KR1
      common D(12),Sc,beta,k1,ns,nre,nkin,xj0,jg,jg1,j1,i1,i1gre,
     1 a1(12,0:50,100),a2(12,0:50,100),a9(100),vi2(100),dvi(100),
     1 aj1(50),aj2(50),f(12,0:50),r(50),c(12),KR1
c
      write(*,*)' For following mechanism (number in parentheses'
      write(*,*)'   is species index):'
      write(*,*)
      write(*,*)'  A(1) ---> B(2) + e            disc'
      write(*,*)'  C(3) ---> D(4) + e                '
      write(*,*)'  E(5) ---> F(6) + e                '
      write(*,*)'  G(7) ---> H(8) + e                '
      write(*,*)'   I(9) ---> J(10) + e              '
      write(*,*)'   K(11) ---> M(13) + e             '
      write(*,*)'   L(12) ---> N(14) + e             '
      write(*,*)
      write(*,*)'  C(3) ---> D(4) + e            ring'
      write(*,*)
      write(*,*)'  2B(2) -k1 ---> C(3)   homogeneous kinetics'
      write(*,*)'  C(3) + B(2) -k2 ---> D(4) + A(1)  '
      write(*,*)'  2D(4)         -k3 ---> G(7)       '
      write(*,*)'  D(4) + B(2) -k4 ---> E(5)         '
      write(*,*)'  E(5) + B(2)  -k5 ---> F(6)  + A(1) '
      write(*,*)'  F(6) + B(2)  -k6 ---> G(7)        '
      write(*,*)'  F(6) + D(4)  -k7 ---> I(9)        '
      write(*,*)' G(7) + B(2)  -k8 ---> H(8) + A(1) '
      write(*,*)' H(8) + B(2)  -k9 ---> I(9)        '
      write(*,*)' H(8) + D(4)  -k10 ---> K(11)       '
      write(*,*)' H(8) + F(6)  -k11 ---> L(12)       '
      write(*,*)
      write(*,*)'  There is no need to track species J, K & L.'
c
c          ns  = number of species involved in simulation
c          nre = index of species that is electroactive at
c               ring (c(nre,jring,x=0) = 0 is presumed)
c          nkin= index of species kinetically disappearing
c               (nkin = 0 indicates no such species).
c          n   = 1 for species that is electroactive at disc,
c               i.e.: c(1,0,x=0) = 0.
c          c(n)= initial concentration of nth species.
c
      ns=12
      nkin=2
      nre=3
      c(1)=1
      c(2)=0
      c(3)=0
      c(4)=0
      c(5)=0
      c(6)=0
      c(7)=0
      c(8)=0
      c(9)=0
      c(10)=0
      c(11)=0
      c(12)=0
      return
      end
c
c     ----------------------------------------------------------
      SUBROUTINE surflux(j)
c
c         Subroutine to compute surface flux at disc (j=0) and
c          ring (j >= jg1).
c
c          Remember: f(n,j) terms are subtracted in computation.
c
      real k1,knorm,KR1
      common D(12),Sc,beta,k1,ns,nre,nkin,xj0,jg,jg1,j1,i1,i1gre,
     1 a1(12,0:50,100),a2(12,0:50,100),a9(100),vi2(100),dvi(100),
     1 aj1(50),aj2(50),f(12,0:50),r(50),c(12),KR1
c
c
      if(j.eq.0) then
        f(1,0)=2*D(1)*a1(1,0,1)
        f(2,0)=-f(1,0)
        f(3,0)=2*D(3)*a1(3,0,1)
        f(4,0)=-f(3,0)
        f(5,0)=2*D(5)*a1(5,0,1)
        f(6,0)=-f(5,0)
        f(7,0)=2*D(7)*a1(7,0,1)
        f(8,0)=-f(7,0)
        f(9,0)=2*D(9)*a1(9,0,1)
        f(10,0)=-f(9,0)
        f(11,0)=2*D(11)*a1(11,0,1)
        f(12,0)=2*D(12)*a1(12,0,1)
       return
      endif
c
      if(j.ge.jg1) then
       f(1,j)=0
       f(2,j)=0
       f(3,j)=2*D(3)*a1(3,j,1)
       f(4,j)=-f(3,j)
       f(5,j)=0
       f(6,j)=0
       f(7,j)=0
       f(8,j)=0
       f(9,j)=0
       f(10,j)=0
       f(11,j)=0
       f(12,j)=0
       return
      endif
c
      f(1,j)=0
      f(2,j)=0
      f(3,j)=0
      f(4,j)=0
      f(5,j)=0
      f(6,j)=0
      f(7,j)=0
      f(8,j)=0
      f(9,j)=0
      f(10,j)=0
      f(11,j)=0
      f(12,j)=0
      return
c
      end
c
c     ----------------------------------------------------------
      SUBROUTINE homkin
c
c         Subroutine to compute homogeneous kinetics at disc, gap,
c           and ring.  For second-order dimerization ECE case :
c             zeroed in initialization.
c
c
      real k1,knorm,KR1
      common D(12),Sc,beta,k1,ns,nre,nkin,xj0,jg,jg1,j1,i1,i1gre,
     1 a1(12,0:50,100),a2(12,0:50,100),a9(100),vi2(100),dvi(100),
     1 aj1(50),aj2(50),f(12,0:50),r(50),c(12),KR1
c     reset and kinetics for disc (j=0)
c
c     Note: kinetic parameters operate on a1(n,j,i).  This is
c      equivalent to including the kinetic term in subexp0 or
c      subexp1 instead of in SUBROUTINE reset.  It is much more
c      accurate than operating on  a2(n,j,i).
c
      do 1000 i=1,i1
      a1(1,0,i)=a2(1,0,i)+(KR1*k1*a1(2,0,i)*a1(3,0,i))
     1          +(KR1*k1*a1(2,0,i)*a1(5,0,i))
     1          +(KR1*k1*a1(2,0,i)*a1(7,0,i))
      a1(2,0,i)=a2(2,0,i)-(k1*a1(2,0,i)*a1(2,0,i))
     1          -(KR1*k1*a1(2,0,i)*a1(3,0,i))
     1          -(KR1*k1*a1(2,0,i)*a1(4,0,i))
     1          -(KR1*k1*a1(2,0,i)*a1(5,0,1))
     1          -(KR1*k1*a1(2,0,i)*a1(6,0,1))
     1          -(KR1*k1*a1(2,0,i)*a1(7,0,1))
     1          -(KR1*k1*a1(2,0,i)*a1(8,0,1))
      a1(3,0,i)=a2(3,0,i)+(k1*a1(2,0,i)*a1(2,0,i))
     1          -(KR1*k1*a1(2,0,i)*a1(3,0,i))
      a1(4,0,i)=a2(4,0,i)+(KR1*k1*a1(2,0,i)*a1(3,0,i))
     1          -(KR1*k1*a1(4,0,i)*a1(4,0,i))
     1          -(KR1*k1*a1(4,0,i)*a1(2,0,1))
     1          -(KR1*k1*a1(4,0,i)*a1(6,0,i))
     1          -(KR1*k1*a1(4,0,i)*a1(8,0,i))
      a1(5,0,i)=a2(5,0,i)+(KR1*k1*a1(2,0,i)*a1(4,0,i))
     1          -(KR1*k1*a1(2,0,i)*a1(5,0,1))
```

```
      a1(6,0,i)=a2(6,0,i)+(KR1*k1*a1(2,0,i)*a1(5,0,i))
     1          -(KR1*k1*a1(6,0,i)*a1(2,0,1))
     1          -(KR1*k1*a1(6,0,i)*a1(4,0,1))
      a1(7,0,i)=a2(7,0,i)+(KR1*k1*a1(4,0,i)*a1(4,0,i))
     1          +(KR1*k1*a1(6,0,i)*a1(2,0,1))
     1          -(KR1*k1*a1(7,0,i)*a1(2,0,1))
      a1(8,0,i)=a2(8,0,i)+(KR1*k1*a1(7,0,i)*a1(2,0,i))
     1          -(KR1*k1*a1(8,0,i)*a1(2,0,1))
     1          -(KR1*k1*a1(8,0,i)*a1(4,0,1))
     1          -(KR1*k1*a1(8,0,i)*a1(6,0,1))
      a1(9,0,i)=a2(9,0,i)+(KR1*k1*a1(6,0,i)*a1(4,0,i))
     1          +(KR1*k1*a1(8,0,i)*a1(2,0,1))
      a1(11,0,i)=a2(11,0,i)+(KR1*k1*a1(8,0,i)*a1(4,0,i))
 1000 a1(12,0,i)=a2(12,0,i)+(KR1*k1*a1(6,0,i)*a1(8,0,i))
c
c     reset and kinetics for ring and gap
c
      do 2000 j=1,j1
      do 2000 i=1,i1gre
      a1(1,j,i)=a2(1,j,i)+(KR1*k1*a1(2,j,i)*a1(3,j,i))
     1          +(KR1*k1*a1(2,j,i)*a1(5,j,i))
     1          +(KR1*k1*a1(2,j,i)*a1(7,j,i))
      a1(2,j,i)=a2(2,j,i)-(k1*a1(2,j,i)*a1(2,j,i))
     1          -(KR1*k1*a1(2,j,i)*a1(3,j,i))
     1          -(KR1*k1*a1(2,j,i)*a1(4,j,i))
     1          -(KR1*k1*a1(2,j,i)*a1(5,j,1))
     1          -(KR1*k1*a1(2,j,i)*a1(6,j,1))
     1          -(KR1*k1*a1(2,j,i)*a1(7,j,1))
     1          -(KR1*k1*a1(2,j,i)*a1(8,j,1))
      a1(3,j,i)=a2(3,j,i)+(k1*a1(2,j,i)*a1(2,j,i))
     1          -(KR1*k1*a1(2,j,i)*a1(3,j,i))
      a1(4,j,i)=a2(4,j,i)+(KR1*k1*a1(2,j,i)*a1(3,j,i))
     1          -(KR1*k1*a1(4,j,i)*a1(4,j,i))
     1          -(KR1*k1*a1(4,j,i)*a1(2,j,1))
     1          -(KR1*k1*a1(4,j,i)*a1(6,j,i))
     1          -(KR1*k1*a1(4,j,i)*a1(8,j,1))
      a1(5,j,i)=a2(5,j,i)+(KR1*k1*a1(2,j,i)*a1(4,j,i))
     1          -(KR1*k1*a1(2,j,i)*a1(5,j,1))
      a1(6,j,i)=a2(6,j,i)+(KR1*k1*a1(2,j,i)*a1(5,j,i))
     1          -(KR1*k1*a1(6,j,i)*a1(2,j,1))
     1          -(KR1*k1*a1(6,j,i)*a1(4,j,1))
      a1(7,j,i)=a2(7,j,i)+(KR1*k1*a1(4,j,i)*a1(4,j,i))
     1          +(KR1*k1*a1(6,j,i)*a1(2,j,1))
     1          -(KR1*k1*a1(7,j,i)*a1(2,j,1))
      a1(8,j,i)=a2(8,j,i)+(KR1*k1*a1(7,j,i)*a1(2,j,i))
     1         -(KR1*k1*a1(8,j,i)*a1(2,j,1))
     1         -(KR1*k1*a1(8,j,i)*a1(4,j,1))
     1         -(KR1*k1*a1(8,j,i)*a1(6,j,1))
      a1(9,j,i)=a2(9,j,i)+(KR1*k1*a1(6,j,i)*a1(4,j,i))
     1         +(KR1*k1*a1(8,j,i)*a1(2,j,1))
      a1(11,j,i)=a2(11,j,i)+(KR1*k1*a1(8,j,i)*a1(4,j,i))
 2000 a1(12,j,i)=a2(12,j,i)+(KR1*k1*a1(6,j,i)*a1(8,j,i))
c
      return
c
      end
c
c     ---------------------------------------------------------
      SUBROUTINE subexp0
c
c         Subroutine for the disc:
c           Explicit HS computation
c
      real k1,knorm,KR1
      common D(12),Sc,beta,k1,ns,nre,nkin,xj0,jg,jg1,j1,i1,i1gre,
     1 a1(12,0:50,100),a2(12,0:50,100),a9(100),vi2(100),dvi(100),
     1 aj1(50),aj2(50),f(12,0:50),r(50),c(12),KR1
      call surflux(0)
      do 105 n=1,ns
105   a2(n,0,1)=a1(n,0,1)*(1-D(n)+vi2(1))+(D(n)-vi2(1))*
     1 a1(n,0,2)-f(n,0)
 110  do 120 i=2,i1
      do 120 n=1,ns
 120  a2(n,0,i)=a1(n,0,i)*(1-2*D(n)+dvi(i))+(D(n)-vi2(i))*
     1 a1(n,0,i+1)+(D(n)+vi2(i-1))*a1(n,0,i-1)
      return
      end
c
c     ---------------------------------------------------------
      SUBROUTINE subexp1
c
c     Subroutine for gap and ring:
c       Explicit HS computation
c
      real k1,knorm,KR1
      common D(12),Sc,beta,k1,ns,nre,nkin,xj0,jg,jg1,j1,i1,i1gre,
     1 a1(12,0:50,100),a2(12,0:50,100),a9(100),vi2(100),dvi(100),
     1 aj1(50),aj2(50),f(12,0:50),r(50),c(12),KR1
c
      do 2000 j=1,j1
      jp=j+1
      jm=j-1
      jmm=jg1-2
      do 10 n=1,ns
10      a1(n,j,i1gre+1)=a1(n,0,i1gre+1)
c
      if(j.eq.1) then
        rji=aj2(j)
        rjpi=aj2(j)
        rjmi=-2*aj1(j)
        rjmmi=0
        goto1000
      endif
c
      if((j.eq.jg).or.(j.eq.j1)) then
        rji=2*aj2(j)+1
        rjpi=0
        rjmi=-aj2(j)-aj1(j)
        rjmmi=0
        goto1000
      endif
c
      if(j.eq.jg1) then
        rji=aj2(j)
        rjpi=aj2(j)
        rjmi=-3*aj1(j)
        rjmmi=aj1(j)
        goto1000
      endif
c
        rji=1
        rjpi=aj2(j)
        rjmi=-aj1(j)
        rjmmi=0
c
1000    call surflux(j)
      do 100 n=1,ns
100     a2(n,j,1)= a1(n,j,1)*(1-D(n)-dvi(1)*(1-rji))+a1(n,j,2)*
     1 (D(n)-vi2(1))+dvi(1)*(a1(n,jp,1)*rjpi+a1(n,jm,1)*rjmi+
     1 a1(n,jmm,1)*rjmmi)-f(n,j)
c
      do 200 i=2,i1gre
      do 200 n=1,ns
200     a2(n,j,i)=a1(n,j,i)*(1-2*D(n)-dvi(i)*(1-rji))+a1(n,j,i+1)*
     1 (D(n)-vi2(i))+a1(n,j,i-1)*(D(n)+vi2(i-1))+dvi(i)*(a1(n,jp,i)*
     1 rjpi+a1(n,jm,i)*rjmi+a1(n,jmm,i)*rjmmi)
2000   continue
c
       return
       end
c
c      -----------------------------------------------------------
       SUBROUTINE levart
c
c        Subroutine to compute coefficients for the computation of
c          hydrodynamic velocities according to Levart and Shuhmann)
c
       real k1,knorm,KR1
       common D(12),Sc,beta,k1,ns,nre,nkin,xj0,jg,jg1,j1,i1,i1gre,
     1 a1(12,0:50,100),a2(12,0:50,100),a9(100),vi2(100),dvi(100),
     1 aj1(50),aj2(50),f(12,0:50),r(50),c(12),KR1
       dimension aa(150),bb(150),cc(150)
       aa(1)=0
       aa(2)=.510232619
       bb(1)=1
       bb(2)=-.615922
       bb(3)=0
       do 100 i=2, 95
       sa=0
       sb=0
       do 200 kk=1,i-1
       k=kk-1
       sa=sa+(i-3*k-1)*aa(k+1)*aa(i-k-1)/(i-k-1)-bb(k+1)*bb(i-k-1)
       if (i.ge.3)then
       sb=sb+aa(k+1)*bb(i-k-1)-k*aa(i-k-1)*bb(k+1)/(i-k-1)
       endif
 200   continue
       aa(i+1)=sa/(i*(i-1))
       if (i.ge.3) bb(i+1)=2*sb/(i*(i-1))
       cc(i+1)=-2*aa(i)/i
 100   continue
       do300i=1,95
       a9(i)=2*aa(i)/i
 300   continue
       return
       end
c
c      -----------------------------------------------------------
       SUBROUTINE subab1(r2,r3)
c
```

```
c      Subroutine (with subab2) to compute the collection
c        efficiencies according to to the equations of Albery and
c          Bruckenstein (assuming an infinite Schmidt number).
c
      real k1,knorm,KR1
      common D(12),Sc,beta,k1,ns,nre,nkin,xj0,jg,jg1,j1,i1,i1gre,
     1 a1(12,0:50,100),a2(12,0:50,100),a9(100),vi2(100),dvi(100),
     1 aj1(50),aj2(50),f(12,0:50),r(50),c(12),KR1
      xj0=jg/(r2-1)
      j1=1+int(xj0*(r3-1))
      jg1=jg+1
      a=r2**3-1
      do 140 j=1,jg
 140  r(j)=0
      do 150 k=jg1,j1
      r3=1+k/xj0
      b=r3**3-r2**3
      z=a/b
      call subab2(z,fsub)
      f1=fsub
      z=a
      call subab2(z,fsub)
      f2=fsub
      z=(a/b)*(1+a+B)
      call subab2(z,fsub)
      f3=fsub
 150  r(K)=1-f1+b**(2./3.)*(1-f2)-(1+A+B)**(2./3.)*(1-f3)
      write(*,*)'Expected collection efficiencies (inf. Sc) are:'
      do 160 j=jg1,j1
 160  write(*,*)'For J=',j,'  n=', r(j)
      write(*,*)
      return
      end
c
c     -------------------------------------------------------
      SUBROUTINE subab2 (z,fsub)
c
c     Subroutine (with subab1) to compute the collection
c       efficiencies according to to the equations of Albery and
c         Bruckenstein (assuming an infinite Schmidt number).
c
      pi=3.14159
      fsub=0
      z1=(2*z**(1./3.)-1)/sqrt(3.)
      m1=1
      if (z1.ge.1.) then
      m1=-1
      fsub=pi/2
      endif
      do 100 i=1,1000
      m=2*i-1
      t=-m1*(-1)**i*(z1**m)**m1/m
      fsub=fsub+t
      if (abs(t/fsub).le.1e-6) goto 500
 100  continue
 500  fsub=sqrt(3.)*alog((1+z**(1./3.))**3/(1+z))/(4*pi)+1.5*
     1 fsub/pi+.25
      return
      end
c
c     ----------------------------------------------------------
      SUBROUTINE subvel
c
c      Subroutine to compute velocity terms (see paper).
c
      real k1,knorm,KR1
      common D(12),Sc,beta,k1,ns,nre,nkin,xj0,jg,jg1,j1,i1,i1gre,
     1 a1(12,0:50,100),a2(12,0:50,100),a9(100),vi2(100),dvi(100),
     1 aj1(50),aj2(50),f(12,0:50),r(50),c(12),KR1
      b2=beta/2
      b3=(beta/(a9(2)*sc*D(1)))**(1./3.)
      if (b3.lt.1e-4) b3=1e-4
      vi2(1)=0
      do 200 i=1,i1
      w7=0
      do 180 k=2,95
      k2=k-2
      w6=-b2*i**2*a9(k)*(b3*I)**k2/a9(2)
      w7=w7+w6
      if (k.gt.2) then
      if (abs(w6/w7).lt.1e-10) goto 190
      endif
  180 continue
  190 vi2(I)=w7
      if (i.gt.1)dvi(i)=vi2(i)-vi2(i-1)
  200 continue
      dvi(1)=vi2(1)
      do 300 j=1,j1
      aj2(j)=(xj0+j)**2/(2*(xj0+j)-1)
300    aj1(j)=(xj0+j-1)**2/(2*(xj0+j)-1)
```

```
return
end
```